



MONASH University

**Experimental Study on the Fundamental Combustion
Characteristics of Biogas and Multiwalled Carbon
Nanotubes blended Palm Oil Biodiesel**

Dastan Nurmukan

Supervisor: Dr. Manh-Vu Tran

Co-Supervisor: A/Prof. Hung Yew Mun

Department of Mechanical Engineering

Monash University Malaysia

A thesis submitted for the degree of

Doctor of Philosophy

May 2021

Copyright notice

© Dastan Nurmukan 2021.

I certify that I have made all reasonable efforts to secure copyright permissions for third-party content included in this thesis and have not knowingly added copyright content to my work without the owner's permission.

Abstract

Understanding of combustion behavior of biofuels requires an extensive study of the fundamental combustion characteristics such as laminar burning velocity, blowoff velocity, flammability limits, liftoff velocity, liftoff height, and emission production. A coflow bunsen burner was employed to experimentally investigate the combustion behavior of biogas and pre-vaporized palm oil biodiesel fuels.

The premixed biogas flame studies have been conducted at various experimental conditions such as elevated unburnt gas temperatures (298, 373, and 440 K), the varied concentration of CO₂ in the mixture (30, 35, and 40% by volume), and the hydrogen enrichment within the range of 0 to 40% by volume. The results revealed that both the laminar burning velocity and blowoff velocity were improved with an addition of hydrogen into the mixture. On the other hand, the increasing content of CO₂ in the mixture resulted in lower laminar burning velocity. In addition to that, the experimental observation showed that the presence of tip opening in premixed biogas flames was due to the hydrogen addition and independent of mixture flow rate at the nozzle. Furthermore, the blowoff velocity of biogas mixtures experienced a linear increase with an increasing temperature of unburnt gas, regardless of the biogas composition.

In the case of liquid fuel, palm oil biodiesel premixed flames were investigated using the slightly modified coflow bunsen burner with the addition of heating elements to ensure complete vaporization. Furthermore, the combustion characteristics of multiwalled carbon nanotubes (MWCNTs) blended palm-oil biodiesel/air mixtures were studied at a wide range of equivalence ratios, 0.7-1.6. Concentrations of the MWCNTs in the mixture were varied from 25 to 200 ppm for two different groups of nanotubes having outer diameter ranges of 10-20 nm and 30-50 nm. The results showed that both laminar burning velocity and blowoff velocity were increased with the additions of MWCNTs. Besides, the flammability limits of MWCNTs

blended biodiesel/air premixed flames were also extended at both fuel-lean and fuel-rich conditions. It was also noticed that while smaller nanoparticles experienced more noticeable improvements in the combustion characteristics, a very high concentration of nanoparticles in the mixture resulted in lesser improvement in the laminar burning velocities of the premixed flames. The study also showed that the addition of MWCNTs increased nitrogen oxides and decreased carbon monoxide concentrations in the combustion products.

Lastly, experimental studies on non-premixed flames of palm oil biodiesel fuel have been conducted to investigate the liftoff behavior. The biodiesel fuel was pre-vaporized and mixed with pre-heated nitrogen at a range of fuel mole fractions of 0.01 – 0.02. The unburnt gas temperature was varied from 500 K to 650 K and measured at the center of the nozzle exit. The results revealed that a higher jet velocity increased the liftoff height of non-premixed flames. On the contrary, an increase in fuel mole fraction and unburnt mixture temperature resulted in a lower liftoff height. It was shown that jet velocity, which was normalized with the stoichiometric laminar burning velocity, correlated well with the liftoff height regardless of unburnt mixture temperature and fuel mole fraction in the mixture. Furthermore, the correlation between the stoichiometric laminar burning velocity and the buoyancy velocity adapted liftoff velocity showed the significance of the buoyancy effect near the region of the nozzle exit.

Declaration

This thesis is an original work of my research and contains no material which has been accepted for the award of any other degree or diploma at any university or equivalent institution and that, to the best of my knowledge and belief, this thesis contains no material previously published or written by another person, except where due reference is made in the text of the thesis.

Dastan Nurmukan

May 2021

Acknowledgments

Many people contributed towards the completion of the present work, both in terms of academic guidance and assistance, as well as personal support.

First of all, I would like to express my gratitude to my supervisor Dr. Manh-Vu Tran. Not only did he give me a chance to take on this journey, but he also supported me throughout my entire candidature. While the research journey brings its own set of challenges, the outbreak of COVID-19 around the world made the process more complicated. However, the guidance and the leadership of my supervisor during this trying time will forever be appreciated. Furthermore, I would like to thank A/Prof. Hung Yew Mun for his continuous support during my research journey.

I would also like to extend my thanks to Drs. Cheng Tung Chong and Gianfranco Scribano for their continuous support and discussions provided, especially on the topic of premixed flames combustion, during my Ph.D. candidature.

As I mentioned earlier, the continuation of the research during the year of 2020 up to the present day was not the easiest period of my life due to COVID-19. The limited access, and at times no access at all, to the laboratories definitely did not help in the progress of my research. However, I am forever indebted to Dr. Poh Phaik Eong, Technical Officers of the Laboratories, Management Office, and many others who I might not know, who did their best to support the graduate students throughout this pandemic.

I can never forget the support, assistance, and discussions from my research teammates, Amsal Mohamed and Chia Chun Lee. However, besides the academic contribution, I highly appreciate the times we have shared together, with all the laughter, arguments, and jokes which came with it.

Many thanks go to Monash University Malaysia, for granting me with the scholarship and providing me with an opportunity to pursue my Doctoral degree.

At last but definitely not least, my endless gratitude goes to my, now wife, Aliesha Nadira Binti Safirul Azli. I am grateful for everything she has done for me, for making me feel at peace, for her patience in listening to things she cannot understand, for her tireless support during this long and tiring journey. I am forever and ever will be indebted to her.

First author publications resulted from this thesis

[A1] Nurmukan D, Chen TJM, Hung YM, Ismadi M-Z, Chong CT, Tran M-V. Enhancement of biogas/air combustion by hydrogen addition at elevated temperatures. *Int J Energy Res.* 2020;44:1519–1534.

[A2] Nurmukan D, Tran M-V, Foo JJ, Scribano G, Chong CT, Huynh TC. Experimental study on laminar lifted flames of pre-vaporized palm oil biodiesel. *Fuel* 2021;288:119697.

[A3] Nurmukan D, Tran M-V, Hung YM, Scribano G, Chong CT. Effect of Multi-walled Carbon Nanotubes on Pre-vaporized Palm Oil Biodiesel/air Premixed Flames. *Accepted in Fuel Communications.*

The published work can be viewed in Appendix A.

Co-Author publications

[B1] Lee CC, Nurmukan D, Scribano G, Chong CT, Tran M-V. Liftoff and Stabilisation of Pre-Vapourised Palm Biodiesel with Nitrogen Dilution in Laminar Coflow Jet. *In Review with Energy*

Table of Contents

1. Introduction	1
1.1. Motivation	1
1.2. Background	2
1.3. Biofuels overview	3
1.4. Objectives.....	5
1.5. Research scope	6
1.6. Thesis organization	7
1.7. References	9
2. Combustion characteristics of biogas/air mixture	11
2.1. Introduction	11
2.2. Measurement of laminar burning velocity	14
2.2.1. Tube method	16
2.2.2. Flat flame (Heat flux) method.....	18
2.2.3. Spherical bomb method	22
2.2.4. Stagnation (Counterflow) method.....	25
2.2.5. Bunsen burner method	29
2.3. Measurement of blowoff velocity	34
2.4. Experiment	35
2.4.1. Measurement uncertainties	38
2.5. Numerical simulation	39
2.6. Results & Discussion	41
2.6.1. Experimental validation	42
2.6.2. Effect of elevated initial temperatures	43
2.6.3. Effect of hydrogen addition	46
2.6.4. Effect of CO ₂ composition in biogas mixture.....	52
2.6.5. Comparison between numerical and experimental flames	56
2.7. Conclusion.....	58
2.8. References	60
3. Combustion characteristics of pre-vaporized palm oil biodiesel/air premixed flames	66
3.1. Introduction	66
3.2. Literature review on nano-additives.....	69
3.2.1. Metal-based nanoparticles	71
3.2.2. Metal-oxide-based nanoparticles	73

3.2.3.	Magnetic nanofluids.....	76
3.2.4.	Organic nanoparticles	77
3.2.5.	Mixed nano-additives.....	78
3.3.	Carbon-based nanoparticles	79
3.4.	Experiment	82
3.5.	Results & Discussion	87
3.5.1.	Experimental validation	87
3.5.2.	Blowoff velocity	89
3.5.3.	Laminar burning velocity	95
3.5.4.	Emissions	100
3.6.	Conclusion.....	103
3.7.	References	104
4.	Combustion characteristics of pre-vaporized palm oil biodiesel diffusion flames	111
4.1.	Introduction	111
4.2.	Literature review on lifted flames	113
4.3.	Experiment	116
4.4.	Results & Discussion	119
4.4.1.	Experimental validation	119
4.4.2.	Stabilization of non-premixed laminar lifted flames	120
4.4.3.	Effect of elevated unburnt gas temperature	124
4.4.4.	Jet flow velocity of lifted flames	128
4.4.5.	Diesel-Biodiesel blends	131
4.5.	Conclusion.....	134
4.6.	References	135
5.	Future Work.....	138
6.	Appendix	140

List of Figures

Chapter 1

Figure 1-1: Biomass Processing Chart (the chart is adapted from [17]).....	4
--	---

Chapter 2

Figure 2-1: (a) The proposed Annular stepwise diverging tube [46], (b) upgraded setup with cavity [47]	18
Figure 2-2: The schematic diagram of flat flame burner configuration, [48]	19
Figure 2-3: (a) Heat flux burner, (b) top view of burner plate showing the perforation pattern, [51].....	20
Figure 2-4: Schematics of spherically propagation premixed flames, [29]	22
Figure 2-5: (a) Jet-wall stagnation burner, (b) premixed flat flame, [65].....	27
Figure 2-6: The schematic diagram of the counterflow burner, [29].....	28
Figure 2-7: Flame angle method of measuring the laminar burning velocity, [70].....	30
Figure 2-8: Various flame fronts based on the imaging technique, [70]	32
Figure 2-9: (a) Flame image captured by shadowgraph technique, (b) grey scaled direct photograph. Shadow boundary thickness changes with the distance between the camera and the flame, (c) 0.4856 mm, (d) 0.6143 mm.	32
Figure 2-10: Measurement of the flame surface area using MATLAB	33
Figure 2-11: Schematic diagram of the experimental setup	37
Figure 2-12: (a) Geometry and (b) computational grid of the coflow burner with its boundary conditions.....	41
Figure 2-13: Comparison of the experimental and numerical data for CH ₄ /air mixture: (a) blowoff velocity, (b) laminar flame speed.	42
Figure 2-14: Effect of elevated unburned gas temperature on the blowoff velocity of stoichiometric biogas/air mixtures at atmospheric pressure conditions.	44
Figure 2-15: Direct photographs of stoichiometric premixed bunsen flame (BG1) with elevated temperatures; (a) all three flames are at the same inlet velocity of 35 cm/s, (b) flames are at their critical velocity just prior to blowoff.	45
Figure 2-16: Effect of hydrogen addition on the blowoff velocities of stoichiometric biogas/air mixtures.....	47
Figure 2-17: Effect of the hydrogen addition on: (a) blowoff velocity and (b) laminar burning velocity of BG1 mixture over the wide range of equivalence ratios.	48

Figure 2-18: Direct photographs of stoichiometric premixed bunsen flames (BG2) with H ₂ additions; (a) all five flames are at the same inlet velocity of 40 cm/s, (b) flames are at their critical velocity just prior to blowoff.	50
Figure 2-19: Laminar burning velocity of biogas/air mixtures (a) with 40% of H ₂ addition and (b) pure biogas/air mixtures, at room temperature and atmospheric pressure.	53
Figure 2-20: Effect of CO ₂ on the laminar burning velocity	54
Figure 2-21: Comparison of stoichiometric biogas/air with three different compositions at room temperature and atmospheric pressure.	56
Figure 2-22: Comparison between numerical and experimental results: (a) CH ₄ /air mixtures at $\phi = 0.8, 1.0$, and 1.2 (from left to right), (b) biogas/air mixtures at the stoichiometric condition ($\phi = 1.0$).	58

Chapter 3

Figure 3-1: Schematic diagram of the experimental setup.	84
Figure 3-2: (a) Schlieren image, (b) direct photograph of PME/air flame at $\phi = 1.1$ and $U_{jet} = 100$ cm/s.	87
Figure 3-3: Laminar burning velocities of n-heptane/air flame at atmospheric pressure and the unburnt gas temperature of 470 K obtained from the present study and literature.	88
Figure 3-4: Direct photographs of PME/air premixed flames without and with MWCNTs (10-20 nm) of 100 ppm addition at lean, rich, and stoichiometric conditions at $U_{jet} = 120$ cm/s. ...	90
Figure 3-5: Direct photographs of very rich PME/air premixed flames without and with MWCNTs (10-20 nm) of 100 ppm addition.	91
Figure 3-6: Comparison of blowoff velocities of PME/air premixed flames without and with MWCNTs (10-20 nm) of 100 ppm addition.	92
Figure 3-7: Direct photographs of PME/air premixed flames, (a) increasing the jet velocity until blowoff at $\phi = 1.0$, (b) presence of tip opening with the increasing of equivalence ratio at $U_{jet} = 90$ cm/s.	94
Figure 3-8: Comparison of laminar burning velocities of PME/air premixed flames without and with MWCNTs (10-20 nm) of 100 ppm addition.	96
Figure 3-9: Enhancement of laminar burning velocities of PME/air premixed flames with MWCNTs addition with the outer diameters of (a) 10-20 nm, (b) 30-50 nm.	99
Figure 3-10: Direct photographs of PME/air premixed flames (a) without MWCNTs and with MWCNTs addition of 175 ppm with the outer diameter of (b) 10-20 nm, (c) 30-50 nm, at $\phi = 1.0$ and $U_{jet} = 120$ cm/s.	100
Figure 3-11: NO _x and CO emissions from PME/air premixed flames at the stoichiometric condition with MWCNTs (10-20 nm) addition.	101

Chapter 4

Figure 4-1: Non-premixed flames, (a) schematic diagram of the flame structure [12], (b) non-premixed flame of palm oil biodiesel fuel at $T=550\text{K}$ and atmospheric pressure.	113
Figure 4-2: Schematic diagram of the experimental setup.	118
Figure 4-3: Comparison of the liftoff heights with literature values for (a) n-heptane, (b) iso-octane.	120
Figure 4-4: Visible images of the laminar diffusion flames of biodiesel.	121
Figure 4-5: Liftoff heights for various (a) jet flow velocities at $T_0 = 500\text{ K}$ and $X_F = 0.02$, (b) unburnt gas temperatures at $U_0 = 0.6\text{ m/s}$ and $X_F = 0.02$	122
Figure 4-6: The domain of existence of the lifted flames.	124
Figure 4-7: Liftoff height as a function of jet flow velocity for various unburnt gas temperatures and fuel mole fractions.....	126
Figure 4-8: Liftoff height as a function of jet flow velocity scaled by the stoichiometric laminar burning velocity for various unburnt gas temperatures and fuel mole fractions.	128
Figure 4-9: Liftoff velocity as a function of the stoichiometric laminar burning velocity for various unburnt gas temperatures and fuel mole fractions.	129
Figure 4-10: Effect of the buoyancy-induced velocity on the liftoff with respect to stoichiometric laminar burning velocity for various unburnt gas temperatures and fuel mole fractions.....	131
Figure 4-11: Visible images of the laminar diffusion flames of various biodiesel/diesel blends. B100 represents pure biodiesel, D100 represents pure diesel, B50/D50 represents 50% biodiesel/50% diesel blend.	132
Figure 4-12: Liftoff height as a function of jet flow velocity for various biodiesel/diesel blends at $T_0 = 550\text{ K}$ and $X_F = 0.02$	133

Appendix

Figure 6-1: GCMS analysis of palm oil biodiesel sample

Figure 6-2: The specification sheet of palm oil biodiesel provided by the manufacturer

Figure 6-3: Schematic diagram of the coflow bunsen burner

List of Tables

Chapter 2

Table 2-1: Biogas compositions used in this present work.....	37
---	----

Chapter 3

Table 3-1: Palm methyl esters (PME) properties.....	85
Table 3-2: Compositions of fatty acids in palm methyl esters (PME).....	86
Table 3-3: Properties of the MWCNTs.....	86

Chapter 4

Table 4-1: Diesel and Palm methyl esters (PME) properties.....	118
Table 4-2: Compositions of fatty acids in palm methyl esters (PME).....	119

Appendix

Table 6-1: Summary of literature findings of the effect of various nano additives on the engine performance and emission characteristics	
Table 6-2: Summary of literature findings of the effect of CNTs on the engine performance and emission characteristics (all based on experimental methods)	
Table 6-3: Specifications of the MWCNTs (10-20 nm)	
Table 6-4: Specifications of the MWCNTs (30-50 nm)	
Table 6-5: The list of main components in the present experimental configuration	

1. Introduction

1.1. Motivation

Understanding the physical process of combustion is historically known to be quite substantial towards the progress of society. Over the past few centuries, since the first industrial revolution, the interest in understanding the combustion process has increased. While there were many attempts to understand the behavior of combustion phenomena via the analytical investigation of isolated experimentations, it is yet to be fully explained due to the complexity of the combustion process [1]. Despite the limited knowledge of the fundamental combustion characteristics, combustion science was still widely adopted in many industrial sectors such as manufacturing, space, military, transport industries, etc. The understanding of combustion and flame phenomena plays a significant role in heating devices, explosives, rocket propulsion systems, and internal combustion engines [2]. The general idea in all the mentioned applications is based on the combustion of various types of fuels, such as gases, solids (wood/coal), and liquid, to generate steam, high-pressure combustion propulsion, and mechanical power. Nevertheless, the increase in applications of combustion processes has raised the demand in the understanding of combustion and flame phenomena. It should be highlighted that the increased interest in combustion brought a number of new challenges to face. In the present days, it became apparent that it is essential to understand the effect of combustion products on the environment as well as human health prior to the diversification of fuels and modification of current engine models.

While the scientific community fully supports sustainability, in many industries, combustion is still considered the primary electricity generation method, as such being the main power source. Therefore, as currently structured, it is impractical and impossible to shift to a fully sustainable energy source. However, it should not imply that the potential danger of emission production and current fuel depletion threats may be ignored. Instead, it means that

the current scientific community should diligently address the situation and produce the most optimal execution plan. The specific experimental investigations, together with the detailed computational analysis, must be carried out in order to understand the combustion behavior per given application. The past progress that has been achieved so far highlights the importance of combustion research. Hence, it is the motivation to deepen the understanding of combustion phenomena, as well as to link the theoretical discoveries with experimental observations and computational analysis.

1.2. Background

It is apparent to state that there is a continuous increase in energy consumption worldwide due to reasons such as the growing world population, elevated comfort levels, and recent developments in technology [3-5]. However, with the current demand for energy consumption, there is also a very high demand for traditional fossil fuels, bringing a number of concerns such as the current state of the environment and the potential risk of fuel depletion. These threads have incited a rapidly growing interest in utilizing renewable and alternative fuels such as biofuels [6,7]. A substantial amount of research is reported on the emission production and performance of internal combustion engines with biofuels of different feedstocks [8,9]. Furthermore, in a gaseous state, biogas fuels are also studied to a great extent under various experimental conditions [10-12]. Despite these findings, it is highly important to emphasize that the vast majority of the studies, related to liquid fuels, are limited to the application of internal combustion engines. In the case of gaseous fuels, there are still existing knowledge gaps where the fundamental combustion characteristics of biogas fuels are underinvestigated. In fact, the knowledge of the fundamental combustion characteristics of the particular fuel is essential in developing its flame modeling.

In the present study, the main interest is to study the behavior of the fundamental combustion characteristics of biofuels. The combustion parameters such as laminar burning velocity, blowoff velocity, flammability limits, liftoff behavior, tip opening, and emission production are experimentally measured using a coflow burner. The database generated from these experiments can be helpful in modeling premixed bunsen flames, non-premixed attached and lifted flames, as well as in various practical applications.

1.3. Biofuels overview

As a result of a rapid rate of global industrialization as well as the exponential expansion of the transport industry over the past few decades, the demand for traditional fossil fuels is peaking [13]. This leads to a conundrum over the potential depletion of non-renewable sources of energy. The extensive reliance of the world on the usage of traditional fossil fuels results in other concerns associated with the combustion products, such as emissions of greenhouse gases, which have negative environmental influence. Hence, the increased interest in developing renewable alternatives is associated with this awareness of the negative impact of fossil fuels on global warming and climate change [14].

Biofuels are considered as one of the most promising renewable fuels, among many other alternatives [15]. The attention of the scientific community is growing on biofuels due to their availability as well as their wide range of feedstock sources. Furthermore, based on the existing literature, it is shown that biofuels result in cleaner combustion compared to the traditional fossil fuels, all the while requiring minimal to no modification of the existing engines [10]. Based on the type of feedstock used, biomass can be converted into all three states of fuels, such as solid, liquid, and gaseous fuels. While the solid biomass can be combined with the existing solid fuels, such as coal, to generate power in power plant

applications, liquid and gaseous fuels can easily be integrated into various combustion applications such as gas turbines, furnaces, and internal combustion engines, etc. [10,16].

Many processes can be employed in order to convert biomass into biofuel. Based on the existing literature, these methodologies can be split into two main categories known as thermochemical conversion and biochemical conversion, as shown in Fig. 1.1 [17-22]. In the case of thermochemical conversion of biomass, the feedstock is thermally decomposed by the processes of heating in a closed and pressurized environment. These methods are also known as gasification and pyrolysis, which differ from each other merely based on the applied temperature and oxygen content used in the conversion process. As a result of these processes, synthetic gas (also known as syngas) can be obtained, which can be used in the practical applications of combustion cycles. On the other hand, some of the extracted hot fuel vapors can be condensed into bio-oil, which in turn, showed some promising results in the application of diesel engines. Unfortunately, due to the nature of having high viscosity, modifications of the existing engines are required to obtain the optimal performance of the engine.

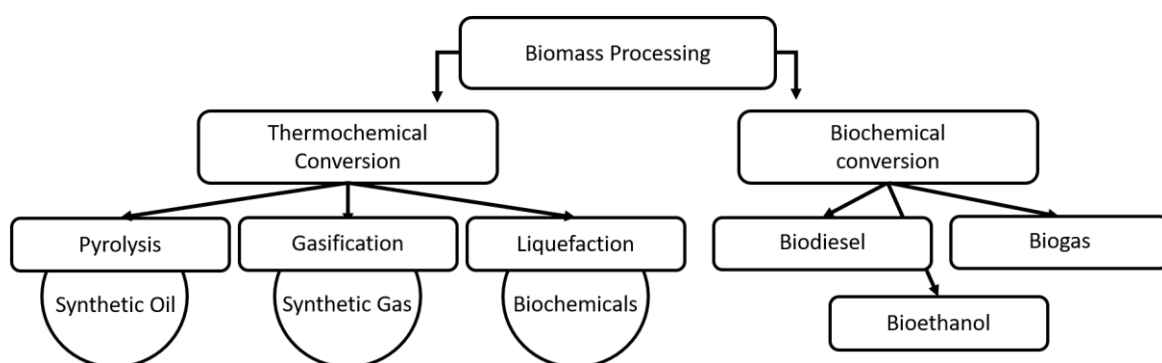


Figure 1-1: Biomass Processing Chart (the chart is adapted from [17])

In the case of biochemical conversion, the methodology is widely known as transesterification [21,22]. It is based on the process of converting the various types of feedstocks into fatty acid methyl esters, also known as FAME, by reacting a glyceride and alcohol together with a catalyst. These methyl esters are generally used in the production of biodiesel fuel. Some of the common feedstocks used in this process are animal fats and vegetable oils, such as sunflower, soybean, and palm oil. It should be noted that the results in the existing literature suggest that biodiesel, produced as a result of transesterification, can be used purely or in blends with commercial diesel fuels in diesel engines.

Despite these promising results reported in the literature, it is unanimously accepted that traditional fossil fuels still possess superior physiochemical properties such as heating value, flame stability, combustion rate, etc. Thus, the interest grows for the studies on the improvement of combustion parameters of biofuels. One of the cost-effective and widely accepted methods of improving fuel combustion characteristics without a significant engine modification is fuel enrichment. In the present study, it is of interest to investigate the impact of hydrogen enrichment on biogas and the effect of nanoparticles on the combustion of biodiesel fuels.

1.4. Objectives

The main objective of the present work is to perform an experimental investigation on the fundamental combustion characteristics of biofuels, both in gaseous as well as liquid form. The results obtained from the experiment are expected to be useful in the modeling of combustion behavior for biogas and palm-oil biodiesel under various experimental conditions. Furthermore, the present research aims to contribute to understanding the combustion of biogas

with hydrogen addition and palm oil biodiesel with multiwalled carbon nanotubes in the mixture. The following pointers are the main objectives of the research:

- (a) To establish an experimental setup and technique capable of measuring the *laminar burning velocity and blowoff velocity* of gaseous (biogas) and liquid (biodiesel) fuels.
- (b) To measure the *laminar burning velocity* of biogas/air with the addition of hydrogen at elevated temperatures of the unburnt mixture.
- (c) To measure the *blowoff velocity* of biogas/air with the addition of hydrogen at elevated temperatures of the unburnt mixture.
- (d) To perform *computational analysis* on how the *composition of carbon dioxide (CO₂) in biogas mixture* affects the combustion parameters of biogas/air flames
- (e) To establish and analyze the *liftoff behavior* of the laminar non-premixed palm oil biodiesel flames
- (f) To measure the *laminar burning velocity* of the premixed palm oil biodiesel/air flames
- (g) To measure the *blowoff velocity* of the premixed palm oil biodiesel/air flames
- (h) To investigate the effect of *Multiwalled Carbon Nanotubes, MWCNTs*, (concentration in the mixture and nanoparticles size) on the combustion parameters of palm oil biodiesel flames

1.5. Research scope

The main interest of the present study is to perform an experimental investigation on the behavior of fundamental combustion characteristics of biofuels, such as biogas and palm oil biodiesel. The findings from this research can be utilized to develop the chemical kinetic mechanisms, laminar premixed bunsen flames modeling, and laminar non-premixed lifted flames modeling for the associated fuels. The present study is split into two major parts with their subsections, respectively. The first part of the research is focused on the combustion

behavior of various biogas/air mixtures with the addition of hydrogen at the elevated temperatures of the unburnt mixture. The kinematic analysis was provided in order to explain the findings from the experiments further. It was followed by the experimental investigation of combustion behavior for palm-oil biodiesel in the second part of the research. In this part, the study of palm oil biodiesel flames was split further into premixed and non-premixed categories. Regarding non-premixed flames, the focus of the study was the lifted phenomena at various fuel concentrations in the mixture and different unburnt mixture temperatures. On the other hand, the experiments on the premixed flames were focused on the effect of multiwalled carbon nanotubes on the laminar burning velocity and blowoff velocity of palm oil biodiesel flames.

1.6. Thesis organization

There are five chapters in the present thesis. It is started with Chapter 1, where an explanation of the motivation behind this research and the general overview on biofuels is presented. Furthermore, Chapter 1 highlights the main objectives and determines the research scope of the present study.

Chapter 2 provides an in-depth literature review on the measurement of laminar burning velocity based on various experimental configurations, measurement of blowoff velocity and primarily focuses on the combustion behavior of biogas/air mixtures. These combustion parameters were obtained over the wide range of equivalence ratios, 0.8-1.2. The experimental investigation of the laminar premixed biogas/air flames aims to describe the changes in laminar burning velocity and blowoff velocity due to the change in biogas composition between methane and carbon dioxide (CO_2), the addition of hydrogen into the mixture as well as the change in unburnt temperature of the mixture. It is followed by the numerical examination of biogas/air flames using CHEMKIN PREMIX Code, with a modified GRI Mech 3.0 kinematic

mechanism. It should be noted that some of the findings from Chapter 2 were utilized to prepare the first manuscript (A1) for publication purposes.

Chapter 3 focuses on the combustion behavior of the laminar premixed flames of pre-vaporized palm oil biodiesel fuel. Furthermore, the effect of multiwalled carbon nanotubes on the fundamental combustion characteristics is experimentally studied. The chapter includes an in-depth literature review on the various types of nano additives. It is followed by the measurement of laminar burning velocity and blowoff velocity of palm oil biodiesel with and without the addition of carbon-based nanotubes. The chapter also provides detailed discussions on the correlations between the changing parameters, changes in the flame structure, and the overall change in combustion characteristics. It should be noted that some of the findings from Chapter 3 were utilized to prepare the second manuscript (A3) for publication purposes.

Chapter 4 introduces non-premix flames in the study and shows the findings from the existing literature related to lifted flames. This chapter provides results and discussion related to the liftoff effect of laminar non-premixed flames of palm oil biodiesel fuel. The lifted flames are experimentally obtained at different fuel concentrations as well as at various temperatures of the unburnt mixture. The results in Chapter 4 suggest that there are correlations between the liftoff height of the flame and the associated jet velocity at a given temperature of the unburnt mixture when the jet velocity is normalized with regards to the stoichiometric laminar burning velocity. Furthermore, it should be noted that some of the findings from Chapter 4 were utilized to prepare the second manuscript (A2) for publication purposes.

At last, the overall summary of the present study, major conclusions based on the findings, and suggestions for future work are presented in Chapter 5. It is followed by the Appendix section, where the reader can find all the published work and proposed manuscripts, some of the additional tables, figures, and files related to the present study.

1.7. References

- [1] Raghavan V. Combustion Technology: Essentials of Flames and Burners. Chichester: John Wiley & Sons Ltd., 2016.
- [2] Lackner M, Palotas AB, Winter F. Combustion: From Basics to Applications. 1st ed. Weinheim: Wiley-VCH, 2013.
- [3] Nejat P, Jomehzadeh F, Taheri MM, Gohari M, Majid MZA. A global review of energy consumption, CO₂ emissions and policy in the residential sector (with an overview of the top ten CO₂ emitting countries). *Renew Sust Energy Rev* 2015;43:843-862.
- [4] Ahmad T, Zhang D. A critical review of comparative global historical energy consumption and future demand: The story told so far. *Energy Rep* 2020;6:1973-1991.
- [5] Dong K, Dong X, Jiang Q. How renewable energy consumption lower global CO₂ emissions? Evidence from countries with different income levels. *World Econ* 2020;43:1665-1698.
- [6] Jiang Y, Xin F, Lu J, Dong W, Zhang W, Zhang M, Wu H, Ma J, Jiang M. State of the art review of biofuels production from lignocellulose by thermophilic bacteria. *Bioresour Technol* 2017;245:1498-1506.
- [7] Vinod BM, Madhu MK, Amba PRG. Butanol and pentanol: The promising biofuels for CI engines – A review. *Renew Sust Energy Rev* 2017;78:1068-1088.
- [8] Oh YK, Hwang KR, Kim C, Kim JR, Lee JS. Recent developments and key barriers to advanced biofuels: A short review. *Bioresour Technol* 2018;257:320-333.
- [9] Leong WH, Lim JW, Lam MK, Uemura Y, Ho YC. Third generation biofuels: A nutritional perspective in enhancing microbial lipid production. *Renew Sust Energy Rev* 2018;91:950-961.
- [10] Pizutti L, Martins CA, Lacava PT. Laminar burning velocity and flammability limits in biogas: A literature review. *Renew Sust Energy Rev* 2016;62:856-865
- [11] Zhen HS, Leung CW, Cheung CS, Huang ZH. Combustion characteristic and heating performance of stoichiometric biogas–hydrogen–air flame. *Int J Heat Mass Transf* 2016;92:807-814.
- [12] Qian Y, Sun S, Ju D, Shan X, Lu X. Review of the state-of-the-art of biogas combustion mechanisms and applications in internal combustion engines. *Renew Sust Energy Rev* 2017;69:50-58.
- [13] Sultana WR, Sahoo SK, Sukchai S, Yamuna S, Venkatesh D. A review on state of art development of model predictive control for renewable energy applications. *Renew Sust Energy Rev* 2017;76:391-406.
- [14] Bharathiraja B, Sudharsanaa T, Bharghavi A, Jayamuthunagai J, Praveenkumar R. Biohydrogen and Biogas – An overview on feedstocks and enhancement process. *Fuel* 2016;185:810-828.

- [15] Skolrud TD, Galinato GI, Galinato SP, Shumway CR, Yoder JK. The role of federal Renewable Fuel Standards and market structure on the growth of the cellulosic biofuel sector. *Energy Econ* 2016;58:141-151.
- [16] Jiaqiang E, Pham M, Zhao D, Deng Y, Le DH, Zuo W, Zhu H, Liu T, Peng Q, Zhang Z. Effect of different technologies on combustion and emissions of the diesel engine fueled with biodiesel: A review. *Renew Sust Energy Rev* 2017;80:620-647.
- [17] Demirbas A. Progress and recent trends in biofuels. *Prog Energy Combust Sci* 2007;33:1-18.
- [18] Kasmuri NH, Kamarudin SK, Abdullah SRS, Hasan HA, A.Md. Som. Process system engineering aspect of bio-alcohol fuel production from biomass via pyrolysis: An overview. *Renew Sust Energy Rev* 2017;79:914-923.
- [19] Bridgwater AV. Renewable fuels and chemicals by thermal processing of biomass. *Chem Eng J* 2003;91:87-102.
- [20] McKendry P. Energy production from biomass (part 1): overview of biomass. *Bioresour Technol* 2002;83:37-46.
- [21] Chen H, Wang L. *Technologies for Biochemical Conversion of Biomass*. London: Elsevier Inc., pp. 137-164, 2017.
- [22] Manochio C, Andrade BR, Rodriguez RP, Moraes BS. Ethanol from biomass: A comparative overview. *Renew Sust Energy Rev* 2017;80:747-755.

2. Combustion characteristics of biogas/air mixture

It must be highlighted that some parts of Chapter 2 were used to prepare the manuscript [A1] on the combustion behavior of biogas/air flames. The work has successfully been published in the International Journal of Energy Research.

2.1. Introduction

With the continuous decline of the environmental conditions as well as the increasing demand in energy supply, the interest in the development of renewable clean fuels has peaked over the last decade. Due to its strong accessibility, the abundance of its sources, and environmentally friendly combustion, biogas has drawn lots of attention in the field of combustion research [1]. Although biogas brings these benefits, it has particular challenges restricting its use in the application of engines [2]. One of the significant problems of biogas is the high content of carbon dioxide (CO_2) in the mixture, which also varies in composition with the primary hydrocarbon, methane (CH_4), based on the change of the temperature, pressure, and the production method. This situation leads to the lower heating value, slower combustion speed, and the poor stability of a flame compared to natural gas [3].

To enhance the combustion characteristics of biogas, the addition of another fuel, having a high calorific value into the flowing stream of biogas, can be an effective solution. The past research [1,3–12] showed that hydrogen (H_2) could be used as an additive to improve fuel combustion characteristics. Besides, from elevating the reactivity of the fuel blend, hydrogen is known as an environmentally friendly fuel as well, based on the production method. Mustafa et al. [4] showed that the increasing hydrogen content results in a considerable decrease in the production of carbon monoxide, CO, emission. Results from this experimental

study are in good agreement with the trends obtained via the numerical investigations performed by Jeong et al. [5] and Esmail et al. [6]. While Hu and Zhang [7] investigated the effect of hydrogen on the combustion characteristics of the low calorific value fuels using the constant volume combustion bomb, Yang and Wu [11] studied the influence of hydrogen on the properties of propane/air flames, using the burner with granular ceramic beds. They found that the addition of hydrogen in the fuel mixture led to a noticeable improvement in the flame propagation rate, regardless of the applied techniques and base fuel. Sun et al. [12] used the constant-pressure spherical flame technique in order to calculate the laminar flame speeds of CO/H₂/air and CO/H₂/O₂/helium mixtures. The results showed that both mixtures experienced significant flame speed improvements with the increase of H₂ content in the mixture. Hu and Zhang [1] discussed the effect of the CO₂/H₂ ratio on the development of the flame cells. It was shown that with the rising hydrogen ratio, the cellular instability of the flame increased, resulting in faster flame propagation. Wei et al. [3] investigated the effect of different compositions of CO₂ and H₂ on the heat transfer characteristics of biogas/hydrogen flames. It was shown that the increase in H₂ content resulted in the enhancement of the total heat transfer rate up to 50%, which varied depending on the CO₂ contents. Based on these studies, it is expected that the addition of hydrogen into biogas leads to positive effects in terms of improved laminar burning velocity, heat transfer rate, and flame temperature. This statement is further supported by numerous researches, which can be referred to for the detailed analyses [2,8,10–14]. On the contrary, there is a research gap regarding the effect of hydrogen addition on the blowoff velocity of premixed biogas/air mixtures. In the case of a premixed laminar flame, the blowoff velocity is one of the primary critical limits to ensure static stability. Furthermore, in some applications of low emission gas turbines, knowing blowout velocities is crucial to prevent any severe problems in the case of the re-ignition system failure [15]. As such, it can be understood that the study of the hydrogen effect on the blowoff velocity is required.

Most of the studies mentioned above for biogas have conducted their investigations at room temperature conditions. The effect of the initial temperature on the combustion of various fuels such as syngas and natural gas has been found in a few studies [16–18]. Natarajan et al. [16] conducted experiments in a bunsen burner and found that the laminar burning velocity of syngas was improved with the higher pre-heated temperature of the unburned gas. Robin et al. [17] and Ai et al. [18] employed the burner with the diverging channel and the spherical bomb configuration, respectively. All three reports showed that the temperature of the adiabatic flame was increased by heating the mixture of unburned gases, which consequently led to the improved laminar flame speed. Other research groups [19–21] conducted experiments with different fuels, such as oxy-methane, methylcyclohexane, and methanol. They reported the same trends and supported the idea of increasing the temperature of the mixture enhanced combustion performance.

Besides the experimental studies mentioned earlier, there have been numerical studies determining the combustion characteristics of biogas fuels with various chemical mechanisms [19,20]. Quintino et al. [22] and Xiang et al. [23] assessed the effect of CO₂ on the combustion characteristics of CH₄/air flames using CANTERA with USC-Mech chemical-kinetic mechanism and PREMIX code with the GRI-Mech 3.0 chemical reaction mechanism, respectively. Furthermore, researchers [24–26] performed numerical simulations of laminar premixed bunsen flames with different base fuels and chemical mechanisms. While these studies have been performed in-depth, and, additionally, there is available literature on the usage of the GRI-Mech 3.0 chemical mechanism in order to study the combustion characteristics of biogas/air flames [27], the results were obtained based on the full mechanisms imposing a heavy computational burden. Thus, the applicability of the reduced chemical mechanisms for modeling of the premixed bunsen flames becomes of importance.

Thus, this work aims to experimentally investigate the enhancement of blowoff and laminar burning velocities with the addition of hydrogen at elevated initial temperatures of the unburned gases for different biogas compositions. Moreover, it is of interest to fill the knowledge gap on the application of the reduced GRI-Mech 3.0 chemical mechanism to simulate the biogas flames using ANSYS Fluent software. It is then followed by the chemical kinetic analysis of the premixed biogas/air flames using the PREMIX code. At last, the computationally obtained conical flames will be in direct comparison with the experimental bunsen flames to justify the use of the kinetic mechanism.

2.2. Measurement of laminar burning velocity

The understanding of the combustion behavior of different fuels is essential in the development process of fuel economy. Over the past few decades, various combustion techniques such as flame cooling, lean-fuel premixed combustion, recirculation of exhaust gas, and combustion at elevated initial temperatures were developed to achieve cleaner and more efficient combustion [28]. However, the implementation of these techniques is not necessarily straightforward in practical applications due to the lack of knowledge on the combustion behavior of various fuels. One of the most crucial fundamental combustion characteristics of fuel, for understanding the combustion behavior, is the laminar burning velocity of premixed fuel and oxidizer mixture [29].

By definition, the laminar burning velocity is the combustion parameter of premixed fuel and oxidizer mixture that shows the speed of propagation for planar combustion wave relative to the unburnt mixture ahead, at given pressure and temperature of the mixture [30]. As the physicochemical property of the mixture, the laminar burning velocity can measure the overall reactivity of the fuel. Hence, in general, the higher laminar burning velocity of the fuel

can indicate the faster combustion rate in an engine compared to the fuel with a lower laminar burning velocity [29]. Some of the essential flame behavior, such as the liftoff effect, flame stabilization, blowoff/blowout, and flashback effect, can be described based on the laminar burning velocity of the given flame [30]. Furthermore, the database of the laminar burning velocity of various fuel mixtures at different experimental conditions can be very useful in the development processes of chemical kinetic mechanisms. As long as the transport and thermodynamic parameters are adequately established, these mechanisms can then be used to model some practical applications such as industrial furnaces, internal combustion engines, and gas turbines [29,31].

The increasing interest in combustion research led to the development of various techniques for measuring the laminar burning velocity of fuel/air mixtures. Some of the common methodologies are known as the tube method [32,33], flat flame method [34,35], spherical bomb method [35,36], stagnation or counter-flow method [36,37], and bunsen burner method [38]. There are several research groups that have performed an in-depth and critical review on the previously mentioned methodologies. The research group led by Egolfopoulos [39] performed a thorough review of the spherical bomb and counterflow methods in measuring the laminar burning velocity of different fuel/air mixtures.

While the main objective of all the above mentioned methods is to accurately measure the laminar burning velocity of a given fuel/air mixture, it is essential to understand that each method brings sets of its own advantages and disadvantages. Besides the spherical bomb and counterflow configurations, another widely known configuration in studying the flame behavior is the tube method. One of the most significant benefits of using the tube method is the ability to study the effect of flame stretch and curvature [40]. Based on the findings from the current literature, it is clear to conclude that the studies with the tube method were beneficial in establishing the correlations of stretched flames between planar and curved flames.

Flat flame and jet wall stagnation are other widely used configurations used in determining the laminar burning velocity of a given fuel mixture. While the earlier setup of the flat flame method could only accommodate the mixtures at low burning velocities such as 15 cm/s or less, the recent design modifications extended the upper limit [41]. As the name suggests, the setup consists of a burner and stagnation plate placed at a distance from the nozzle rim in the jet wall stagnation method. While the current literature results show that the presence of a wall does not influence the measurement of the laminar burning velocity, it was reported that the flammability limits of the given fuel mixture are sensitive to the distance between the nozzle rim and stagnation plate [29].

Lastly, one of the earliest methodologies of measuring laminar burning velocity and understanding the various flame behavior is the bunsen burner method. Due to the conical structure of a flame, the flame experiences a negative stretch at the tip. The literature findings suggest that the presence of negative stretch leads to tip opening of the laminar premixed bunsen flames [42]. Furthermore, the presence of strain and curvature influences the measurement of laminar burning velocity using the bunsen burner method. However, using the weighted average of the area over the entire flame surface method can produce an adequate accuracy of measured laminar burning velocities [43].

The following subchapters intend to provide some of the latest updates and a brief literature review of the previously mentioned methodologies for the laminar burning velocity measurements.

2.2.1. Tube method

In this method, the experimental setup can be considered reasonably simple as it consists of a long cylindrical tube with one end being open and the other end closed. The tube

is filled with the combustible mixture, and the flames generated in this configuration can be hemispherical or ellipsoidal. The flame speed is defined as the rate of flame propagation in the tube and can be calculated as shown in the following expression:

$$S_L = \frac{u_m \pi R^2}{A_f} \quad (1)$$

where S_L is the laminar burning velocity, u_m is the flame velocity in the tube, R is the inner radius of the tube and A_f is the area of a flame, which is usually approximated as the cross-section area of the tube [40].

While this method appears to be very simple in its setup, there are some inherent flaws in this methodology. One of the primary sources of errors in this method is heat loss due to the cooling effect from the tube walls. Furthermore, the presence of the buoyancy effect can result in the non-uniformity in the flame structure, which influences the calculation of laminar burning velocity. As the flame propagates through the vertical tube, it is subjected to the experience of quenching effect, which in return can affect the measured flame velocity [29, 40].

Over the last few decades, one of the recently modified methods of measuring the laminar burning velocity was developed, known as the Annual Stepwise Diverging Tube method (ASDT). Unlike in the simple tube method, the principle of ASDT is to establish the stationary flat flames within the tube. The location of the stabilized flame and flow rate of the mixture is then used to measure the laminar burning velocity of the mixture. The research group led by Kim [44,45] performed multiple experimental investigations, which showed that the flame propagation velocity could represent the laminar burning velocity as long as the flames are remained flat with no significant distortion. Therefore, Liu et al. [46] implemented stepwise core in Annular Diverging Tube in order to achieve more stable and flatter flames, as shown in Fig. 2.1(a). The results showed that the finer steps in the tube structure led to more accurate

results of laminar burning velocity. Furthermore, Liu et al. [47] suggested separate fabrication of step-units to control the number of step-units used in the setup and create the cavity between each unit-step to minimize the heat transfer along the core of the tube, as shown in Fig. 2.1(b). While these modifications make the current methodology more accurate than its previous configurations, more studies are required to show that this method can be applied over a wide range of fuel mixtures.

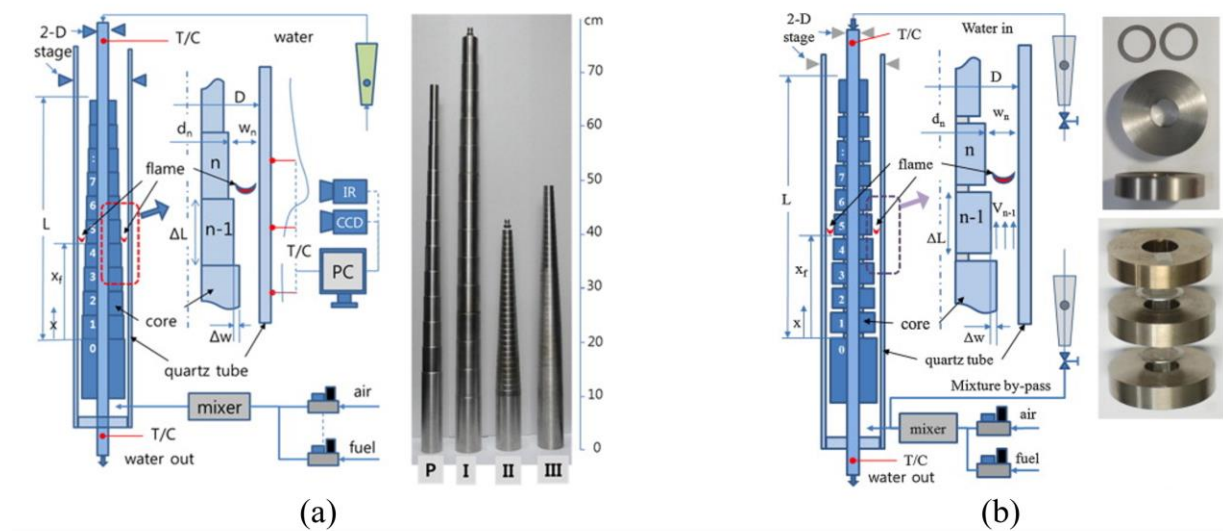


Figure 2-1: (a) The proposed Annular stepwise diverging tube [46], (b) upgraded setup with cavity [47]

2.2.2. Flat flame (Heat flux) method

In this method, a gas mixture travels through the series of honeycomb filters and porous metal plates and is ignited at the burner exit, as shown in Fig. 2-2. As a result of the heat loss that takes place at the burner exit, the ignited mixture formulates the flat flame. The mixture is initially ignited at a very high flow rate and then decreased till the flat flame is achieved. The

flame velocity is then calculated as the diameter of the stabilized flat flame divided by the flow rate of the unburnt mixture [48]. As the flow rate of the unburnt mixture influences the overall heat loss at the burner exit, one of the biggest disadvantages of this method is that the application of this method is restricted to mixtures with low burning velocities. Some research groups attempted to improve the flat flame burner method to measure the fuels with higher flame velocities by cooling the porous metal sheets [49] or by measuring the temperature profile of the metal sheets [50]. While the results were positive, the loss of active radical to the metal sheets during the heating and combustion makes it difficult to accurately measure the laminar burning velocity of various fuels.

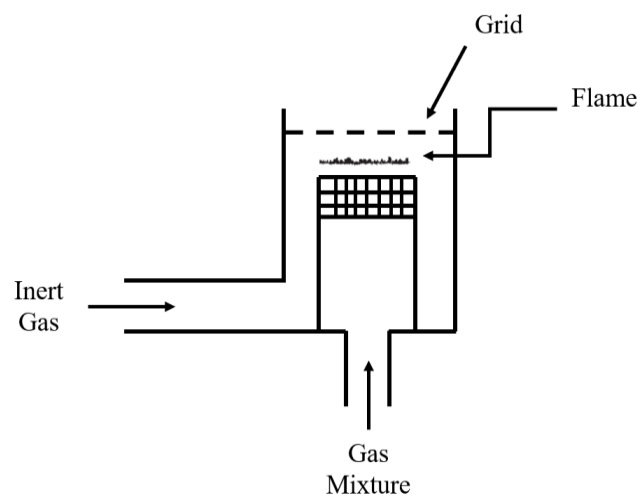


Figure 2-2: The schematic diagram of flat flame burner configuration, [48]

With the inclusion of significant modifications to the flat flame burner, the heat flux method is used to establish stable adiabatic flat flames [35,51]. Figure 2-3 illustrates the schematic diagram of the heat flux burner, adapted from [51]. External heating of the burner plate results in the elevated temperature of the unburnt gas mixture, which in return,

compensates for the heat loss from the flame at the burner exit. The external heating is achieved by the circulation of hot water at the burner head [51]. It was shown both experimentally and numerally that the heat flux method can establish the flat flames to measure the adiabatic laminar burning velocity of various fuels [35,51,52].

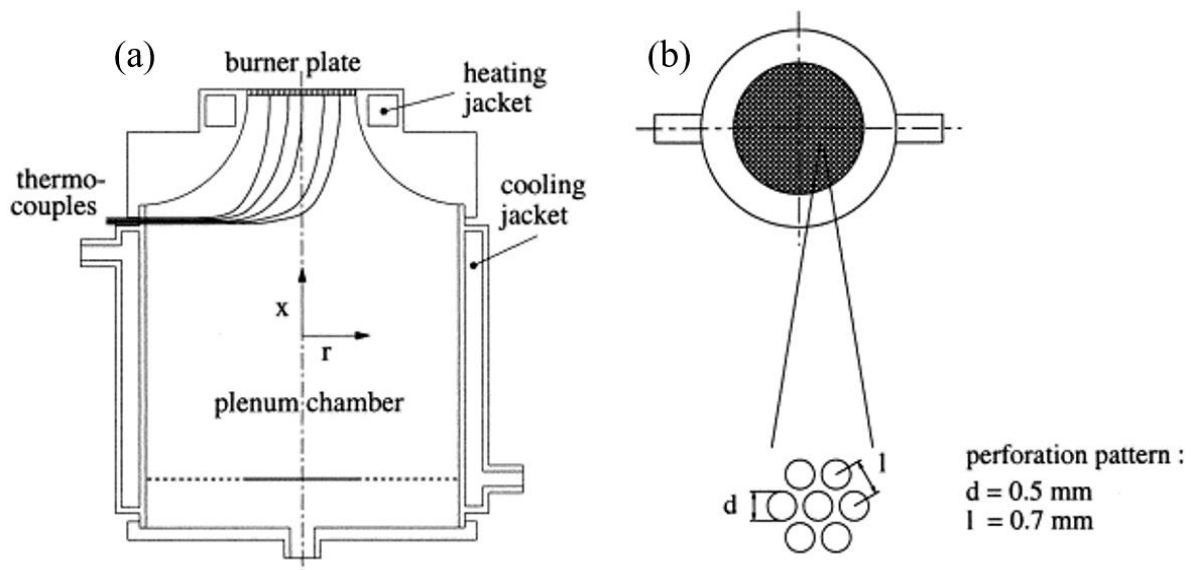


Figure 2-3: (a) Heat flux burner, (b) top view of burner plate showing the perforation pattern,

[51]

The flat flame method was initially used mainly with gaseous fuels. However, with the development of the heat flux method, the usage of the flat flame configuration was extended to various liquid fuels to measure the laminar burning velocity. One of the earliest applications of the heat flux method was measuring the laminar burning velocity of premixed ethanol + air mixtures at various unburnt mixture temperatures [53]. Rau et al. [54] conducted an experimental investigation on the combustion behavior of isooctane+ethanol+air mixtures using the heat flux method. The results showed that the measured laminar burning velocity data

was in good agreement with the existing literature results. However, Knorsch et al. [55] introduced further modifications to the existing setup of the heat flux burner to improve the accuracy of the measured adiabatic burning velocities of various liquid fuels. In general, the heat flux method results [54-56] were in good agreement with the existing data. Hence, the usage of the heat flux method can produce adequate results on the measurement of laminar burning velocity both for gaseous and liquid fuel mixtures.

Despite the positive findings from the literature regarding the heat flux method, Alekseev et al. [56] presented a number of factors in the experiment that can potentially affect the uncertainties in the results. After the extensive analysis of the experimental setup, it was shown that accuracy of mass flow controllers, quality of mixing, ambient pressure around the burner, radiation, and asymmetric heating at the burner head could be considered as some of the primary sources of uncertainties. Upon further investigation, some of the significant difficulties in the execution of the experiment were found and stated below.

1. The heat flux method is restricted to the fuels with the laminar burning velocity below 80 cm/s. While this issue can be addressed by reducing the nozzle size, this will, in return, increase the difficulty and inaccuracy of the manufacturing of the burner.
2. The experimental conditions such as elevated temperatures of the unburnt mixture result in the loss of radicals to the metal plate as the quenching increases. Hence, the experiment is restricted to low temperature conditions.
3. The stabilization of the flat flames becomes more difficult with the increasing ambient pressure of the experiment.

While these difficulties may limit the range of applications, by taking the required conditions into account, the heat flux method can still provide very accurate results for laminar

burning velocity and provide meaningful information to understand the combustion behavior of various fuel mixtures.

2.2.3. Spherical bomb method

In this method, the constant volume chamber contains the premixed fuel/air mixtures at specified experimental conditions such as equivalence ratio, pressure, and temperature of the unburnt mixture. It is followed by the ignition of this premixed mixture by a spark at the center of the constant volume, where the quiescent combustible mixture formulates a spherical flame and propagates outwardly. Figure 2-4 illustrates the behavior of outwardly propagating spherical flames where r represents the radius of the chamber, $r_f(t)$ is the flame radius at a given instant, and S_b is the laminar burning velocity per the given coordinates of the experimental setup [29].

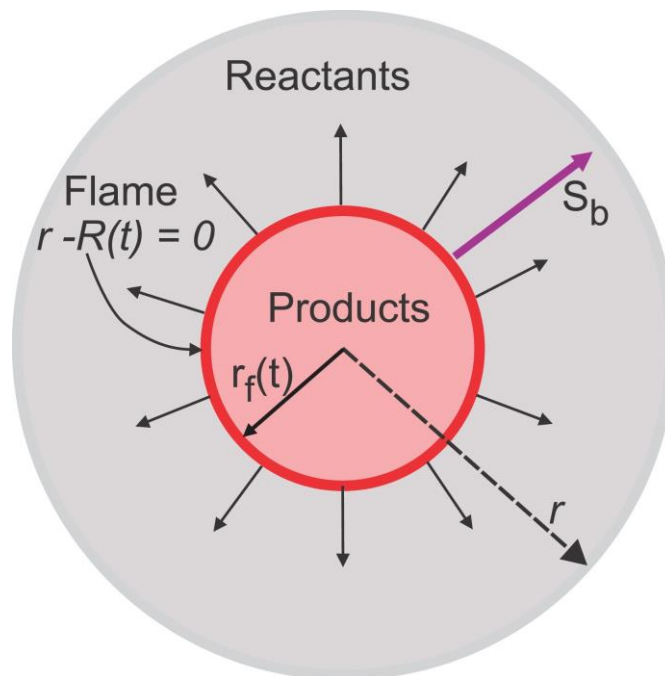


Figure 2-4: Schematics of spherically propagation premixed flames, [29]

Furthermore, generally, the spherical flame propagation results in the adiabatic compression of the unburnt mixture, resulting in the continuous change in pressure. Based on the radius of the flame and its pressure at the given instant, the laminar burning velocity of the mixture can be calculated using the following equation:

$$S_L = \left(1 - \frac{R^3 - r^3}{3p\gamma_u r^2} \frac{dp}{dr}\right) \frac{dr}{dt} \quad (2)$$

where S_L is the laminar burning velocity, R is the radius of the sphere, r is the radius of the flame at the given instant, p is the pressure at the given instant, and γ_u is the specific heat ratio of the unburnt mixture [57]. While the flame spherically propagates outwards, the presence of flame curvature and the unsteady propagation of the flame front, diffusional effects, and the heterogeneous state of the flow field results in the flame stretch effect. The existence of flame stretch impacts the flame propagation speed, and as a result, the laminar burning velocity of the fuel mixture. Therefore, it is essential to distinguish the measured values between the stretched and unstretched flame speed.

The unstretched laminar burning velocity can be derived by the method of extrapolation using the images of continuous propagation of spherical flames. Firstly, the stretched laminar burning velocity, S_n , can be obtained via the well-known flame expansion method [58], which uses the data of continuously increasing flame radius and its associated time, as shown below.

$$S_n = \frac{dr_u}{dt} \quad (3)$$

where r_u is the radius of the instantaneous flame measured from the flames images (obtained via imaging techniques such as schlieren imaging), t is the time of the flame propagation. Based on Equation 3, the flame stretch rate, α , is then defined as follows.

$$\alpha = \frac{1}{A} \frac{dA}{dt} = \frac{2}{r_u} \frac{dr_u}{dt} = \frac{2}{r_u} S_n \quad (4)$$

where A is the area of the flame front. Thus, based on the relationship between S_n and α , the Markstein length, L_b , associated with the unstretched laminar burning velocity, S_L , can be expressed as follows.

$$S_L - S_n = L_b \alpha \quad (5)$$

Hence, the value of the unstretched laminar burning velocity can be obtained at the condition of $\alpha = 0$ [29,58]. While there are some limitations associated with this method, such as the presence of buoyancy effect, heat loss due to the presence of spark plug, and cellular instabilities, this method is still one of the few configurations that produced adequate results in good agreement with the existing literature data. Furthermore, these uncertainties are also present in other experimental configurations, but the higher pressure conditions can be studied in the spherical bomb method.

It is also important to highlight that there are two main variations of the spherical flame method to measure the laminar burning velocity of various fuel mixtures, known as constant pressure [59,60] and constant volume [60-62] methods. In the constant pressure spherical flame method, the combustion chamber is large enough to mitigate the significance of the pressure rise during the flame propagation. Furthermore, the imaging techniques such as Schlieren or Shadowgraph imaging are used to visualize the flame front propagation within the chamber. These imaging methods can reveal the cellular instabilities within the flame structure during the outward propagation. In addition, in the constant pressure method, the change in pressure and temperature can be neglected, so there is a stage in the propagation where the flame speed can be expressed as the function of the stretch effect, as shown in Equation 5. The extrapolation methods can be followed, where linear, non-linear, linear based on curvature, non-linear with three fitting parameters models can be used to calculate the value of unstretched laminar burning velocity. The detailed review of these extrapolation models can be viewed in the work

of Konnov et al. [29]. In the constant volume method, the thick-walled spherical chamber is employed, where the fast-response pressure transducer is used to register the instantaneous value of the pressure during the propagation of the flame front [61]. In this method, the laminar burning velocity of various fuel/air mixtures can be obtained at elevated temperatures and high pressure conditions.

It is clear that the spherical flame method is one of the most accurate and versatile methods in obtaining the laminar burning velocity. However, this method has its own sets of limitations, such as the size of the chamber should be large enough with the aspect ratio of unity to produce accurate results. Two chambers are required if the goal is to match some of the operating conditions of the engine applications. Furthermore, the synthesized oxidizer with the helium content is needed to offset the flame front instabilities at higher pressures. Overcoming these and some other limitations of the spherical flame method leads to the need for the complex design of the combustion chamber.

2.2.4. Stagnation (Counterflow) method

Simmons and Wolfard [63] proposed the use of stagnation flame configuration to conduct extensive experimental studies to investigate the flame structure, flame stability, and flammability behavior of premixed and non-premixed flames of various fuel mixtures. For example, Law et al. [64] used the stagnation flame method to experimentally measure the flammability limits of propane/air mixtures at fuel-lean conditions. Konnov et al. [29] produced a comprehensive review on the measurement methods of laminar burning velocities of different fuel/air mixtures. In their work, it was explained that the stagnation flame method results in stabilization of one dimensional (1-D) steady flame at the stagnation flow field. This stagnation

flow field can be achieved either in jet-wall stagnation configuration or counterflow flame configuration.

In the jet-wall stagnation method, the experimental setup consists of a single burner and an impinging plate placed at a distance from the burner outlet, which is illustrated in Fig. 2-5(a). After the ignition of the fuel mixture, a one dimensional steady flat flame is stabilized upon the impingement of the premixed flame/air mixture with the wall, as shown in Fig. 2-5(b). This process is associated with the hydrodynamic strain [29,64,65]. As the unburnt mixture approaches the flame front, the flow velocity of the unburnt mixture continuously decreases. In contrast, the flow velocity of the unburnt mixture raises upon entering the reaction zone and passing through the flame due to the gas expansion phenomena. This is followed by the gradual deceleration of the mixture velocity near the stagnation wall. At the location where the unburnt mixture is just about to enter the reaction zone and experience the flow velocity acceleration, the reference flame speed can be measured. In addition to that, the velocity gradient at the upstream region of the flame can be used to quantify the strain rate of the flame front. As a result, the reference flame speed and the strain rate of the flame can be used to obtain the unstrained laminar burning velocity of the fuel mixture via the extrapolation method.

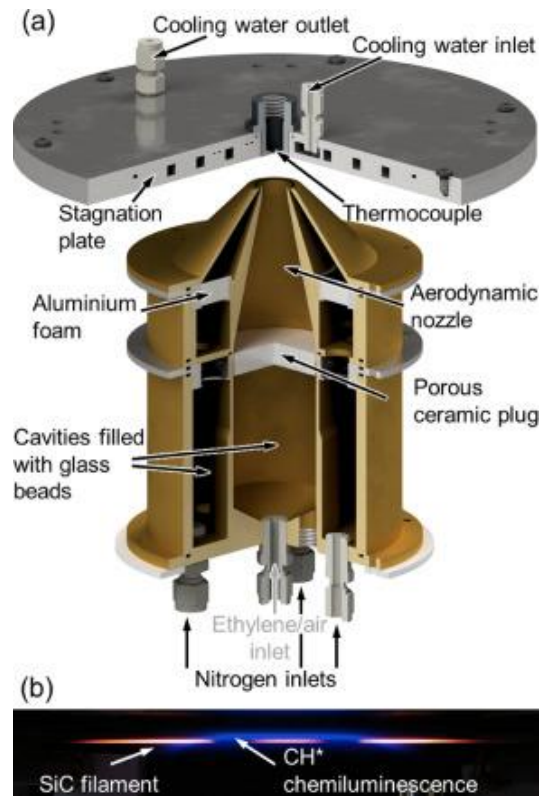


Figure 2-5: (a) Jet-wall stagnation burner, (b) premixed flat flame, [65]

In counterflow flame configuration, the setup consists of two identical burners placed in opposite directions. Figure 2-6 shows that two identical premixed one dimensional steady flat flames are formed as a result of the impingement of two identical flow fuel/air mixtures [29]. In this configuration, one of the main advantages is that there is no heat loss in the downstream area of the flame as the two flames are identical to each other. It was reported that the only component that can contribute to the overall heat loss is radiative heat which is often assumed to be negligible [39]. Hence, as a result of hydrodynamic strain, the flame stretch is the only external factor that influences the stabilization of the flat flames [40,66]. In the case of ideal counterflow flame configuration, the flame stretch effect can be associated with the velocity gradient of the mixture flow in the axial direction.

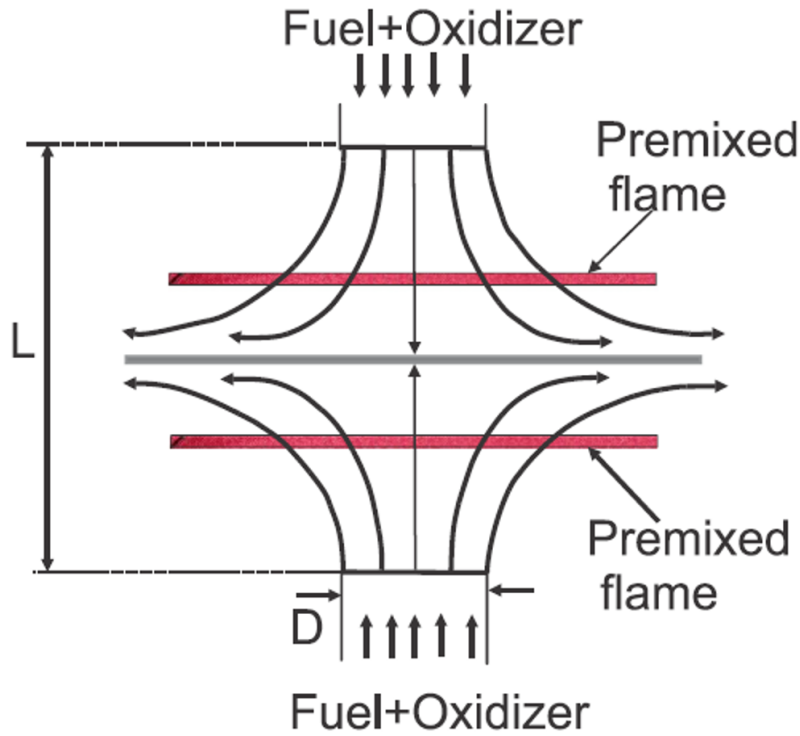


Figure 2-6: The schematic diagram of the counterflow burner, [29]

The straight tubes in the stagnation flow configurations were used to numerically investigate the effects of the flow field on the laminar burning velocity of various fuel/air flames [67,68]. The results showed that there are some discrepancies between the results of 1D and 2D flames. This behavior was associated with the momentum equation in the 1D model, where the pressure derivative is assumed to be constant [29]. Furthermore, the nozzle shape and its diameter on the flat flame in counterflow configuration are analyzed and computationally tested using the 1D model [69]. The results revealed that the 1D model could produce reliable data, and the significance of radial direction becomes smaller as the nozzle diameter increases.

While the measurement of laminar burning velocity was done by several groups [29,64-66], the vast majority of the literature is focused on gaseous fuel/air mixtures. There are some difficulties that come with the use of liquid fuels in the counterflow flame configuration. One of the most prominent challenges is the accurate measurement of the flow rate, as most of the

mass flow controllers are designed for gaseous flows and not for liquid or vapor. Another difficulty is preparing the homogeneous liquid fuel/air mixture, where the equivalence ratio is significant in the experiment. These and many other issues can result in higher uncertainties in measuring the laminar burning velocity of liquid fuel/air mixtures [29].

2.2.5. Bunsen burner method

In the present study, the fundamental combustion characteristics of biogas/air flames are studied using the coflow bunsen burner. Konnov et al. [29] reported a comprehensive review of measurements and data analysis of laminar burning velocities for various fuel/air mixtures in a wide range of various experimental configurations such as spherical bomb, counterflow, jet-wall stagnation, flat flame as well as bunsen burner. It is worth noting that each of these experimental methods has its advantages and drawbacks. In the case of the bunsen burner method, there are two well-known approaches in calculating the laminar burning velocity, namely the flame angle [70] and the flame area methods [43,71]. In the flame angle method, the laminar burning velocity, S_L , is determined based on the nozzle exit velocity, v_0 , and the cone apex angle, θ , as shown in Fig. 2-7 [70]. Furthermore, it is worth noting that the accuracy of this method significantly depends on the uniformity of the gas velocity along the radial direction.

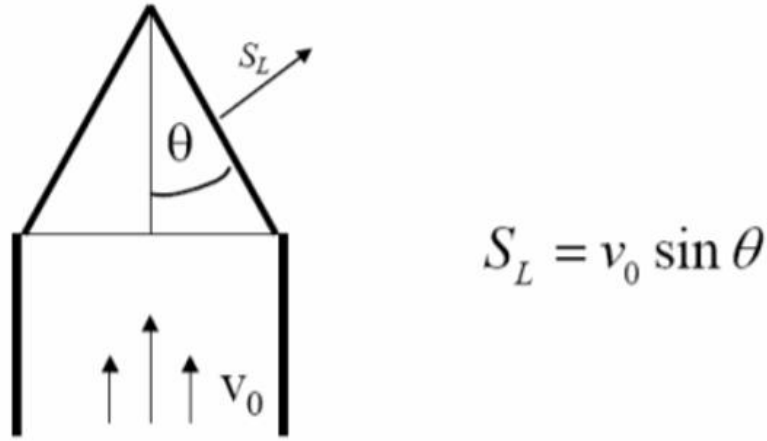


Figure 2-7: Flame angle method of measuring the laminar burning velocity, [70]

However, due to the non-uniform nature of the velocity distribution in the burner nozzle, the flame angle method cannot be used in this study. Hence, the bunsen burner with the flame area method was employed to obtain the laminar flame speed values. The laminar burning velocity of a premixed bunsen flame can be calculated using the following expression.

$$S_u^0 = \frac{Q_u}{A_b} \quad (6)$$

While the experimental conditions define the volumetric flow rate of the unburned gas, Q_u , the area of the flame surface, A_b , is found based on the image processing method of the given flame. The most challenging part of this segment is to identify the location of the flame front. Theoretically, the most accurate edge of the flame front is the location where the deviation of the fresh gas temperature starts to occur [70]. The most known imaging process methods are schlieren, shadow graphing, and the direct photographs of the flame; each of the mentioned methods produces different flame boundaries [70]. It was reported in Ref. [29] that the boundary with the highest brightness in a flame can be used as the flame front for calculation purposes. It is worth noting in Ref. [70] that the inner boundary of the visible flame was shown

to be coinciding or slightly overlapping with the outer edge of the shadow boundary, as shown in Fig. 2-8. In order to validate this statement in the present study, the shadowed image of a premixed bunsen flame was obtained as shown in Fig. 2-9(a), whereas Fig. 2-9(b) illustrates the greyscaled version of the flame captured by direct imaging. The inner boundary of the visible flame was highlighted by identifying the highest rate of change in pixel brightness in each column of the direct flame image, as displayed by the red dots in Fig. 2-9(b). As such, by identifying the pixel location and overlaying them on the shadowgraph image of the respective flame, Fig. 2-9(a), it was shown that both direct imaging and shadow graphing methods produce almost identical outcomes of flame surface area, which is used in calculation of the laminar burning velocity. For comparison purposes, the laminar burning velocity of CH₄/air mixture at $\phi=1$ was calculated to be 34.78 cm/s by shadow graphing and 34.57 cm/s by direct imaging. However, employing the shadow graphing method brings additional difficulties as the thickness of the flame varies based on the distance between the flame and the camera [70]. This phenomenon is clearly shown in Figs. 2-9(c) and (d). Hence, it was decided to use the inner boundary of a visible flame from the direct photographs to define the area of the flame surface in this study. The image post-processing analysis was done using the MATLAB program.

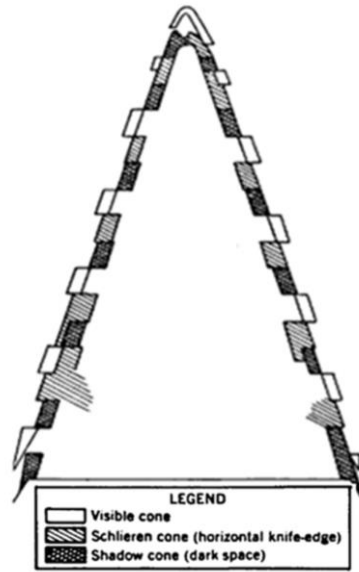


Figure 2-8: Various flame fronts based on the imaging technique, [70]

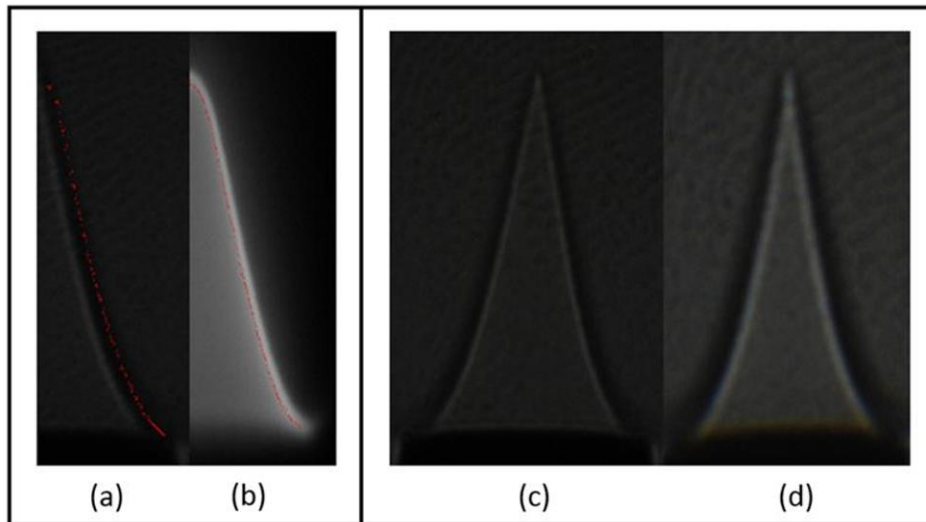


Figure 2-9: (a) Flame image captured by shadowgraph technique, (b) grey scaled direct photograph. Shadow boundary thickness changes with the distance between the camera and the flame, (c) 0.4856 mm, (d) 0.6143 mm.

Figure 2-10 illustrates the flow of the image processing in determining the flame surface area from the direct images of the premixed biogas/air flames. The greyscaled version of Fig. 2-10(a) can be obtained using the built-in MATLAB function of *rgb2gray*, resulting in Fig. 2-10(b). Based on the existing literature [72], the boundary with the highest brightness in a greyscaled image of the flame can be used as the flame front to measure the surface area of the flame, which can result in Fig. 2-10(c). Hence, using the curve fitting feature in MATLAB and Equation 7, the surface area of the premixed flame, A_b , can be calculated, as shown in Fig. 2-10(d,e).

$$A_b = \pi r^2 \sqrt{r^2 + h^2} \quad (7)$$

where h is the flame height, and r is the radius of the conical flame at its base [43,71,72].

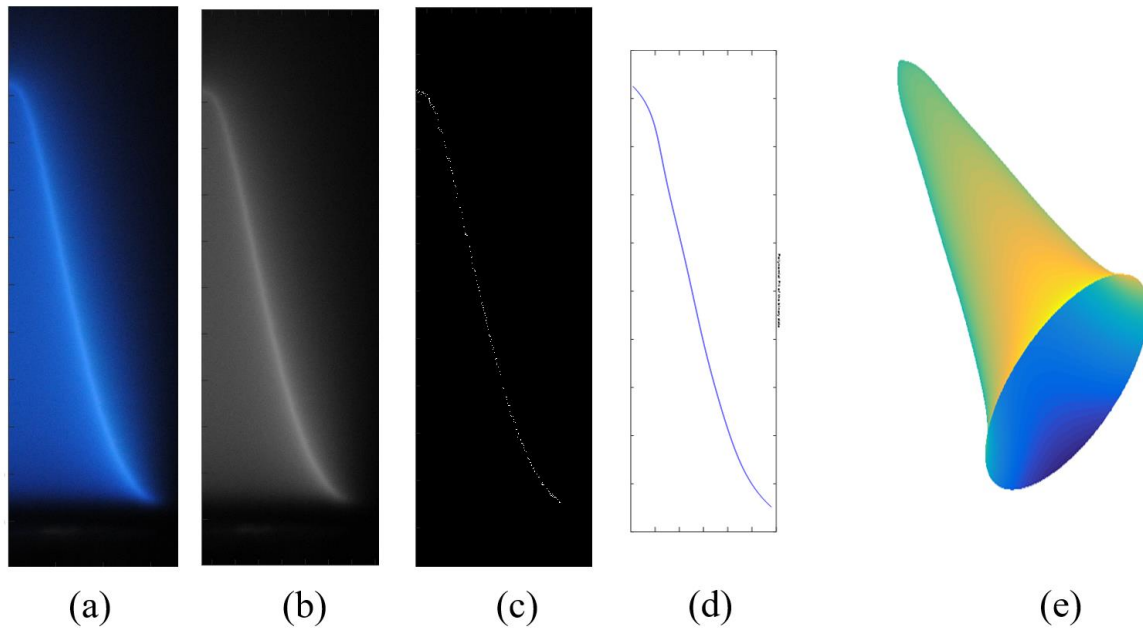


Figure 2-10: Measurement of the flame surface area using MATLAB

This method has some flaws, such as the presence of stretch effect due to the curvature at the tip of the flame. However, in the case of fuels with small laminar burning velocities such as methane, propane, etc., the bunsen burner method produces accurate results as the difference of the laminar burning velocity obtained from the flame surface area and unstretched propagating flame could be negligible [73,74]. In the case of heavier fuels, which possess higher laminar burning velocities, imaging technique such as Schlieren Imaging can help to improve the accuracy of the measurement [29]. Furthermore, as shown by Dong et al. [43], the results obtained from the flame surface area method were in good agreement with the results obtained from other methodologies.

2.3. Measurement of blowoff velocity

The root of the premixed conical bunsen flame is the anchoring point that connects to the nozzle rim and leads to the stabilization of the flame as a result of the heat transfer between these two mediums. Increasing the speed of the supplied mixture, relative to the velocity at which the flame is stable, pushes the flame further from the nozzle of a burner. As this distance increases, the heat transfer mechanism weakens, resulting in instability of the flame, consequently leading to its blowoff at a specific flow velocity [70]. This critical nozzle exit velocity is known as the blowoff velocity of the flame. It is assumed that in order to experimentally determine this critical velocity, the premixed flame should firstly be established on the nozzle rim and followed by the continuous increase in the flow velocity until the flame blows off while maintaining the constant equivalence ratio of the mixture. Here equivalence ratio is defined as a measure of the fuel-air mixture relative to stoichiometric conditions. Among many factors that affect the blowoff phenomenon, laminar burning velocity plays an integral role in the behavior of the blowoff velocity. It showed that these two parameters, i.e., blowoff and laminar burning velocities, had similar trends over the same range of equivalent

ratio [75]. It is also known that the laminar burning velocity is dependent on the mixture's composition and temperature. Once the premixed flame is stabilized on the rim of the nozzle, there is a heat loss to the nozzle that causes a drop in the flame temperature. This occurrence negatively affects the laminar flame speed. On the other hand, the laminar burning velocity can get benefit from the heated nozzle as the flame elevates the initial temperature of the mixture at the nozzle exit. Hence when measuring the blowoff velocity, the time required to perform the measurements and change the velocity of the mixture would play a significant role in the outcome of the experiment. It was reported that using an increasing flow rate method could lead to inconsistent results [75].

Based on this observation, it was concluded that the decreasing flow rate method should be employed to determine the blowoff velocity of the premixed flame. In this study, the nozzle exit velocity was initially set at a high value where the flame was unable to be established. It is followed by the continuous decrease in the flow velocity when keeping the equivalence ratio constant until the flame was ignitable and stable at the nozzle rim. By following this approach, the heat loss from the flame to the nozzle was avoided, and the initial temperature of the unburned mixture was kept constant at the desirable conditions.

2.4. Experiment

To perform the experimental investigation, the setup consisted of a coflow burner, multiple mass flow controllers, heating ropes, variable autotransformer variac, multiple thermocouples, and a digital camera (Nikon D3000), as schematically shown in Fig. 2-11. The central nozzle of the coflow burner was made of stainless steel with an inner diameter of 7.55 mm, the thickness of 1 mm, and the length to be over 500 mm. This geometric profile was chosen to establish a fully developed parabolic profile of the velocity at the exit of the nozzle, regardless of the flow conditions [76]. The coflow burner was filled with glass beads and

covered with a honeycomb in order to ensure a uniform coflow. Nitrogen (N_2) coflow was used to prevent the secondary diffusion flame while stabilizing premixed bunsen flame. The nitrogen coflow was set at 5 cm/s and was used for all the conditions. Mass flow controllers (MKS, 1179 A) were used to control the flow rate of the gases via readout controller (MKS, 247D 4 channel). The calibration of these MFCs was done using a dry-test gas meter (Bios, Definer 220M). Methane (CH_4) and carbon dioxide (CO_2) were supplied to imitate the biogas fuel based on various compositions, referring to Table 1.

The biogas/air mixture was pre-heated by heating ropes (Omega) to investigate the effect of the temperature of the unburned mixture. The temperature of the heating ropes was controlled based on the supplied voltage from the autotransformer variac. The measurement of the temperature was done via a thermocouple (Omega, DP32PT) at the nozzle exit to ensure the temperature of the mixture was set at the desired condition. In order to confirm the uniformity of the heating, multiple thermocouples were attached throughout the supply line which was heated via the heating ropes. The temperature values were recorded by the temperature readout unit (midi LOGGER GLB20). Furthermore, the supplied mixture was ignited only when the temperature readout showed the desired value for the temperature, with an uncertainty of ± 1 K, of the unburned gas to ensure the accuracy of the experiment.

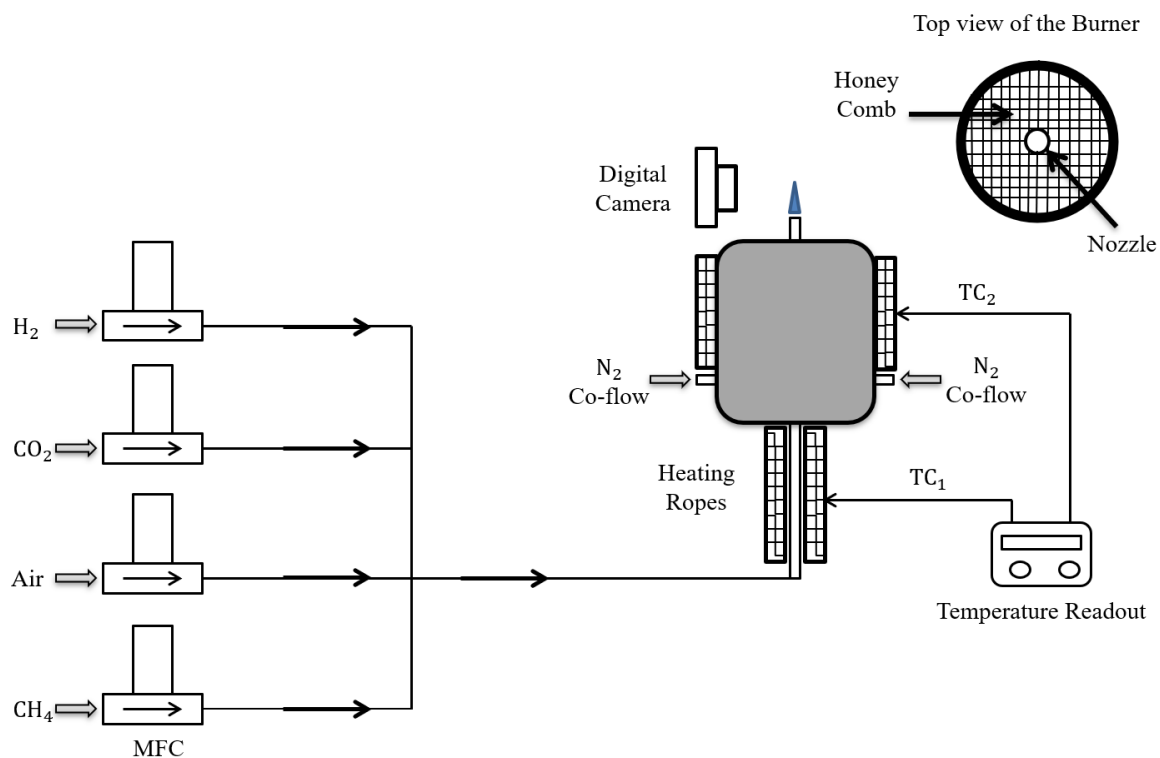


Figure 2-11: Schematic diagram of the experimental setup

Table 2-1: Biogas compositions used in this present work

Mixture name	Biogas	H ₂ addition to biogas (% by vol.)	Gas concentration in fuel mixture (% by vol.)		
	composition				
	(% by vol.)		CH ₄	CO ₂	H ₂
BG1		0	60	40	0
BG1H10	CH ₄ –CO ₂ 60%–40%	10	54	36	10
BG1H20		20	48	32	20
BG1H30		30	42	28	30
BG1H40		40	36	24	40
BG2	CH ₄ –CO ₂	0	65	35	0

BG2H10	65%–35%	10	58.5	31.5	10
BG2H20		20	52	28	20
BG2H30		30	45.5	24.5	30
BG2H40		40	39	21	40
BG3		0	70	30	0
BG3H10	CH ₄ –CO ₂ 70%–30%	10	63	27	10
BG3H20		20	56	24	20
BG3H30		30	49	21	30
BG3H40		40	42	18	40

2.4.1. Measurement uncertainties

In this experimental study, there are two primary sources of uncertainties; one is associated with the flow metering system, which corresponds to the determination of the blowoff velocity, while the other comes from the calculation of a flame area to obtain the laminar burning velocity of the flame [29]. As mentioned earlier, the gases were supplied via mass flow controllers calibrated using the dry-test gas meter, which resulted in $\pm 2\%$ accuracy per gas. Hence, based on the Root Sum of Squares (RSS) method, the combined uncertainty for the total mixture (4 gases) is calculated to be around $\pm 4\%$. In the case of the flame area calculation, five images were captured for each flame, and due to the axisymmetric nature of the bunsen flame, the calculation was done using half image at a time. The final conical flame surface area was the average value of the five flames. The maximum deviation in the flame front area between a single image and the averaged value based on all the images is roughly $\pm 3\%$. This produces the accuracy of $\pm 1\%$ for the mean flame area used in the calculation of the laminar burning velocity. Thus, the maximum uncertainty in the measurement of blowoff velocity is calculated to be $\pm 4\%$, while for the laminar flame speed is $\pm 5\%$.

2.5. Numerical simulation

A steady-state simulation was modelled with non-swirling 2D axis-symmetric geometry using ANSYS Fluent 17.2. The reactive fluid flow was solved with three fundamental conservation equations in steady-state forms [77,78]:

1) continuity equation,

$$\nabla \cdot (\rho \vec{U}) = 0 \quad (8)$$

2) Navier-Stoke equation,

$$\nabla \cdot (\rho \vec{U} \vec{U}) = -\nabla p + \nabla \cdot \bar{\bar{\tau}} + \rho \vec{g} \quad (9)$$

3) energy equation,

$$\nabla \cdot \left[\vec{U} \left(\rho \left(h - \frac{p}{\rho} + \frac{U^2}{2} \right) + p \right) \right] = \nabla \cdot \left[k \nabla T - \sum_i h_i \vec{J}_i + (\bar{\bar{\tau}} \cdot \vec{U}) \right] - \sum_i \frac{h_i^0}{M_i} \mathfrak{R}_i \quad (10)$$

where

$$\nabla \cdot \vec{U} = \frac{\partial U_x}{\partial x} + \frac{\partial U_y}{\partial y} \quad (11)$$

and,

$$\bar{\bar{\tau}} = \nabla \cdot \mu \left[(\nabla \vec{U} + \nabla \vec{U}^T) - \frac{2}{3} \nabla \cdot \vec{U} \bar{\delta} \right] \quad (12)$$

Pressure-based solver was chosen with laminar as a viscous model. Species transport species model was chosen for ideal gas with volumetric reaction activated and wall reaction deactivated. GRI-Mech 3.0 chemical mechanism [79] containing 325 reactions and 53 species was chosen. However, for the purpose of the present study, the dimension reduction was carried out to yield 13 species (H₂, H, O, O₂, OH, H₂O, HO₂, CH₃, CH₄, CO, CO₂, CH₂O, N₂) as recommended and proved by the number of research groups [80-82] to account for methane and biogas only. This reduced mechanism was used to lessen the computational burden, while

producing the same level of results, by employing the most relevant reactions and species on the combustion in the given chemical mechanism. Stiff chemistry solver, which uses ISAT table to increase solving speed [77], was configured with ISAT error tolerance of 5×10^{-5} . Coupled solver scheme with second-order upwind spatial discretization was selected for higher accuracy.

Figure 2-12 shows the geometry and the computational grid of the coflow burner for simulation. It is worth mentioning the importance of the inlet location for fuel/air mixture in the geometry of the model. Based on the main findings from the studies related to the combustion of the bunsen flames [83,84], the present study adopted the idea of setting the fuel/air inlet at 70 mm upstream from the nozzle exit. This is done in order to promote a more realistic velocity profile at the nozzle exit, as applying the fuel inlet boundary conditions at the nozzle exit tends to produce an overestimation of the results. Mesh convergence test was performed by comparing the temperature profile along the central axial direction. Based on the mesh convergence results, the geometry with the total mesh elements of 44,104 quadrilateral cells with radial edge element sizing of 0.2 mm, 2/3 mm, 1 mm for fuel-air inlet, nozzle wall, coflow inlet, and axial edge sizing of 0.2 mm was selected for the simulation study. Nozzle dimensions followed those of the experiment. Coflow velocity was radially uniform at 5 cm/s while fuel/air mixture velocity followed a parabolic function with maximum velocity $U_{\max} = 2U_0$. Non-slip wall condition and inlet temperature of 298 K were applied. Volume was initialized at 298 K and 1 atm.

For the first 200 iterations, reaction was deactivated to ensure a steady flow. Then the activation of reaction to solve for the following 2500 iterations was selected to achieve steady bunsen flame. Temperature contour was plotted to define flame geometry.

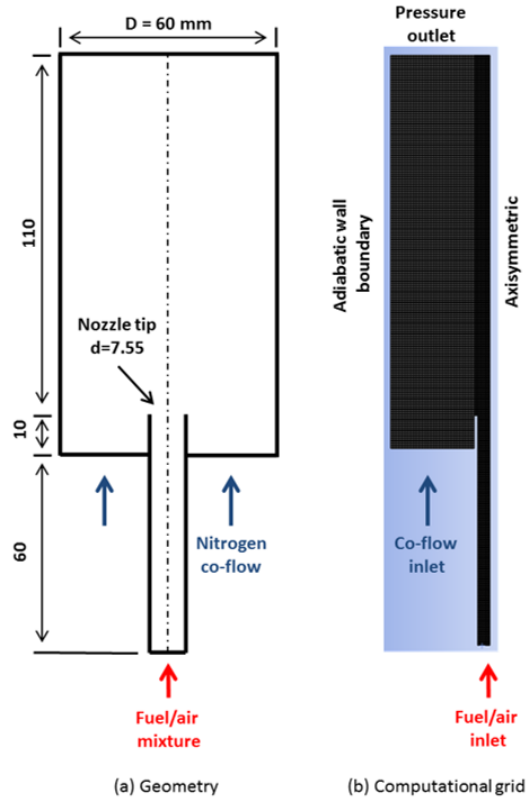


Figure 2-12: (a) Geometry and (b) computational grid of the coflow burner with its boundary conditions

2.6. Results & Discussion

The main objective of this work is to investigate the blowoff velocity of various biogas/air mixtures, specifically, to understand the behavioral change in blowoff velocity due to the addition of hydrogen and the elevated temperatures of the unburned mixture. Moreover, in order to fill the knowledge gap in this field of research, the numerical investigation of the biogas/air flame, using the reduced GRI-Mech 3.0 chemical mechanism, was conducted. In this section, experimental and numerical results for CH_4/air flame are compared with literature data to validate our experimental setup and numerical model. Then, the effects of hydrogen addition, elevated initial temperature, and CO_2 composition in the biogas/air mixtures are discussed next.

2.6.1. Experimental validation

In order to validate the above-mentioned methodologies, combustion characteristics such as blowoff and laminar burning velocities were experimentally determined at room temperature and atmospheric pressure conditions for methane/air flames and illustrated in Figs. 2-13(a) and (b), respectively. As shown in Fig. 2-13, both values, from the present study, are in good agreement with the literature data [75,85–88]. Although there are some minor discrepancies between this study and the literature, the similarity in the trends is obvious. Moreover, these differences can be caused by the variation in the experimental setup as well as in the methods of determining these parameters [29]. However, the discrepancies are within the calculated uncertainties range represented by the error bars. Thus, the proposed methodologies, as well as the reduced GRI-Mech 3.0 chemical mechanism were validated and could be used for the determination of the laminar flame speed of the biogas/air mixture.

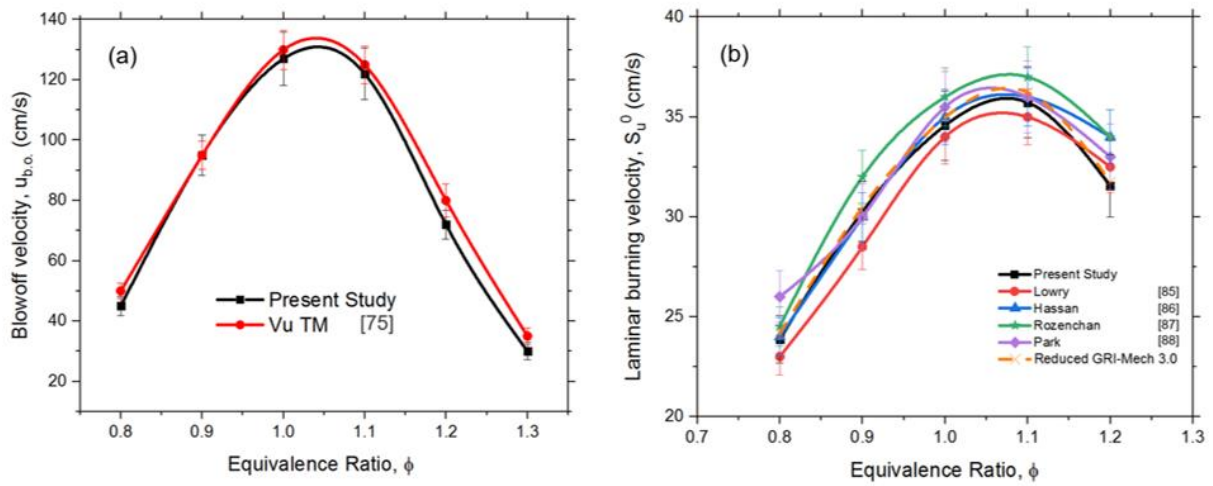


Figure 2-13: Comparison of the experimental and numerical data for CH₄/air mixture: (a) blowoff velocity, (b) laminar flame speed.

2.6.2. Effect of elevated initial temperatures

The unburned gas temperature of the biogas/air mixture was heated within the range of 298–440 K, with the incremental steps of 20 K. Figure 2-14 illustrates the effect of initial temperature variation on the blowoff velocity of various stoichiometric biogas/air mixtures, with different CH₄ and CO₂ compositions. It is clearly seen that blowoff velocities are linearly increasing with the initial temperature of the mixture, regardless of CO₂ content. This behavior occurs as the result of a higher content of enthalpy present in the heated biogas mixture. To observe the impact of elevated initial temperatures of the unburned gas, flame photographs at three different initial temperatures of the unburned gas, i.e., 298, 373, and 440 K, were taken at the same inlet velocity of 35 cm/s for the fuel sample BG1, as shown in Fig. 2-15(a). Moreover, the settings in the digital camera were kept constant (1/60 s and $f = 1.2$) for the purpose of the direct comparison between the flame observations. From Fig. 2-15(a), it was found that the height of the flame had decreased with an increase in the initial temperature of the mixture. As an example, for the fuel sample BG1 at $\phi = 1.0$, the flame height was reduced from 2.281 mm to 2.016 mm at the initial temperatures of 298 K and 440 K, respectively. As the local flow velocity was kept constant for comparison purposes, it was observed that the reduction in flame height resulted in an increase in the cone angle. It is also known that the calculation of the laminar burning velocity is closely associated with the cone angle and the local flow velocity. Therefore, the change in flame height can be considered as the indicator of change in both laminar burning velocity as well as blowoff velocity.

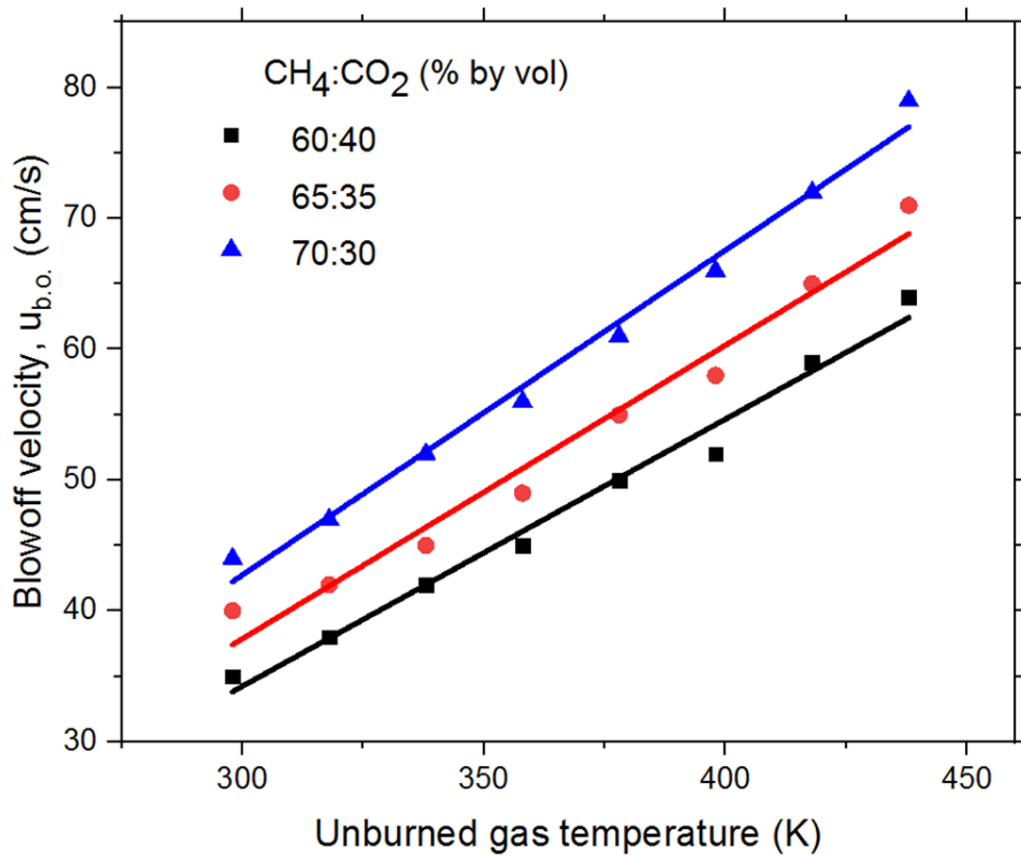


Figure 2-14: Effect of elevated unburned gas temperature on the blowoff velocity of stoichiometric biogas/air mixtures at atmospheric pressure conditions.

The standoff distance, which is the distance between the flame base and the nozzle rim, plays an essential role in the flame stabilization as the heat transfer occurs between these two mediums [75,89]. Although the anchoring mechanism of the flame based on the nozzle rim is complicated and consists of various combustion properties, the standoff distance of the flame can be another indicator to predict the behavior of the blowoff velocity. This situation is in good agreement with the observation of flame images from Fig. 2-15(a). It can be seen that the standoff distance of the flame was decreased with the elevated temperature of the biogas/air mixture, which results in a stronger stabilization mechanism indicating the increase in blowoff velocity. Figure 2-15(b) illustrates the enhancement in the blowoff velocity of the BG1 flames

with regard to their respective elevated initial temperatures. The blowoff velocities were found to be 35, 50, and 64 cm/s for initial temperatures of 298, 373, and 440 K, respectively. Although the increase in flame height can be attributed to the increased flow rate of the unburned mixture, the decrease in standoff distance can be observed, which indicates the stronger anchoring mechanism at the nozzle rim.

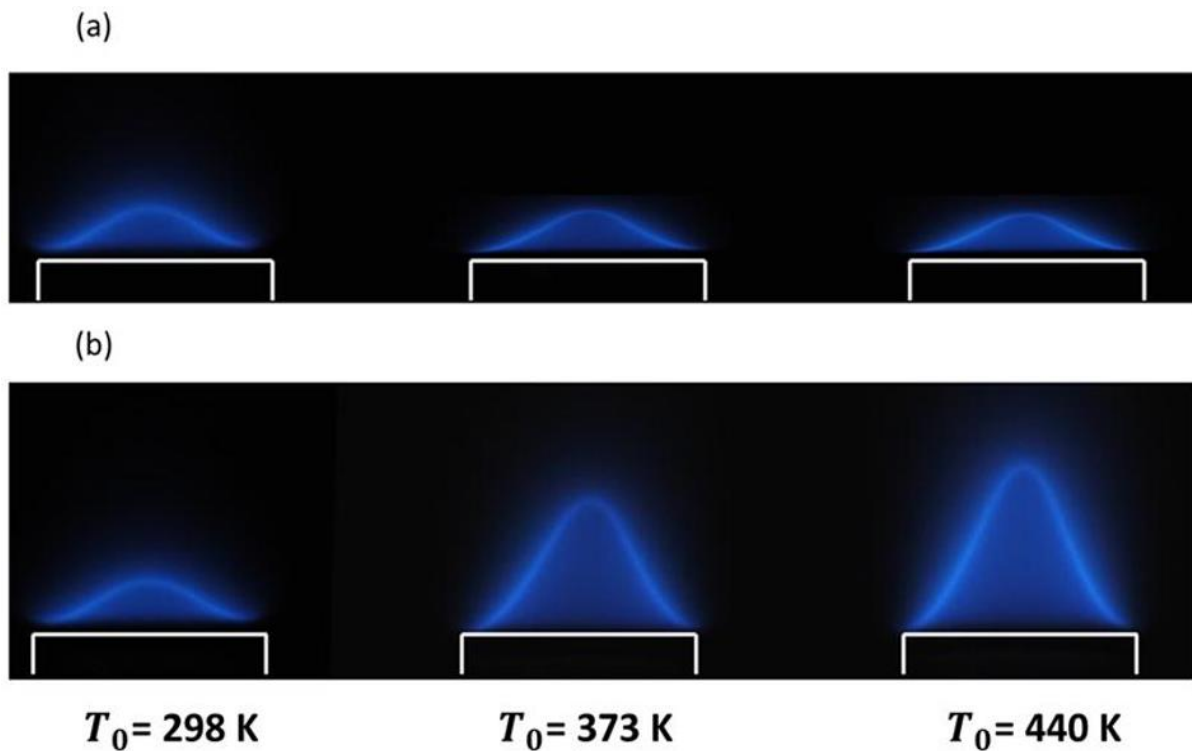


Figure 2-15: Direct photographs of stoichiometric premixed bunsen flame (BG1) with elevated temperatures; (a) all three flames are at the same inlet velocity of 35 cm/s, (b) flames are at their critical velocity just prior to blowoff.

2.6.3. Effect of hydrogen addition

All three compositions of biogas were enriched with the hydrogen in the range of 10–40%, as shown in Table 1. The effect of this additive on the blowoff velocity was experimentally investigated at atmospheric pressure and 298 ± 1 K, over the wide range of equivalence ratios, i.e., 0.8–1.3.

Figure 2-16 shows the enhancement of blowoff velocities of biogas/air mixtures with the addition of hydrogen at the stoichiometric condition. Unlike the linear increase of the blowoff velocity due to the elevated temperature of the unburned gas, the blowoff velocity increased non-linearly with the increasing content of hydrogen in the mixture, for all three biogas compositions, BG1, BG2, and BG3. It is obvious to note that the fuel sample with the lower content of CO₂ underwent a more significant rise in blowoff velocity with the hydrogen enrichment. This behavior is more apparent with the increasing content of the hydrogen in the mixture. For example, with 20% of hydrogen content in the mixture, BG1, BG2, and BG3 achieved the improvements of 100, 140, and 170 % in the blowoff velocities, respectively. It can be explained based on the fact that the temperature of the combustion and the active radicals are increased with the higher content of H₂ as well as the lower concentration of CO₂ added into the biogas mixtures. This behavior is similar to the case of the laminar burning velocity of hydrogen-enriched fuels, which was shown in the literature [2,3,10].

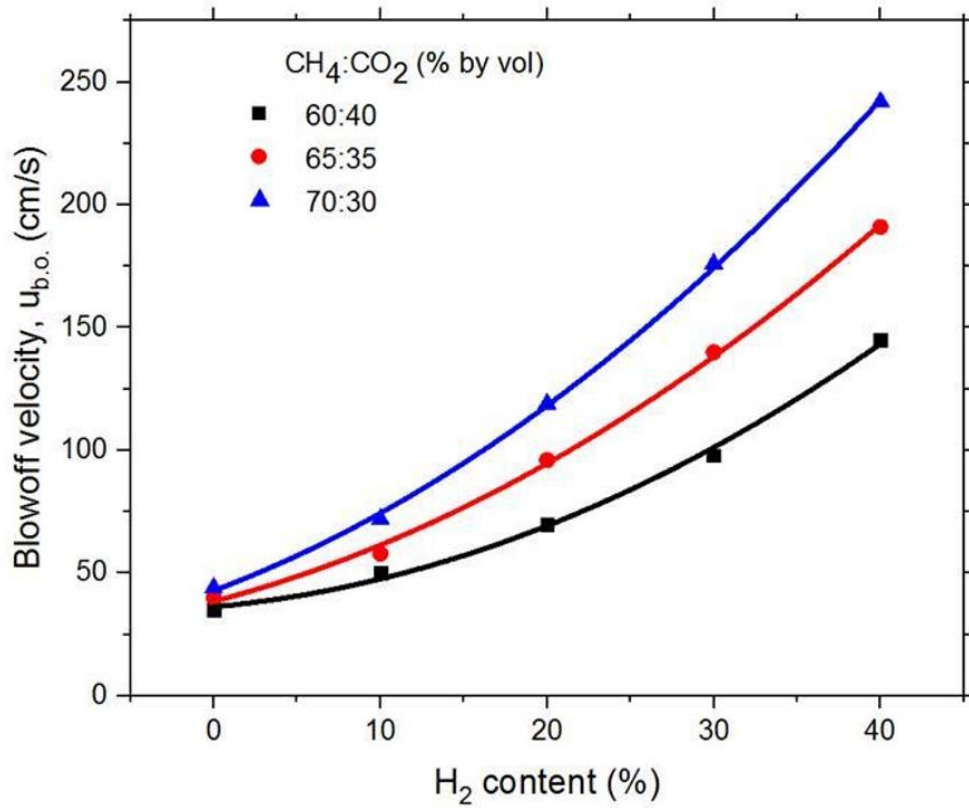


Figure 2-16: Effect of hydrogen addition on the blowoff velocities of stoichiometric biogas/air mixtures.

Figures 2-17(a) and (b) depict the effect of hydrogen addition on the blowoff as well as the laminar burning velocities of the BG1 mixture over the wide range of equivalence ratios. As a result of the addition of hydrogen into the mixture, more active radicals are produced, and the temperature of the unburned mixture is increased. These changes lead to the enhancement of the thermal diffusivity. This phenomenon was discussed by Wei et al. [3], who also predicted that the thermal diffusivity was higher in the rich hydrogen-enriched-biogas mixtures compared to the lean mixtures. This prediction is in good agreement with the experimental results of the present study, shown in Fig. 2-17(a), as the improvements in stoichiometric and rich mixtures were more apparent compared to lean mixtures. Moreover, it is worth noting that the significant growth in the burning velocity can be attributed to the higher contribution of hydrogen towards

the combustion process of the fuel blends. Erjiang et al. [90] performed a numerical investigation on the combustion of methane/hydrogen/air mixture and showed that there were three regimes of the combustion. One of them is the transition regime where the combustion was governed by both hydrogen and methane fuels. As a result of their combined physiochemical properties, the growth in flame burning velocity was non-linear compared to the linear increase for purely methane or hydrogen dominated combustion regimes. Jun et al. [91] reported a similar observation while studying the combustion characteristics of hydrogen/ammonia/air mixture. The results showed that the changes in the burning velocity are non-linear with the hydrogen content of 30–50 % in the mixture. The effect of this non-linear growth can be seen in Fig. 2-17, where the improvements in blowoff and laminar burning velocities change dramatically with the hydrogen fraction of 30% and above.

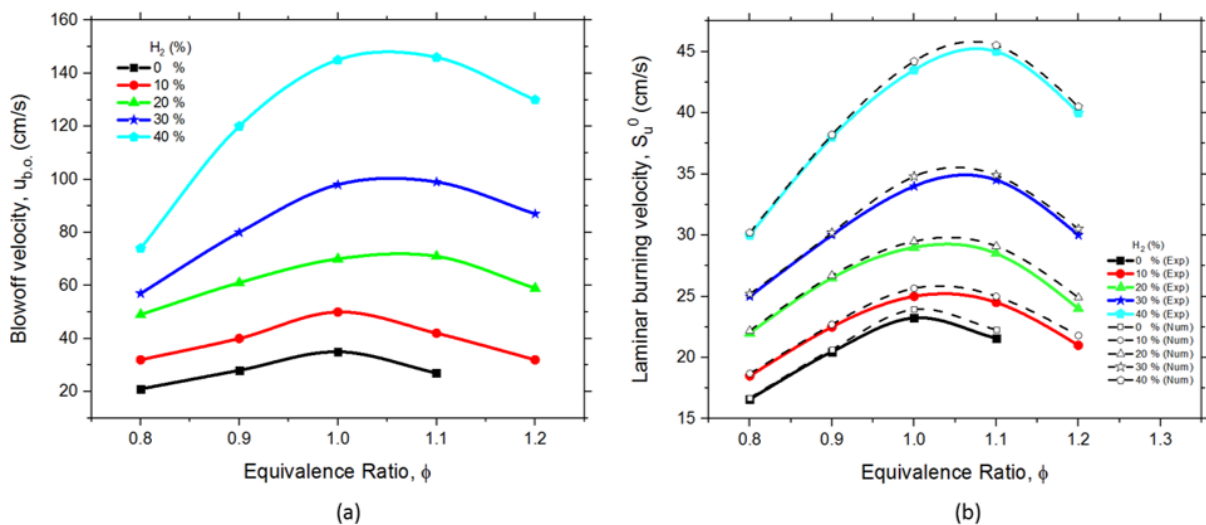


Figure 2-17: Effect of the hydrogen addition on: (a) blowoff velocity and (b) laminar burning velocity of BG1 mixture over the wide range of equivalence ratios.

Blowoff velocity of a flame can generally be predicted by the trend of the laminar burning velocity for a given flame. This is because the laminar burning velocity is associated with the temperature of the flame, which plays a major role in the heat transfer mechanism

between the root of the premixed bunsen flame and the nozzle. This is in good agreement with the present results, illustrated in Figs. 2-17(a) and (b). However, it must be noted that the relationship between these two characteristics is far more complex due to the possible occurrence of the stretch of the flame surface, heat losses, quenching effects as well as the dilution with the ambient gas.

To perform the flame observation, the direct photographs of stoichiometric premixed bunsen flames of BG2 mixture with different concentrations of hydrogen, 0–40%, are shown in Fig. 2-18(a). For the purpose of the comparison, the flame photographs were taken at the same inlet velocity of 40 cm/s. In Fig. 2-18(b), the flames were taken at their respective blowoff velocities, which were found to be 40, 58, 96, 140, and 191 cm/s for 0–40% of hydrogen addition, respectively. As the hydrogen content increases in the mixture, the diffusion rate drops in the reaction zone and enhances in the preheat zone. This leads to the following changes: more active radicals, elevated temperature of the unburned gas, rise in the rates of reactions, as well as the improved blowoff and laminar flame speed. On the contrary, the upstream side of the flame experiences early low-temperature reactions, which lead to a steeper temperature gradient of the flame. Hence, the reaction zone thickness is decreased, as seen in Fig. 2-18(a). This observation is in good agreement with the mathematical relation discussed by Kanury [92]. It showed that the ratio of the temperature difference between burned and unburned gases to the maximum temperature gradient of the flame could be used to represent the flame thickness [92].

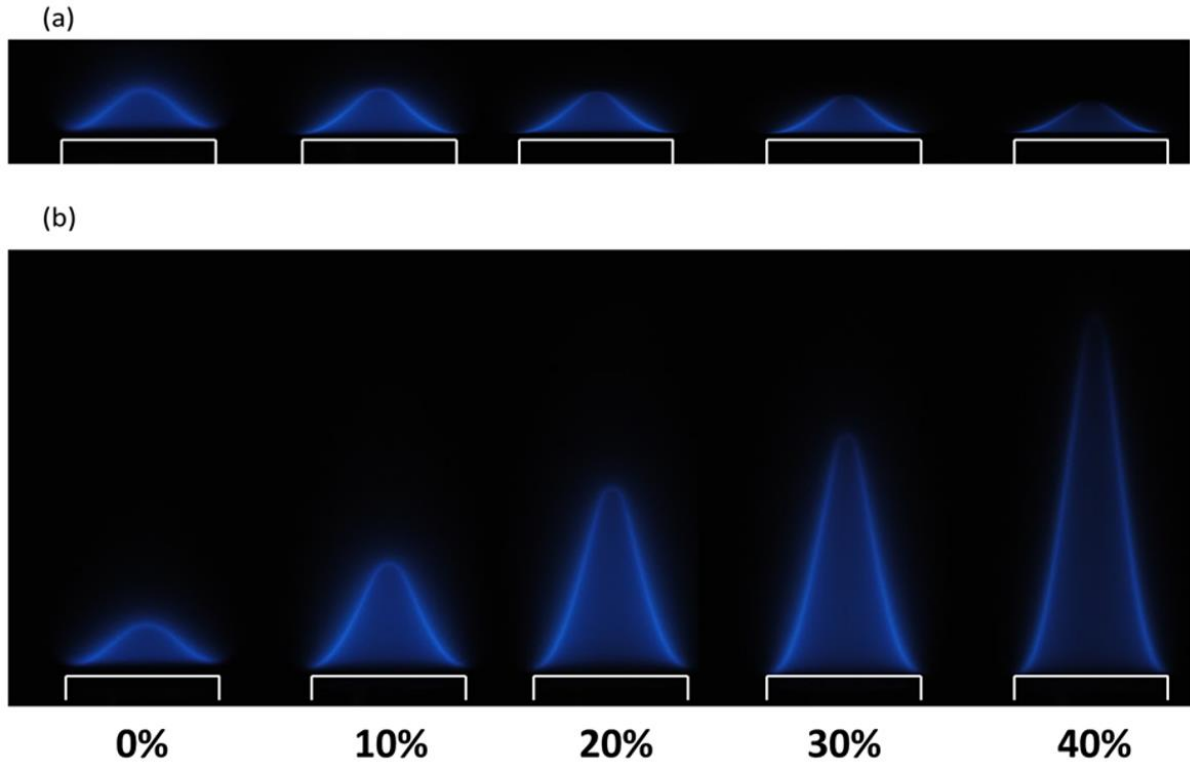


Figure 2-18: Direct photographs of stoichiometric premixed bunsen flames (BG2) with H₂ additions; (a) all five flames are at the same inlet velocity of 40 cm/s, (b) flames are at their critical velocity just prior to blowoff.

Another observation from the flame images, shown in Fig. 2-18(a), is the existence of the flame tip opening at 40% H₂ addition in the fuel blends. The two main factors associated with the tip opening of premixed bunsen flames are stretch rate, which is characterized by the curvature of the flame tip, and the preferential diffusion, which is associated with the disproportion of molecular diffusion of the components within the mixture [93]. As illustrated in Fig. 2-18(a), fuel enrichment with hydrogen resulted in the reduction in the flame height at the given unburned gas velocity. The reduction in flame height increases the curvature at the flame tip, which dominates the stretch effect and weakens the negative stretch. Moreover, flow strain exists due to the high mass diffusivity of hydrogen, causing the positive stretch effect.

Yasuhiro et al. [26] conducted a numerical study to understand the tip opening mechanism of bunsen flames. The results of the simulation showed that the fuel concentration is not homogeneous throughout the flame structure. It decreases along the direction of the flow, i.e., in the axial direction, due to the outward radial diffusion, while the oxidant concentration is constant. As such, there was a reduction in the fuel consumption rate in the downstream of the flame, due to the leaner nature of the mixture, which led to the lower local combustion intensity at the flame tip. Hence, there is a competitive relationship between the impact of the flame curvature and the fuel consumption rate at the tip of the flame. With the higher fraction of H_2 in the mixture, the flame height reduces while increasing the curvature of the flame tip at the given unburned gas velocity. On the other hand, the intensity of the combustion at the flame tip enhances due to the increased hydrogen ratio. Thus, the tip opening depends on whichever of the two mentioned effects are more dominant at the given hydrogen concentration. This behavior is more apparent with the higher concentration of hydrogen, which is consistent with the present experimental results. In this work, the tip opening of the flame occurred at 40% addition of H_2 , where the flame curvature weakened the negative flame stretch, and its influence was more dominant compared to the local combustion intensity at the tip of the flame. Additionally, Vu et al. [42] showed that the existence of tip opening was independent of the unburned gas velocity at the given equivalence ratio, which is supported with the present study findings shown in Fig. 2-18. The flame images were taken at the same gas velocity of 40 cm/s as shown in Fig. 2-18(a) whereas in Fig. 2-18(b), the flame images were taken at their respective blowoff velocities. In both scenarios, the tip opening of the flame was present at the hydrogen concentration of 40%, irrespective of the jet velocity.

2.6.4. Effect of CO₂ composition in biogas mixture

Figures 2-19(a) and (b) illustrate the variation of the laminar flame speed of biogas/air mixtures over the wide range of equivalence ratios, for all three mixture compositions with and without H₂ addition respectively. It can be observed that the increase in CO₂ content in the mixture causes a consistent reduction in the laminar burning velocity of the biogas/air mixtures. In addition, the reduction of laminar burning velocity due to the dilution with CO₂ is noticeably higher for richer biogas mixtures compared to lean and stoichiometric conditions. Figure 2-19(a) shows that the peak of the laminar burning velocity of biogas with H₂ addition shifts from the richer towards stoichiometric mixture conditions with the increase of CO₂ content in biogas fuel, while the peak of laminar burning velocity is at stoichiometric for the biogas without H₂ enrichment as can be seen from Fig. 2-19(b). These behaviors can be explained by the combination of dilution, thermal, and chemical effects of CO₂ in the mixture [22,94]. One of the widely known methods of performing the quantitative analysis on these effects is by employing the fictitious species in the mixture [95,96]. Figure 2-20 shows the impact of CO₂ on the laminar burning velocity of CH₄/air mixture in terms of chemical, thermal, and dilution effects, which was evaluated using PREMIX Code. The fictitious species of CO₂, named FCO₂, was introduced into the mixture, which possesses similar thermodynamic and transport properties as the real CO₂ but cannot participate in any of the chemical reactions. Hence, the difference between the results of laminar burning velocity with CO₂ and FCO₂ can be associated purely with the chemical effect. Based on the literature [97,98], it is also known that N₂ can be considered to be an inert gas. It was also supported by the results where the values of laminar burning velocity between fictitious species, FN₂, and real N₂ blended mixture showed no difference, as shown in Fig. 2-20. The difference in the laminar burning velocity between the mixtures with FCO₂ and FN₂ can be associated with the thermal effect. Hence, the difference in laminar burning velocity of CH₄/air mixture and FN₂ can be associated with the

dilution effect. Furthermore, CO₂ is a chemically passive agent, and its addition to the mixture can result in the reduction of the fuel content due to the dilution effect. Thermal effect is characterized by the reduction in adiabatic flame temperature, due to the non-reactive nature of CO₂, which plays the role of the heat sink in the mixture [94]. Hence, the laminar flame speed decreased with the higher dilution ratio of CO₂, as shown in Fig. 2-19(b), due to its dependency on the temperature of the flame. The result is in good agreement with our numerical adiabatic flame temperatures, which were recorded to be 2110, 2130, and 2158 K for BG1, BG2, and BG3 respectively.

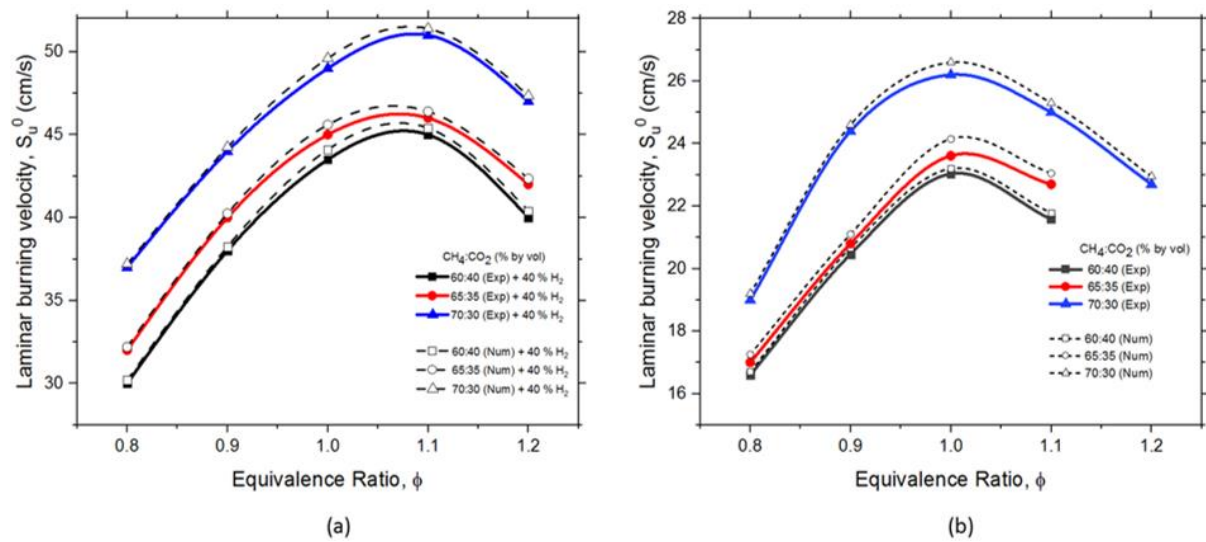


Figure 2-19: Laminar burning velocity of biogas/air mixtures (a) with 40% of H₂ addition and (b) pure biogas/air mixtures, at room temperature and atmospheric pressure.

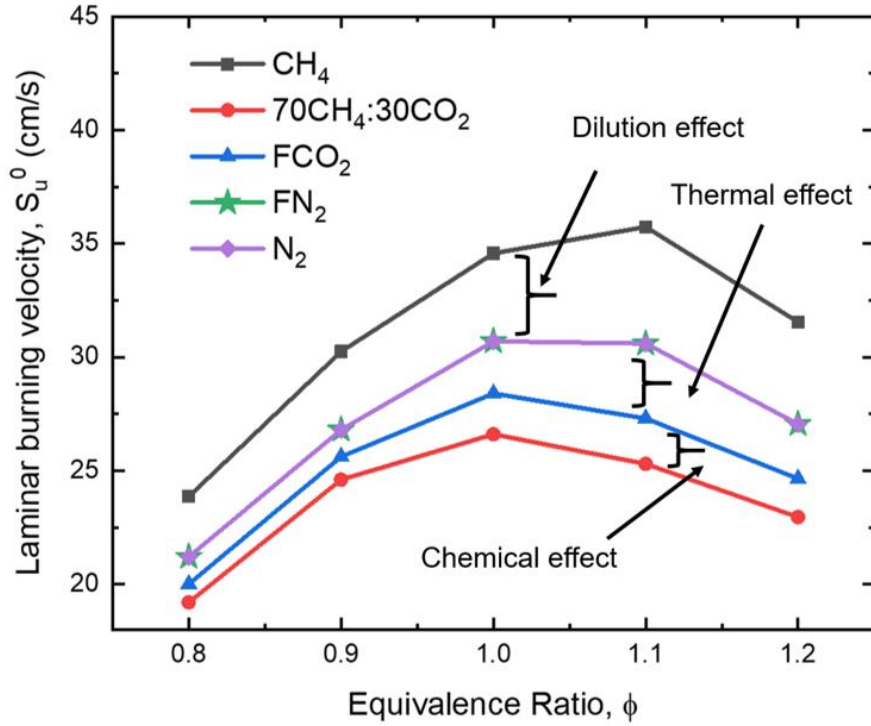


Figure 2-20: Effect of CO₂ on the laminar burning velocity

Besides, CO₂ is one of the major products of combustion. It has been reported the chemical kinetics of fuel/air mixture modifications, invoked by the addition of CO₂, can be associated with the following major reactions [22,23,27,94]:



The presence of CO₂ in the mixture results in the reduction of H radicals through the reverse reaction of $\text{CO} + \text{OH} = \text{CO}_2 + \text{H}$. Whereas, $\text{H} + \text{O}_2 = \text{O} + \text{OH}$ reaction is the most influential on the combustion, based on the sensitivity analysis. Therefore, the lack of H radicals resulted by Equation 13 influences Equation 14, thereby decreasing the reaction rate of the overall combustion for the given mixture. However, it is important to note that the chemical effect of CO₂ is more pronounced near stoichiometric conditions. The content of the fuel increases with

the equivalence ratio, allowing more H radicals in the mixture to be available in Equation 14, thereby strengthening the effect of chemical kinetics for the rich fuel mixtures. This can explain the shift in the peak of laminar burning velocity from the rich side of biogas with H₂ addition, Fig. 2-19(a), to the stoichiometric side of biogas without H₂ addition, Fig. 2-19(b).

Figure 2-19(b) shows that the richer biogas mixtures experience a more notable reduction in laminar burning velocities with CO₂ dilution rate. This is attributed to the radiation effect of CO₂ in the mixture. Carlos et al. [99] reported the existence of the linear relation between the temperature loss through radiation and CO₂ dilution rate. In addition, with both experiment and numerical simulation, Lee et al. [100] reported that CO₂ can be considered as a radiating medium, and thereby resulting in the radiation heat loss as well as the total heat loss.

Another observation from Figs. 2-19(a) and (b) is the drastic change in laminar burning velocity of the biogas mixtures between BG2 and BG3. This behavior can be explained by the findings from Lee et al. [100], where the steeper temperature drops were observed through the radiation loss, between 30% and 40% of CO₂ dilution in the mixture. This difference has also exerted its influence on the physical appearance of the bunsen flames. To further support the above-mentioned statement, the flame observations for all three compositions were conducted, as shown in Fig. 2-21. The results, indeed, showed that BG3 depicted the brightest flame indicating the highest flame temperature as well as the highest presence of active radicals among the three tested biogas mixtures, which directly affects the rates of reactions in the combustion process.

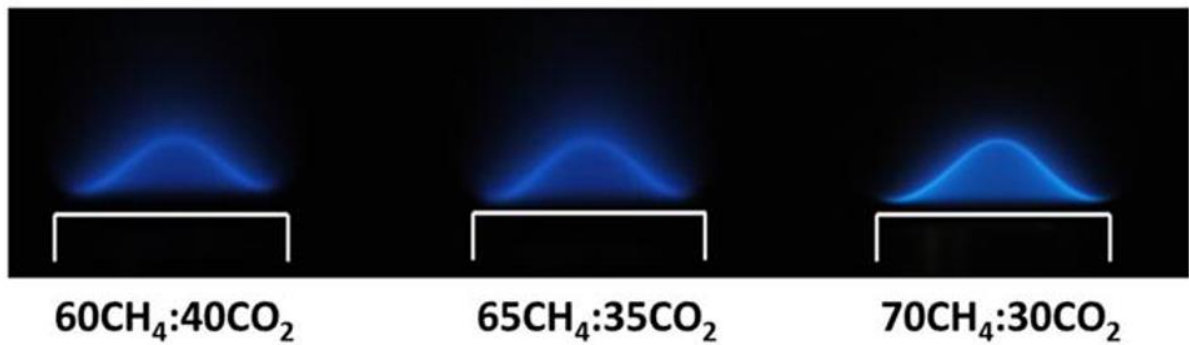


Figure 2-21: Comparison of stoichiometric biogas/air with three different compositions at room temperature and atmospheric pressure.

2.6.5. Comparison between numerical and experimental flames

While there is a number of studies on combustion characteristics of biogas/air flames using the GRI-Mech 3.0 chemical mechanism, the information on the application of reduced GRI-Mech 3.0 chemical mechanism is scarce. Thus, the applicability of the reduced chemical mechanisms for modeling of the premixed biogas/air flames becomes of importance.

In this study, the reduced GRI-Mech 3.0 mechanism is applied to study the combustion of CH₄/air flames in order to ensure the accuracy of the model. This is done as CH₄ is one of the major components in the biogas fuel, which is the main interest of this study. The numerically obtained data of laminar burning velocity, then, was compared to the experimental results, as shown in Fig. 2-13(b). It can be seen that the results are in good agreement and well within the literature scatter.

Upon the completion of the numerical study on CH₄/air flames, the same reduced mechanism was applied to investigate the effect of CO₂ and H₂ content on the combustion characteristics of the biogas/air flames. As expected, the laminar burning velocity decreased with a higher concentration of CO₂ in the mixture and increased with the addition of H₂. These

behaviors are in good agreement with the experimental results. Figure 2-19 shows the laminar burning velocity of biogas/air mixtures with different concentrations of CO₂ and their enrichment with H₂ addition. As can be seen, numerical and experimental results are in good agreement with each other. While Fig. 2-19(a) shows only 40% of H₂ addition to the three different biogas compositions, Fig. 2-17(b) can be referred to view the change in laminar burning velocity of BG1 fuel sample with the various H₂ concentrations.

Figures 2-22(a) and (b) illustrate the direct comparison of the flame structures between the numerically and experimentally obtained premixed bunsen flames, for both CH₄/air and biogas/air flames. In ensuring the validity of the results, CH₄/air flames were compared at three equivalence ratio conditions such as fuel-lean ($\phi = 0.8$, $U_0 = 50$ cm/s), stoichiometric ($\phi = 1.0$, $U_0 = 125$ cm/s) and fuel-rich ($\phi = 1.2$, $U_0 = 80$ cm/s) as shown in Fig. 2-22(a). Whereas in Fig. 2-22(b), the flame of biogas/air mixtures were captured at the stoichiometric condition with their respective gas flow velocities of 35 cm/s (for 60CH₄:40CO₂), 40 cm/s (for 65CH₄:35CO₂) and 44 cm/s (for 70CH₄:30CO₂). From the observation, it is clear to note that both flame heights and standoff distances of the experimental flames are in good agreement with the computational results. It must be highlighted that the location of the fuel/air inlet boundary condition is essential as it highly affects the velocity profile at the nozzle exit. It was found that applying the fuel/air inlet boundary condition at the nozzle exit area leads to an overestimation in flame height and standoff distance.

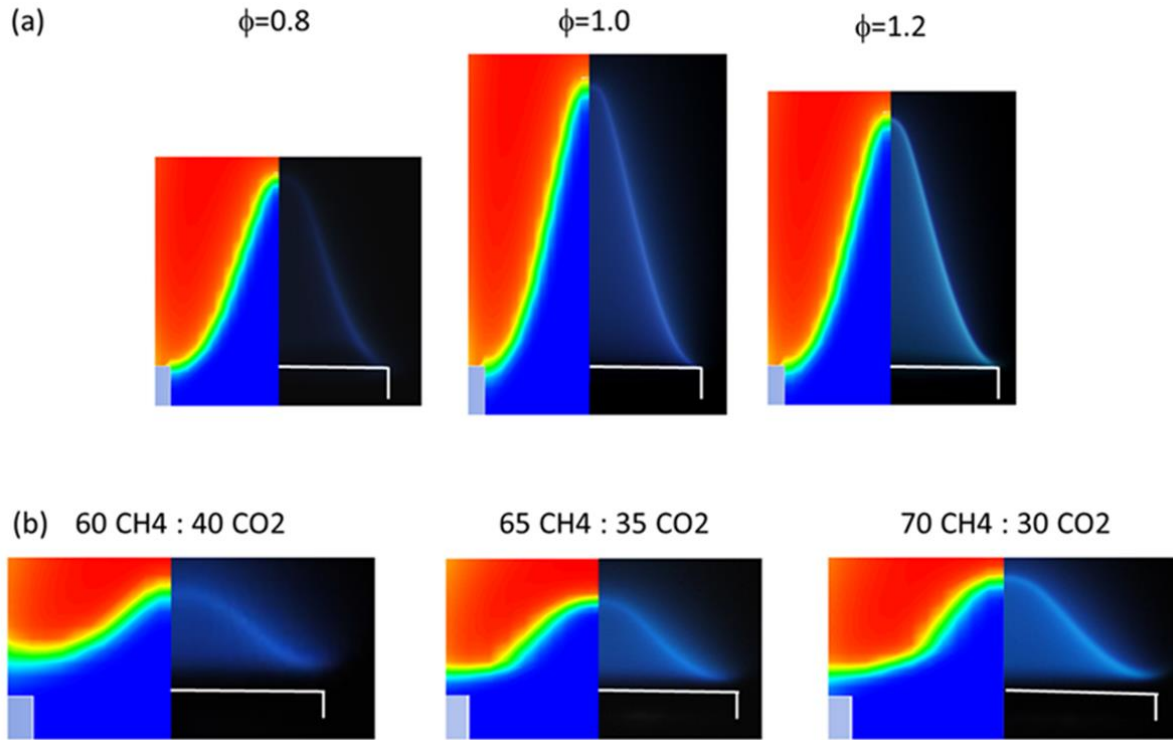


Figure 2-22: Comparison between numerical and experimental results: (a) CH₄/air mixtures at $\phi = 0.8$, 1.0 , and 1.2 (from left to right), (b) biogas/air mixtures at the stoichiometric condition ($\phi = 1.0$)

2.7. Conclusion

In the present study, the biogas mixtures with the CO₂ concentration of 30–40% were enriched by H₂ within the range of 0–40% by volume and preheated in the range of 298–440 K. Combustion characteristics, such as blowoff and laminar burning velocities, of these biogas/air flames were experimentally examined using the bunsen burner method. The computational results were obtained using the ANSYS Fluent with reduced GRI-Mech 3.0 chemical mechanism and compared with the experimental results of the premixed bunsen flames. The major conclusions of the study are as follows:

1. Blowoff velocity increases linearly with the increase of the 3. temperature. The improvements in blowoff velocity are indicated by the reduction in flame height as well as the shortening of standoff distance.
2. Blowoff and laminar burning velocities of biogas/air flames increase with the H₂ enrichment of the mixture. The relationship of blowoff velocity and H₂ addition is non-linear and attributed to the dominance of methane-inhibited hydrogen combustion process. The improvements in burning velocities are more apparent in the stoichiometric and rich fuels compared to lean mixtures. Additionally, the tip opening of the flame was observed with the H₂ concentration of 40% in the mixture irrespective of the jet velocity.
3. Laminar burning velocity decreases with the addition of CO₂ into the biogas/air mixture. The flame structure changes in terms of the brightness of the flame as well as the reduction in flame temperature. The dilution, chemical, and thermal effect of CO₂ addition on the laminar burning velocity of biogas/air mixture were quantitatively explained using fictitious species. Furthermore, the fuel samples with 30% of CO₂ (BG3) show a big difference in laminar burning velocity compared to BG1 (40%) and BG2 (35%).
4. The reduced GRI-Mech 3.0 chemical mechanism is suitable to simulate the premixed bunsen flames of biogas/air mixtures. The flame height and standoff distance, and the laminar burning velocity are in good agreement between the computational and experimental results. It is highlighted that setting the fuel/air inlet boundary condition at 70 mm upstream is required as applying the inlet boundary conditions at the nozzle exit leads to an overestimation of the results.

2.8. References

- [1] Hu Z, Zhang X. Experimental study on flame stability of biogas/hydrogen combustion. *Int J Hydrogen Energy* 2019;44:5607–5614.
- [2] Liu J, Zhang X, Wang T, Hou X, Zhang J, Zheng S. Numerical study of the chemical, thermal and diffusion effects of H₂ and CO addition on the laminar flame speeds of methane-air mixture. *Int J Hydrogen Energy* 2015;40:8475–8483.
- [3] Wei ZL, Leung CW, Cheung CS, Huang ZH. Effects of H₂ and CO₂ addition on the heat transfer characteristics of laminar premixed biogas–hydrogen Bunsen flame. *Int J Heat Mass Transf* 2016;98:359–366.
- [4] Mustafa İ, İlker Y. Experimental analysis of the effects of hydrogen addition on methane combustion. *Int J Energy Res* 2012;36:643–647.
- [5] Jeong P, Dong JH, June SP, Jeong SK, Sang IK, Han CC, Dong SN, Tae KK. Hydrogen utilization as a fuel: Hydrogen-blending effects in flame structure and NO emission behavior of CH₄–Air flame. *Int J Energy Res* 2007;31:472–485.
- [6] Esmail MAM, Yinka SS, Mohamed AH. Numerical study of hydrogen-enriched methane-air combustion under ultra-lean conditions. *Int J Energy Res* 2016;40:743–762.
- [7] Hu Z, Zhang X. Study on laminar combustion characteristic of low calorific value gas blended with hydrogen in a constant volume combustion bomb. *Int J Hydrogen Energy* 2019;44:487–493.
- [8] Zhen HS, Leung CW, Cheung CS. Effects of hydrogen addition on the characteristics of a biogas diffusion flame. *Int J Hydrogen Energy* 2013;38:6874–6881.
- [9] Leung T, Wierzbka I. The effect of hydrogen addition on biogas non-premixed jet flame stability in a co-flowing air stream. *Int J Hydrogen Energy* 2008;33:3856–3862.
- [10] Li Z, Cheng X, Wei W, Qiu L, Wu H. Effects of hydrogen addition on laminar flame speeds of methane, ethane and propane: Experimental and numerical analysis. *Int J Hydrogen Energy* 2017;42:24055–24066.
- [11] Yang SI, Wu MS. Properties of premixed hydrogen/propane/air flame in ceramic granular beds. *Int J Hydrogen Energy* 2014;39:17347–17357.
- [12] Sun HY, Yang SI, Jomaas G, Law CK. High-pressure laminar flame speeds and kinetic modeling of carbon monoxide/hydrogen combustion. *Proc Combust Inst* 2007;31:439–446.
- [13] Ma F, Wang Y, Liu H, Li Y, Wang J, Ding S. Effects of hydrogen addition on cycle-by-cycle variations in a lean burn natural gas spark-ignition engine. *Int J Hydrogen Energy* 2008;33:823–831.
- [14] Porpatham E, Ramesh A, Nagalingam B. Effect of hydrogen addition on the performance of a biogas fuelled spark ignition engine. *Int J Hydrogen Energy* 2007;32:2057–2065.
- [15] Schefer RW. Hydrogen enrichment for improved lean flame stability. *Int J Hydrogen Energy* 2003;28:1131–1141.
- [16] Natarajan J, Kochar Y, Lieuwen T, Seitzman J. Pressure and preheat dependence of laminar flame speeds of H₂/CO/CO₂/O₂/He mixtures. *Proc Combust Inst* 2009;32:1261–1268.
- [17] Robin JV, Harshal K, Vishnu H, Sudarshan K. Effect of CO content on laminar burning velocities of syngas-air premixed flames at elevated temperatures. *Fuel* 2018;214:144–153.

- [18] Ai Y, Zhou Z, Chen Z, Kong W. Laminar flame speed and Markstein length of syngas at normal and elevated pressures and temperatures. *Fuel* 2014;137:339–345.
- [19] Hu X, Yu Q. Effect of the elevated initial temperature on the laminar flame speeds of oxy-methane mixtures. *Energy* 2018;147:876–883.
- [20] Vladimir AA, Sergey SM, Ivan VC, Sergey GM. Laminar burning velocities of methylcyclohexane + air flames at room and elevated temperatures: A comparative study. *Combust Flame* 2018;196:99–107.
- [21] Amit K, Asad M, Minaev S, Sudarshan K. Measurement of laminar burning velocities of methanol–air mixtures at elevated temperatures. *Fuel* 2016;182:57–63.
- [22] Quintino FM, Fernandes EC. Analytical correlation to model diluent concentration repercussions on the burning velocity of biogas lean flames: Effect of CO₂ and N₂. *Biomass Bioenergy* 2018;119:354–363.
- [23] Xiang L, Chu H, Ren F, Gu M. Numerical analysis of the effect of CO₂ on combustion characteristics of laminar premixed methane/air flames. *J Energy Inst* 2018;92(5):1487–1501.
- [24] Wang J, Zhilong W, Senbin Y, Wu J, Yongliang X, Meng Z, Zuohua H. Effects of stretch and preferential diffusion on tip opening of laminar premixed Bunsen flames of syngas/air mixtures. *Fuel* 2016;148:1–8.
- [25] Zerrin T-R, Rajnish NS, Robert RR. Two-dimensional simulation of premixed laminar flame at microscale. *Chem Eng Sci* 2015;138:414–431.
- [26] Yasuhiro M, Taisuke N, Tadao T. Numerical study of tip opening of hydrogen/air Bunsen flame. *Proc Combust Inst* 2019;37:1775–1781.
- [27] Nonaka HOB, Pereira FM. Experimental and numerical study of CO₂ content effects on the laminar burning velocity of biogas. *Fuel* 2016;182:382–390.
- [28] Lackner M, Palotas AB, Winter F. *Combustion: From Basics to Applications*. 1st ed. Weinheim: Wiley-VCH, 2013.
- [29] Konnov AA, Mohammad A, Kishore VR, Kim NI, Prathap C, Kumar S. A comprehensive review of measurements and data analysis of laminar burning velocities for various fuel + air mixtures. *Prog Energy Combust Sci* 2018;68:197–267.
- [30] Bernard L, Guenther VE. *Combustion, Flames and Explosions of Gases*. 2nd ed. Pittsburgh, Pennsylvania: Academic Press, INC, 1961.
- [31] Pizutti L, Martins CA, Lacava PT. Laminar burning velocity and flammability limits in biogas: A literature review. *Renew Sust Energy Rev* 2016;62:856–865.
- [32] Kim GT, Kim NI. Laminar burning velocity predictions by meso-scale flames in an annularb diverging tube. *Fuel* 2011;90:2217–2223.
- [33] Kim NI, Maruta K. A numerical study on propagation of premixed flames in small tubes. *Combust Flame* 2006;146:283–301.
- [34] Alekseev VA, Christensen M, Berrocal E, Nilsson EJK, Konnov AA. Laminar premixed flat non-stretched lean flames of hydrogen in air. *Combust Flame* 2015;162:4063–4074.
- [35] Naucier JD, Nilsson EJK, Konnov AA. Laminar burning velocity of nitromethane + air flames: A comparison of flat and spherical flames. *Combust Flame* 2015;162:3803–3809.

- [36] Jayachandran J, Zhao R, Egolfopoulos FN. Determination of laminar flame speeds using stagnation and spherically expanding flames: Molecular transport and radiation effects. *Combust Flame* 2014;161:2305-2316.
- [37] Faghih M, Chen Z. The constant-volume propagating spherical flame method for laminar flame speed measurement. *Sci* 2016;61:1296-1310.
- [38] Zhen HS, Leung CW, Cheung CS, Huang ZH. Characterization of biogas-hydrogen premixed flames using Bunsen burner. *Int J Hydrog Energy* 2014;39:13292-13299.
- [39] Egolfopoulos FN, Hansen N, Ju Y, Kohse-Hoinghaus K, Law CK, Qi F. Advances and challenges in laminar flame experiments and implications for combustion chemistry. *Progr Energy Combust Sci* 2014;43:36–67.
- [40] Glassman I. *Combustion*. 3rd ed. San Diego, California, USA: Academic Press, 1996.
- [41] Powling J. A new burner method for the determination of low burning velocities and limits of inflammability. *Fuel* 1949;28:25-28.
- [42] Vu TM, Cha MS, Lee BJ, Chung SH. Tip opening of premixed bunsen flames: Extinction with negative stretch and local Karlovitz number. *Combust Flame* 2015;162:1614–1621.
- [43] Dong C, Zhou Q, Zhao Q, Zhang Y, Xu T, Hui S. Experimental study on the laminar flame speed of hydrogen/carbon monoxide/air mixtures. *Fuel* 2009;88:1858-1863.
- [44] Kim NI, Kataoka T, Maruyama S, Maruta K. Flammability limits of stationary flames in tubes at low pressure. *Combust Flame* 2005;141:78-88.
- [45] Kim NI, Do Lee U, Shin HD. Laminar premixed flame propagation using large axial velocity variation. *Proc Combust Inst* 2000;28:1867-1874.
- [46] Liu Z, Lee MJ, Kim NI. Direct prediction of laminar burning velocity using an adapted annular stepwise diverging tube. *Proc Combust Inst* 2013;34:755-762.
- [47] Liu Z, Kim NI. An assembled annular stepwise diverging tube for the measurement of laminar burning velocity and quenching distance. *Combust Flame* 2014;161:1499-1506.
- [48] Glassman I, Yetter RA. *Combustion*. 4th ed. San Diego, California, USA: Academic Press, 2008.
- [49] Botha JP, Spalding DB. The laminar flame speed of propane/air mixtures with heat extraction from the flame. *Proc Royal Soc London A Math Phy Sci* 1954;225:71-96.
- [50] Van Maaren A, Thung DS, De Goey LRH. Measurement of flame temperature and adiabatic burning velocity of methane/air mixtures. *Combust Sci Technol* 1994;96:327-344.
- [51] Bosschaart KJ, de Goey LPH. Detailed analysis of the heat flux method for measuring burning velocities. *Combust Flame* 2003;132:170-180.
- [52] Wang Z, Wang S, Whiddon R, Han X, He Y, Cen K. Effect of hydrogen addition on laminar burning velocity of CH₄/DME mixtures by heat flux method and kinetic modeling. *Fuel* 2018;232:729-742.
- [53] Konnov AA, Meuwissen RJ, de Goey LPH. The temperature dependence of the laminar burning velocity of ethanol flames. *Proc Combust Inst* 2011;33:1011-1019.

- [54] Rau F, Hartl S, Voss S, Still M, Hasse C, Trimis D. Laminar burning velocity measurements using the Heat Flux method and numerical predictions of iso-octane/ethanol blends for different preheat temperatures. *Fuel* 2015;140:10-16.
- [55] Knorsch T, Demmelmeyer M, Wensing M, Leipertz A. A novel heat flux burner system to determine the laminar flame velocity of liquid fuels. *Fuel Process Technol* 2013;107:119-125.
- [56] Alekseev VA, Naucier JD, Christensen M, Nilsson EJK, Volkov EN, de Goey LPH, Konnov AA. Experimental Uncertainties of the Heat Flux Method for Measuring Burning Velocities. *Combust Sci Technol* 2016;188:853-894.
- [57] Kuo KK. Principles of combustion. 2nd ed. John Wiley & Sons Ltd., 2005.
- [58] Liao SY, Jiang DM, Huang ZH, Zeng K, Cheng Q. Determination of the laminar burning velocities for mixtures of ethanol and air at elevated temperatures. *Appl Therm Eng* 2007;27:374-380.
- [59] Shu T, Xue Y, Zhou Z, Ren Z. An experimental study of laminar ammonia/methane/air premixed flames using expanding spherical flames. *Fuel* 2021;290:120003.
- [60] Chen Z, Burke MP, Ju Y. Effects of compression and stretch on the determination of laminar flame speeds using propagating spherical flames. *Combust Theory Model* 2009;13:343-364.
- [61] Tippa M, Subbiah S, Prathap C. Impact of chamber volume on the measurement of laminar burning velocity using constant volume spherical flame method. *Fuel* 2019;256:115936.
- [62] Faghih M, Chen Z. The constant-volume propagating spherical flame method for laminar flame speed measurement. *Sci Bull* 2016;61:1296-1310.
- [63] Simmons RF, Wolfhard HG. Some limiting oxygen concentrations for diffusion flames in air diluted with nitrogen. *Combust Flame* 1957;1:155-161.
- [64] Law CK, Ishizuka S, Mizomoto M. Lean-limit extinction of propane/air mixtures in the stagnation-point flow. *Symp (Int) Combust* 1981;18:1791-1798.
- [65] Dreyer JAH, Bringley EJ, Manuputty MY, Akroyd J, Kraft M. Temperature and CH* measurements and simulations of laminar premixed ethylene jet-wall stagnation flames. *Proc Combust Inst* 2021;38:2083-2091.
- [66] Williams FA. Combustion theory. 2nd ed. Redwoodcity, CA: Addison-Wesley, 1985.
- [67] Burrell RR, Zhao R, Lee DJ, Burbano H, Egolfopoulos FN. Two-dimensional effects in counterflow methane flames. *Proc Combust Inst* 2017;36:1387-1394.
- [68] Wang W, Karatas AE, Groth CPT, Gulder OL. Experimental and numerical study of laminar flame extinction for syngas and syngas-methane blends. *Combust Sci Technol* 2018;190:1455-1471.
- [69] Bergthorson JM, Sone K, Mattner TW, Dimotakis PE, Goodwin DG, Meiron DI. Impinging laminar jets at moderate Reynolds numbers and separation distances. *Phys Rev E* 2005;72:066307.
- [70] Bernard L, Guenther VE. Combustion, Flames and Explosions of Gases. 2nd ed. Pittsburgh, Pennsylvania: Academic Press, INC, 1961.

- [71] Munajat NF, Erlich C, Fakhrai R, Fransson TH. Influence of water vapour and tar compound on laminar flame speed of gasified biomass gas. *Appl Energy* 2012;98:114-121.
- [72] Hu X, Yu Q, Liu J, Sun N. Investigation of laminar flame speeds of CH₄/O₂/CO₂ mixtures at ordinary pressure and kinetic simulation. *Energy* 2014;70:626-634.
- [73] Wei L, Yong J, Yi J, Xianli Z. Investigation of the influence of DMMP on the laminar burning velocity of methane/air premixed flames. *Fuel* 2019;235:1294-1300.
- [74] Yi W, Bjorn R, Vincent M, Xilong Y, Linlin W, Frédéric G. Laminar flame speed of lignocellulosic biomass-derived oxygenates and blends of gasoline/oxygenates. *Fuel* 2017;202:572-582.
- [75] Vu TM, Won SH, Ombrello T, Cha MS. Stability enhancement of ozone-assisted laminar premixed Bunsen flames in nitrogen co-flow. *Combust Flame* 2014;161:917-26.
- [76] White FM. *Fluid Mechanics*. 4th ed. New York: McGraw-Hill, p. 331, 1998.
- [77] ANSYS, ANSYS Fluent 15.0 Theory Guide, Canonsburg, PA, 2013, pp. 2-4, pp. 133-5, pp. 187-8, pp. 289-90.
- [78] Batchelor GK. *An Introduction to Fluid Dynamics*. Cambridge: Cambridge Uni. Press, 2000.
- [79] Smith GP, Golden DM, Frenklach M, Moriarty NW, Eiteneer B, Goldenberg M, Bowman CT, Hanson RK, Song S, Gardiner WC, Lissianski Jr VV, Qin Z. GRI-MECH 3.0. Available at http://www.me.berkeley.edu/gri_mech/.
- [80] Ren Z, Goldin GM, Hiremath V, Pope BS. Simulations of a turbulent non-premixed flame using combined dimension reduction and tabulation for combustion chemistry. *Fuel* 2013;105:636-44.
- [81] Belcadi A, Assou M, Affad E, Chatri E. Construction of a reduced mechanism for modeling premixed combustion of methane-air. *Combust Theory Model* 2007;11:603-13.
- [82] Kuo KK. *Principles of Combustion*. 2nd ed. John Wiley & Sons, Inc., p. 732.
- [83] Cha MS, Son JW, Yoon SH, Luong HT, Deanna AL, Sohn CH. Vortex formation mechanism within fuel streams in laminar nonpremixed jet flames. *Combust Flame* 2019;199:46-53.
- [84] Nasreldin MM, Fuwu Y, Yu W. Effects of fuel inlet boundary condition on aromatic species formation in coflow diffusion flames. *J Energy Inst* 2018;92:288-97.
- [85] Lowry W, de Vries J, Krejci M, Petersen E, Serinyel Z, Metcalfe W, Curran H, Bourque G. Laminar flame speed measurements and modeling of pure alkanes and alkane blends at elevated pressures. *J Eng Gas Turbines Power* 2011;133(9):091501-9.
- [86] Hassan MI, Aung KT, Kwon OC, Faeth GM. Properties of laminar premixed hydrocarbon / Air flames at various pressures. *J Propuls Power* 1998;14:479-488.
- [87] Rozenchan G, Zhu D, Law C, Tse S. Outward propagation, burning velocities, and chemical effects of methane flames up to 60atm. *Proc Combust Inst* 2002;29:1461-1470.
- [88] Park O, Veloo PS, Liu N, Egolfopoulos FN. Combustion characteristics of alternative gaseous fuels. *Proc Combust Inst* 2011;33:887-894.

- [89] Hu X, Yu Q, Liu J, Sun N. Investigation of laminar flame speeds of CH₄/O₂/CO₂ mixtures at ordinary pressure and kinetic simulation. *Energy* 2014;70:626–634.
- [90] Erjiang H, Zuohua H, Jiajia H, Chun J, Jianjun Z. Experimental and numerical study on laminar burning characteristics of premixed methane–hydrogen–air flames. *Int J Hydrogen Energy* 2009;34:4876–4888.
- [91] Jun L, Hongyu H, Noriyuki K, Zhaohong H, Yoshihiro N. Study on using hydrogen and ammonia as fuels: Combustion characteristics and NO_x formation. *Int J Energy Res* 2014;38:1214–1223.
- [92] Kanury AM. *Introduction to Combustion Phenomena*. New York: Breach Science Publishers, 1975.
- [93] Jinhua W, Zhilong W, Senbin Y, Wu J, Yongliang X, Meng Z, Zuohua H. Effects of stretch and preferential diffusion on tip opening of laminar premixed Bunsen flames of syngas/air mixtures. *Fuel* 2015;148:1–8.
- [94] Chen Z, Tang C, Fu J, Jiang X, Li Q, Wei L, Huang Z. Experimental and numerical investigation on diluted DME flames: Thermal and chemical kinetic effects on laminar flame speeds. *Fuel* 2012;102:567–573.
- [95] Liu F, Guo H, Smallwood GJ. The chemical effect of CO₂ replacement of N₂ in air on the burning velocity of CH₄ and H₂ premixed flames. *Combust Flame* 2003;133:495–497.
- [96] Xiang L, Chu H, Ren F, Gu M. Numerical analysis of the effect of CO₂ on combustion characteristics of laminar premixed methane/air flames. *J Energy Inst* 2019;92:1487–1501.
- [97] Glarborg P, Bentzen LLB. Chemical Effects of a High CO₂ Concentration in Oxy-Fuel Combustion of Methane. *Energy Fuel* 2008;22:291–296.
- [98] Galmiche B, Halter F, Foucher F, Dagaut P. Effects of Dilution on Laminar Burning Velocity of Premixed Methane/Air Flames. *Energy Fuel* 2011;28:948–954.
- [99] Carlos DG, Arrieta AA, Suárez JL. Comparison of combustion properties of simulated biogas and methane. *C.T.F Cienc. Tecnol. Futuro* 2009;3:225–236.
- [100] Lee K, Kim H, Park P, Yang S, Ko Y. CO₂ radiation heat loss effects on NO_x emissions and combustion instabilities in lean premixed flames. *Fuel* 2013;106:682–689.

3. Combustion characteristics of pre-vaporized palm oil biodiesel/air premixed flames

It must be highlighted that some parts of Chapter 3 were used to prepare the manuscript [A3] on the combustion behavior of premixed biogas/air flames. The work has successfully been published in Fuel Communications.

3.1. Introduction

The primary use of traditional fossil fuels in agriculture, manufacturing as well as transportation applications has led to the apparent concerns of fuel supply capacity. Furthermore, the combustion of fossil fuels produces a large amount of greenhouse, which, in turn, directly influences the rate of climate change [1]. Thus, there is a demand for developing alternative fuels that can replace or supplement the existing hydrocarbon based fuels. One of the ways to reduce emission production is to employ cleaner combustion. In this regard, the studies [2, 3] showed that biodiesel fuels can be considered as one of the most promising renewable and sustainable solutions. The results of the SWOT (Strength, Weakness, Opportunities, and Threats) analysis, conducted by Semwal et al. [4], showed that biodiesel fuels possess higher cetane number resulting in a better quality of ignition, the lack of aromatics and sulphur content resulting in a lower soot emission, cleaner combustion, and better biodegradability compared to traditional fossil fuels. Another factor that makes biodiesel fuels highly competitive, among all the available alternatives, is the similarity in the fuel and combustion properties with diesel fuels. On that note, the existing literature [5] has shown that the blends between diesel and biodiesel fuels can be obtained without the participation of any blending agents. Hence, biodiesel fuels can be used in the application of internal combustion

engines with no or slight modifications in the current designs. There is also no inherent danger or complexity in the storage and handling processes of biodiesel fuels. Furthermore, biodiesel fuels can be obtained from a variety of feedstock sources such as vegetable oils (palm, soybean, and canola) and animal fats via the transesterification process [6].

It is a growing belief that B100 (pure biodiesel fuel) can become the primary fuel in engine applications due to its environmental benefits. The results from the experimental investigations [7-9] of using biodiesel fuels in diesel engines showed a reduction in smoke density. This observation was similar in behavior regardless of the feedstock used, as one group [7] used the biodiesel derived from soybean, whereas the other group [8] derived the fuel from rapeseed. However, it is important to note that there are some instances [10] where the increase in smoke density was observed while operating with biodiesel derived from karanja. In terms of the power generated from the combustion of biodiesel fuels, the results [5,7-12] are mixed. This observation can be associated with the type of engine used for the testing (various engine designs), injection timing (fuel delivery), engine operations load, etc. While the absolute values may differ based on the feedstock and experimental conditions, the use of biodiesel fuels in diesel engines generally results in the reduction of CO, PM, and HC but cause a slight increase in NO_x emissions [5].

Despite all these positive findings, there are still some disadvantages of using biodiesel fuels compared to traditional fossil fuels. Some of the most glaring flaws of biodiesel fuels are the lower heat content as well as the mediocre spray characteristics. In addition to that, as mentioned earlier, biodiesel fuels can result in, overall, cleaner combustion by reducing the soot, particulate matter production, CO, and CO₂ emissions. However, the studies [13,14] showed that the use of biodiesel can, at times, increase the production of NO_x in diesel engine applications.

It is worth noting that biodiesel fuel is among the top alternative fuels not only for its cleaner combustion but also for its availability due to its wide range of feedstocks. One of the most commonly used feedstocks in the production of biodiesel is palm oil due to its abundance, cost efficiency, and high oil yield content [15]. Chong et al. [16] performed an experimental investigation to assess the effect of pure palm oil biodiesel fuel on the engine performance using a 4-stroke direct injection diesel engine at the operating speed of 2000-3000 rpm and brake mean effective pressure of 3 bar. The results revealed that the thermal efficiency was improved due to the enhanced combustion resulting from extra oxygen molecules available in biodiesel fuels. In contrast, biodiesel fuels resulted in a higher brake specific fuel consumption due to the lower heating value compared to fossil diesel fuels. It was also reported that the use of palm oil biodiesel reduced the production of CO and HC emissions while increased the production of NO_x. This behavior was in agreement with the findings of other research groups [17,18] that conducted experimental studies on the combustion of palm oil biodiesel fuels. Furthermore, in the work of Ozsezen and Canakci [19], combustion and injection characteristics of biodiesel, derived from waste palm oil, were experimentally studied using the six cylinder diesel engine. The shorter ignition delay, observed in the study, was attributed to the higher cetane number and rapid gasification of palm oil biodiesel fuels.

In the process of understanding the behavior of fundamental combustion characteristics of palm oil biodiesel fuels, it is essential to study the fuels in both premixed and non-premixed states. In this chapter, it is of interest to study the behavior of laminar premixed flames of palm oil biodiesel/air flames. In contrast, Chapter 4 will focus on the combustion behavior of non-premixed palm oil biodiesel flames. Any homogeneous mixture where the fuel and oxidizer are mixed together prior to the ignition (combustion) can be categorized as the premixed mixture. One of the most well known experimental configurations of studying the premixed flames, which is also used in the present study, is the coflow bunsen burner. By carefully

choosing the appropriate diameter of the nozzle as well as its length, it is possible to achieve laminar premixed flames of fuel/air mixture. This, in return, enables the studies of laminar burning velocity, blowoff velocity, flammability limits, and bunsen flame tip opening, etc.

3.2. Literature review on nano-additives

As it has been explained above, biodiesel fuels are among the top contenders to be the alternatives for the traditional fossil fuels. While the existing literature [5-19] shows a great potential of biodiesel fuels, it is essential to note that traditional fuels such as natural gas, petrol, and diesel possess higher heating values, faster combustion rates, and better stability of a flame. Hence, the enhancement methods of biodiesel fuels became one of the fast growing areas of interest [20].

Fuel enrichment is one of the most widely accepted methods of altering the fuel combustion properties in order to improve the performance characteristics of engines without modification in design. Over the past decade, there has been an increasing interest in the application of various nano-particles as an additive to biodiesel fuels [21-30]. These studies showed that nano-additives could, in fact, enhance combustion parameters, overall engine efficiency, reduce fuel consumption, and lower the production of harmful exhaust emissions as well as the change in some of the fuel properties such as viscosity, flash point, etc. It is essential to note that there are different classes of nano-additives such as metal-based, metal-oxide-based, magnetic nano-fluids, nano-organic additives, carbon-based, as well as mixed nano-particles [22,24]. The interest of the current research, on the investigation of the fundamental combustion characteristics of nanoparticle blended biodiesels, was primarily triggered by the works conducted by these research groups led by Khond and Kriplani [31] and Manzoore [32]. They carried out a comprehensive review on the impact of various nano-additives in diesel-

biodiesel fuel blends using a CI engine. They showed that the presence of metallic or oxygenated nano-additives resulted in the reduction of UBHC, CO, and PM due to the improved combustion and ignition parameters. However, some nano-additives such as magnetic nanofluids caused the opposite behavior in the case of CO production [33]. Furthermore, while the metal-based nano-additives reduced some of the properties such as the viscosity, density, and flashpoint of the fuel blends, they have also negatively impacted engine performance parameters such as brake thermal efficiency and brake specific fuel consumption due to their cooling effect. In both independent research studies [31,32], it was highlighted that carbon-based nanotubes showed very promising results in terms of both emission reduction and engine performance. Sivakumar et al. [21] and Venu and Madhavan [25] showed a reduction in the brake specific fuel consumption (BSFC), improvement in the brake thermal efficiency, and reduced concentrations of oxides of nitrogen (NO_x), unburnt hydrocarbon (UHC), and carbon monoxide (CO) productions with the addition of aluminum oxide (Al₂O₃) to the fuel. It was also reported that similar behavior was observed by Sajith et al. [26] and Vairamuthu et al. [27] when cerium oxide (CeO₂) nanoparticles were used as a fuel additive. Manigandan et al. [23] and Chen et al. [28] conducted comparative studies between various nano-additives and, in contrast, showed that carbon nanotubes (CNTs) could provide a different effect as compared to other nano-particles due to their properties such as free metal compound nature, higher energy density, and higher thermal conductivity. While the majority of nano-particles resulted in the lower production of UHC, CO, and carbon dioxide (CO₂) emissions, Chen et al. [28] showed that the addition of CNTs to diesel fuel led to a reduction of NO_x concentration and an increase in UHC, CO, and CO₂ emissions. However, it was also highlighted that the engine load also influenced the behavior of emission production. In addition, Ghanbari et al. [29] experimentally showed that the engine's brake power and torque were increased while decreasing the BSFC at any load, with the addition of CNTs to the fuel.

Najafi [30] conducted an experiment to analyze the changes in the combustion behavior of CNTs blended diesel and biodiesel mixtures. The results revealed that CNTs blended fuels experienced a shorter ignition delay, lower pressure in the cylinder, and faster heat release rate. These findings were attributed to the catalytic nature of CNTs, which acted as an agent accelerating fuel combustion reaction. While the studies mentioned above claim the benefits of nano-additives on the combustion of fuels, it is apparent to conclude that all the experiments were conducted to merely assess the performance of engines rather than understanding the fundamental combustion characteristics of CNTs added fuels, creating the knowledge gap in this research area.

As mentioned earlier, most nano-additives can be categorized under one of the following classes of nanoparticles, namely, metal-based, metal-oxide-based, magnetic nano-fluids, nano-organic additives, carbon-based, as well as mixed nano-particles. Understanding nanoparticles and their role as additives in various liquid fuels have drawn significant attention in the combustion research field. The following subchapters (3.2.1-3.2.5) intend to provide some of the latest updates and a brief literature review of the various categories of nano additives.

3.2.1. Metal-based nanoparticles

In recent years, metal-based nano-additives were employed to promote the combustion of various liquid fuels due to their catalytic and superparamagnetic nature, high energy release and reactivity, ignition promotion, and low temperature requirement for the thermal sintering [22]. There have been several studies [32,34,35] that investigated the effect of various metal-based nano-additives to achieve complete combustion, improve fuel consumption, and reduce the production of harmful emissions. These studies were performed using the laboratory-scaled experimental configurations and different nanoparticles such as aluminum, iron, boron, and

ferric chloride. While Abdali [36] performed an experimental investigation to study the combustion behavior and ignition characteristics of aluminum nano-additives blended diesel and biodiesel fuels, Mehregan and Moghiman [37] conducted a computational study on the emission production, and combustion characteristics of aluminum nanoparticles blended liquid fuels. Abdali [36] used the ultrasonic bath in order to improve the mixing between the fuels and the nanoparticles. It was highlighted that the properties of the final mixture were influenced by the mechanism of mixing, such as the duration of ultrasonication, frequency, and power rating. Abdali [36] sonicated the samples at least for 30 minutes at 45 kHz and 140 watts of power rating. Furthermore, no surfactants were used in the fuel mixture preparation process to avoid the secondary influence of surfactants on combustion behavior. The experiments were conducted using the static constant volume (bomb) calorimeter to measure the heat release during the combustion process and the hot plate setup to investigate the ignition probability of various fuel mixtures. The results showed that there is an almost 44% increase in ignition probability with the addition of 0.5% (by volume) of aluminum nano-additives into the fuel mixtures. The author also concluded that the reduction in the evaporation time of the nanoparticles blended fuel mixtures can suggest that aluminum nano-additives can favorably influence the ignition delay. Mehregan and Moghiman [37] performed a numerical study on the combustion behavior of ethanol and n-decane with the addition of 2.5 % (by volume) aluminum nano-additives. The study revealed that nanoparticles in the fuel mixtures reduced droplet evaporation rate and resulted in a lower flame temperature for both ethanol and n-decane. Furthermore, it was shown that the production of NO_x was reduced, which can be associated with the reduction in flame temperature. Mehregan and Moghiman [37] also stated that the aluminum nano-additives improved the overall combustion of the liquid fuels, which led to the reduction in CO emission.

Kannan et al. [38] found that some engine performance parameters such as brake specific fuel consumption and brake thermal efficiency can be improved with the addition of ferric chloride nano-additives into biodiesel fuel mixtures at specific operating conditions. The authors attributed these changes in engine performance to the catalytic nature of the nanoparticles, which can promote complete combustion in an engine. The experimental investigation was performed using the single cylinder, direct injection diesel engine, which was capable of generating 5.2 kW of power at a constant speed of 1500 rpm. Metal-based nano-additives were added to 100 ml of biodiesel at a dose ranging from 0.01 to 0.2 g. The mixture was stirred for 30 minutes via a magnetic stirrer and checked for the homogeneity and long term stability of the mixture. Other metal-based nano-additives such as iron and boron also show promising results, as shown by the work of Mehta et al. [39]. These nanoparticles were blended with diesel fuel and tested with a single cylinder CI engine. The results showed that the presence of these metal-based nano-additives led to an increased evaporation rate, which can be an indicator of reduced ignition delay.

3.2.2. Metal-oxide-based nanoparticles

Based on the existing literature, there is a wide range of available metal-oxide-based nanoparticles, namely aluminum oxide, silicon dioxide, cerium oxide, titanium dioxide, zinc oxide, manganese oxide, copper oxide, etc. All these nanoparticles have been extensively researched as potential fuel additives in order to improve the combustion characteristics and reduce the production of harmful pollutants.

Kalaimurugan et al. [40] performed an experimental investigation of the effect of cerium oxide on the combustion behavior of diesel-biodiesel blends. The study was performed using a single cylinder air-cooled engine, and the concentration of cerium oxide in the mixture

was varied from 25 to 100 ppm. The results revealed that net heat release rate and in-cylinder pressure are both recorded higher for the fuel blends with the addition of cerium oxide as compared to baseline diesel biodiesel blends. This behavior was associated with the high surface to volume ratio property of nano-additives which can promote the combustion rate. Furthermore, upon the closer investigation of the engine, it was revealed that the nanoparticles blended fuels resulted in a reduced carbon deposit on the cylinder walls. Chen et al. [28] used a single cylinder diesel engine in order to study emissions production and combustion characteristics of diesel fuels enriched with the nano-additives such as silicon oxide and aluminum oxide. The concentration of nanoparticles in fuel blends were varied from 25 to 100 ppm, with pure diesel being the baseline fuel in this experimental study. The results showed that both aluminum oxide and silicon oxide improved the overall performance of the engine via improved thermal efficiency and reduced brake specific fuel consumption compared to the baseline diesel fuel. However, based on the direct comparison of the recorded data between these two nanoparticles blended fuels, it is clear to note that silicone oxide blends result in better combustion characteristics such as CO emission production, in-cylinder pressure from the combustion, and lower brake specific fuel consumption. Another commonly known metal-oxide-based nano-additive is titanium oxide. EL-Seesy et al. [41] studied the combustion and emission characteristics of diesel biodiesel blends with the addition of titanium oxide nanoparticles into the fuel mixture. The experimental investigation was conducted using a single cylinder direct injection diesel engine, and the concentrations of nanoparticles in the mixture were set at 25 and 50 mg/L. It was shown that there was a slight increase in the peak pressure and heat release rate with the presence of titanium oxide nano-additives in the mixture. These behaviors were attributed to the fact that titanium oxide promoted combustion initiation and resulted in shorter ignition delay. Furthermore, there was a noticeable reduction in CO and UHC emissions by about 30% and 50%, respectively, while the NO_x production was increased.

The authors highlighted that the presence of nanoparticles did not have any negative influence on the engine components and engine performance. However, it was recognized that this conclusion could not be fully finalized without a long-term inspection. Selvaganapthy et al. [42] used zinc oxide as a nano additive at very high concentrations, such as 250 and 500 ppm, to study the change in combustion characteristics due to the presence of nanoparticles in fuel blends. The results revealed a similarity in general combustion characteristics behavior to the results generated using other metal-oxide-based nanoparticles. Those behaviors include the reduction in ignition delay, higher heat release rate, improved thermal efficiency and increased in-cylinder peak pressure, etc.

Based on the existing literature, it is clear to note that metal-oxide-based nanoparticles can result in a substantial reduction of harmful pollutants. One of the ways, how the presence of metal-oxide-based nano-additives can reduce the formation of unwanted emission species, is the formation of OH radicals due to a reaction between metals and water vapor. This, in return, leads to a process of improved soot oxidation which reduces the soot formation [43]. Another potential reason can be associated with the catalytic nature of metal oxides, which can reduce the oxidation temperature during the reaction with carbon atoms [22]. Hence, the oxidation can be improved for the process of conversion from CO to CO₂, which in return leads to reduced production of CO emission.

The results from the existing literature show that the improvement of combustion characteristics, as well as the reduction of harmful pollutants, can be achieved with the addition of metal-oxide-based nanoparticles into the fuel mixtures. Despite knowing that these metal nanoparticles are considered very harmful to human health, it is clear to note that the vast majority of existing literature neglected the possibility for the presence of metal nanoparticles deposit in the exhaust. In the future, the studies should also focus on the long-term performance of engines with metal-oxide-based nano-additives.

3.2.3. Magnetic nanofluids

Nanoparticles were experimentally found to be quite promising in the improvement of combustion characteristics as well as the reduction of emissions production. The literature findings [44] show that the specific property of nano-additives such as high surface to volume ratio improves the mixing between the fuel and oxidizer, and in return, promotes the combustion rate. Furthermore, the presence of nano-additives in the fuel mixture tends to influence the time scale of chemical reactions and the thermophysical properties of the fuel mixture. However, it must be noted that while these benefits were observed across multiple studies [24,32,33,42,45], the stability of these nanoparticles was always a concern. On that note, there is a growing interest in using ferrofluids as additives in liquid fuels. Ferrofluids are technically suspended nano-sized ferromagnetic (or ferrimagnetic) particles in a liquid medium. These fluids are known to respond upon the application of a magnetic field. One of the distinct differences between the ferrofluid additives and other metal, metal-oxide-based nanoparticles is the improved stability of the nanofluids in a homogeneous mixture.

Shafii et al.[33] conducted one of the earliest studies to show the influence of ferrofluids on the combustion characteristics of liquid fuels using a diesel engine. During the preparation of nanofluid fuel blends, it was revealed that the magnetic particles did not agglomerate nor experienced phase separation. Furthermore, the study results showed a noticeable improvement in thermal efficiency and reduction in brake specific fuel consumption. In more recent years, Devarajan et al. [46] performed an experimental investigation on the effect of magnetic nanofluids on engine performance, combustion characteristics, and neat biodiesel emission production derived from mahua oil. In that experimental study, the size of magnetites was 14 nm, and the fuel blend included 1% ferrofluid and 0.3% surfactant by volume. The analysis of the results revealed that the addition of magnetic nanofluids into the neat biodiesel led to 5.27% improvement in brake thermal efficiency and 5.37% decrease in brake specific fuel

consumption. Furthermore, ferrofluids resulted in a reduction of emissions such as CO, HC, and NO_x. The same behavior of combustion characteristics and emission production was recorded by Ramanan et al. [47], who studied the effect of magnetite nanofluids on the combustion of methyl ester.

While these studies show the promising aspect of using magnetic nanofluids, it is essential to highlight that most of the existing studies are very similar in their experimental conditions. More studies are required to understand the effect of various concentrations of magnetic particles in the mixture, sensitivity towards the experimental conditions such as pressure and temperature variation, etc.

3.2.4. Organic nanoparticles

Up to date, the studies on the effect of organic nanoparticles on combustion characteristics are very scarce. Yang et al. [48] were the first to treat nano organic particles as nano-additives in order to influence the combustion behavior of liquid fuels. In their experimental study, glycerin was used as an additive and blended with water diesel emulsion. The authors suggest that the presence of nano organic particles in the mixture led to micro explosion phenomena, which in return increased the fuel evaporation rate, improved the fuel and oxidizer mixing, and promoted the combustion rate. Furthermore, the analysis of the results revealed that the brake thermal efficiency was improved by approximately 14% compared to the baseline diesel fuel. However, it should be noted that due to the process of intellectual protection, the authors could not reveal the process of mixing nano organic particles with the baseline fuel nor reveal the concentrations used in the experiment. This work was followed up by different research group [49], also led by Yang, where polyethoxyester was used as a nano additive. The results showed a similar behavior as the findings from the previous work. Brake

thermal efficiency was improved, while the engine power and generated torque were reduced. In recent years, Mohsen et al. [50] conducted an experimental study to assess the engine performance of biodiesel fuel with the addition of nano organic particles. Like Yang et al. [48], Mohsen et al. [50] used glycerin as a nano organic additive, and tested the fuel mixtures in a diesel engine. However, in this study, the nano organic additive was also compared to carbon-based and metal-oxide-based nano-additives. The results showed some contradicting behavior compared to findings from Yang et al. [49]. Mohsen et al. [50] found that the addition of 3% (by volume) glycerin into the fuel mixture reduced the brake thermal efficiency by 6.6 %. However, compared to carbon-based and metal-oxide-based nano-additives, nano organic particles reduced the smoke opacity, CO, and NO_x emissions.

Out of all the nano-additive classes, the information available on nano organic particles is very limited. Hence, more studies are required to make any definitive conclusions on the effectiveness of nano organic particles as fuel additives.

3.2.5. Mixed nano-additives

While metal-based, metal-oxide-based, carbon-based, and magnetic nano-additives are all extensively researched, there is very limited literature on the potential of mixed nano additives in improving the combustion characteristics. One of the earliest attempts to mix various types of nanoparticles in a fuel mixture was made by Basha and Anand [51]. The experimental study was conducted using a diesel engine, and the baseline fuel (biodiesel) was blended with a mixture of aluminum oxide and carbon nanotubes. The authors showed that the brake thermal efficiency and the combustion rate of biodiesel were improved with mixed nano-additives. The high surface to volume ratio and the high heat conductivity of the nano-additives led to the shortening of ignition delay and increased heat transfer rate. Furthermore, the

combination of different types of nanoparticles resulted in changes in some thermophysical properties of the fuel mixture. One of the most recent studies related to the effect of mixed nano-additives on the performance of an engine was carried out by Vali et al. [52]. Unlike Basha and Anand [51], Vali et al. [52] combined two nanoparticles of the same class (metal oxides), namely aluminum oxide and titanium oxide additives. In this study, diesel-ethanol was blended with mixed nano-additives at the concentration of 50 and 100 ppm. The results showed noticeable improvements in the engine performance parameters such as brake thermal efficiency and brake specific fuel consumption with an increasing concentration of mixed nano-additives. Furthermore, the emissions such as CO, UBHC, and NO_x were continuously reduced with the higher content of nanoparticles in the mixture. It can be noted that these improvements are more noticeable at the higher loads of the engine.

Despite these findings, it is clear to conclude that the knowledge on the use of mixed nano-additives is still at its early stages, and more studies are required.

3.3. Carbon-based nanoparticles

Among all the previously discussed nanoparticles, it can be noted that the addition of metal and metal-oxide-based nano-additives showed the most promising improvement in both engine performance and emission production. However, the stability of a homogeneous mixture and the potential deposit of toxic metal particles in the exhaust gas are the main challenges of utilizing the metallic nano-additives for fuel enrichment purposes. In contrast, magnetic nanofluids showed promising results in stable mixing between the nano-additives and baseline fuel. However, similar to nano organic and mixed nano-additives, there is limited information on the effect of magnetic nanofluids on the combustion characteristics of various

fuels. Hence, more studies are required to make any definitive conclusions on the effectiveness of these nano additives.

One other type of nanoparticles that can become an effective additive to fuels is carbon-based nanoparticles. It was reported that there are also some challenges regarding the stability of the mixture with the addition of carbon-based nanoparticles [24,32]. However, these nano-additives have the potential to result in much cleaner and efficient combustion due to their free metal compound nature, high energy density, high surface-to-volume ratio, and high thermal conductivity. One of the most widely known carbon-based nanoparticles is carbon nanotubes, also famously named the “Wonder material of the 21st century” [53]. There are two main carbon nanotubes types depending on the number of layers present in the structure, namely singlewalled carbon nanotubes and multiwalled carbon nanotubes. As the name suggests, SWCNTs consist of a single layer of the graphene sheet, whereas MWCNTs have multilayers of graphene sheets in the structure. The attention towards carbon nanotubes has increased over the last decade due to the potential usage of these nanoparticles in a wide range of applications across various engineering fields [24,54,55]. In terms of engine applications, Hosseini et al. [56] performed an experimental investigation on the effect of carbon nanotubes on the combustion characteristics of diesel-biodiesel blends. The study was conducted using a single cylinder CI engine and CNTs with concentrations of 30, 60, and 90 ppm in the fuel mixture with the diameter of nanotubes ranging from 10 to 20 nm. The authors implied that the nano-additives blended mixture were prepared employing the ultrasonication process, and with no addition of surfactants. Engine power and torque generated have improved with increasing concentration of nanoparticles in the mixture. Furthermore, the addition of carbon nanotubes reduced CO and UHC production but resulted in elevated production of NO emission. Basha and Anand [57] carried out one of the early studies related to the effect of MWCNTs on engine performance. The experimental investigation was performed using a single cylinder diesel

engine to study the combustion characteristics of varying concentrations of carbon nanotubes blended water diesel emulsion fuels. The results showed that there are improvements in both brake thermal efficiency as well as brake specific fuel consumption. These improvements are associated with the thermal properties of CNTs, such as high thermal conductivity and high calorific value. Multiple other research groups further supported these claims by varying the operational conditions, using the different base fuels, changing the engine configurations and CNTs concentrations [28-30,56-67]. Najafi [30] conducted an experiment to analyze the changes in combustion activities such as cylinder pressure, heat release rate, and ignition delay of nano-additives blended in diesel and biodiesel mixtures. The author concluded that with the presence of CNTs in the fuel, the ignition delay was shortened by almost 9%. This can be associated with the increased cetane number of the CNTs blended fuel, as cetane number can be addressed as the indicator of the combustion speed. Moreover, it was shown that the heat release rate is improved with the addition of nanoparticles due to the improved mixing of fuel and oxidizer in the mixture. Consequently, the peak pressure was increased, which led to stronger power stroke and better combustion. Appendix B can be referred to view the tabulated summary of the literature review on the effect of carbon nanotubes (both single and multiwalled) on engine performance and emission production.

As explained before, the laminar burning velocity, blowoff velocity, flammability limits, and emissions production are amongst the main fundamental combustion characteristics of fuels. These parameters are essential in understanding the fuel behavior in various practical applications such as internal combustion engines, gas turbines, industrial furnaces, and as data in the development of kinetic mechanisms [68]. As such, many studies have been conducted to measure the laminar burning velocity of gaseous fuels over a wide range of equivalence ratios, ϕ , at different pressures [69] and temperatures [70], using various methodologies [71]. However, regarding liquid fuels, the vast majority of the existing literature is focused on single

component hydrocarbon fuels [72-78]. Even though the existing literature has shown an increasing interest in biodiesel fuels, there are limited data, both experimental and numerical, on the fundamental combustion characteristics such as laminar burning velocity. The lack of such data can be attributed to the complexity of the fuel structure and variability of the composition, depending on the feedstock sources. In the case of laminar premixed flame, blowoff velocity is another important parameter from which the critical burning limits of a given fuel can be analyzed. Furthermore, knowing the limits of flame stability is crucial in preventing potential system failures due to re-ignition behavior in applications such as low emission gas turbines.

Although the potential benefits of carbon-based nano-additives have drawn a lot of attention, it can be noticed that the current knowledge is mainly limited to compression ignition engine applications. In addition to that, data on the fundamental combustion characteristics of palm oil biodiesel flames, such as laminar burning velocity and blowoff velocity, are still scarce. In this regard, the present study focused on investigating the fundamental combustion characteristics of pre-vaporized palm oil biodiesel premixed flames with and without the addition of multi-walled carbon nanotubes, MWCNTs. The present study results could provide an adequate set of data on MWCNTs blended palm oil biodiesel and pure palm oil biodiesel, which can be helpful in practical applications and the development of kinetic mechanisms.

3.4. Experiment

A detailed schematic of the present setup is illustrated in Figure 3-1. The overall system consisted of a coflow burner, a syringe pump (NE-300) that delivered the liquid fuel to a stainless steel supply line wrapped with heating ropes (Omega, FGR-060). The temperature of the heating ropes was controlled by a variable autotransformer variac and measured via

thermocouples, TC₁₋₃ (Omega, SA3-K-72), at multiple locations to ensure the desired temperature. The temperatures measured by TC₁₋₃ were displayed by a temperature readout unit (midi Logger GLB20). The setup also included two mass flow controllers (MKS, 1179 A) and a readout controller (MKS, 247D 4 channel) to deliver the air and nitrogen coflow to the system. The mass flow controllers were calibrated using a dry-test gas meter (Bios, Definer 220M) to improve the accuracy of the experiment. The central nozzle of the coflow burner was made of a stainless steel tube with an inner diameter of 7.55 mm and a thickness of 1 mm. The length of this tube was set to be over 500 mm in order to achieve a fully parabolic velocity profile at the nozzle rim [70]. It should be noted that the coflow gas is supplied to the burner independently from the mainstream fuel/air premixed mixture. As such, it is possible to maintain the same flow rate of the coflow gas for all the velocity conditions of fuel/air mixture in the experiment. To stabilize a premixed flame while preventing secondary diffusion flame development, nitrogen gas was employed as a coflow gas and set at 10 cm/s for all the experimental conditions. Based on the existing literature [70,71], it was shown that the impact of a coflow velocity is negligible on the measurement of laminar burning velocity. Since the boiling temperature of the palm oil biodiesel is 483 K, the liquid fuel was preheated and mixed with air at a constant temperature of 550 K in the system to ensure complete vaporization. The stainless steel supply line and burner were insulated by ceramic wool to minimize the heat loss to the environment and avoid any potential condensation of vaporized fuel.

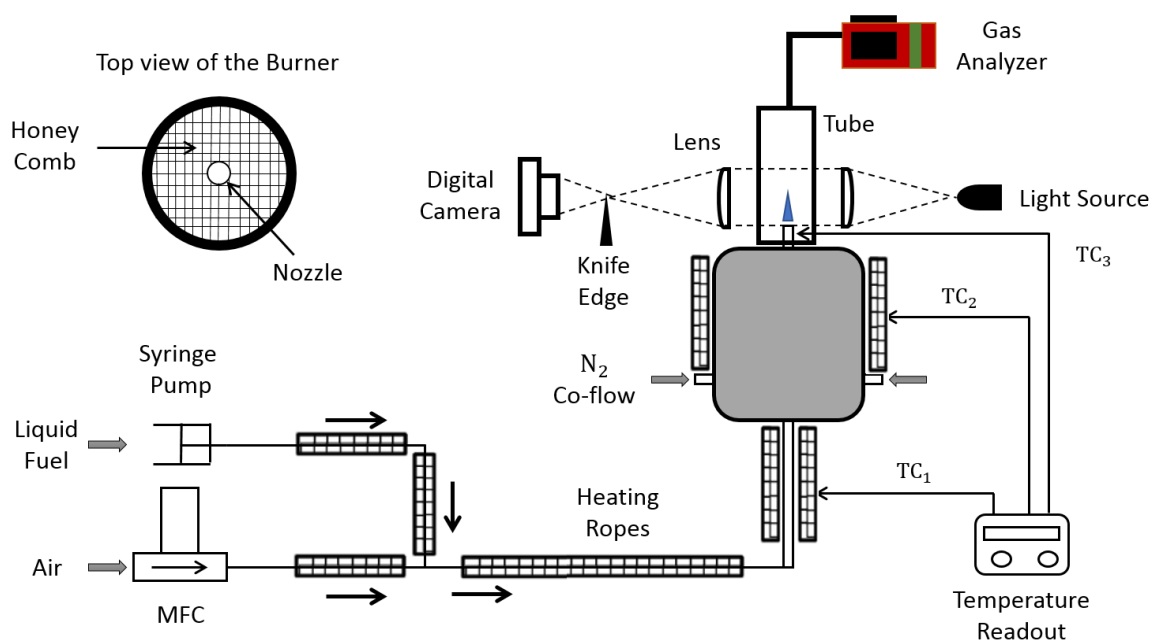


Figure 3-1: Schematic diagram of the experimental setup.

In the present study, the palm oil biodiesel, also known as palm methyl esters (PME), was supplied by Mewah Oils Sdn. Bhd., Malaysia. Furthermore, GC-MS analysis, using Agilent 7890 A (GC) & 5975C (MS), was performed to obtain the composition of PME used in the experiment [79]. The sample result of GC-MS analysis of PME can be viewed in Appendix C. Table 3-1 shows the fuel properties, which are well within the European Union's EN14214 standards, while Table 3-2 illustrates the composition of PME. Multi-walled carbon nanotubes having outer diameter ranges of 10-20 and 30-50 nm were supplied by BT Science Sdn. Bhd., Malaysia, and their properties are illustrated in Table 3-3. The detailed table of specifications, provided by the suppliers, for palm oil biodiesel and multiwalled carbon nanotubes can be viewed in Appendix D. The concentration of nano-additives in the mixture was varied from 25 to 200 ppm. It is worth mentioning that MWCNTs with the outer diameter of 10-20 nm were used as the main additive to study the effect of the nanotubes on the

combustion characteristics of the fuel, while the nanotubes with an outer diameter of 30-50 nm were employed to analyze the significance of nanotubes geometry. MWCNTs blended fuel samples were prepared using an ultrasonicator (Cole Parmer) at the amplitude of 55% and the pulse of 10/5 for 45 minutes. The images of premixed flames were captured via direct photography using a digital camera (Sony, A6000). In the case of the emission measurement, the concentrations of NO_x and CO in the exhaust gases were obtained via an exhaust gas analyzer (Kane, 905), which was placed at the end of the quartz tube aligned with the central nozzle.

Table 3-1: Palm methyl esters (PME) properties.

Properties	Value
Density at 25 °C [kg/m^3]	872
Kinematic viscosity at 40 °C [mm^2/s]	4.1
Flash point [°C]	101
Boiling point [°C]	> 210
Cetane number [-]	51
Molecular weight [g/mol]	281
High heating value [MJ/kg]	39.9

Table 3-2: Compositions of fatty acids in palm methyl esters (PME).

Fatty acid	No. of carbon: double bond	Composition (% wt.)
Palmitic	(C16:0)	47.50
Oleic	(C18:1)	39.55
Linoleic	(C18:2)	8.42
Stearic	(C18:0)	4.53

Table 3-3: Properties of the MWCNTs.

Property	10-20 nm	30-50 nm
Purity (carbon content, wt.%)	97	97
Inner diameter (nm)	5-10	5-12
Length (μm)	10-30	10-20
Specific surface area (m^2/g)	> 200	> 60
True density (g/cm^3)	2.1	2.1
Estimated number of walls (-)	8-23	27-67

The measurement of the blowoff velocity of pre-vaporized liquid fuel was conducted based on the methodology explained in the previous chapter, section 2.3. Furthermore, the flame area method, explained in section 2.2.5, was used to calculate the laminar burning velocity. The flame surface area in the present chapter was defined based on the visible flame boundary from the schlieren images, as shown in Fig. 3-2. The flame boundary was identified using the image processing tools from MATLAB, which was used to calculate the surface area of the revolution.

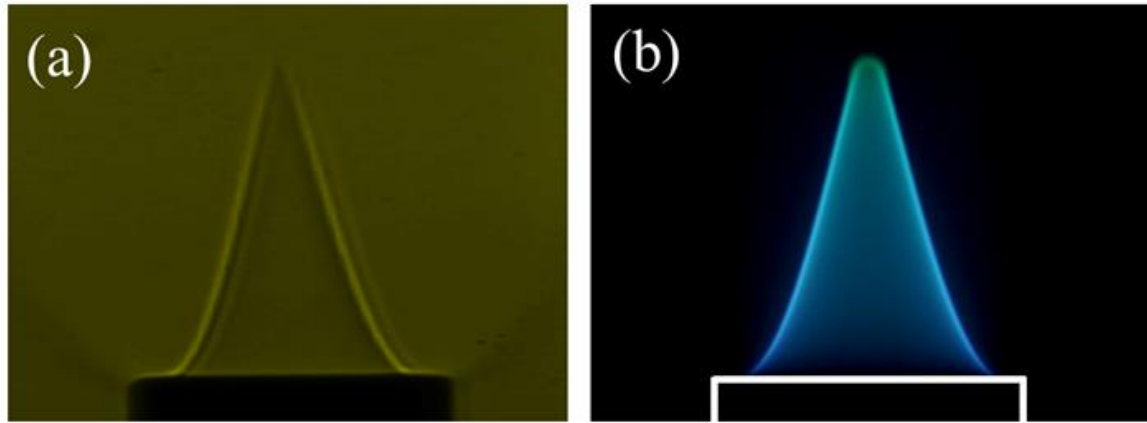


Figure 3-2: (a) Schlieren image, (b) direct photograph of PME/air flame at $\phi = 1.1$ and $U_{\text{jet}} = 100$ cm/s.

3.5. Results & Discussion

In the present study, the effect of MWCNTs addition on fundamental combustion characteristics of the PME/air premixed flames was experimentally investigated. Laminar burning velocities were obtained over the wide range of equivalence ratios, $\phi = 0.7$ -1.3, and at the unburnt gas temperature of 550 K and atmospheric pressure. The blowoff effect was achieved at all the equivalence ratios, and the changes in flammability limits were identified at both fuel-lean and fuel-rich regions. Lastly, the exhaust gas analyzer was used to measure NO_x and CO concentrations as the result of the combustion of MWCNTs blended PME fuel.

3.5.1. Experimental validation

Based on the literature findings, there are some studies done on laminar burning velocity and blowoff velocity of liquid fuels such as *n*-heptane [75-77,80], while data for PME/air premixed flame are still limited. Hence, the laminar burning velocity of *n*-heptane

flame was measured using the present setup in order to validate the accuracy of the current experiment. To perform a direct comparison, experiments were conducted at the same conditions as the literature conditions at the atmospheric pressure with the unburnt gas temperature of 470 K and the equivalence ratio varying from 0.7 to 1.4. Furthermore, the experimental results were also compared with the numerically obtained results using PREMIX code of Chemkin, with CRECK mechanism [81]. As illustrated in Fig. 3-3, it can be seen that the results from the present study are well within the range of the literature findings [75-77,80] and in good agreement with the numerical results. The discrepancies between the literature results can be attributed to the differences in the experimental setups and the use of different burner configurations.

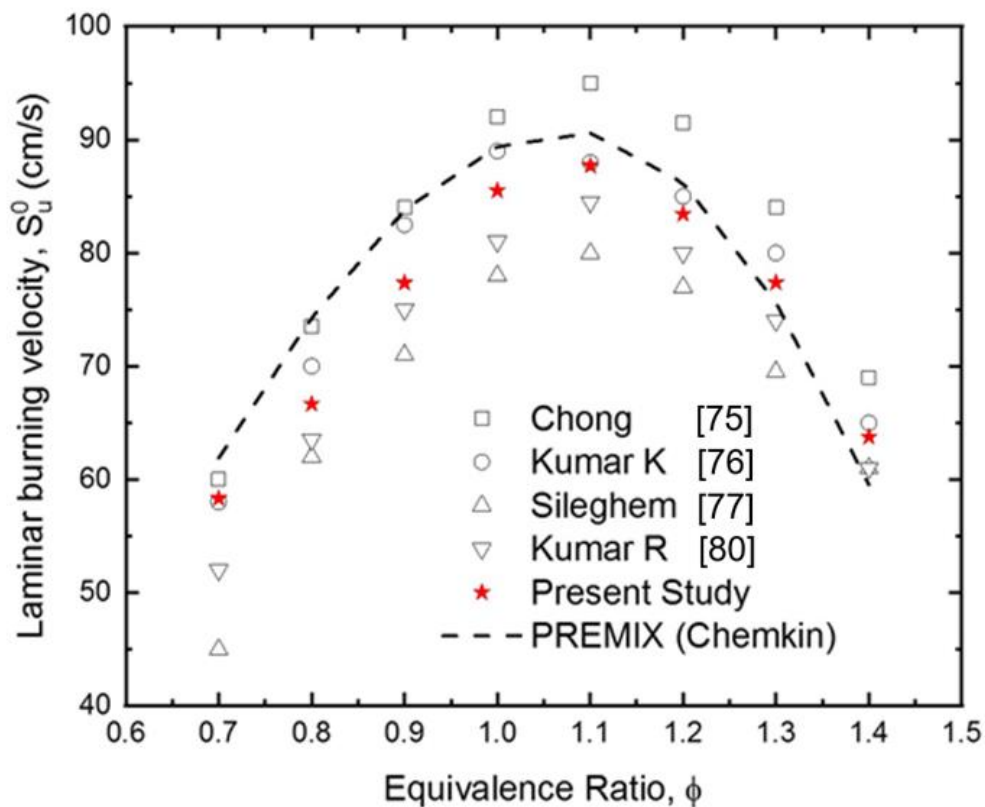


Figure 3-3: Laminar burning velocities of n-heptane/air flame at atmospheric pressure and the unburnt gas temperature of 470 K obtained from the present study and literature.

3.5.2. Blowoff velocity

PME/air premixed mixtures were enriched with MWCNTs of 10-20 nm at the concentration of 100 ppm to study the effect of nano-additives on the behavior of the premixed flames. Figure 3-4 illustrates the laminar premixed flames stabilized at the nozzle rim, for all three, lean ($\phi = 0.8$), rich ($\phi = 1.2$) and stoichiometric ($\phi = 1.0$) conditions at the jet velocity of 120 cm/s. All direct images were captured at the same camera settings (ISO, shutter speed, and white balance) in order to perform the direct comparison in the structure of premixed flames with and without the addition of MWCNTs.

As can be seen from Fig. 3-4, the flame height was shorter when MWCNTs were added to the mixture regardless of the equivalence ratio. As an example, for the PME/air flame at the rich condition, the height was decreased from 12.6 mm to 11.9 mm with MWCNTs of 100 ppm addition to the mixture. This behavior can be attributed to the improved fuel-air mixing with the presence of nanotubes in the mixture due to the occurrence of micro explosions during the vaporization and combustion process. In other words, MWCNTs helped the fuel react with more oxygen in the mixture. This is in alignment with the observations made by Hua et al. [82] and Mazas et al. [83], where they showed that the height of the reaction zone in flames decreased with the higher content of oxygen in the fuel/air mixtures. In regard to the structure of a premixed bunsen flame, the balance between the laminar burning velocity and the local flow velocity determines the flame tip angle. Hence, it is understood that any changes in the two parameters can lead to a change in the conical premixed flame angle, resulting in a flame height modification. In fact, when the jet velocity is kept constant for the mixture with and without MWCNTs addition, a decrease in the flame height of the premixed flame is a good indicator of the improvement in laminar burning velocity and blowoff velocity.

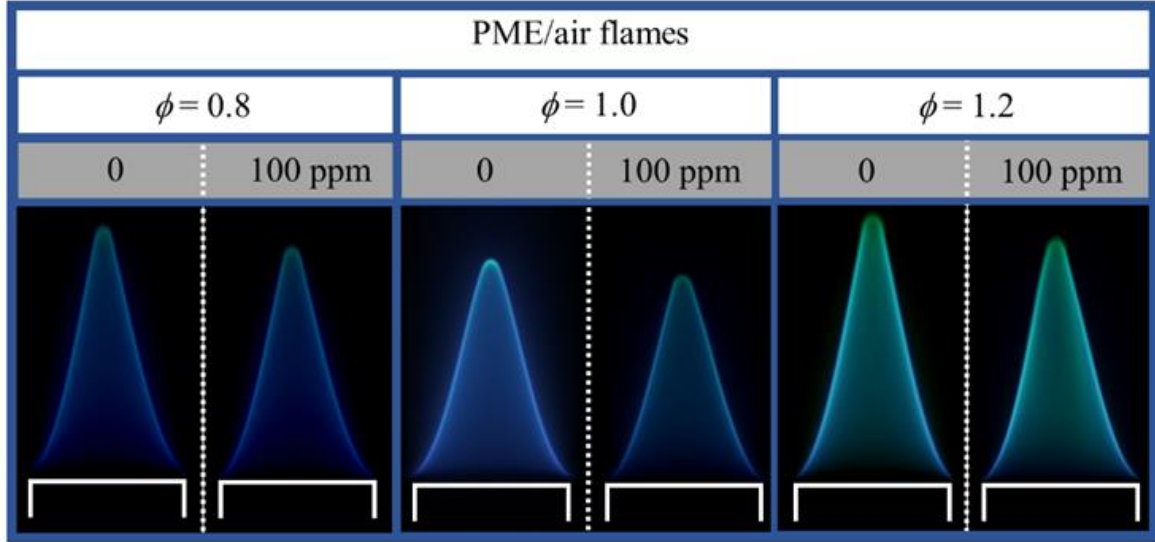


Figure 3-4: Direct photographs of PME/air premixed flames without and with MWCNTs (10-20 nm) of 100 ppm addition at lean, rich, and stoichiometric conditions at $U_{\text{jet}} = 120$ cm/s.

In premixed flame, standoff distance, which is defined as the height of the flame base from the nozzle rim, determines the heat transfer mechanism between the flame and the nozzle rim. Blowoff occurs when the standoff distance reaches its critical value at a certain jet velocity [68]. Hence, it can be understood that the standoff distance is another parameter in predicting the behavior of the blowoff velocity of a premixed bunsen flame. The effect of MWCNTs on the PME/air premixed flames was further investigated at the fuel-rich conditions of the mixture by increasing the equivalence ratio towards the rich limit. It can be observed from Fig. 3-5 that there is a decrease in the standoff distance of the flame with the addition of MWCNTs. Furthermore, the typical conical shape of the premixed bunsen flames was distorted, and the rotating flames were observed at $\phi \geq 1.35$. By gradually increasing the equivalence ratio of the PME/air mixture, the extinction limit of the flame without the addition of MWCNTs was found to be at $\phi = 1.6$. However, it was found that the flammability was further extended to $\phi = 1.65$ with the MWCNTs of 100 ppm addition to the mixture. While it is an adequate conclusion to

state that the nano-additives could improve the stability of the premixed flames, it should be highlighted that a more detailed study of the chemical kinetics involving the MWCNTs blended PME/air premixed flames is required.

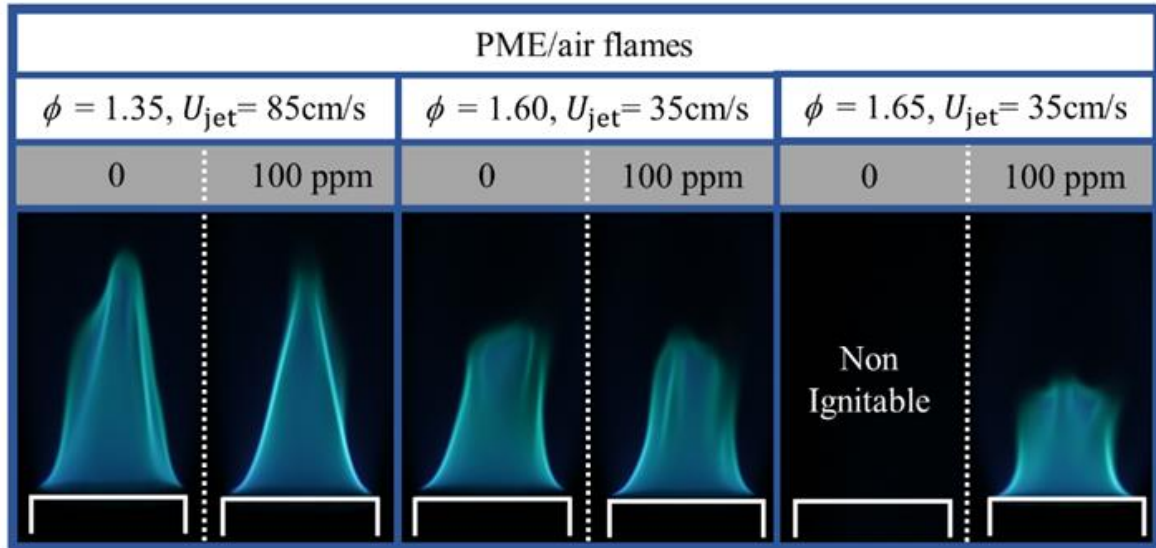


Figure 3-5: Direct photographs of very rich PME/air premixed flames without and with MWCNTs (10-20 nm) of 100 ppm addition.

Figure 3-6 depicts the effect of MWCNTs on the blowoff velocity of PME/air flames over the wide range of equivalence ratios. The results showed that there was an improvement in blowoff velocities regardless of the equivalence ratio. From the absolute values of blowoff velocities, it can be observed that the flames around the stoichiometric condition experienced the most significant improvement. However, it is worth noting that, based on the enhancement percentage, the flames at very rich conditions ($\phi \geq 1.4$) experienced a more improvement compared to the flames at $\phi < 1.4$. Furthermore, the flammability limits at both lean and rich regions were improved with the addition of 100 ppm of MWCNTs to PME/air premixed flames. The improvements of blowoff velocities were associated with the enhancement of the heat

transfer to the nozzle rim due to the decrease of standoff distance, as can be seen in Fig. 3-5. In their studies, Hosseini et al. [56] and El-Seesy et al. [67] showed two favoring properties of carbon-based nanotubes, such as high thermal conductivity and high surface-to-volume ratio, made them a promising fuel-borne catalyst. Hence, it can be understood that the high surface to volume ratio of MWCNTs enabled an improved thermal exchange between nano-additives and fuel-air droplets, leading to the occurrence of micro explosions during the vaporization and combustion processes. This resulted in improving combustion performance due to the enhancement of fuel-air mixing, which, in turn, improved the oxidation of the mixture.

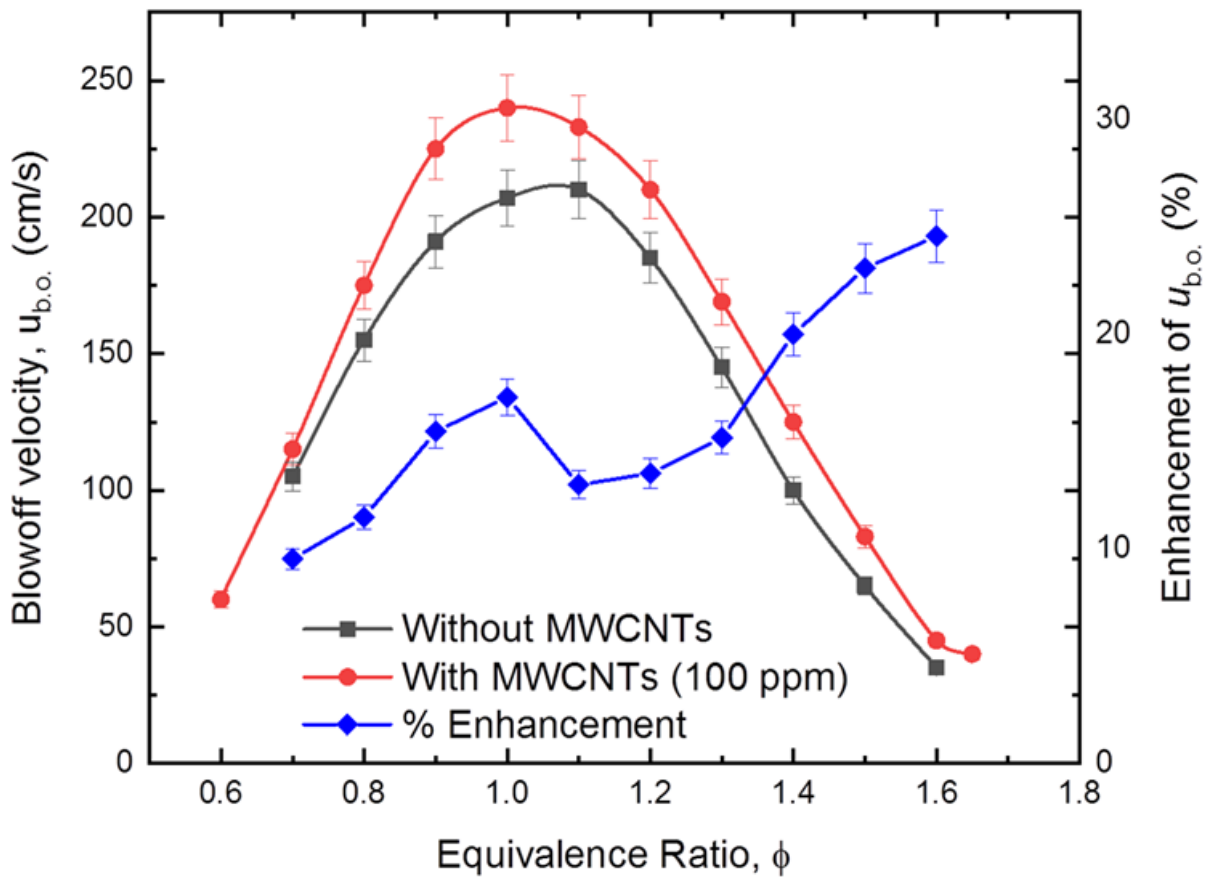


Figure 3-6: Comparison of blowoff velocities of PME/air premixed flames without and with MWCNTs (10-20 nm) of 100 ppm addition.

Another observation made during the present study regarding the flame structure was the presence of tip opening in the premixed bunsen flame. Figure 3-7(a) illustrates the typical behavior of the premixed flame with the increasing jet velocity, $U_{\text{jet}} = 100, 125, 150, \text{ and } 200$ cm/s, at the stoichiometric condition of the mixture. As can be seen in Fig. 3-7(a), the flame tip did not open even though the flame experienced the blowoff effect. This indicates the independence of the tip opening with regard to the jet velocity of the flame. Figure 3-7(b) shows the premixed flames with the increasing equivalence ratio, $\phi = 1.1, 1.2, 1.35, 1.4, \text{ and } 1.45$, at the jet velocity of 90 cm/s. It can be observed that the flame did not experience any tip opening at the equivalence ratios of 1.1 and 1.2. However, it started experiencing the flame structure breakouts at $\phi = 1.35$ and followed by the clear tip opening at $\phi = 1.4$, which grew wider when the mixture became richer, at $\phi = 1.45$. It was observed that the presence of tip opening led to the stabilization of the flame front, and the breakouts of the flame structure disappeared. In general, the occurrence of flame tip opening is associated with the negative stretch rate of the curvature at the flame tip and the preferential diffusion, represented by the Lewis number, from the imbalance of thermal and mass diffusions in the flame [84,85]. Regarding the premixed bunsen flames, Mizobuchi et al. [86] showed that the fuel concentration was not homogeneous throughout the flame structure as it decreased along the axial direction. Furthermore, the findings from [84,85] showed a gradual decrease in the maximum concentration of OH radicals downstream along the flame front with the increasing equivalence ratio of the rich mixtures. In addition to that, the localized concentration of OH radicals was weakened at the tip for the flames that experienced the tip opening phenomenon [84]. Hence, the preferential diffusion between the fuel and oxidant molecules led to a weaker local combustion intensity at the flame tip. Additionally, it can be seen from Fig. 3-7(b) that the flame height was increased with the increasing equivalence ratio of the premixed flame, which, in turn, caused a stronger flame stretch rate at the tip. As such, the flame tip opening

can be addressed with the weaker combustion intensity and the stronger flame stretch rate at the tip of the flame with the increasing equivalence ratio of the mixture.

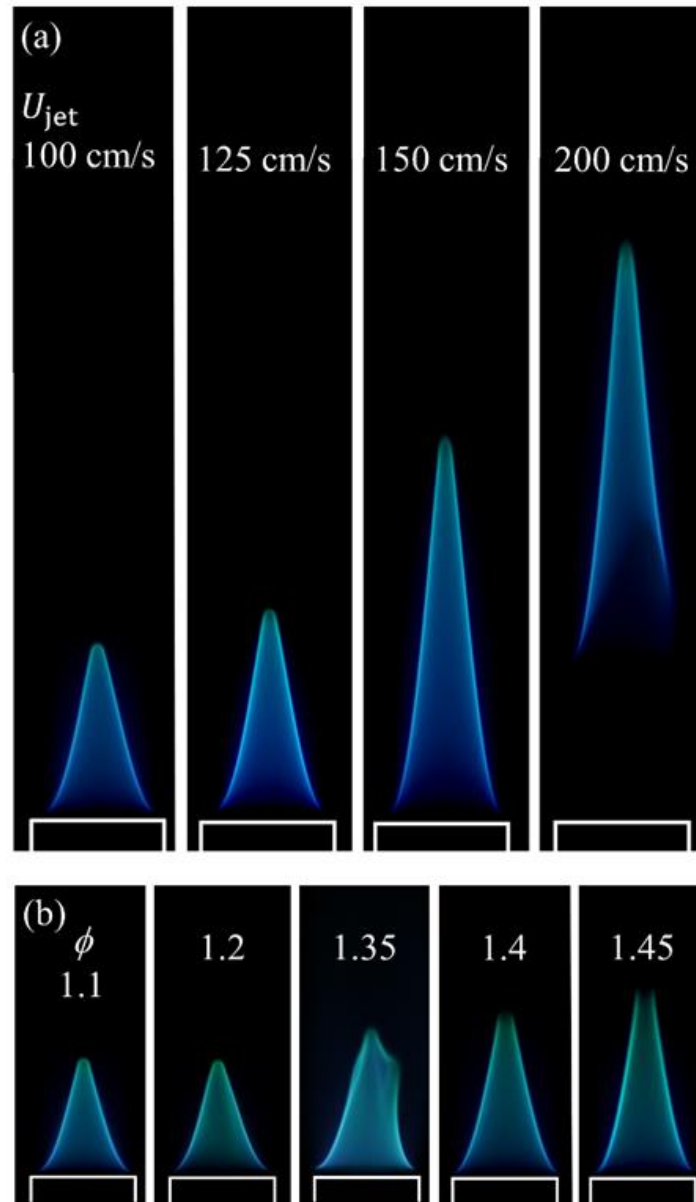


Figure 3-7: Direct photographs of PME/air premixed flames, (a) increasing the jet velocity until blowoff at $\phi = 1.0$, (b) presence of tip opening with the increasing of equivalence ratio at

$$U_{\text{jet}} = 90 \text{ cm/s.}$$

3.5.3. Laminar burning velocity

Figure 3-8 shows the laminar burning velocities of PME/air premixed flames with and without MWCNTs addition over the wide range of equivalence ratios, $\phi = 0.7-1.3$, at atmospheric pressure and the preheat temperature of 550 K. While the richer mixtures, $\phi = 1.35-1.6$, were ignitable, it is essential to highlight that the measurement of laminar burning velocity was limited to $\phi = 1.3$. Regarding the premixed bunsen flame, laminar burning velocity can be obtained either via angle or flame surface area method. It is worth noting that both mentioned methods require the assumption of a flame being in a conical shape with symmetry about its axial direction. Hence, as shown in Fig. 3-5, the flames with $\phi > 1.3$ can be considered irregular and asymmetrical. Furthermore, the existence of tip opening at the fuel-rich conditions can result in greater uncertainties in calculating the surface area method, which in return leads to errors in the calculation of laminar burning velocity. As illustrated in Fig. 3-8, the results showed that the laminar burning velocities of PME/air premixed flames were noticeably improved with the addition of MWCNTs for all the experimental cases. Alenezi et al. [87] explained that the presence of MWCNTs in the fuel blends led to an accelerated fuel reaction in the combustion process due to the catalytic nature of carbon-based nanotubes. It was further explained that the thermos-physical properties, such as thermal conductivity and mass diffusivity, of the fuel were enhanced with the addition of nano-additives, resulting in improving combustion performance [88]. In addition to the overall improvement of laminar burning velocity, the results from the present study showed that the effect of nano-additives was more impactful at the fuel-rich and stoichiometric conditions as compared to the fuel-lean conditions of PME/air mixtures, as represented by the enhancement percentage curve in Fig. 3-8. This behavior is quite similar in trend to the enhancement percentage for the blowoff velocity at the specific range of equivalence ratios, $\phi = 0.7-1.3$, as shown in Fig. 3-6. Furthermore, the laminar burning velocity against the equivalence ratio trend is similar to the

trend of blowoff velocity for PME/air premixed flames, as compared between Figs. 3-6 and 3-8. As such, it can be stated that the behavior of the laminar burning velocity can be used as a preliminary parameter to predict the behavior of the blowoff velocity per given mixture. Although these two parameters have codependency with each other, it is essential to highlight that the relationship is far more complex due to the potential coupling effect of the flame stretch, heat losses as well as quenching.

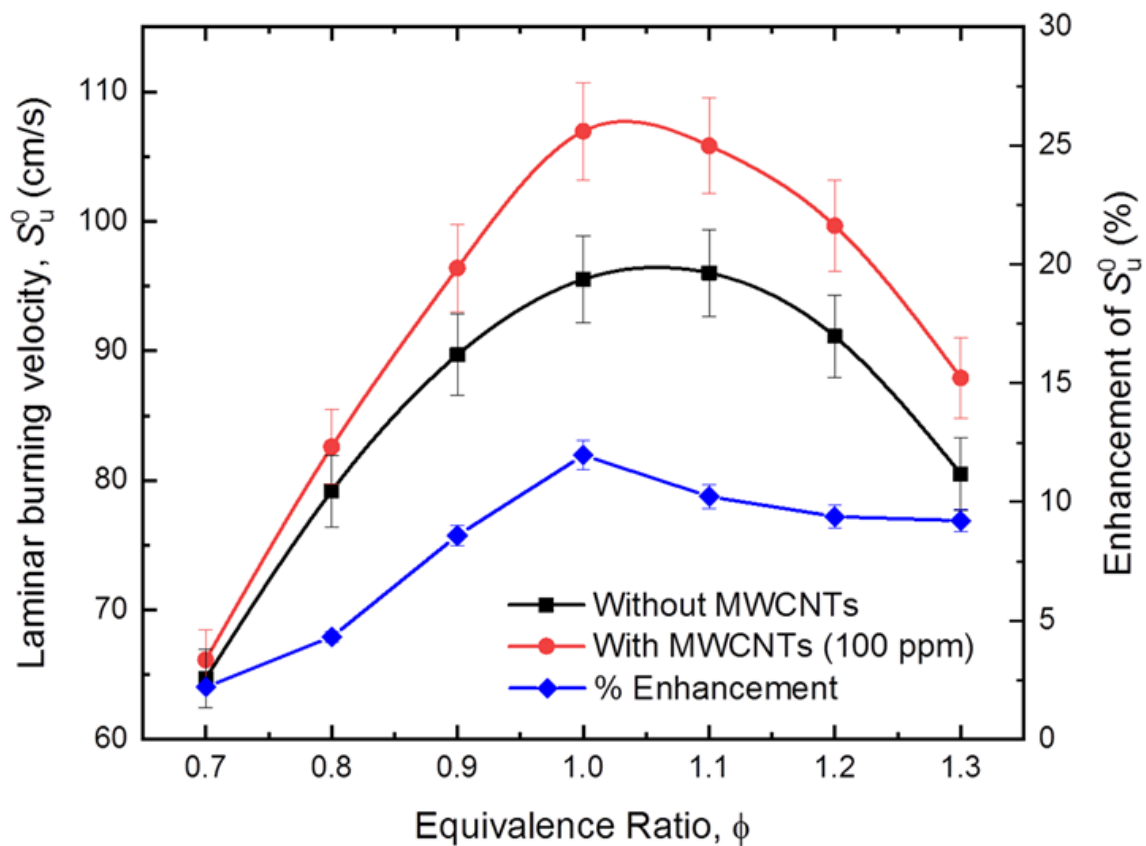


Figure 3-8: Comparison of laminar burning velocities of PME/air premixed flames without and with MWCNTs (10-20 nm) of 100 ppm addition.

To further understand how the carbon-based nanotubes affect the combustion of PME/air premixed flames, the concentration of MWCNTs in the mixture was varied between

25 and 200 ppm. Furthermore, to assess the significance of nanotubes' diameter on the laminar burning velocity of the premixed flame, the mixture was blended with two different groups of nano-additives, 10-20 nm, and 30-50 nm diameter ranges. As can be seen from Fig. 3-9(a), the maximum improvement of 13.6% in laminar burning velocity was achieved at the stoichiometric condition with 125 ppm of MWCNTs (10-20 nm) addition. It was followed by the flames at fuel-rich conditions, which experienced the most improvement in laminar burning velocity at 150 ppm of MWCNTs. On the other hand, the flames at lean conditions experienced the least improvement in the laminar burning velocity, which peaked at about 125 ppm of MWCNTs in the mixture to reach about 4% improvement. From these observations, it can be concluded that for the smaller MWCNTs (10-20 nm), the MWCNTs of 125-150 ppm range can be considered as the optimal concentration across the equivalence ratios. On the other hand, PME/air mixtures with the addition of larger MWCNTs (30-50 nm) experienced a much lower improvement in laminar burning velocity, as shown in Fig. 3-9(b). The highest increase in laminar burning velocity with larger MWCNTs (30-50 nm) is about 6% compared to 13.6% improvement with smaller MWCNTs (10-20 nm). This behavior can be explained based on the difference in surface-to-volume ratio, which can be quantified from the specific surface area of the MWCNTs. As can be seen from Table 3-3, the specific surface area of the smaller nanotubes is much higher than that of the larger nanotubes, indicating the higher thermal conductivity of the smaller nanotubes. This is in good agreement with the findings of Fujii et al. [89], where it was reported that the thermal conductivity of MWCNTs increased as their outer diameter decreased. This phenomenon is associated with the number of walls per nanotube as nanotubes with larger outer diameter contain a higher number of walls than smaller nanotubes. Furthermore, the present results revealed that the biodiesel flames with larger MWCNTs addition showed an unpredictable behavior in enhancing the laminar burning velocity. As can be seen from Fig. 3-9(b), the fuel-rich and stoichiometric mixtures experienced

the most enhancement in the laminar burning velocity of PME/air with MWCNTs (30-50 nm) of 100-125 ppm addition. In contrast, the fuel-lean mixture experienced less impact, in which the most enhancement in laminar burning velocity occurred at 75 ppm. While it was expected that the laminar burning velocity would gradually increase with the concentration of MWCNTs in the mixture, it was observed that the mixtures experienced lesser improvements in laminar burning velocity when the MWCNTs concentration reached a critical value in the mixture, regardless of the size of the nanotubes and equivalence ratio. For both groups of nanotubes, with diameters of 10-20 nm and 30-50 nm, the decline in the laminar burning velocity was associated with the excessive concentration of nano-additives in the mixture. While MWCNTs possess beneficial thermos-physical properties that can enhance the combustion of the given fuel, exceeding a specific concentration of nano-additives could dilute the overall mixture. The dilution effect was confirmed when some blends could not even get ignited with concentrations of MWCNTs above 150 ppm, as shown in Fig. 3-9(b). Furthermore, it can be explained that the heat absorption of the MWCNTs in the mixture becomes more significant with the increasing of concentration, resulting in a reduction in the temperature of the unburnt mixture. This observation is in agreement with the findings of Hariram et al. [90], where the effect of CNTs on the CI engine performance running with oxygenated jojoba biodiesel-diesel blends was investigated. The results suggested that the fuel sample with 100 ppm of MWCNTs resulted in the optimal engine performance compared to the fuel samples with 50 and 150 ppm of MWCNTs.

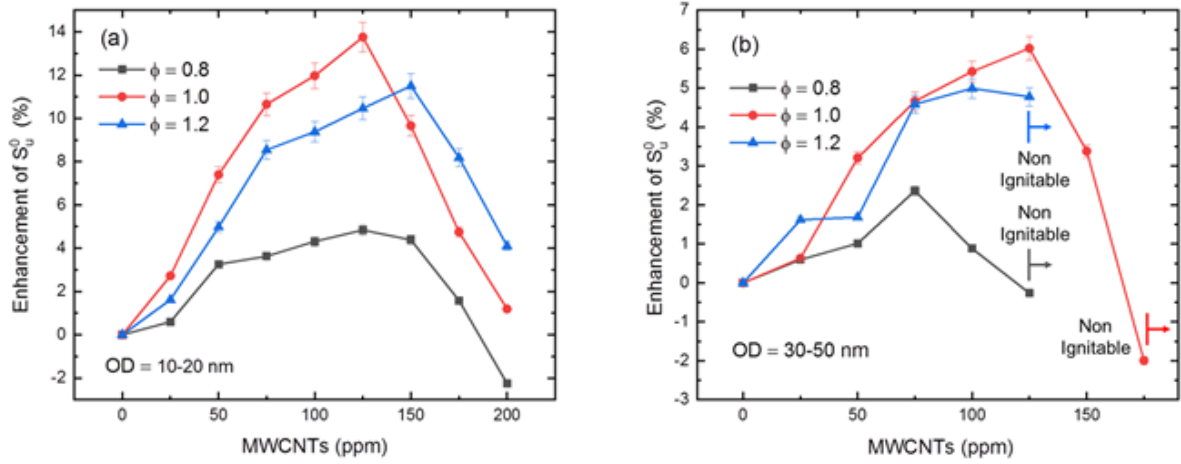


Figure 3-9: Enhancement of laminar burning velocities of PME/air premixed flames with MWCNTs addition with the outer diameters of (a) 10-20 nm, (b) 30-50 nm.

The flame structure changes, such as flame height and standoff distance, with the presence of MWCNTs with two different outer diameters, were visualized in Fig. 3-10. While Fig. 3-10(a) shows the premixed flame with no nanotubes in the mixture, Figs. 3-10(b and c) show the flames of the same mixture with the addition of MWCNTs of 175 ppm with 10-20 and 30-50 nm outer diameters, respectively. The jet velocity was kept constant at 120 cm/s to perform the direct comparison between the flames. As can be observed from Fig. 3-10, the height of the flame with MWCNTs (10-20 nm) addition was decreased by 7.4%, whereas the flame with MWCNTs (30-50 nm) addition was increased by 3.9% as compared to the flame without MWCNTs. Furthermore, the standoff distance became shorter for the flame with MWCNTs (10-20 nm) addition, whereas the flame with MWCNTs (30-50 nm) addition was pushed further away from the nozzle rim. These changes in the flame structure can be attributed to the changes in the laminar burning velocity of premixed flames with the presence of MWCNTs. From Fig. 3-9(a), it can be viewed that the laminar burning velocity of the stoichiometric mixture was enhanced by about 4% by adding MWCNTs (10-20 nm) of 175 ppm. Hence, this improvement in laminar burning velocity resulted in shorter flame height and

standoff distance. On the contrary, Fig. 3-9(b) shows that the laminar burning velocity of the stoichiometric mixture was reduced by about 2% with MWCNTs (30-50 nm) of 175 ppm addition. Besides, it can also be observed that the intensity of flame luminosity decreased with the addition of carbon-based nanotubes.

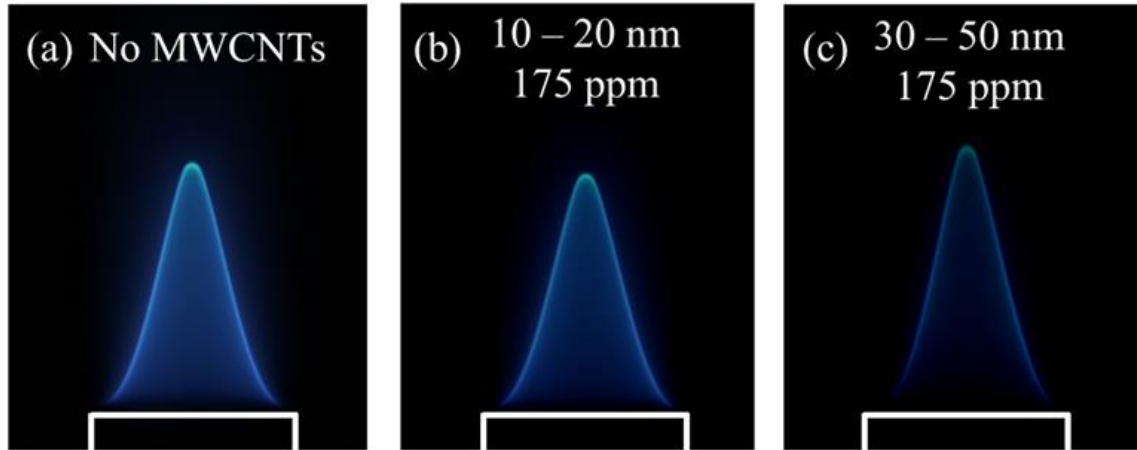


Figure 3-10: Direct photographs of PME/air premixed flames (a) without MWCNTs and with MWCNTs addition of 175 ppm with the outer diameter of (b) 10-20 nm, (c) 30-50 nm, at $\phi = 1.0$ and $U_{\text{jet}} = 120$ cm/s.

3.5.4. Emissions

It is known that transportation is one of the most significant sectors in terms of fossil-based fuel consumption. As such, they are recognized as one of the main contributors towards the production of pollutant emissions. Based on the literature, the usage of biodiesel in diesel engines allows reducing the concentration of UHC, CO_2 , CO, and solid particles in the exhaust gases. However, this also leads to a higher content of NO_x emissions [29]. In regard to this behavior, Fig. 3-11 illustrates the effect of MWCNTs in the mixture on the NO_x and CO emissions. The results showed that NO_x was continuously increasing while CO gradually

decreased with the increasing content of MWCNTs in the mixture. It can also be observed that with the content of MWCNTs of 150 ppm and higher, the changes in the concentration of pollutants were relatively small, which were less than 2% for both NO_x and CO productions.

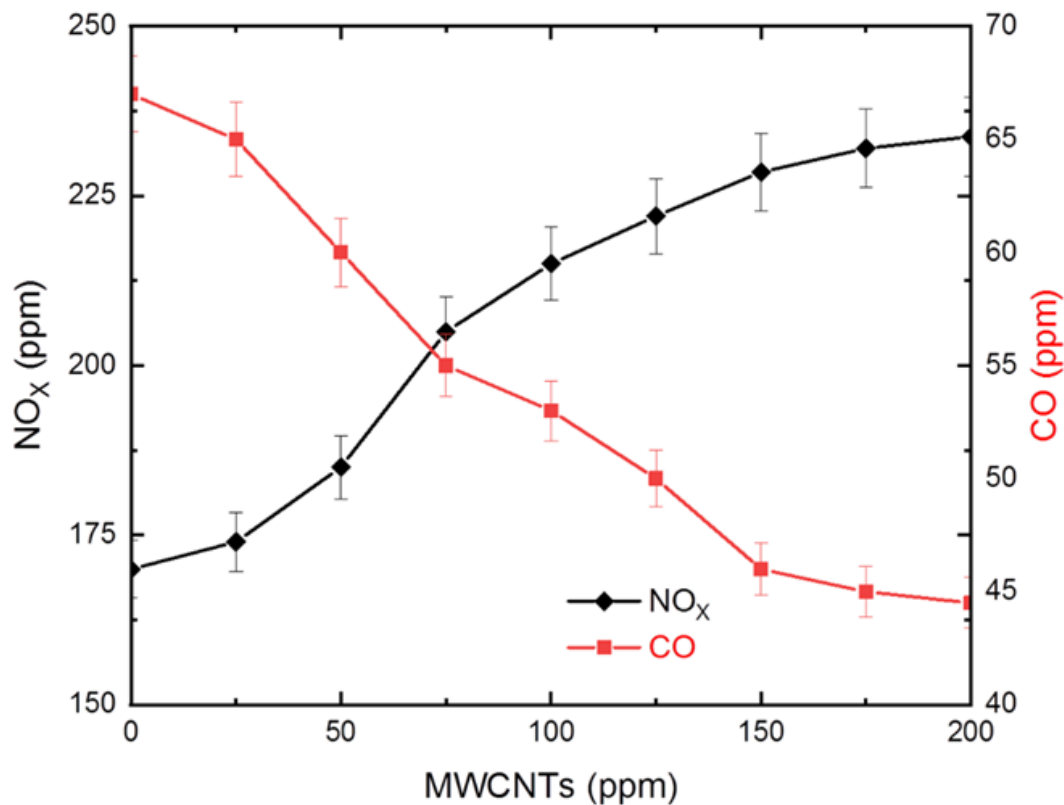


Figure 3-11: NO_x and CO emissions from PME/air premixed flames at the stoichiometric condition with MWCNTs (10-20 nm) addition.

The reduction in CO was mainly attributed to the enhancement of combustion performance with the presence of MWCNTs. Furthermore, MWCNTs in the fuel-air mixture could improve the chemical reactivity of the overall blend [67,87]. It could be attributed to the properties of the carbon-based nanotubes, such as a high surface area to volume ratio and high thermal conductivity, which resulted in the accelerated combustion of the mixture, thereby

leading to a higher heat release rate. This resulted in mitigating the chemical energy loss in the process, which depends on CO emissions production. Furthermore, the process of CO oxidization in the preheated zone could be improved due to the increased temperature of the premixed flames.

In engine application, the formation of NO_x emission is predominantly dependent on the parameters such as injection timing, combustion timing, heat release rate, and temperature of the fuels. In the present laboratory scaled experiment, the injection and combustion timing were not considered to be the relevant parameters. Furthermore, based on different combustion configurations, NO_x formation can be associated with various mechanisms such as prompt NO_x fuel-bound NO_x , intermediate N_2O to NO formation, and thermal NO_x mechanism [91]. As the name suggests, the fuel-bound NO_x formation mechanism implies that the main fuel in the mixture primarily consists of nitrogen species. Desantes et al. [92] explained that prompt NO_x formation is sensitive towards the equivalence ratio and plays a significant role in the case of very fuel-rich conditions. On the other hand, Loffler et al. [93] stated that the production NO_x emission in the combustion is resulted from the conversion of N_2O into NO at fuel-lean and medium temperature conditions. In the present study, the addition of MWCNTs to PME/air mixture could raise the flame temperature as a result of the enhancement of combustion performance due to the presence of MWCNTs in the mixture. Hence, the increase in NO_x formation can be attributed to the thermal NO_x mechanism. This is also in good agreement with the improvements found in laminar burning velocity, as it has been reported that the higher flame temperature leads to a higher laminar burning velocity. Furthermore, the improved chemical reactivity of the blend could result in a higher heat release rate. As such, these changes in the combustion behavior, due to the presence of MWCNTs in the mixture, resulted in a higher content of NO_x production.

3.6. Conclusion

In the present study, the fundamental combustion characteristics of PME/air premixed mixtures with the addition of MWCNTs were investigated using the coflow burner configuration. The parameters such as laminar burning velocity, blowoff velocity, and NO_x and CO concentrations were experimentally measured over the wide range of equivalence ratios at atmospheric pressure and the preheated temperature of 550 K. The main findings are as follows:

1. Blowoff velocity increased with MWCNTs addition to the mixture regardless of the equivalence ratio. The impact of nano-additives was more significant in fuel-rich conditions, whereas the fuel-lean mixtures experienced less improvement in blowoff velocity. Furthermore, the flammability limits were extended at both lean and rich conditions.

2. Laminar burning velocity increased with MWCNTs addition to the mixture, with the highest enhancement observed around the stoichiometric condition. However, further increase the concentration of nano-additives in the mixture beyond the critical concentrations (125-150 ppm and 75-125 ppm for MWCNTs of 10-20 nm and 30-50 nm, respectively) generally caused less improvement in the laminar burning velocities of the premixed flames. It was observed that the nanotubes with the larger outer diameter were less effective than the smaller nanotubes.

3. The improvements in blowoff velocity and laminar burning velocity were indicated by the reduction in standoff distance and shortening of flame height with the addition of MWCNTs. Furthermore, PME/air premixed flames experienced tip opening at very fuel-rich conditions ($\phi \geq 1.4$). It was shown that the tip opening occurred irrespective of the jet velocity and was primarily affected by the fuel concentration in the mixture.

4. NO_x was continuously increasing, while CO gradually decreased with the increasing content of MWCNTs in the mixture. These emissions production behaviors were mainly attributed to the accelerated and enhanced combustion performance due to the presence of MWCNTs in the mixture.

3.7. References

- [1] Martin U, Dieter B, Christine B, Bert B, Georg F, Rolf L, Martin M, Kevin S, Jennifer S, Olaf S, Ulrike S, Helmut T, Edgar R, Richard W, Markus W, Jürgen K. Action areas and the need for research in biofuels. *Fuel* 2020;268:117227.
- [2] Digambar S, Dilip S, Shyam LS, Sumit S, Deepika K. Chemical compositions, properties, and standards for different generation biodiesels: A review. *Fuel* 2019;253:60–71.
- [3] Anantha RL, Deepanraj B, Rajakumar S, Sivasubramanian V. Experimental investigation on performance, combustion and emission analysis of a direct injection diesel engine fuelled with rapeseed oil biodiesel. *Fuel* 2019;246:69–74.
- [4] Semwal S, Arora AK, Badoni R, Tuli DK. Biodiesel production using heterogeneous catalysts. *Bioresour Technol* 2011;102:2151–2161.
- [5] Tamilselvan P, Nallusamy N, Rajkumar S. A comprehensive review on performance, combustion and emission characteristics of biodiesel fuelled diesel engines. *Renew Sust Energ Rev* 2017;79:1134-1159.
- [6] Medhat E, Hagar AEB, Khaled KE, Ahmed MR, Hitesh P, Kishor KS, Deepalekshmi P, Rashmi W. Experimental studies on the biodiesel production parameters optimization of sunflower and soybean oil mixture and DI engine combustion, performance, and emission analysis fueled with diesel/biodiesel blends. *Fuel* 2019;255:115791.
- [7] Canakci M. Performance and emissions characteristics of biodiesel from soybean oil. *P I Mech Eng D-J Aut* 2005;219:915–922.
- [8] Aldhaidhawi M, Chiriac R, Badescu V. Ignition delay, combustion and emission characteristics of Diesel engine fueled with rapeseed biodiesel – A literature review. *Renew Sust Energ Rev* 2017;73:178-186.
- [9] Vellaiyan S. Combustion, performance and emission evaluation of a diesel engine fueled with soybean biodiesel and its water blends. *Energy* 2020;201:117633.
- [10] Patel C, Chandra K, Hwang J, Agarwal RA, Gupta N, Bae C, Gupta T, Agarwal AK. Comparative compression ignition engine performance, combustion, and emission characteristics, and trace metals in particulates from Waste cooking oil, Jatropha and Karanja oil derived biodiesels. *Fuel* 2019;236:1366-1376.
- [11] Rajasekar E, Selvi S. Review of combustion characteristics of CI engines fueled with biodiesel. *Renew Sust Energ Rev* 2014;35:390-399.
- [12] Zhu L, Cheung CS, Zhang WG, Haung Z. Emission characteristics of a diesel engine operating on biodiesel and biodiesel blended with ethanol and methanol. *Sci Total Environ* 2010;408:914-921.
- [13] Hoekman SK, Robbins C. Review of the effects of biodiesel on NO_x emissions. *Fuel Process Technol* 2012;96:237-249.
- [14] Hribernik A, Kegl B. Influence of Biodiesel Fuel on the Combustion and Emission Formation in a Direct Injection (DI) Diesel Engine. *Energy Fuel* 2007;21:1760-1767.
- [15] Ong HC, Mahlia TMI, Masjuki HH, Norhasyima RS. Comparison of palm oil, Jatropha curcas and Calophyllum inophyllum for biodiesel: A review. *Renew Sust Energ Rev* 2011;15:3501-3515.

- [16] Chong CT, Ng JH, Ahmad S, Rajoo S. Oxygenated palm biodiesel: ignition, combustion and emissions quantification in a light-duty diesel engine. *Energy Convers Manag* 2015;101:317–25.
- [17] Ozsezen AN, Canakci M, Turkcan A, Sayin C. Performance and combustion characteristics of a DI diesel engine fueled with waste palm oil and canola oil methyl esters. *Fuel* 2009;88:629-636.
- [18] Xue J. Combustion characteristics, engine performances and emissions of waste edible oil biodiesel in diesel engine. *Renew Sust Energ Rev* 2013;23:350-365.
- [19] Ozsezen AN, Canakci M. Determination of performance and combustion characteristics of a diesel engine fueled with canola and waste palm oil methyl esters. *Energy Convers Manag* 2011;52:108-116.
- [20] Liu J, Zhang X, Wang T, Hou X, Zhang J, Zheng S. Numerical study of the chemical, thermal and diffusion effects of H₂ and CO addition on the laminar flame speeds of methane-air mixture. *Int J Hydrogen Energy* 2015;40:8475-8483.
- [21] Sivakumar M, Sundaram NS, Kumar RR, Thasthagir MHS. Effect of aluminium oxide nano-particles blended pongamia methyl ester on performance, combustion and emission characteristics of diesel engine. *Renew Energy* 2018;116:518-526.
- [22] Lee CC, Tran M-V, Tan BT, Scribano G, Chong CT. A comprehensive review on the effects of additives on fundamental combustion characteristics and pollutant formation of biodiesel and ethanol. *Fuel* 2021;288:119749.
- [23] Manigandan S, Sarweswaran R, Devi PB, Sohret Y, Kondratiev A, Venkatesh S, Vimal MR, Joshua JJ. Comparative study of nanoadditives TiO₂, CNT, Al₂O₃, CuO and CeO₂ on reduction of diesel engine emission operating on hydrogen fuel blends. *Fuel* 2020;262:116336.
- [24] Shaafi T, Sairam K, Gopinath A, Kumaresan G, Velraj R. Effect of dispersion of various nanoadditives on the performance and emission characteristics of a CI engine fuelled with diesel, biodiesel and blends – A review. *Renew Sust Energ Rev* 2015;49:563-573.
- [25] Venu H, Madhavan V. Effect of Al₂O₃ nano-particles in biodiesel-diesel-ethanol blends at various injection strategies: Performance, combustion and emission characteristics. *Fuel* 2016;186:176-189.
- [26] Sajith V, Sobhan CB, Peterson GP. Experimental Investigations on the Effects of Cerium Oxide Nanoparticle Fuel Additives on Biodiesel. *Adv Mech Eng* 2015;2:1-6.
- [27] Vairamuthu G, Sundarapandian S, Kailasanathan C, Thangagiri B. Experimental investigation on the effects of cerium oxide nano-particle on *Calophyllum inophyllum* (Punnai) biodiesel blended with diesel fuel in DI diesel engine modified by nozzle geometry. *J Energy Inst* 2016;89:668-682.
- [28] Chen AF, Adzmi MA, Adam A, Fahmi M, Kamal M, Mrwan AG. Combustion characteristics, engine performances and emissions of a diesel engine using nano-particle-diesel fuel blends with aluminium oxide, carbon nanotubes and silicon oxide. *Energy Convers Manag* 2018;171:461-477.
- [29] Ghanbari M, Najafi G, Ghobadian B, Yusaf T, Carlucci AP, Kiani Deh Kiani M. Performance and emission characteristics of a CI engine using nano particles additives in biodiesel-diesel blends and modeling with GP approach. *Fuel* 2017;202:699-716.

- [30] Najafi G. Diesel engine combustion characteristics using nano-particles in biodiesel-diesel blends. *Fuel* 2018;212:668-678.
- [31] Khond VW, Kriplani VM. Effect of nanofluid additives on performances and emissions of emulsified diesel and biodiesel fueled stationary CI engine: A comprehensive review. *Renew Sust Energy Reviews* 2016;59:1338-1348.
- [32] Manzoore EM, Nik NNG, Kalama A, Badruddinb IA, Banapurmathc NR , Naveed Akrama. The effect of nano-additives in diesel-biodiesel fuel blends: A comprehensive review on stability, engine performance and emission characteristics. *Energy Conv Management* 2018;178: 146-177.
- [33] Shafii MB, Daneshvar F, Jahani N, Mobini K. Research article effect of ferrofluid on the performance and emission patterns of a four stroke diesel engine. *Adv Mech Eng* 2011:1-5.
- [34] Saxena V, Kumar N, Saxena VK. A comprehensive review on combustion and stability aspects of metal nanoparticles and its additive effect on diesel and biodiesel fuelled C.I. engine. *Renew Sust Energ Rev* 2017;70:563-588.
- [35] Basu S, Miglani A. Combustion and heat transfer characteristics of nanofluid fuel droplets: A short review. *Int J Heat Mass Transf* 2016;96:482-503.
- [36] Abdali JK. Enhancement Combustion And Ignition Characteristics Of Biodiesel/Diesel Fuel Mixtures By Nano Aluminium (N-Al) And Nano Aluminium Oxide (N-Al₂O₃) Additives. *Int J Civ Eng Technol* 2019;10:2337-2347.
- [37] Mehregan M, Moghiman M. Effect of aluminum nanoparticles on combustion characteristics and pollutants emission of liquid fuels – A numerical study. *Fuel* 2014;119:57-61.
- [38] Kannan GR, Karvembu R, Anand R. Effect of metal based additive on performance emission characteristics of diesel engine fuel led with biodiesel. *Appl Energy* 2011;88:3694-3703.
- [39] Mehta RN, Chakraborty M, Parikh PA. Nanofuels: Combustion, engine performance and emissions. *Fuel* 2014;120:91-97.
- [40] Kalaimurugan K, Karthikeyan S, Periyasamy M, Mahendran G. Combustion studies on CI engine with cerium oxide nanoparticle added neochloris oleoabundans biodiesel-diesel fuel blends. *Mater Today Proc* 2020;33:2886-2889.
- [41] El-Seesy AI, Hassan H. Combustion Characteristics of a Diesel Engine Fueled by Biodiesel-Diesel-N-Butanol Blend and Titanium Oxide Additives. *Energy Procedia* 2019;162:48-56.
- [42] Selvaganapthy A, Sundar A, Kumaragurubaran B, Gopal P. An experimental Investigation to study the effects of various nanoparticles with diesel on Di diesel engine. *ARNP J Sci Technol* 2013;3:112–115.
- [43] Hewett KB, Anderson LC, Rosynek MP, Lunsford JH. Formation of hydroxyl radicals from the reaction of water and oxygen over basic metal oxides. *J Am Chem Soc* 1996;118:6992–6997.
- [44] Rosensweig RE. Magnetic Fluids. *Annu Rev Fluid Mech* 1987;19:437-461.

- [45] Nasrin SS, Abdulali F, Ehsan E-B and Massoud M. Effects of Magnetic Nanofluid Fuel Combustion on the Performance and Emission Characteristics. *J Disper Sci Technol* 2014;35:1745-1750.
- [46] Devarajan Y, Munuswamy DB, Mahalingam A. Performance, combustion and emission analysis on the effect of ferrofluid on neat biodiesel. *Process Saf Environ Prot* 2017;111:283-291.
- [47] Ramanan MV, Yuvarajan D. Emission analysis on the influence of magnetite nanofluid on methyl ester in diesel engine. *Atmos Pollut Res* 2016;7:477-481.
- [48] Yang WM, An H, Chou SK, Vedharaji S, Vallinagam R, Balaji M, Mohammad FEA, Chua KJE. Emulsion fuel with novel nano-organic additives for diesel engine application. *Fuel* 2013;104:726-731.
- [49] Yang WM, An H, Chou SK, Chua KJ, Mohan B, Sivasankaralingam V, Raman V, Maghbouli A, Li J. Impact of emulsion fuel with nano-organic additives on the performance of diesel engine. *Appl Energy* 2013;112:1206-1212.
- [50] Mohsen MK, Oleksiy A, Heinz PB. Experimental analysis of the effect of nano-metals and novel organic additives on performance and emissions of a diesel engine. *Fuel Process Technol* 2019;196:106166.
- [51] Basha JS, Anand RB. The influence of nanoadditive blended biodiesel fuels on the working characteristics of a diesel engine. *J Braz Soc Mech Sci Eng* 2013;35:257-264.
- [52] Vali RH, Wani MM. The effect of mixed nano-additives on performance and emission characteristics of a diesel engine fuelled with diesel-ethanol blend. *Mater Today Proc* 2021;43:3842-3846.
- [53] Malik SR, Maqbooi, Hussain S, Irfan H. Carbon nanotubes: description, properties and applications. *J Pak Mater Soc* 2008;2:21-36.
- [54] Study on the Possibility of Improving the Environmental Performance of Diesel Engine Using Carbon Nanotubes as a Petroleum Diesel Fuel Additive. *Energies* 2019;12:4345.
- [55] Luo C, Xie H, Wang Q, Luo G, Liu G. A Review of the Application and Performance of Carbon Nanotubes in Fuel Cells. *J Nanomater* 2015.
- [56] Hosseini HS, Alisaraei AT, Ghobadian B, Mayvan AA. Performance and emission characteristics of a CI engine fuelled with carbon nanotubes and diesel-biodiesel blends. *Renew Energy* 2017;111:201-213.
- [57] Basha JS, Anand RB. An experimental investigation in a diesel engine using carbon nanotubes blended water–diesel emulsion fuel. *Proceedings of the Institution of Mechanical Engineers Part A: Journal of Power and Energy* 2011;225:279-288.
- [58] Prajwal T, Eshank D, Banapurmath NR, Yaliwal VS. Experimental investigations on a diesel engine fuelled with multiwalled carbon nanotubes blended biodiesel fuels. *International Journal of Emerging Technology and Advanced Engineering* 2013;3:72-76
- [59] Basha JS, Anand RB. Performance, emission and combustion characteristics of a diesel engine using Carbon Nanotubes blended Jatropha Methyl Ester Emulsions. *Alexandria Engineering Journal* 2014;53:259-273.

- [60] Balaji G, Cheralathan M. Effect of CNT as additive with biodiesel on the performance and emission characteristics of a DI diesel engine. *International Journal of ChemTech Research* 2015;7:1230-1236.
- [61] Singh N, Bharj RS. Effect of CNT-Emulsified Fuel on Performance Emission and Combustion Characteristics of Four Stroke Diesel Engine. *International Journal of Current Engineering and Technology* 2015;5:477-485.
- [62] Ghafoori M, Ghobadian B, Najafi G, Layeghi M, Rashidi A, Mamat R. Effect of nanoparticles on the performance and emission of a diesel engine using biodiesel-diesel blend. *International Journal of Automotive and Mechanical Engineering* 2015;12:3097-3108.
- [63] Maleney KH, Alisaraei AT, Ghobadian B, Mayvan AA. Analyzing and evaluation of carbon nanotubes additives to diesohol-B2 fuels on performance and emission of diesel engines. *Fuel* 2017;196:110-123.
- [64] Praveen A, Rao GLN, Balakrishna B. The combined effect of multiwalled carbon nanotubes and exhaust gas recirculation on the performance and emission characteristics of a diesel engine. *International Journal of Ambient Energy*
- [65] Basha JS. Impact of Carbon Nanotubes and Di-Ethyl Ether as additives with biodiesel emulsion fuels in a diesel engine e An experimental investigation. *J Energy Inst* 2018;91:289-303.
- [66] Hoseini SS, Najafi G, Ghobadian B, Mamat R, Ebadi M, Yusaf T. Novel environmentally friendly fuel: The effects of nanographene oxide additives on the performance and emission characteristics of diesel engines fuelled with *Ailanthus altissima* biodiesel. *Renew Energy* 2018;125:283-294.
- [67] El-Seesy AI, Abdel-Rahman AK, Bady M, Ookawara S. Performance, combustion, and emission characteristics of a diesel engine fueled by biodiesel-diesel mixtures with multi-walled carbon nanotubes additives. *Energy Convers Manag* 2017;135:373-393.
- [68] Bernard L, Guenther VE. *Combustion, Flames and Explosions of Gases*. 2nd ed. Pittsburgh, Pennsylvania: Academic Press, INC, 1961.
- [69] Yi W, Bjorn R, Vincent M, Xilong Y, Linlin W, Frédéric G. Laminar flame speed of lignocellulosic biomass-derived oxygenates and blends of gasoline/oxygenates. *Fuel* 2017;202:572-582.
- [70] Nurmukan D, Chen TJM, Hung YM, Ismadi M-Z, Chong CT, Tran M-V. Enhancement of biogas/air combustion by hydrogen addition at elevated temperatures. *Int J Energy Res* 2020;44:1519–1534.
- [71] Konnov AA, Mohammad A, Kishore VR, Kim NI, Prathap C, Kumar S. A comprehensive review of measurements and data analysis of laminar burning velocities for various fuel + air mixtures. *Prog Energy Combust Sci* 2018;68:197–267.
- [72] Wei L, Yong J, Yi J, Xianli Z. Investigation of the influence of DMMP on the laminar burning velocity of methane/air premixed flames. *Fuel* 2019;235:1294-1300.
- [73] Sileghem L, Alekseev VA, Vancoillie J, Van Geem KM, Nilsson EJK, Verhelst S, Konnov AA. Laminar burning velocity of gasoline and the gasoline surrogate components iso-octane, n-heptane and toluene. *Fuel* 2013;112:355-365.
- [74] Rau F, Hartl S, Voss S, Still M, Hasse C, Trimis D. Laminar burning velocity

measurements using the Heat Flux method and numerical predictions of iso-octane/ethanol blends for different preheat temperatures. *Fuel* 2015;140:10-16.

[75] Chong CT, Hochgreb S. Measurements of laminar flame speeds of liquid fuels: Jet-A1, diesel, palm methyl esters and blends using particle imaging velocimetry (PIV). *Proc Comb Inst* 2011;33:979-986.

[76] Kumar K, Freeh JE, Sung CJ, Huang Y. Laminar Flame Speeds of Preheated Iso-Octane/O₂/N₂ and n-Heptane/O₂/N₂Mixtures. *J Propul Power* 2007;23:428-436.

[77] Sileghem L, Alekseev VA, Vancoillie J, Van Geem KM, Nilsson EJK, Verhelst S, Konnov AA. Laminar Burning Velocity of Gasoline and the Gasoline Surrogate Components Iso-Octane, nHeptane and Toluene. *Fuel* 2013;112:355-365.

[78] Meng Z, Liang K, Fang J. Laminar burning velocities of iso-octane, toluene, 1-hexene, ethanol and their quaternary blends at elevated temperatures and pressures. *Fuel* 2019;237:630-636.

[79] Nurmukan D, Tran M-V, Foo JJ, Scribano G, Chong CT, Huynh TC. Experimental study on laminar lifted flames of pre-vaporized palm oil biodiesel. *Fuel* 2021;288:119697.

[80] Kumar R, Singhal A, Katoch A, Kumar S. Experimental Investigations on Laminar Burning Velocities of n-Heptane + Air Mixtures at Higher Mixture Temperatures Using Externally Heated Diverging Channel Method. *Energy Fuels* 2020;34:2405-2416.

[81] Ranzi E, Frassoldati A, Stagni A, Pelucchi M, Cuoci A, Faravelli T. Reduced kinetic schemes of complex reaction systems: Fossil and biomass-derived transportation fuels. *Int J Chem Kinetics* 2014;46:512-542.

[82] Hua Y, Qiu L, Liu F, Qian Y, Meng S. Numerical investigation into the effects of oxygen concentration on flame characteristics and soot formation in diffusion and partially premixed flames. *Fuel* 2020;268:117398.

[83] Mazas AN, Fiorina B, Lacoste DA, Schuller T. Effects of water vapor addition on the laminar burning velocity of oxygen-enriched methane flames. *Combust Flame* 2011;158:2428-2440.

[84] Vu TM, Cha MS, Lee BJ, Chung SH. Tip opening of premixed bunsen flames: Extinction with negative stretch and local Karlovitz number. *Combust Flame* 2015;162:1614-1621.

[85] Wang J, Nie Y, Cai X, Guo S, Zhang W, Xie Y, Huang Z. Investigation on the highly negative curved syngas Bunsen flame and the critical local Karlovitz number when tip opening. *Fuel* 2018;215:429-437.

[86] Mizobuchi Y, Nambu T, Takeno T. Numerical study of tip opening of hydrogen/air Bunsen flame. *Proc Comb Inst* 2019;37:1775-1781.

[87] Alenezi RA, Norkhizan AM, Mamat R, Erdiwansyah, Najafi G, Mazlan M. Investigating the contribution of carbon nanotubes and diesel-biodiesel blends to emission and combustion characteristics of diesel engine. *Fuel* 2021;285:119046.

[88] Ficarella A, Carlucci AP, Chehroudi B, Laforgia D, Strafella L. Multi-Walled Carbon Nanotubes (MWCNTs) bonded with Ferrocene particles as ignition agents for air-fuel mixtures. *Fuel* 2017;208:734-745.

- [89] Fujii M, Zhang X, Xie H, Ago H, Takahashi K, Ikuta T, Abe H, Shimizu T. Measuring the thermal conductivity of a single carbon nanotube. *Phys Rev Lett* 2005;95:065502.
- [90] Hariram V, Udhayakumar V, Karthick P, Abraham Eben Andrews A, Arunraja A, Seralathan S, Micha Premkumar T. Effect of Carbon Nanotubes on Oxygenated Jojoba Biodiesel-Diesel Blends in Direct Injection CI Engines. *Int J Vehicle Structures & Systems* 2018;10:423-432.
- [91] Miller JA, Bowman CT. Mechanism and modeling of nitrogen chemistry in combustion. *Prog Energy Comb Sci* 1989;15:287-338.
- [92] Desantes JM, Lopez JJ, Redon P, Arregle J. Evaluation of the Thermal NO formation mechanism under low-temperature diesel combustion conditions. *Int J Engine Res* 2012;13:531-539.
- [93] Loffler G, Wargadalam VJ, Winter F, Hofbauer H. Decomposition of Nitrous Oxide at Medium Temperatures. *Combust Flame* 2000;120:427-438.

4. Combustion characteristics of pre-vaporized palm oil biodiesel diffusion flames

It must be highlighted that some parts of Chapter 4 were used to prepare the manuscript [A2] on the combustion behavior of non-premixed lifted palm oil biodiesel fuels. The work has successfully been published in Fuel.

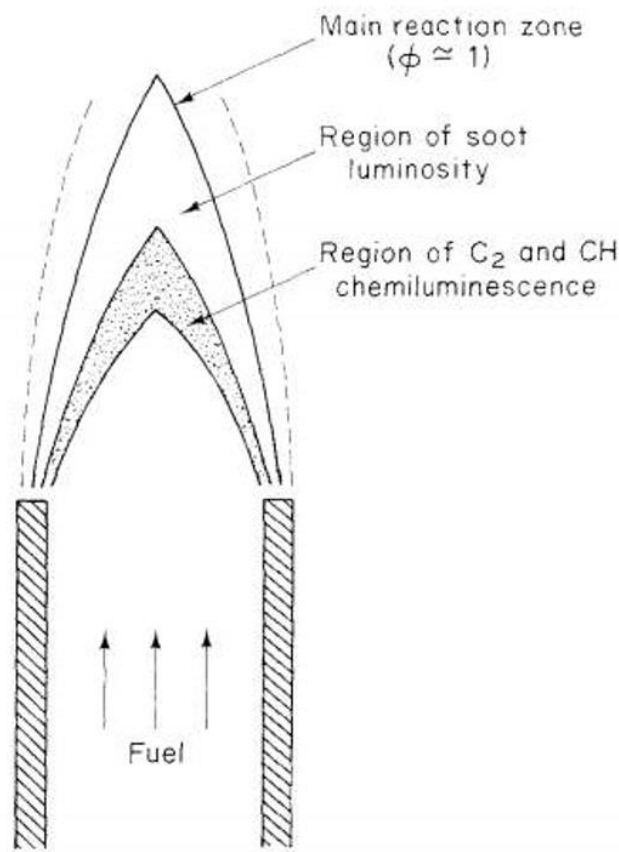
4.1. Introduction

Economic development due to the spikes in oil prices, ongoing debates on the possible shortage of the fossil fuels in the future, and the currently increasing awareness on the effect of greenhouse gasses on global warming and climate change have led to an increased interest in the development of the renewable clean fuels [1-5]. Among many available options, biodiesel fuel has drawn the attention of the scientific community due to its availability and variety of its feedstock sources, and its cleaner combustion nature compared to the traditional fossil fuels, all the while requiring minimal to no modification of the existing engines [6].

The existing literature shows [7-10] that there is still a lack of understanding of the combustion behavior of various biodiesel fuels due to the complexity of associated physical and chemical processes. In the present study, it is of interest to investigate biodiesel combustion behavior under various experimental conditions and also, to generate data that can be helpful in developing the chemical kinematic mechanisms. In the previous chapter, the premixed flames of pre-vaporized palm oil biodiesel fuel were studied to understand the behavior of fundamental combustion characteristics. The parameters such as the laminar burning velocity, blowoff velocity, flammability limits were investigated using coflow bunsen burner. While the fuel and oxidizer must be mixed prior to the ignition to generate premixed flames, the mixing

of fuel and oxidizer molecules occurs only after the reaction to establish non-premixed flames or also known as diffusion flames. It should be noted that many practical applications employ a non-premixed combustion method due to the safety aspect. Since the fuel and oxidizer are delivered to the reaction zone independently from each other, the possibility of accidents before the ignition, such as autoignition or explosion is mitigated. The mixing can be achieved by means of molecular diffusion, convection process as well as the turbulence of the flow [11]. However, in the present study, the laminar non-premixed flames are of interest, and the basic structure is shown in Fig. 4-1(a), adapted from [12]. While the equivalence ratio values can characterize the quality of mixing for premixed flames, the equivalence ratio values are not homogeneous throughout the flame structure for non-premixed flames [12,13]. The equivalence ratio varies from zero (for pure air in the mixture) to infinity (for pure fuel in the mixture). There are two main zones associated with most laminar non-premixed flames of hydrocarbon fuels: the primary reaction zone and region of luminosity. The outer layer of the reaction zone is usually blue in color and coincides with the stoichiometric line representing the visible flame front. The blue areas along the flame front and at the base of the flame are visible due to the radiation produced from CH radicals. On the other hand, the bright yellow part of the flame is the region of soot luminosity. These features are illustrated in Fig. 4-1(b), where the laminar non-premixed flame of biodiesel is ignited and stabilized on the burner at the atmospheric temperature, and the unburnt mixture temperature of 550 K.

The study of laminar non-premixed flames allows for the investigation of some flame combustion characteristics such as flame height and lifted flame behavior under various experimental conditions. Hence, Chapter 4 focuses on the combustion behavior of lifted laminar non-premixed flames of pre-vaporized palm oil biodiesel fuel.



(a)



(b)

Figure 4-1: Non-premixed flames, (a) schematic diagram of the flame structure [12], (b) non-premixed flame of palm oil biodiesel fuel at $T=550\text{K}$ and atmospheric pressure.

4.2. Literature review on lifted flames

It was explained in the previous chapters that the primary fuel of the study is biodiesel. As one of its advantages, biodiesel can be produced from a wide range of feedstocks, both from edible [14] and non-edible sources [15]. A number of research groups have studied combustion characteristics of different biodiesels such as soybean, coconut, rapeseed, sunflower, palm oil, and others [14-17]. Upon their observations, the results showed that palm oil biodiesel has a slight advantage over the other fuels because it has a higher cetane number and calorific value. Moreover, this fuel tends to achieve complete combustion due to the presence of oxygen in

palm oil biodiesel, leading to lower soot production compared to traditional fuels. Despite all the positive findings of palm oil biodiesel, it has some significant drawbacks such as low heating value as well as high freezing point. Thus, biodiesel is mainly blended with the standard fossil fuel in order to obtain the optimal fuel characteristics in terms of cleanliness and combustion efficiency [18,19]. Since palm oil biodiesel is generally blended with traditional diesel fuels, it is of utmost importance to identify the limitation of the flame stability for biofuels to avoid the degradation of the fuel blend.

There are three main parameters that can characterize the stabilization mechanism of laminar non-premixed flames in practical combustors, known as liftoff velocity (ULO), liftoff height (HL), and blowoff velocity (UBO). Understanding the behavior of the lifted flames is also critical in the development of industrial burners [20]. There is a wide range of applications where the lifted flames occur, such as gas turbines, power systems, and traditional diesel engines [21]. As such, the stabilization of the lifted flames has been extensively studied both numerically and experimentally at various conditions such as fuel types, dilution effect, the inclusion of partial premixing as well as different coflow velocities [21-29]. Chung [25] showed that the lifted laminar non-premixed flames exhibit tribrachial flame edge under non-autoignited experimental conditions. In his work, the tribrachial flame edge was defined as the intersection location where three flame brunches, such as lean and rich premixed flame wings as well as the diffusion flame, are connected and extended from a single point. The balance mechanism between the local flow velocity along the contour of stoichiometry and the flame burning velocity enables the stabilization of lifted non-premixed flame experiencing the tribrachial flame edge. Hence, based on this mechanism, it can be understood that the relationship between the height of lifted flames and the corresponding jet velocity can be established [30,31]. Choi and Chung [27] reported that the fuel could experience the behavior of lifted flames under non-autoignited conditions provided Schmidt number (Sc) of the given

fuel is higher than unity. Schmidt number can be defined as the ratio between momentum and mass diffusivity. It should be noted that Schmidt number of the fuel can be derived based on the exponent of the mathematical correlation between the jet velocity and the liftoff height of the flame. On the contrary, within the autoignited regime, authors [27] showed that the lifted flames experienced mild combustion, which resulted in a different flame structure and liftoff behavior compared to the flames under non-autoignited conditions. Based on the experimental results, it was concluded that the autoignited non-premixed lifted flames could be obtained even at the condition of Schmidt numbers being less than unity. Furthermore, Van et al. [28] performed numerical and experimental studies to investigate the liftoff behavior of nitrogen-diluted methane jet flames. The authors showed that the stationary lifted flames can be obtained even with the fuels having Schmidt number less than unity. These findings were in good agreement with the findings of Won et al. [32], who also studied the liftoff behavior of nitrogen-diluted methane flames. Choi and Chung [23] also established a mathematical relationship between the liftoff height and the corresponding jet velocity normalized by the stoichiometric laminar burning velocity of the n-heptane fuel mixture. A similar study was conducted by Al-Noman et al. [24] to investigate the behavior of iso-octane flames. The results showed that the flames experienced higher liftoff heights for iso-octane than n-heptane, which was associated with the prolonged ignition delay and lower laminar burning velocity of iso-octane compared to n-heptane.

It should be noted that the existing literature on the liftoff behavior of biofuels is still limited to a certain extent. The laminar non-premixed jet flames of dimethyl ether [26,33,34] and syngas [21,35] are among the few biofuel flames studied in the past. Xue and Ju [34] illustrated, both experimentally and analytically, the significance of flame stretch and oxygen enrichment in the mixture on the behavior of lifted flames of dimethyl ether fuel. The results revealed that Schmidt number and flame liftoff height was affected by the presence of flame

stretch. Furthermore, the oxygenated fuel mixtures experienced the shift from the direct liftoff regime to the direct blowout regime. While the study provided significant insight into the liftoff phenomena of dimethyl ether and other hydrocarbon fuels, it is essential to highlight that the studies were conducted for single-component fuels. On that note, Quattrocchi et al. [21] conducted a numerical investigation on the effect of syngas compositions, comprised of CO and H₂, on the flame stability parameters such as liftoff and blowout velocities.

While the existing literature shows promising results, it was found that there is also a lack of studies on the liftoff behavior and the stabilization of non-premixed heavy hydrocarbon flames. It should also be noted that heavy hydrocarbon fuels can provide a better representation of traditional fuels in practical combustion applications. Hence, the understanding of the combustion behavior of heavy hydrocarbon fuels can be very beneficial. As such, palm oil biodiesel fuel was selected for investigation in the present study. The main objective of the present study is to experimentally investigate the characteristics of the laminar lifted flame of the palm oil biodiesel by varying fuel mole fraction at elevated unburnt gas temperatures. This study provides reasonable correlations between the liftoff height and jet flow velocity, as well as the buoyancy effect and liftoff velocity.

4.3. Experiment

The experimental setup, schematically shown in Fig. 4-2, consisted of a coflow burner, fuel supply line, mass flow controllers (MKS, 1179 A), syringe pump (NE-300), heating ropes (Omega), thermocouples (Omega, SA3-K-72), variable autotransformer variac, the temperature readout unit (midi LOGGER GLB20) and a digital camera (Fujifilm X-T20). A stainless-steel tube with an inner diameter of 6.35 mm and a thickness of 1 mm was employed as the central nozzle of the burner. In the case of the central nozzle, in order to achieve a fully

parabolic velocity profile at the outlet of the nozzle, the length of the tube was chosen to be over 500 mm [36]. The palm oil biodiesel was delivered to the central nozzle via a syringe pump, where the fuel was pre-vaporized and diluted by the pre-heated carrier gas of N₂. The autotransformer variac controlled the output of the supplied voltage to the heating ropes to achieve the desired temperature. Multiple thermocouples (TC1-3) were attached throughout the system to confirm the uniformity of heating temperature, and the ceramic wool insulators were installed to mitigate the heat loss to the environment. One of the thermocouples (TC3) was placed at the nozzle exit to ensure the temperature of the mixture was set at the desired conditions. Air was used as the coflow gas to stabilize the lifted flames above the burner. The uniformity of the air coflow was achieved by filling the burner with glass beads and utilizing a honeycomb as a pathway. The air coflow velocity was set at 10 cm/s and was kept constant for all the experimental cases. The flow rates of both air coflow and N₂ carrier gas were controlled by mass flow controllers and readout controller (MKS, 247D 4 channel). To minimize the potential errors, the mass flow controllers were calibrated using a dry-test gas meter (Bios, Definer 220M) for each specific gas accordingly. The pre-heated temperature of N₂ carrier gas was kept constant at 483 K to avoid the condensation of vaporized fuel during the mixing process, as its boiling temperature is 483 K. In this experimental study, the fuel/N₂ mixtures were heated at the temperature range of 500 K – 650 K (unburnt gas temperature), and the fuel mole fraction was varied from 0.01 to 0.02. The lifted flames were visualized via direct photography employing the digital camera, and liftoff heights, which is the distance between the nozzle rim and the base of the lifted flame, were measured in post-analysis via image processing using MATLAB.

The fuel used in this experimental study was palm oil biodiesel, also known as palm methyl esters (PME), supplied by Mewah Oils Sdn. Bhd., Malaysia. The quality of the PME is within the European Union's EN14214 standards. The properties of the fuel and its

composition are shown in Tables 1 and 2. The compositions of PME were obtained via GC-MS analysis using Agilent 7890A (GC) & 5975C (MS) [37,38].

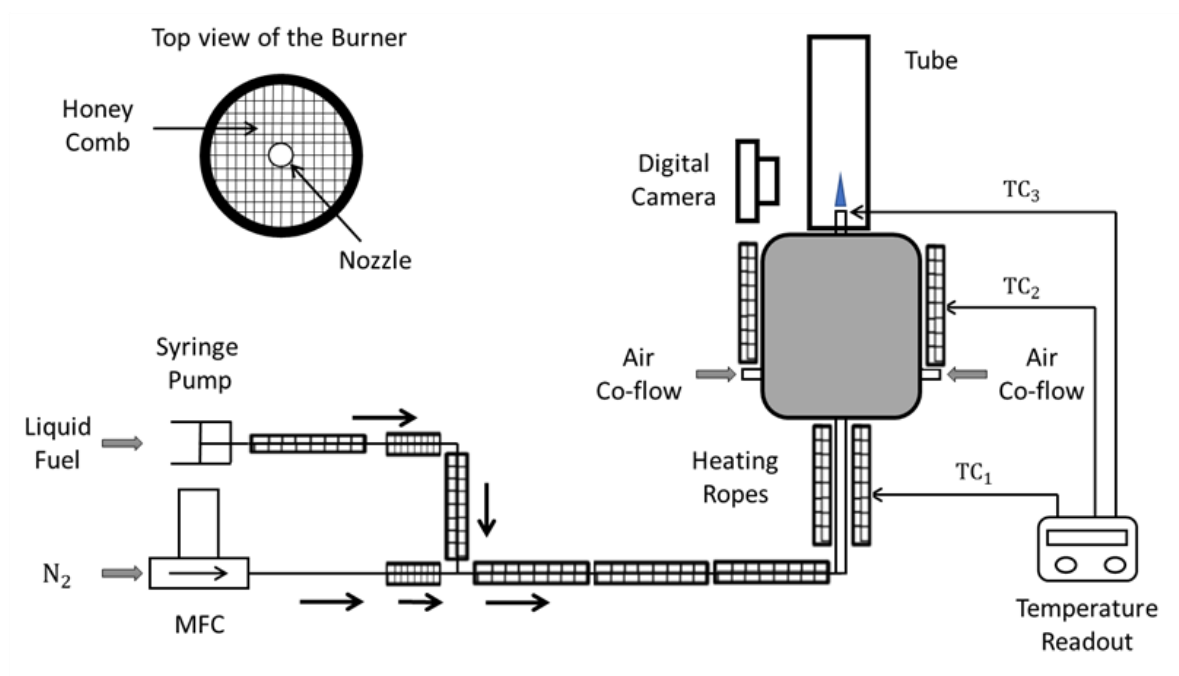


Figure 4-2: Schematic diagram of the experimental setup.

Table 4-1: Diesel and Palm methyl esters (PME) properties.

	Diesel	PME
Density at 25 °C [kg/m ³]	820	872
Kinematic viscosity at 40 °C [mm ² /s]	3.05	4.1
Flash point [°C]	79	101
Boiling point [°C]	> 180	> 210
Cetane number [-]	49	51
Molecular weight [g/mol]	190	281

High heating value [MJ/kg]	46.2	39.9
----------------------------	------	------

Table 4-2: Compositions of fatty acids in palm methyl esters (PME).

Fatty acid	No. of carbon: double bond	Composition (% wt)
Palmitic	(C16:0)	47.50
Oleic	(C18:1)	39.55
Linoleic	(C18:2)	8.42
Stearic	(C18:0)	4.53

4.4. Results & Discussion

The objective of this work was to experimentally study the behavior of the lifted flames of PME for different fuel mole fractions in the mixture at elevated unburnt gas temperatures. The lifted flames were achieved by varying the jet flow velocity at a specified temperature per given fuel mole fraction in the mixture. To describe the behavior of the lifted flames, the correlations between the liftoff height and jet flow velocity, as well as the buoyancy effect and liftoff velocity, were obtained.

4.4.1. Experimental validation

Since the selected fuel of the study was palm oil biodiesel which is a liquid fuel, n-heptane [23] and iso-octane [24] were chosen as the reference fuels in order to validate the accuracy of the present experimental setup. The same conditions were applied, such as the non-autoignited regime and the molar fraction of the fuel, which was kept in the range of 0.02 – 0.04. Figs. 4-3(a) and (b) show the direct comparison between the results from this study and the literature. It can be seen that the results are in good agreement both value-wise as well as

trend-wise. Thus, it can be concluded that the current experimental setup is acceptable to produce adequate results.

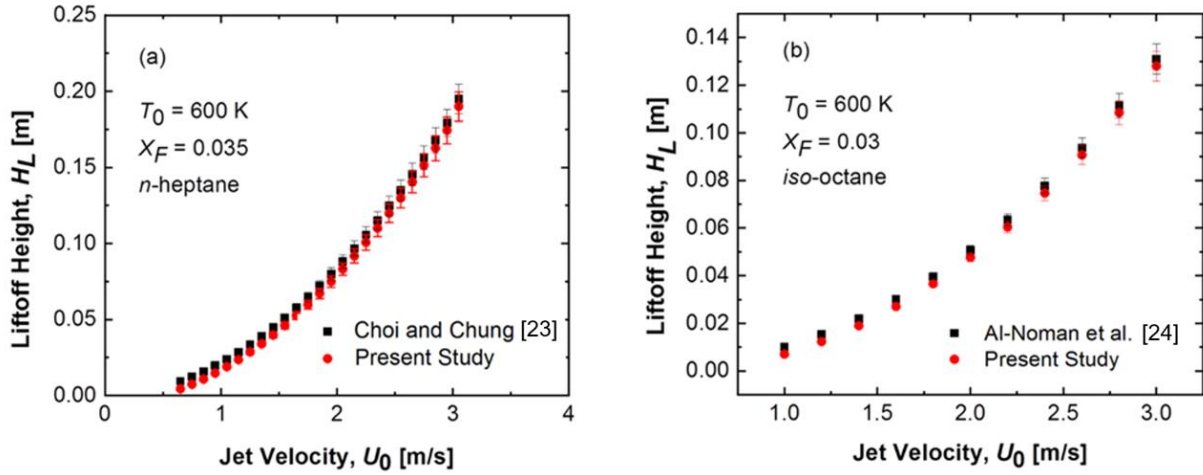


Figure 4-3: Comparison of the liftoff heights with literature values for (a) *n*-heptane, (b) *iso*-octane.

4.4.2. Stabilization of non-premixed laminar lifted flames

The characteristics of laminar lifted flame are influenced by multiple parameters such as the unburnt gas temperature, T_0 , fuel mole fraction in the mixture, X_F , as well as the jet flow velocity, U_0 [29]. Figure 4-4 displays direct photographs of the typical laminar non-premixed lifted flames for palm oil biodiesel fuels. Fig. 4-4(a) shows the effect of increasing U_0 on the liftoff height of the flames and Fig. 4-4(b) illustrates the behavior of the lifted flames for $U_0 = 0.7$ m/s and $X_F = 0.02$ at different unburnt gas temperatures. As can be observed from the direct images, the liftoff height increased with the increasing jet flow velocity (Fig. 4-4(a)). On the contrary, elevation in the unburnt gas temperature led to a reduced liftoff height per given fuel mole fraction (Fig. 4-4(b)). While the edges of the lifted flames were not shown in detail to represent the tribrachial structure, Al-Noman et al. [26] showed that the tribrachial edge was

associated with the lifted flame even when it was not clearly visible from the direct photography. Furthermore, the existence of the tribrachial structure at the edges of lifted flames was shown for both gaseous fuels [27] and liquid fuels [23,24]. This means that the lifted flames have a triple structure where the point of lean and rich premixed flame wings is connected and trailed by a diffusion flame [25]. It should be noted that the edges of the flames remained to have a tribrachial structure regardless of changes in T_0 , X_F , and U_0 .

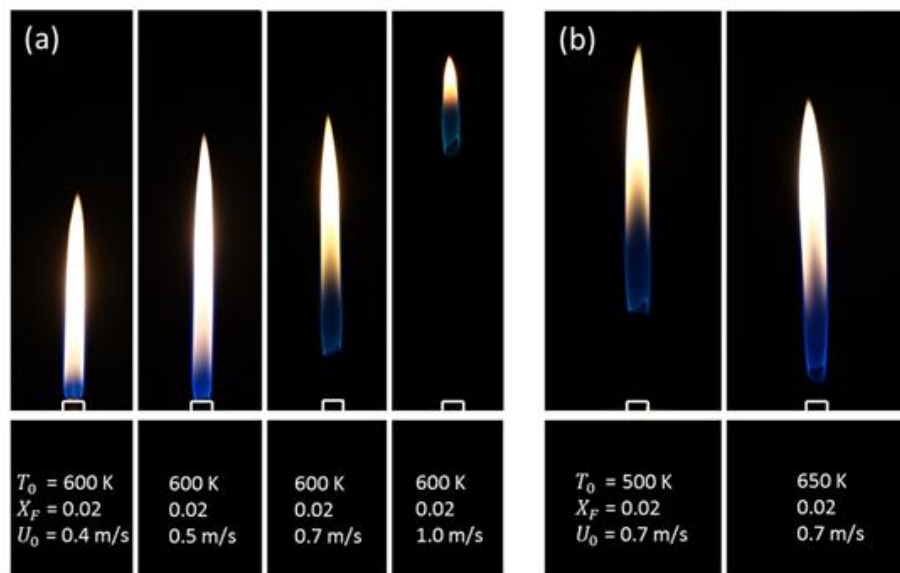


Figure 4-4: Visible images of the laminar diffusion flames of biodiesel.

To further study the behavior of the lifted flames, Fig. 4-5(a) illustrates the lifted flames as a function of jet fuel velocity at $T_0 = 500 \text{ K}$ and $X_F = 0.02$. As can be observed from the graph, the flame was initially established and attached to the nozzle rim at relatively low jet flow velocity ($U_0 \leq 0.35 \text{ m/s}$). As the jet flow velocity increased, the laminar non-premixed flames lifted off from the nozzle rim and stabilized at a specific height. It was followed by a non-linear increment in the liftoff height of the flame until it reached a critical jet flow velocity

where the blowout took place. The non-linear progression, shown in Fig. 4-5(a), can be expressed in terms of a power law with the correlation coefficient of 0.98:

$$H_L = 0.1495 \times U_0^{2.842} \quad (1)$$

As the unburnt gas temperature increases, the heat transfer between the nozzle rim and the lifted flame enhances [36, 39]. This led to a reduced liftoff height of the flames due to the elevated unburnt gas temperatures, which can be seen in Fig. 4-5(b). At the given fuel mole fraction of $X_F = 0.02$ and jet flow velocity of $U_0 = 0.6$ m/s, the flame experienced the liftoff height of 0.036 m at $T_0 = 500$ K and blowout at a slightly lower temperature. In contrast, the flame at the same fuel mole fraction and jet flow velocity is fully attached to the nozzle at the temperature of 650 K.

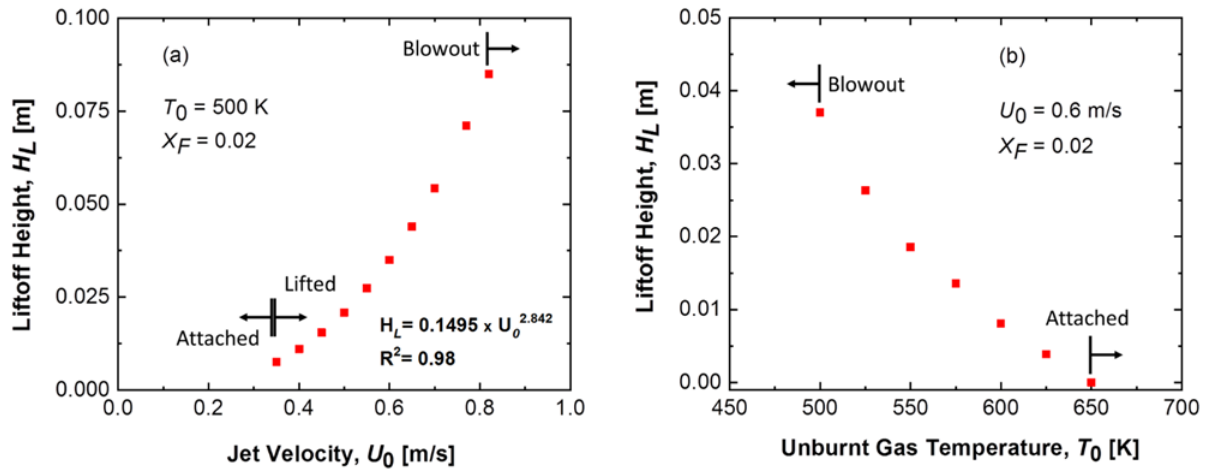


Figure 4-5: Liftoff heights for various (a) jet flow velocities at $T_0 = 500$ K and $X_F = 0.02$, (b) unburnt gas temperatures at $U_0 = 0.6$ m/s and $X_F = 0.02$.

Based on the obtained results, it was expected that the lifted flames could be achieved in a limited domain in terms of the fuel mole fraction and the unburnt gas temperature, as shown

in Fig. 4-6. The blue lines represent the lower limit of the domain. When the fuel mole fraction in the mixture was below the blue lines at a given temperature, the flame could not be stabilized due to the high dilution ratio of the inert gas (N_2). On the contrary, the red lines represent the upper limit of the domain. When the fuel mole fraction in the mixture was above the red lines at a given temperature, the stable flame could be established on the nozzle rim at low jet flow velocities. However, as the jet flow velocity increased and reached a critical value, the flame blew off without having a liftoff effect. In this study, experiments were conducted at the unburnt gas conditions represented with “+” sign, as shown in Fig. 4-6. The results showed that the flames, with the conditions within the domain, experienced all three stages of flame development. The laminar non-premixed flames were established on the nozzle rim at the sufficiently low jet flow velocity, followed by the liftoff due to the increasing jet flow velocity, and experienced the blowout once the velocity reached a critical value. It was noted that 483 K is the lowest set temperature at the nozzle exit to achieve complete vaporization. Below this temperature, the experiments could not be conducted as the fuel could not be vaporized completely.

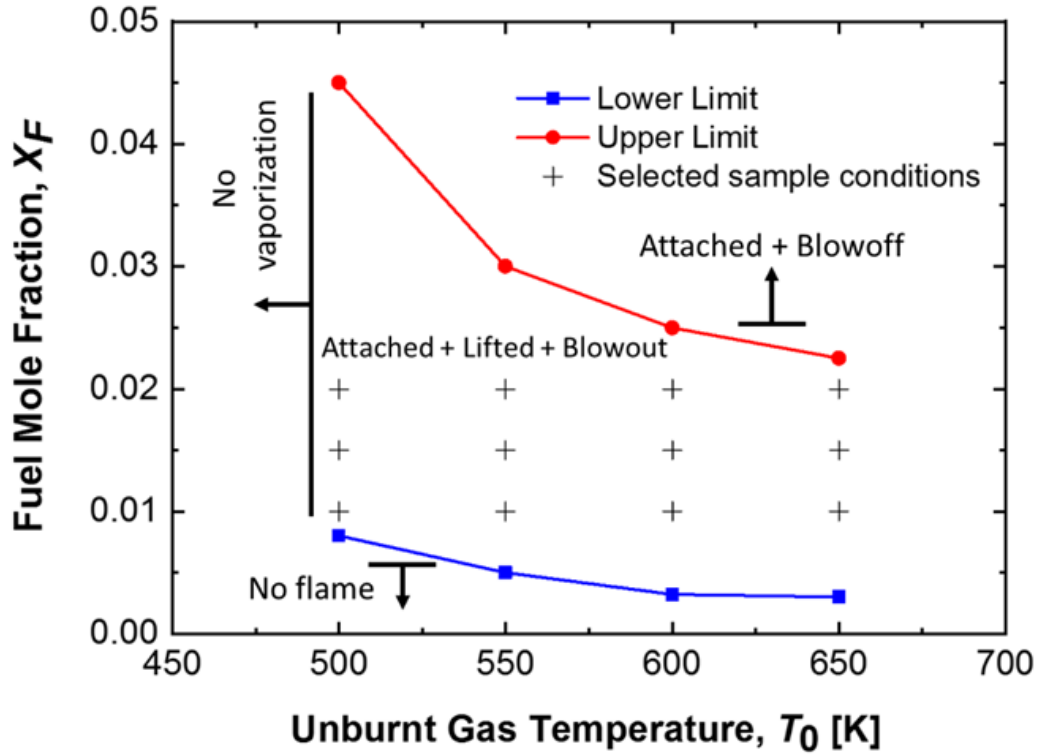


Figure 4-6: The domain of existence of the lifted flames.

4.4.3. Effect of elevated unburnt gas temperature

As mentioned earlier, the liftoff height of the flames can be influenced by multiple parameters such as the unburnt gas temperature, the fuel mole fraction in the mixture as well as the jet flow velocity. Figure 4-7 shows the liftoff height as a function of jet flow velocity for varying fuel mole fraction as well as unburnt gas temperature. In order to highlight the fairly linear correlation between the liftoff heights and the jet flow velocities at different temperatures and fuel mole fractions, a log-log scale was used. However, it was observed that the linear relation between the liftoff heights and the jet flow velocities weakened with an increase in unburnt gas temperature. On the other hand, higher unburnt gas temperatures resulted in a steeper slope of the data, regardless of the fuel mole fraction in the mixture. Furthermore, the linear trend seems to deteriorate only at relatively low liftoff height, which is illustrated by the

points below the dashed-dotted line in Fig. 4-7. This behavior can be explained based on the observation made by Won et al. [40]. They have found that the lifted flames could be stabilized in either developing or developed regions of the jet, which were corresponding to the areas near the nozzle and further away from the nozzle rim, respectively. Won et al. [40] suggested that the length of the developing region is approximated by cold jet theory, where centerline velocity U_{CL} must be smaller than U_{\max} , with U_{\max} the maximum jet flow velocity ($U_{\max} = 2U_0$).

$$U_{CL} = \frac{U_0^2 d^2}{8\nu x} \quad (2)$$

where d is the inner diameter of the nozzle, ν is the kinematic viscosity of the unburnt gas, and x is the axial distance. Since the fuel mole fraction was notably smaller than the mole fraction of the carrier gas, the kinematic viscosity of N_2 was adopted to calculate the centerline velocity. Furthermore, the temperature influences the kinematic viscosity of the gas, hence, the length of the developing region is appreciably influenced by temperature. The changes in slope and non-linearity within the developing region were demonstrated by the dashed-dotted line, which was the locus of cross-points of the experimental results. This behavior is in good agreement with the findings related to the lifted flames of the pre-vaporized *n*-heptane [23] and *iso*-octane [24] but disagrees with the pure gaseous fuels [27,29]. One of the most significant differences between these studies is that pre-vaporized liquid fuels were prepared with a much higher dilution ratio of N_2 as they required a carrier gas, unlike pure gaseous fuels. Thus, to explain the significance of the dilution ratio in gaseous fuels, Van et al. [28] experimentally studied the laminar lifted nitrogen-diluted methane jet flames. Their results showed that, within the developing region of the jet, the highly diluted gaseous flames experienced the non-linear behavior between H_L and U_0 , which agreed with the behavior observed in the present study.

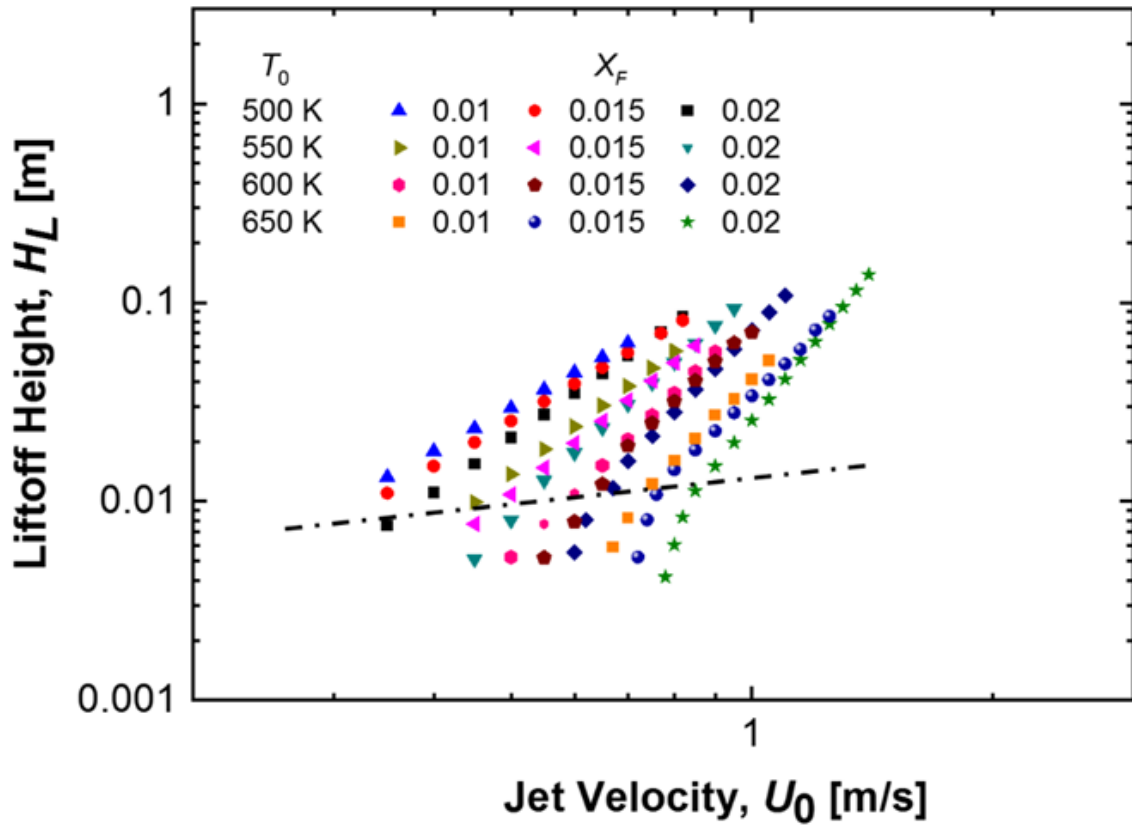


Figure 4-7: Liftoff height as a function of jet flow velocity for various unburnt gas temperatures and fuel mole fractions.

The stabilized lifted flame, having a tribrachial structure, is associated with the balance mechanism between the local flow velocity along the contour of stoichiometry and the burning velocity of the tribrachial flame. The existence of the tribrachial structure in lifted flames implies that there is a relation between the tribrachial edge propagation speed and its associated stoichiometric laminar burning velocity of the given mixture [25]. As such, it can be assumed that the liftoff velocity and, subsequently, liftoff height can be related and dependent on the stoichiometric laminar burning velocity. Hence, all the obtained data were replotted in Fig. 4-8 to further emphasize the role of the stoichiometric laminar burning velocity, S_{st}^0 . The results showed that the liftoff height is significantly influenced by the stoichiometric laminar burning

velocity, regardless of the fuel mole fraction and the unburnt gas temperature. It is noted that the stoichiometric laminar burning velocity of the flame, per given mixture, was obtained via the PREMIX code in Chemkin using the kinetic mechanism developed by Kuti et al. [41]. The compositions of the palm oil biodiesel were used in accordance with the values in Table 4-2. The overall correlation between the liftoff height and dimensionless jet flow velocity, U_0/S_{st}^0 , was successfully established with the correlation coefficient of 0.92. Hence, the changes in the slopes of H_L versus U_0 between developing or developed regions in Fig. 4-7 were attributed to the varying of the unburnt gas temperature as well as the fuel mole fraction in the mixture. This is due to the differential diffusion between the fuel and carrier gas, which directly affects the fuel mole fraction in the stoichiometric region of the flame [29]. As a result, the stoichiometric laminar burning velocity is changed, thereby influencing the burning velocity of the tribrachial flame.

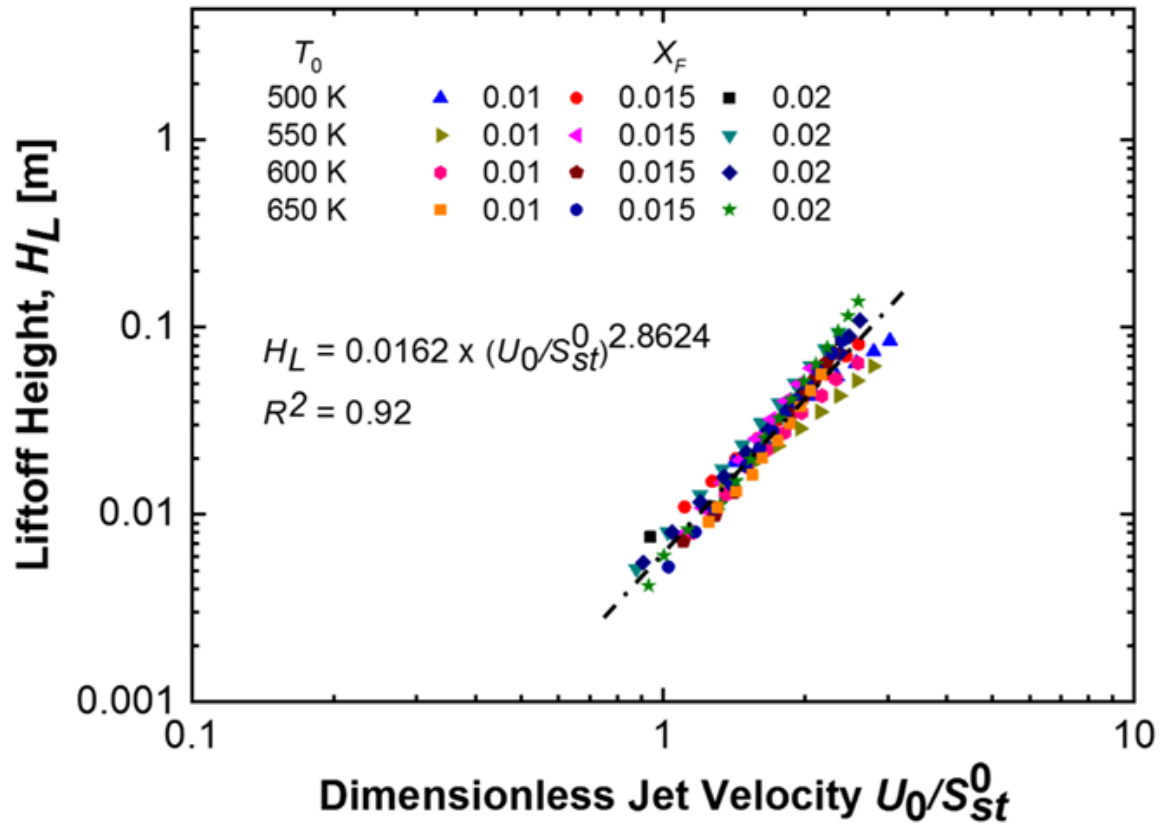


Figure 4-8: Liftoff height as a function of jet flow velocity scaled by the stoichiometric laminar burning velocity for various unburnt gas temperatures and fuel mole fractions.

4.4.4. Jet flow velocity of lifted flames

From Fig. 4-5(a), it can be seen that the flame was initially attached to the nozzle rim at relatively low jet flow velocity. Once it reached a certain velocity, the flame abruptly experienced liftoff. This velocity is known to be the liftoff velocity, U_{LO} . In Fig. 4-9, liftoff velocities of palm oil biodiesel were plotted as a function of stoichiometric laminar burning velocity, together with the liftoff condition shown as the dashed line. Ko and Chung [42] and Lee et al. [43] explained that, for the liftoff to take place, the jet flow velocity must be higher than the stoichiometric laminar burning velocity of the mixture. Hence, the flames that experience $U_{LO} < S_{St}^0$, theoretically, could not be lifted. However, as can be seen from Fig. 4-

9, there are some discrepancies for the previously mentioned statement. This contradiction can be associated with the buoyancy effect [44].

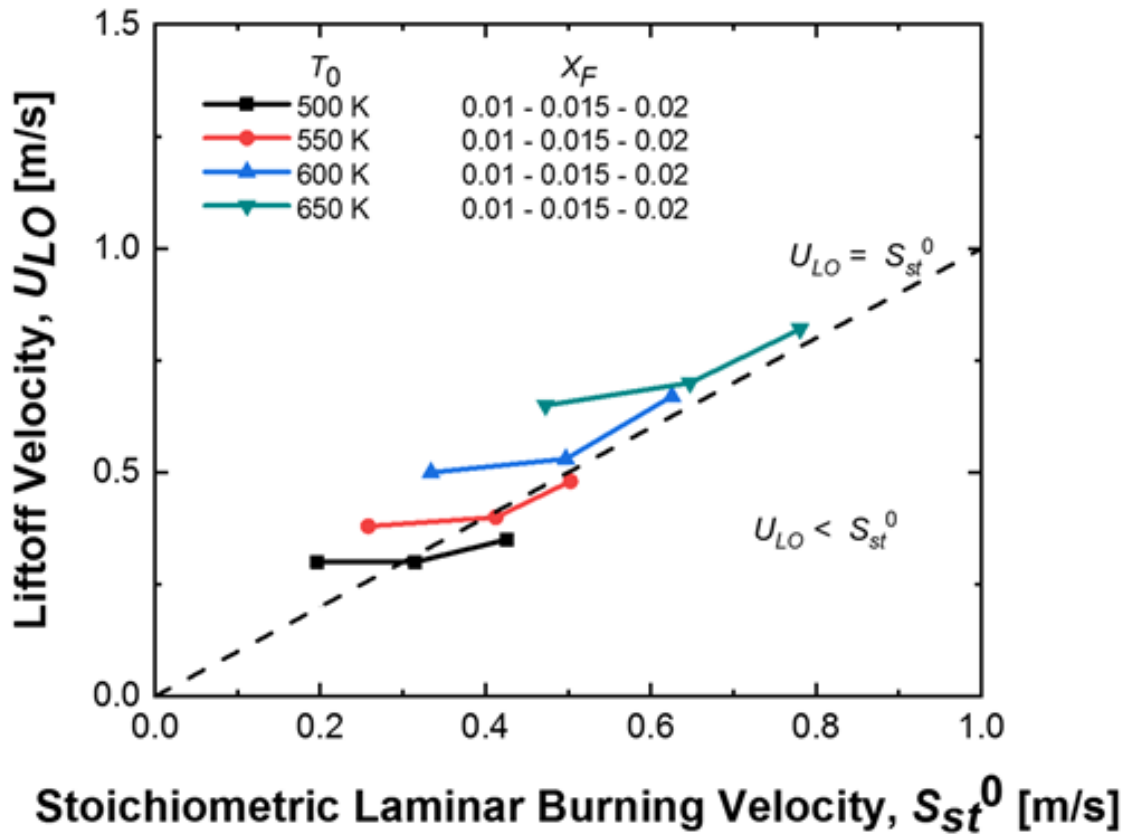


Figure 4-9: Liftoff velocity as a function of the stoichiometric laminar burning velocity for various unburnt gas temperatures and fuel mole fractions.

Based on the general structure of the non-premixed laminar lifted flames, it can be understood that there are temperature and density differences between the unburnt and burnt gases. As a result, the flame can experience a driving force of buoyancy, known as a buoyant force. This force has the highest impact near the nozzle rim, where it leads to an increase in flow velocity as it causes the entrainment of the flow of the mixture, thereby leading to the

buoyancy-induced velocity of the flame, U_B . Therefore, considering the presence of buoyancy, the overall local flow velocity becomes higher, resulting in $U_{LO}^* = U_{LO} + U_B$. Thus, the condition for the existence of lifted flames ($U_{LO}^* > S_{st}^0$), can be fully satisfied.

Bédard and Cheng [44] showed the effect of buoyancy on the premixed flame stabilization. Based on their work, the impact of buoyancy on the flow rate of the mixture was approximated using the following expression:

$$U_B = \sqrt{(\Delta\rho/\rho_u)gd} \quad (3)$$

with the density difference between the unburnt and burnt gases $\Delta\rho = \rho_u - \rho_b$, densities of the unburnt gas ρ_u and burnt gas ρ_b , gravitational acceleration g , and the inner diameter of the nozzle d . Hence, Fig. 4-10 was plotted by including the effect of buoyancy-induced velocity to the liftoff velocity, $(U_{LO}U_B)^{1/2}$. This graph shows that the scaled expression of $(U_{LO}U_B)^{1/2}$ is a good indicator in demonstrating the significance of the buoyancy effect on the lifted flames, with the correlation coefficient of 0.97. This implies, together with the observations from Fig. 4-9, that the buoyancy effect reduced the liftoff velocity of the flame. Lastly, it is essential to note that the expression used for the approximation of the buoyancy, $\sqrt{(\Delta\rho/\rho_u)gd}$, is sensitive to the change in unburnt gas temperature. Hence, with the increasing unburnt gas temperature, the flow entrainment at the nozzle rim caused by the buoyancy is mitigated, as shown in Fig. 4-9.

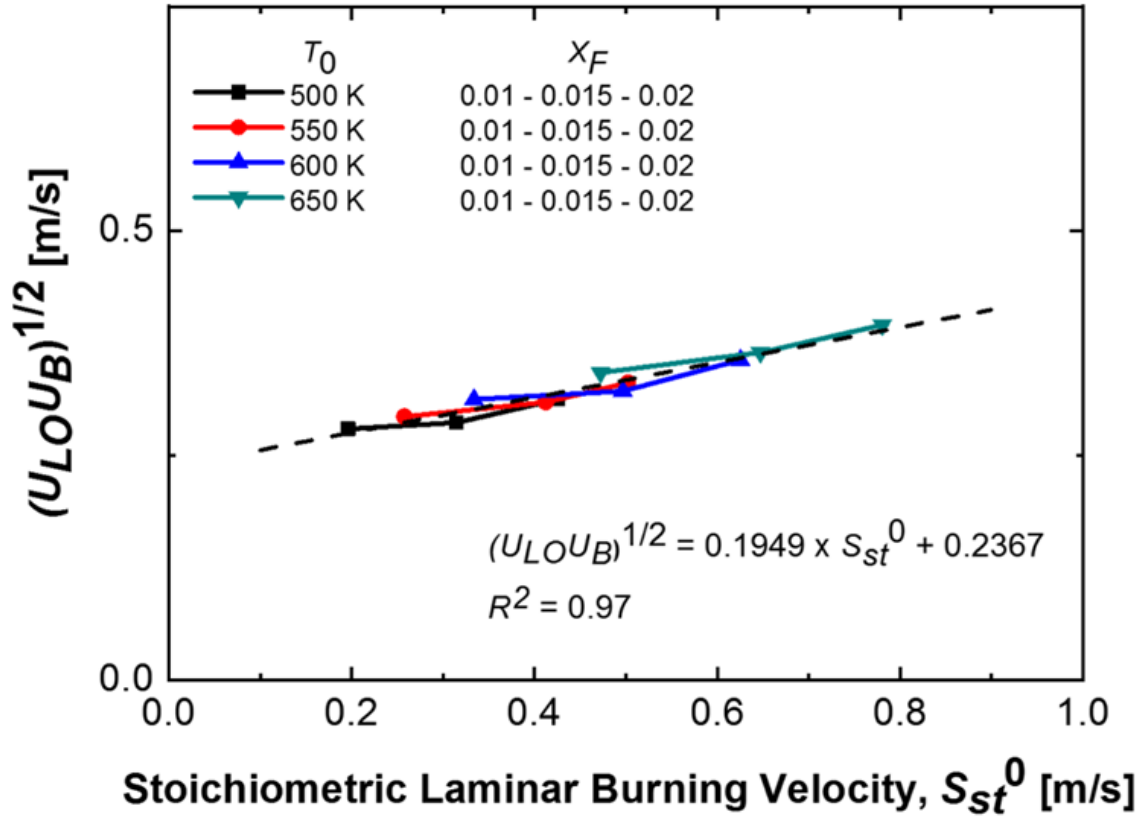


Figure 4-10: Effect of the buoyancy-induced velocity on the liftoff with respect to stoichiometric laminar burning velocity for various unburnt gas temperatures and fuel mole fractions.

4.4.5. Diesel-Biodiesel blends

Fig. 4-11 displays direct photographs of laminar diffusion lifted flames of pure biodiesel (B100), pure diesel (D100), and their blends at the same unburnt gas temperature of 550 K, the fuel mole fraction of 0.02, and jet flow velocity of 0.9 m/s. It can be seen that the liftoff height decreased with the increasing concentration of diesel in the fuel blend. Hence, the pure diesel flame stabilized at a lower liftoff height as compared to pure biodiesel flame at the same conditions. This phenomenon can be attributed to the difference in the laminar burning velocity that plays an essential role in flame stabilization. It is noted that the stoichiometric

laminar burning velocities of biodiesel and diesel at atmospheric pressure and unburnt gas temperature of 550 K were measured to be 103 cm/s and 112 cm/s, respectively.

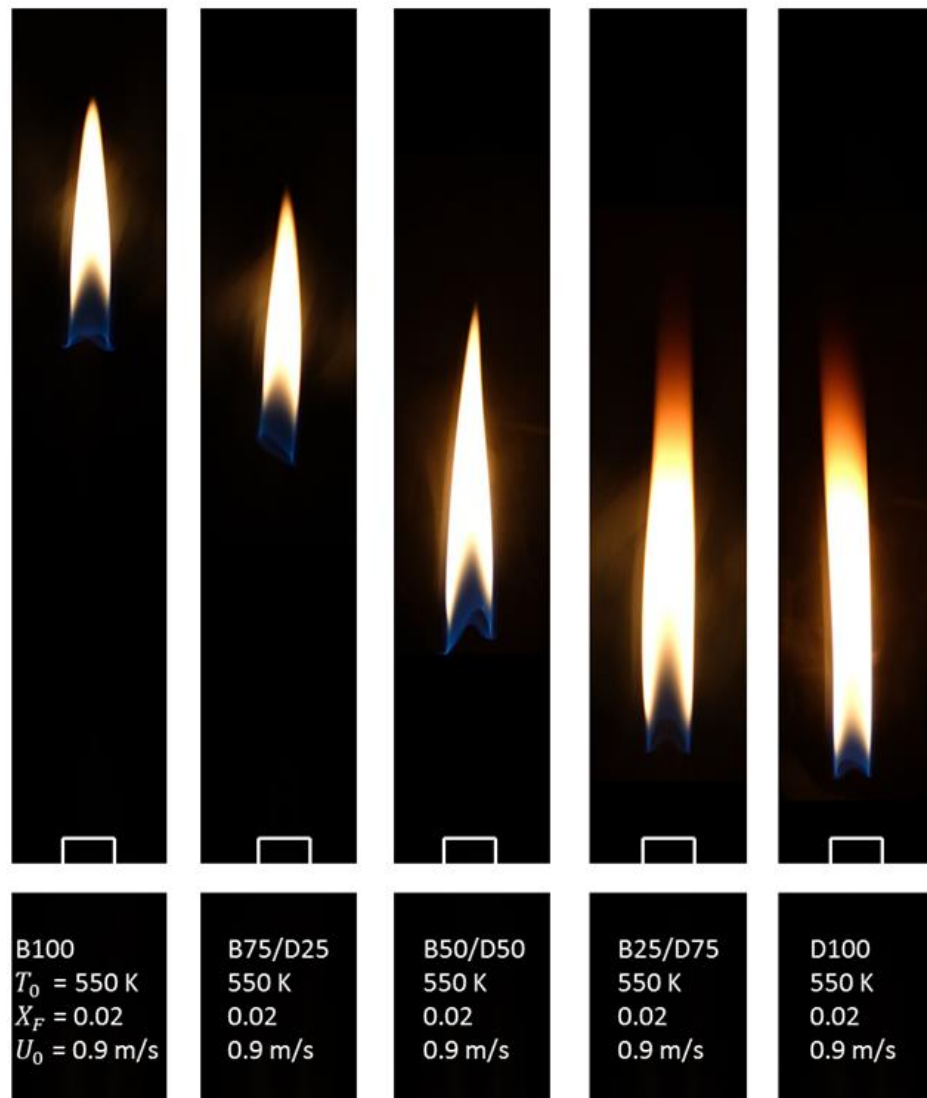


Figure 4-11: Visible images of the laminar diffusion flames of various biodiesel/diesel blends. B100 represents pure biodiesel, D100 represents pure diesel, B50/D50 represents 50% biodiesel/50% diesel blend.

Fig. 4-12 illustrates the liftoff height as a function of jet flow velocity at $T_0 = 550$ K and $X_F = 0.02$ for diffusion flames of B100, D100, and their blends. It can be seen that the liftoff heights of the D100 and biodiesel/diesel diffusion flames increased nonlinearly with jet flow velocity, which is similar to the trend of B100 lifted flame. Also, it can be observed that D100 flames were able to stabilize at a much higher jet flow velocity compared to B100 flame, indicating a stronger stabilization mechanism of diesel fuel. Since we focused on the characteristics of biodiesel lifted flame in the present study, a detailed explanation of the stabilization mechanism of diesel lifted flame should be addressed in a future study, where in-depth experimental and numerical investigations are required.

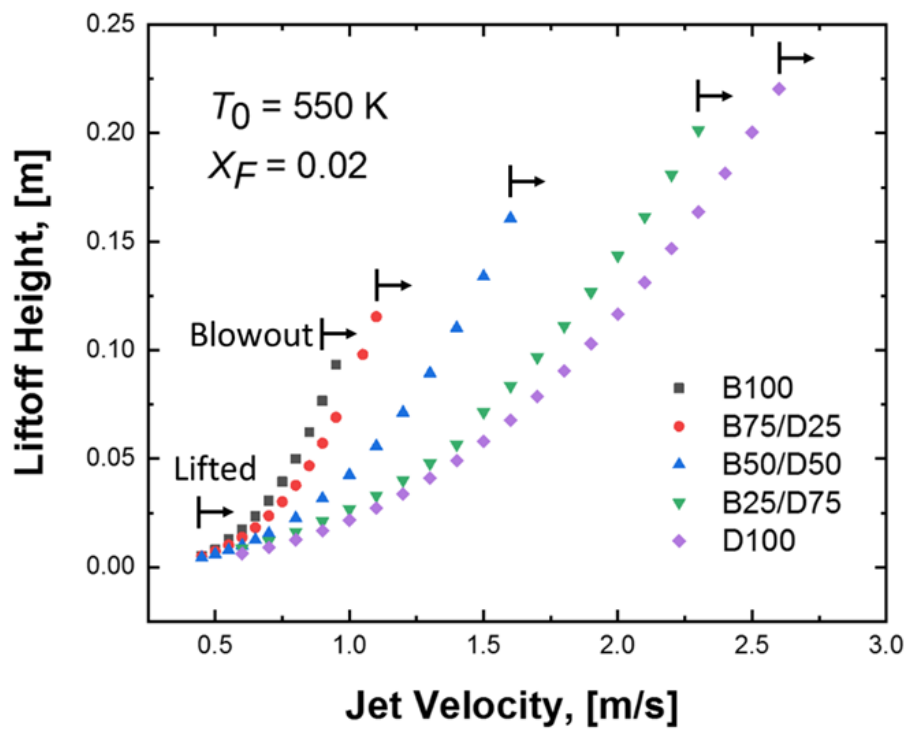


Figure 4-12: Liftoff height as a function of jet flow velocity for various biodiesel/diesel blends at $T_0 = 550$ K and $X_F = 0.02$.

4.5. Conclusion

In the present study, the liftoff characteristics of palm oil biodiesel were studied by varying the jet flow velocity per given fuel mole fraction and unburnt gas temperature. The fuel mole fraction and unburnt gas temperature ranges were 0.01 – 0.02 and 500 K – 650 K, respectively. The fuel was pre-vaporized and mixed with pre-heated nitrogen, which was used as the carrier gas. The major conclusions of the study are as follows:

1. The liftoff height increased with the higher jet flow velocity. The unburnt gas temperature and the fuel mole fraction had a similar effect on the lifted flames, because the increase in either of those parameters enhanced the heat transfer mechanism between the flame base and the nozzle rim, which resulted in lower liftoff heights. Based on these observations, the limited range of the conditions where the lifted flames occurred had been obtained per given unburnt gas temperature and fuel mole fraction.

2. The existence of the tribrachial structure implies the balance between the stoichiometric laminar burning velocity and local jet flow velocity. Thus, the dimensionless jet flow velocity, U_0/S_{st}^0 , was calculated to illustrate its correlation with the liftoff height of the flames. Furthermore, the changes in the slope and non-linear relationship between the liftoff height and the jet flow velocity were attributed to the nature of the developing region of the jet.

3. For the liftoff to take place, the jet flow velocity must be higher than the stoichiometric laminar burning velocity of the given mixture. It was noted that there were few cases where this criterion was not fulfilled, and this behavior was associated with the buoyancy effect on the flames. Hence, buoyancy-induced velocity was calculated and its correlation with the stoichiometric laminar burning velocity was obtained.

4. The liftoff height decreased with the increasing concentration of diesel in the fuel blend. Hence, B100 flame stabilized at higher liftoff height as compared to D100 flame due to

the lower laminar burning velocity of the biodiesel flame. Similar to the B100 lifted flame, the liftoff heights of the D100 and biodiesel/diesel diffusion flames increased nonlinearly with the jet flow velocity.

4.6. References

- [1] Noor CWM, Noor MM, Mamat R. Biodiesel as alternative fuel for marine diesel engine applications: A review. *Renew Sustain Energy Rev* 2018;94:127–142.
- [2] Martin U, Dieter B, Christine B, Bert B, Georg F, Rolf L, Martin M, Kevin S, Jennifer S, Olaf S, Ulrike S, Helmut T, Edgar R, Richard W, Markus W, Jürgen K. Action areas and the need for research in biofuels. *Fuel* 2020;268:117227.
- [3] Adeniyi OM, Azimov U, Burluka A. Algae biofuel: Current status and future applications. *Renew Sustain Energy Rev* 2018;90:316–335.
- [4] Gholamhassan N. Diesel engine combustion characteristics using nano-particles in biodiesel-diesel blends. *Fuel* 2018;212:668–678.
- [5] Medhat E, Hagar AEB, Khaled KE, Ahmed MR, Hitesh P, Kishor KS, Deepalekshmi P, Rashmi W. Experimental studies on the biodiesel production parameters optimization of sunflower and soybean oil mixture and DI engine combustion, performance, and emission analysis fueled with diesel/biodiesel blends. *Fuel* 2019;255:115791.
- [6] Digambar S, Dilip S, Shyam LS, Sumit S, Deepika K. Chemical compositions, properties, and standards for different generation biodiesels: A review. *Fuel* 2019;253:60–71.
- [7] Tamilselvan P, Nallusamy N, Rajkumar S. A comprehensive review on performance, combustion and emission characteristics of biodiesel fuelled diesel engines. *Renew Sust Energy Rev* 2017;79:1134–1159.
- [8] Weiss B, George A, Chen JY, Buchholz BA, Dibble RW. A numerical investigation into the anomalous slight NO_x increase when burning biodiesel; A new (old) theory. *Fuel Process Technol* 2007;88:659–667.
- [9] Xue J, Grift TE, Hansen AC. Effect of biodiesel on engine performances and emissions. *Renew Sustain Energy Rev* 2011;15:1098–1116.
- [10] Jiaqiang E, Minhhieu P, Zhao D, Yaunwang D, DucHieu L, Wei Z, Hao Z, Teng L, Qingguo P, Zhiqing Z. Effect of different technologies on combustion and emissions of the diesel engine fueled with biodiesel: A review. *Renew Sust Energy Rev* 2017;80:620–647.
- [11] Bernard L, Guenther VE. *Combustion, Flames and Explosions of Gases*. 2nd ed. Pittsburgh, Pennsylvania: Academic Press, INC, 1961.
- [12] Flagan RC, Seinfeld JH. *Fundamentals of Air Pollution Engineering*. Englewood Cliffs, New Jersey: Prentice-Hall Inc, 1988.
- [13] Glassman I, Yetter RA. *Combustion*. 4th ed. San Diego, California, USA: Academic Press, 2008.

- [14] Anantha RL, Deepanraj B, Rajakumar S, Sivasubramanian V. Experimental investigation on performance, combustion and emission analysis of a direct injection diesel engine fuelled with rapeseed oil biodiesel. *Fuel* 2019;246:69-74.
- [15] Rui W, Wan-Wei Z, Milford AH, Yu-Ping Z, Pinaki SB, Yan W, Bao-An S, Song Y. Biodiesel preparation, optimization, and fuel properties from non-edible feedstock, *Datura stramonium* L. *Fuel* 2012;91:182-186.
- [16] Chong CT, Chiong MC, Teyo ZY, Ng J-H, Tran M-V, Lam SS, Medina AV. Pool fire burning characteristics of biodiesel. *Fire Technol* 2020;56:1703-1724.
- [17] Moser BR. Influence of blending canola, palm, soybean, and sunflower oil methyl esters on fuel properties of biodiesel. *Energy Fuels* 2008;22:4301-4306.
- [18] İlker T, Ömer C, Bünyamin E. Numerical and experimental investigation of the effect of biodiesel/diesel fuel on combustion characteristics in CI engine. *Fuel* 2020;270:117523.
- [19] Ge JC, Kim HY, Yoon SK, Choi NJ. Optimization of palm oil biodiesel blends and engine operating parameters to improve performance and PM morphology in a common rail direct injection diesel engine. *Fuel* 2020;260:116326.
- [20] Wu Y. *Handbook of Combustion*. Weinheim: Wiley-VCH Verlag GmbH & Co. KGaA, cop. 2010. pp. 121-139.
- [21] Quattrocchi S, Aggarwal SK, Katta VR. Liftoff and blowout characteristics of laminar syngas nonpremixed flames. *Int J Hydrogen Energy* 2018;43:6421-6433.
- [22] Chan SMS, Torii S, Yano T. Enhancement of turbulent jet diffusion flame blowout limits by annular counterflow. *Int J Energy Res* 2001;25:1091-1105.
- [23] Choi SK, Chung SH. Autoignited and non-autoignited lifted flames of pre-vaporized n-heptane in co-flow jets at elevated temperatures. *Combust Flame* 2013;160:1717-1724.
- [24] Al-Noman SM, Choi SK, Chung SH. Autoignition characteristics of laminar lifted jet flames of pre vaporized iso-octane in heated coflow air. *Fuel* 2015;162:171-178.
- [25] Chung SH. Stabilization, propagation and instability of tribrachial triple flames. *Proc Combust Inst* 2007;31:877-892.
- [26] Al-Noman SM, Choi SK, Chung SH. Autoignited lifted flames of dimethyl ether in heated coflow air. *Combust Flame* 2018;195:75-83.
- [27] Choi BC, Chung SH. Autoignited laminar lifted flames of methane, ethylene, ethane, and n-butane jets in coflow air with elevated temperature. *Combust Flame* 2010;157:2348-2356.
- [28] Van K, Jung KS, Yoo CS, Oh S, Lee BJ, Cha MS, Park J, Chung SH. Decreasing liftoff height behavior in diluted laminar lifted methane jet flames. *Proc Combust Inst* 2019;37:2005-2012.
- [29] Kim KN, Won SH, Chung SH. Characteristics of laminar lifted flames in coflow jets with initial temperature variation. *Proc Combust Inst* 2007;31:947-954.
- [30] Chung SH, Lee BJ. On the characteristics of laminar lifted flames in a nonpremixed jet. *Combust Flame* 1991;86:62-72.
- [31] Lee BJ, Chung SH. Stabilization of lifted tribrachial flames in a laminar nonpremixed jet. *Combust Flame* 1997;109:163-172.

- [32] Won SH, Kim J, Hong KJ, Cha MS, Chung SH. Stabilization mechanism of lifted flame edge in the near field of coflow jets for diluted methane. *Proc Combust Inst* 2005;30:339-347.
- [33] Jung KS, Jung BR, Kang SH, Chung SH, Yoo CS. A numerical study of the pyrolysis effect on autoignited laminar lifted dimethyl ether jet flames in heated coflow air. *Combust Flame* 2019;209:225-238.
- [34] Xue Y, Ju Y. Studies On The Liftoff Properties Of Dimethyl Ether Jet Diffusion Flames. *Combust Sci Technol* 2006;178:2219-2247.
- [35] Choi SK, Al-Noman SM, Chung SH. Simulation of Non-Autoignited and Autoignited Laminar Non-Premixed Jet Flames of Syngas in Heated Coflow Air. *Combust Sci Technol* 2015;187:132-147.
- [36] Nurmukan D, Chen TJM, Hung YM, Ismadi M-Z, Chong CT, Tran M-V. Enhancement of biogas/air combustion by hydrogen addition at elevated temperatures. *Int J Energy Res* 2020;44:1519-1534.
- [37] Maulidiyah, Nurdin M, Fatma F, Natsir M, Wibowo D. Characterization of methyl ester compound of biodiesel from industrial liquid waste of crude palm oil processing. *Anal Chem Res* 2017;12:1-9.
- [38] El-Araby R, Amin A, El Morsi AK, El-Ibiari NN, El-Diwani GI. Study on the characteristics of palm oil–biodiesel–diesel fuel blend. *Egypt J Pet* 2018;27:187-194.
- [39] Alekseev VA, Matveev SS, Chechet IV, Matveev SG, Konnov AA. Laminar burning velocities of methylcyclohexane + air flames at room and elevated temperatures: A comparative study. *Combust Flame* 2018;196:99-107.
- [40] Won SH, Chung SH, Cha MS, Lee BJ. Lifted flame stabilization in developing and developed regions of coflow jets for highly diluted propane. *Proc Combust Inst* 2000;28:2093–2099.
- [41] Kuti O, Sarathy M, Nishida K, Roberts W. Numerical studies of spray combustion processes of palm oil biodiesel and diesel fuels using reduced chemical kinetic mechanisms. *SAE Technical Paper* 2014-01-1143.
- [42] Ko YS, Chung SH. Propagation of unsteady tribrachial flames in laminar non-premixed jets. *Combust Flame* 1999;118:151–163.
- [43] Lee J, Won SH, Jin SH, Chung SH, Fujita O, Ito K. Propagation speed of tribrachial (triple) flame of propane in laminar jets under normal and microgravity conditions. *Combust Flame* 2003;134:411–420.
- [44] Bédard B, Cheng RK. Effects of buoyancy on premixed flame stabilization. *Combust Flame* 1996;107:13–26.

5. Future Work

The present study provides valuable data (experimental) on the fundamental combustion characteristics of palm oil biodiesel fuel in terms of both laminar premixed and non-premixed flames. The role of carbon nanotubes on the combustion behavior of palm oil biodiesel/air premixed flames was experimentally investigated using a coflow bunsen burner. While the detailed kinematic mechanism for the combustion of carbon nanotubes is not fully developed yet, the present investigation also highlights the lack of detailed kinematic mechanisms for the combustion of laminar palm oil biodiesel flames. As such, upon the availability of the detailed kinematic mechanisms of palm oil biodiesel for the combustion of laminar premixed and non-premixed flames and the combustion of carbon based nanoparticles, the following suggestions can be considered as a potential future study.

- To develop a detailed kinematic mechanism for the combustion of carbon nanotubes blended palm oil biodiesel fuels. On the contrary, the fictitious species can be introduced to replicate the behavior of carbon nanotubes in the combustion of palm oil biodiesel fuel. The results from the present study can be used for validation purposes.
- Numerical analysis on the concentration of nanoparticles for flame stabilization and emission production. The analysis of the concentration of OH radicals, flame temperature and heat transfer mechanism can be helpful in understanding the flame structure irregularities as well as the production of NO_x and CO.
- To develop a detailed kinematic mechanism for the behavior of pre-vaporized palm oil biodiesel laminar premixed and non-premixed flames. On the contrary, all the existing kinematic mechanisms of biodiesel can be compared to identify the most accurate mechanism for the behavior of laminar premixed and non-premixed flames. Once the

kinematic mechanism is built, or the best option is identified, the numerical analysis on the combustion characteristics of palm oil biodiesel fuel can be performed to deepen the understanding of biodiesel combustion.

- Numerical analysis on the palm oil biodiesel/air premixed flames for tip opening, flame irregularities, flame height, and standoff distance. The analysis of the concentration of OH radicals can be helpful in understanding the tip opening and flame structure irregularities.
- Numerical analysis of the nitrogen diluted palm oil biodiesel laminar non-premixed flames for flame height, liftoff height, and buoyancy effect.
- Numerical analysis on biodiesel combustion with the addition of carbon nanotubes. The effect of nanotube diameter and concentration can be studied.
- Numerical analysis on the combustion characteristics of palm oil biodiesel blended diesel fuel.

6. Appendix

Appendix A1.Nurmukan D, Chen TJM, Hung YM, Ismadi M-Z, Chong CT, Tran M-V. Enhancement of biogas/air combustion by hydrogen addition at elevated temperatures. Int J Energy Res. 2020;44:1519–1534.

Appendix A2.Nurmukan D, Tran M-V, Foo JJ, Scribano G, Chong CT, Huynh TC. Experimental study on laminar lifted flames of pre-vaporized palm oil biodiesel. Fuel 2021;288:119697.

Appendix A3. Nurmukan D, Tran M-V, Hung YM, Scribano G, Chong CT. Effect of Multi-walled Carbon Nanotubes on Pre-vaporized Palm Oil Biodiesel/air Premixed Flames. *Accepted in Fuel Communications*.

Appendix B1. The tabulated findings from the existing literature regarding the nanoadditives.

Table 6-1: Summary of literature findings of the effect of various nanoadditives on the engine performance and emission characteristics

No.	Author & Ref.	Compared fuels	Loading value and additive type	Engine used & conditions	Findings
1	Kao et al. [1]	Diesel	30 cm ³ /L – 50 cm ³ /L of Aqueous aluminum	Single cylinder Constant speed of 2400 rpm	<ul style="list-style-type: none"> • Decreased break specific fuel consumption • Significant reduction in exhaust emission characteristics
2	Selvan et al. [2]	Diesterol (diesel-catoroil biodiesel-ethanol)	Mass fraction of 25-100 ppm of Cerium Oxide + CNTs	Single cylinder Constant speed of 1500 rpm	<ul style="list-style-type: none"> • Maximum 5% increase in thermal efficiency with 100 ppm of nano additives in the fuel • Maximum 12.6% improvement in specific fuel consumption • Higher pressure generated in the cylinder and earlier peak pressure occurrence • Significant reduction in exhaust emission characteristics
3	Basha and Anand [3]	Biodiesel (Jatropha oil)	Mass fraction of 25-50 ppm of Alumina nanoparticles And CNTs	Single cylinder Constant speed of 1500 rpm	<ul style="list-style-type: none"> • Higher pressure generated in the cylinder and earlier peak pressure occurrence • Reduced maximum peak of heat release rate • Improved ignition delay

					<ul style="list-style-type: none"> • Higher brake thermal efficiency compared to base biodiesel fuel, lower compared to CNTs blended biodiesel fuel • Significant reduction in NO_x emissions formation
4	Mehta et al. [4]	Diesel	Aluminum, Iron and Boron nanoparticles	Single cylinder Constant speed of 1500 rpm	<ul style="list-style-type: none"> • Boron and Iron nanoparticles showed no significant improvements in terms of specific fuel consumption, cylinder pressure, and a small increase in brake thermal efficiency at high load • Aluminum particle blended diesel showed significant enhancement in both BTE and BSFC • HC and CO emissions are reduced by 11.2% and 40% with the addition of aluminum nanoparticles at full load • 6% increase in NO_x formation with the addition of aluminum nanoparticles at low load; almost no change at higher loads
5	Basha and Anand [5]	Water-diesel emulsion fuel	Mass fraction of 25-50 ppm of Alumina nanoparticles	Single cylinder Constant speed of 1500 rpm	<ul style="list-style-type: none"> • Increased brake thermal efficiency and reduced brake specific fuel consumption • Lower pressure generated in the cylinder and heat release rate compared to water-diesel emulsion fuels • Significant reduction in NO_x formation
6	Yang et al. [6]	Water-diesel emulsion fuel with various concentrations	10% by mass Organic nano additive (Glycerin)	Four-cylinder Varying engine speed	<ul style="list-style-type: none"> • Brake thermal efficiency is increased by 11.2% with the addition of glycerin; with respect to both brake power as well as engine speed

				(1500-3600 rpm)	<ul style="list-style-type: none"> • Lower torque is produced with the additive blended emulsion fuel • Slight decrease in-cylinder pressure • No change in CO and HC emissions at the engine speed of 2000 rpm and less; more noticeable improvements at the higher engine speeds • Significant improvements with higher brake power conditions for both CO and HC emissions • Almost 19% reduction in NO_x formation compared to base fuel; with respect to both brake power as well as engine speed
7	Shafii et al. [7]	Diesel	0.4-0.8% of water-based ferrofluid to diesel ratio by volume	Four-cylinder Constant speed of 2200 rpm	<ul style="list-style-type: none"> • Additive blended fuel results in 12% enhancement in brake thermal efficiency and 11% reduction in specific fuel consumption relative to the neat diesel • Significant reduction in NO_x emissions formation and increase in CO emission
8	Sajeevan and Sajith [8]	Diesel	Mass fraction of 5-35 ppm of cerium oxide	Single cylinder Constant speed of 1500 rpm	<ul style="list-style-type: none"> • Cerium oxide nanoparticles blended diesel results in 8% increase in brake thermal efficiency at high loads • Brake thermal efficiency increases proportionally with the load and nano additive concentrations • 50% reduction in HC and 30% increase in NO_x
9	Ranjan et al. [9]	WCO biodiesel	Mass fraction of 30 ppm of magnesium oxide	Single cylinder Constant speed of 1500 rpm	<ul style="list-style-type: none"> • No change in brake power at any engine load with the addition of MgO nano additives

					<ul style="list-style-type: none"> • At the maximum power condition: BTE has increased by 5%, whereas BSFC has also increased by 6.2% • Additive blended fuel results in 15.71% decrease in CO, 22.27% decrease in HC, 4.68% reduction in PM formation but 15% increase in NO_x
10	Kumar et al. [10]	Diesel and Pongamia methyle ester biodiesel	0.5-1.5% of ferrofluid by volume	Four-cylinder Constant speed of 1500 rpm	<ul style="list-style-type: none"> • Diesel-biodiesel had an almost 20% decrease in brake thermal efficiency compared to neat diesel • Addition of ferrofluid nanoparticles blended diesel-biodiesel fuel had only 7.42% less thermal efficiency compared to neat diesel, which shows the improvement of almost 13% • With the 1.5% by volume dosage into fuel, there is 31.25% improvement in BSFC compared to neat diesel • 1% by volume dosage of ferrofluid nanoparticles results in cleaner combustion; Reduction in CO, HC, and smoke • Higher NO_x
11	Fangsuwannarak and Triratanasirichai [11]	Palm oil biodiesel	0.15 and 0.2% of TiO ₂ by volume	Single cylinder Varying engine speed (1500-4000 rpm)	<ul style="list-style-type: none"> • Reduction in brake specific fuel consumption • Reduction in kinematic viscosity of the blended fuel • Rise in cetane number with the 0.2% addition of TiO₂ • Reduction in exhaust emissions: CO, HC, and NO_x

12	Sarvestany et al. [12]	Diesel	0.4 and 0.8% of Fe ₃ O ₄ by volume	Single cylinder Constant speed of 2200 rpm	<ul style="list-style-type: none"> • All combustion characteristics were showing improved results with the 0.4% (by vol.) concentration of nanoadditives compared to 0.8% • While there is a significant reduction in the formation of NO_x and SO₂ emissions, CO and smoke emissions have increased with the addition of Fe₃O₄
13	Yang et al. [13]	Water-diesel emulsion fuel with various concentrations	12.6% of nano-organic additives by volume polyethoxyester	Four-cylinder Varying engine speed (1500-3600 rpm)	<ul style="list-style-type: none"> • As a result of a micro explosion which is associated with water droplets in the fuel, brake thermal efficiency, as well as specific fuel consumption, were improved • Lower brake power generated compared to neat diesel • Noticeably lower NO_x and HC emissions production and smoke opacity • Almost no change in CO emissions, specially at lower engine speeds (< 2800 rpm)
14	Ganesh and Gowrishankar [14]	Jatropha biodiesel	100 mg/l of Magnalium Cobalt oxide	Single cylinder Constant speed of 1500 rpm	<ul style="list-style-type: none"> • Nano additive blended fuel showed increased brake thermal efficiency as well as the reduction in specific fuel consumption at the condition of half and full load • Significant reduction in exhaust pollutants characteristics such as HC and CO emissions

15	Ranaware and Satpute [15]	Diesel	0-0.8% of water-based ferrofluid by volume	Single cylinder Constant speed of 2200 rpm	<ul style="list-style-type: none"> • Slight overall increase in brake thermal efficiency, but ferrofluid blended diesel fuel employs higher specific fuel consumption compared to neat diesel • Lower CO emissions production but higher NO_x
16	Lenin et al. [16]	Diesel	100 mg/l of MnO and CuO (nano metal oxides)	Single cylinder Constant speed of 1500 rpm	<ul style="list-style-type: none"> • MnO additive blended fuel results in better engine performance in terms of brake thermal efficiency compared to CuO blended and diesel fuels • Noticable reduction in the ignition delay • Reduction in CO and NO_x emissions; but no change in HC at all load conditions
17	Basha and Anand [17]	Jatropha Biodiesel emulsion fuel	Mass fraction of 25-100 ppm of alumina	Single cylinder Constant speed of 1500 rpm	<ul style="list-style-type: none"> • Brake thermal efficiency increases from 25% to 30% with the addition of alumina additives • Reduction in ignition delay and peak pressure • Slight improvements (3%) in specific fuel consumption compared to base fuel • Reduction in CO and NO_x emissions but increase in HC emissions formation
18	Selvaganapthy et al. [18]	Diesel	Mass fraction of 250-500 ppm of zinc oxide	Single cylinder Constant speed of 1500 rpm	<ul style="list-style-type: none"> • Nanoparticles blended fuel showed improvements in thermal efficiency and overall engine performance • But, led to higher generation of NO_x emissions compared to neat diesel

19	Xin et al. [19]	Heavy Oil	Ce _{0.9} Cu _{0.1} O ₂ and Ce _{0.9} Zr _{0.1} O ₂	Single cylinder Constant speed of 1500 rpm	<ul style="list-style-type: none"> • <u>Nano-sized complex oxide can improve the performance of diesel engine fueled with heavy oil, and reduce the emission of pollutants like NO_x and CO, comparing it with the pure heavy oil</u>
20	Sajith et al. [20]	Jatropha Biodiesel	Mass fraction of 20-80 ppm of CeO ₂	Single cylinder Constant speed of 1500 rpm	<ul style="list-style-type: none"> • Fuel properties such as flash point and viscosity have been increased with the addition of CeO₂ nano additives • Increased brake thermal efficiency, as well as improved specific fuel consumption, compared to pure biodiesel • Significant reduction in exhaust pollutants such as HC and NO_x
21	Kannan et al. [21]	Biodiesel from waste cooking oil	5-50 μmol/L of ferric chloride	Single cylinder Constant speed of 1500 rpm	<ul style="list-style-type: none"> • Addition of Ferric chloride nanoparticles into biodiesel fuel resulted in enhancement of engine performance in terms of brake specific fuel consumption, brake thermal efficiency, and energy consumption; although it should be mentioned that the increase in these parameters are small • But, it was showed that there is a significant reduction in exhaust pollutants such as UHC, CO, and smoke emissions

Table 6-2: Summary of literature findings of the effect of CNTs on the engine performance and emission characteristics (all based on experimental methods)

No.	Author & Ref.	Compared fuels	Loading value	Engine used & conditions	Findings
1	Basha and Anand [22]	Neat diesel, water-diesel emulsion, and MWCNTs blended water-diesel emulsion fuels	Mass fraction of 25-50 ppm of MWCNTs	Single-cylinder Constant speed of 1500 rpm	<ul style="list-style-type: none"> • Lower cylinder peak pressure and heat release rate for CNTs blended fuel compared to water-diesel emulsion fuel; 73.5 bar (25ppm) and 75.4 bar; 36.6 J/deg (50ppm) and 40.8 J/deg, respectively • Reduced ignition delay • Improved brake thermal efficiency from 25 to 28% with CNTs concentration of 50ppm • Reduced brake specific fuel consumption from 0.36 to 0.29 kg/kW-h with the addition of 50ppm of CNTs • Increased cetane number from 44 to 47 with the addition of 50 ppm of CNTs into the mixture • Addition of nanoparticles (50 ppm) reduces CO and HC emissions; with the maximum difference of 12% and 8% respectively • Almost 41% reduction in smoke opacity for MWCNTs blended water-diesel emulsion fuels (50 ppm)
2	Tewari et al. [23]	Neat diesel, biodiesel, and MWCNTs	Mass fraction of 25-50 ppm of MWCNTs	Single-cylinder	<ul style="list-style-type: none"> • Improved break thermal efficiency compared to neat biodiesel fuel (4% increase), but lower with comparison to neat diesel (2% drop)

		blended biodiesel fuels		Constant speed of 1500 rpm	<ul style="list-style-type: none"> • 20% reduction in smoke opacity for MWCNTs blended biodiesel fuels (50 ppm) • The fuel sample with 50 ppm of CNTs produced 18% less HC emissions compared to base biodiesel
		Biodiesel feedstock: HOME			
3	Basha and Anand [24]	Jatropha Methyl Esters and CNT blended JME emulsion fuels	Mass fraction of 25-100 ppm of MWCNTs	Single-cylinder Constant speed of 1500 rpm	<ul style="list-style-type: none"> • Reduced cylinder peak pressure from 79.77 to 72.15 bar with the addition of CNTs (100ppm) at the full load • Reduced heat release rate • Improved brake thermal efficiency from 24.80 to 28.45% with CNTs concentration of 100ppm • 13% reduction in the specific fuel consumption with CNTs concentration of 100ppm in the mixture • Marginal reduction of HC emissions for CNT blended JME emulsion fuels; 9.5% reduction of HC emissions at the full load conditions • Reduction of CO emissions almost by 30% at the full load, with the addition of 100ppm CNTs
4	Balaji and Cheralathan [25]	Neat disel, MENO, and CNT blended MENO fuels	Mass fraction of 100-300 ppm of MWCNTs	Single-cylinder	<ul style="list-style-type: none"> • Improved brake thermal efficiency by 4.17% for CNT blended biodiesel with the concentration of 200ppm • Decreased break specific fuel consumption

					<ul style="list-style-type: none"> • Cases with a concentration higher than 200ppm produced negative impacts on the combustion characteristics • Reduced smoke intensity • HC and CO emissions are reduced by 10.39% and 16.20%, with the additive concentration of 200 ppm • Cases with a concentration higher than 200ppm produced negative impacts on the combustion characteristics
5	Singh and Bharj [26]	Neat diesel, water-diesel emulsion, and MWCNTs blended water-diesel emulsion fuels	Mass fraction of 50-150 ppm of MWCNTs	Single-cylinder Constant speed of 1500 rpm	<ul style="list-style-type: none"> • Water-diesel emulsion fuel produces higher peak cylinder pressure compared to neat diesel • Addition of MWCNTs results in a significant reduction of cylinder pressure; the maximum reduction was recorded to be 25% at the concentration of 150 ppm • MWCNTs blended water-diesel emulsion fuel is associated with lower break specific fuel consumption compared to the water-diesel emulsion and neat diesel fuels • The brake thermal efficiency has increased from 27.2% to 30.5% with the addition of MWCNTs (150 ppm) • Overall, NO_x emissions decrease with the increasing concentration of MWCNTs regardless of the load • However, the difference in the reduction of NO_x emissions between the mixtures with 50, 100, and 150 ppm of MWCNTs, is most noticeable at the full load condition

					<ul style="list-style-type: none"> • There is an increasing trend of CO₂ as a result of the combustion of MWCNTs blended emulsified fuel • There is 34.4% reduction in CO emissions from the combustion of MWCNTs blended emulsified fuels with 150 ppm concentration compared to ordinary emulsion fuel
6	Ghafoori et al. [27]	Neat diesel, biodiesel-diesel blend, and CNTs blended diesel-biodiesel fuels Biodiesel feedstock: WVO	Mass fraction of 50-150 ppm of CNTs	Six-cylinder, Varying engine speed conditions (800 – 1000 rpm)	<ul style="list-style-type: none"> • Break power has increased with the content of nano additives in the mixture, for all engine speeds; the maximum improvement in the engine break power is recorded to be 17%, with 30 ppm of CNTs in the diesel-biodiesel fuel mixture; The same trend was observed for the engine torque with almost 20% enhancement compared to neat diesel • It was shown that the most significant change in the combustion characteristics occur at the engine speed of 1000 rpm • The same behavior occurs with the engine's torque, with the recorded increment of 18% for the fuel that contains 30 ppm of CNTs • Overall, there is a significant reduction in fuel consumption and specific fuel consumption with the addition of nanoparticles into the mixture; But, the increase of CNTs concentration more than 20 ppm in the mixture results in the relatively negative effects on the combustion characteristics • Addition of nanoparticles reduces HC emissions; there is 22% reduction in HC emissions in MWCNTs blended biodiesel-diesel fuel compared to neat diesel • It was also shown that the most reduction occurs either at the highest or lowest speed of the engine,

					<p>1000 and 700 rpm respectively, compared to 800 and 900 rpm</p> <ul style="list-style-type: none"> • There is an increase in CO₂ emissions with the addition of nano additives, whereas CO emissions tend to decrease accordingly • The fuel sample with the concentration of 15 ppm has the most significant changes; the lowest for CO (2 %) and the highest CO₂ (23%)
7	Maleney et al. [28]	<p>Diesel-biodiesel and CNTs blended diesohol fuels</p> <p>Biodiesel feedstock: waste cooking oil</p>	Mass fraction of 20-100 ppm of CNTs	<p>Single-cylinder</p> <p>Varying engine speed conditions (1500 – 3000 rpm)</p>	<ul style="list-style-type: none"> • CNTs blended diesohol fuels showed much higher torque compared to diesel-biodiesel and neat diesel fuels; the increase in torque is almost 21% at full load and 15% at low load • Net power has increased from 4.3 kW to 5.3kW for diesel fuel blended with ethanol and CNTs of 60 ppm • The lowest brake thermal efficiency is produced by pure biodiesel and diesel-biodiesel fuels, whereas the maximum efficiency associates with CNTs blended diesohol fuels (specially with 20 and 60 ppm concentrations) • Reduced specific fuel consumption and exhaust gas temperature • Reduced CO and UHC by 5.47% and 31.72%, respectively • 7% decrease in soot generation • Increase of NO emissions by 12.22% • The fuel sample of CNTs blended diesohol (with 6% ethanol and 60 ppm of CNTs) has shown the most optimal performance

8	Hosseini et al. [29]	Neat diesel, biodiesel, diesel-biodiesel blends, and CNTs blended diesel-biodiesel fuels	Mass fraction of 30-90 ppm of CNTs	Single-cylinder Varying engine speed conditions (1800 – 2800 rpm)	<ul style="list-style-type: none"> • Addition of CNTs into the fuel mixture results in increased Torque regardless of the engine speed • There is a minor enhancement in power with the addition of nanoparticles into the mixture; the most significant changes occur at low engine load • CNTs blended diesel-biodiesel fuels have higher break thermal efficiency compared to neat diesel • Reduced specific fuel consumption and exhaust gas temperature • Reduced fuel consumption and specific fuel consumption with the addition of nanoparticles into the mixture • CNTs blended diesel-biodiesel fuels produced 65.70% less CO, 44.98% less HC, and 29.41% less soot formation compared to neat diesel • Increase of NO emissions by 27.49%
9	Ghanbari et al. [30]	Neat diesel, pure biodiesel, MWCNTs blended diesel, and biodiesel fuels	Mass fraction of 40-120 ppm of MWCNTs	Six-cylinder, Varying engine speed conditions (800 – 1000 rpm)	<ul style="list-style-type: none"> • Slight improvements in the engine break power with the addition of nanotubes into diesel and diesel-biodiesel blends, for all engine speeds • Higher combustion pressure leads to higher torque with 2% increment compared to neat diesel • About 7% decrease in the specific fuel consumption for MWCNTs blended diesel and diesel-biodiesel blends compared to neat diesel • MWCNTs blended diesel fuels produced 22.48% less CO and 14.21% less HC compared to neat diesel

					<ul style="list-style-type: none"> • MWCNTs blended diesel-biodiesel fuels produced 25.17% less CO and 28.56% less HC compared to neat diesel • For both CNTs blended diesel and diesel-biodiesel fuels, NO and CO₂ emissions have increased
10	Chen et al. [31]	Neat diesel and nanoparticle-diesel fuel blends	Mass fraction of 25-100 ppm of CNTs	Single-cylinder Constant speed of 1800 rpm	<ul style="list-style-type: none"> • Brake specific fuel consumption was improved by 19.85% with the addition of CNTs into a diesel fuel • Diesel fuel sample with the concentration of 50 ppm showed the highest improvement in brake thermal efficiency, 18.8%, compared to neat diesel fuel • Addition of CNTs led to a higher pressure during the compression stroke and a lower peak in-cylinder pressure compared to neat diesel fuels • Drastic increase in CO₂ emissions for the fuels with the MWCNTs concentration of 100 ppm, compared to neat diesel fuels • Nanoparticle-diesel fuel blends produced 5% less NO_x emissions compared to neat diesel fuels at low and full load conditions, whereas the highest reduction was recorded to be 35% at the partial load condition
11	Praveen et al. [32]	Diesel-biodiesel blend, EGR and MWCNTs blended diesel-biodiesel fuels	Mass fraction of 40 ppm of MWCNTs	Single-cylinder Constant speed of 1500 rpm	<ul style="list-style-type: none"> • MWCNTs blended diesel-biodiesel fuels produce higher brake thermal efficiency compared to diesel-biodiesel blend fuel; Addition of EGR decreases the brake thermal efficiency

					<ul style="list-style-type: none"> • Reduced specific fuel consumption is recorded with the fuels containing MWCNTs in the mixture • Reduced cylinder pressure and increased heat release rate with the addition of CNTs • Reduced CO and HC emissions by 28% and 11% respectively by the addition of MWCNTs, regardless of the engine load • Reduction of NO_x emissions by both nanoadditives as well as EGR addition • Smoke opacity decreases with the addition of MWCNTs into the fuel, but increases with the addition of EGR
12	Basha et al. [33]	Neat diesel, biodiesel, water-biodiesel emulsion, and CNTs blended water-biodiesel emulsion fuels	Mass fraction of 50 ppm of MWCNTs	Single-cylinder Constant speed of 1800 rpm	<ul style="list-style-type: none"> • Reduced cylinder peak pressure and heat release rate with the addition of CNTs • Shorter ignition delay • Fuel samples containing MWCNTs in the mixture exhibit improved brake thermal efficiency as well as reduced specific fuel consumption • Reduced CO and HC emissions by the addition of MWCNTs • Smoke opacity was reduced by the presence of MWCNTs in the mixture • Exhaust gas temperature decreases with the addition of CNTs in the mixture, regardless of brake power

13	Hoseini et al. [34]	Neat diesel, diesel-biodiesel (Ailanthus altissima oil) blends, and GO blended diesel-biodiesel fuels	Mass fraction of 30-90 ppm of GO	Single-cylinder Constant speed of 2100 rpm	<ul style="list-style-type: none"> • Brake power has increased by 0.5 kW with the addition of GO (90 ppm), at 0 and 100% load condition • The samples with the concentration of 30 and 60 ppm do not show any significant improvements at 0% load but show an increase in power with higher loads • 3.1%, 6%, and 7.2% decrease in specific fuel consumption with the addition of GO nanoparticles with the concentration of 30, 60, and 90 ppm, respectively • GO blended (90 ppm) biodiesel blends produced 18% less CO and 27.47% less UHC • GO blended (90 ppm) biodiesel blends produced 12.54% more CO₂ and 8% more NO_x compared to biodiesel under the same conditions
14	Najafi [35]	Neat diesel, pure biodiesel (waste cooking oil), and CNTs blended biodiesel fuels	Mass fraction of 40-120 ppm of CNTs	Six-cylinder Constant speed of 1000 rpm	<ul style="list-style-type: none"> • CNTs blended biodiesel fuels produce higher in-cylinder gas pressure, peak pressure rise rate as well as heat release rate compared to neat diesel and pure biodiesel fuels • Reduced CO and HC emissions by the addition of CNTs • For both CNTs blended diesel and diesel-biodiesel fuels, NO and CO₂ emissions have increased

References

- [1] Kao M.J, Ting CC, Lin BF, Tsung TT. Aqueous aluminum nanofluid combustion in diesel fuel. *J Test Eval* 2008;36:186-190.
- [2] Selvan VAM, Anand RB, Udayakumar M. Effect of Cerium Oxide Nanoparticles and Carbon Nanotubes as fuel-borne additives in Diesterol blends on the performance, combustion and emission characteristics of a variable compression ratio engine. *Fuel* 2014;130:160-167.
- [3] Basha JS, Anand RB. The influence of nano additive blended biodiesel fuels on the working characteristics of a diesel engine. *J Braz Soc Mech Sci Eng* 2013;35:257-264.
- [4] Mehta RN, Chakraborty M, Parikh PA. Nanofuels: Combustion, engine performance and emissions. *Fuel* 2014;120:91-97.
- [5] Basha JS, Anand RB. Effects of nano particle additive in the water–diesel emulsion fuel on the performance, emission and combustion characteristics of a diesel engine. *Int J Veh Des* 2012;59:164-181.
- [6] Yang WM, An H, Chou SK, Vedharaji S, Vallinagam R, Balaji M, Mohammad FEA, Chua KJE. Emulsion fuel with novel nano-organic additives for diesel engine application. *Fuel* 2013;104:726-731.
- [7] Shafii MB, Daneshvar F, Jahani N, Mobini K. Research article effect of ferrofluid on the performance and emission patterns of a four stroke diesel engine. *Adv Mech Eng* 2011:1-5.
- [8] Sajeevan AC and Sajith V. Diesel Engine Emission Reduction Using Catalytic Nanoparticles: An Experimental Investigation. *J Eng* 2013:1-9.
- [9] Ranjan A, Dawn SS, Jayaprabakar J, Nirmala N, Saikiranc , Sriram SS. Experimental investigation on effect of MgO nanoparticles on cold flow properties, performance, emission and combustion characteristics of waste cooking oil biodiesel. *Fuel* 2018;220:780-791.
- [10] Kumar S, Dinesha P, Bran I. Influence of nanoparticles on the performance and emission characteristics of a biodiesel fuelled engine: An experimental analysis. *Energy* 2017;140:98-105.
- [11] Fangsuwannarak K, Triratanasirichai K. Improvements of palm biodiesel properties by using nano-TiO₂ additive, exhaust emission and engine performance. *Romanian Rev Precis Mech Opt Mechatron* 2013;43:111-118.
- [12] Sarvestany NS, Farzad A, Ebrahimnia-Bajestan E, Mir M. Effects of Magnetic Nanofluid Fuel Combustion on the Performance and Emission Characteristics. *J Disper Sci Technol* 2014;35:1745-1750.
- [13] Yang WM, An H, Chou SK, Chua KJ, Mohan B, Sivasankaralingam V, Raman V, Maghbouli A, Li J. Impact of emulsion fuel with nano-organic additives on the performance of diesel engine. *Appl Energy* 2013;112:1206-1212.
- [14] Ganesh D, Gowrishankar G. Effect of Nano-fuel additive on emission reduction in a Biodiesel fuelled CI engine. *Int Conf Electr Control Eng* 2011:3453-3459.

- [15] Ranaware AA, Satpute ST. Correlation between Effects of Cerium Oxide Nanoparticles and Ferrofluid on the Performance and Emission Characteristics of a C.I. Engine. *Jo Mech Civil Eng* 2012;55-59.
- [16] Lenin MA, Swaminathan MR, Kumaresan G. Performance and emission characteristics of a DI diesel engine with a nanofuel additive. *Fuel* 2013;109:362-365.
- [17] Basha JS, Anand RB. Role of nanoadditive blended biodiesel emulsion fuel on the working characteristics of a diesel engine. *J Renew Sust Energy* 2011;3:023106.
- [18] Selvaganapthy A, Sundar A, Kumaragurubaran B, Gopal P. An Experimental Investigation to Study the Effects of Various Nano Particles with Diesel on Di Diesel Engine. *J Sci Technol* 2013;3: 112-115.
- [19] Xin Z, Tang Y, Man C, Zhao Y, Ren J. Research on the Impact of CeO₂-based Solid Solution Metal Oxide on Combustion Performance of Diesel Engine and Emissions. *J Marine Sci Appl* 2013;12:374-379.
- [20] Sajith V, Sobhan CB, Peterson GP, Experimental Investigations on the Effects of Cerium Oxide Nanoparticle Fuel Additives on Biodiesel. *Adv Mech Eng* 2015;2:1-6.
- [21] Kannan GR, Karvembu R, Anand R. Effect of metal based additive on performance emission characteristics of diesel engine fuel led with biodiesel. *Appl Energy* 2011;88:3694-3703.
- [22] Basha JS, Anand RB. An experimental investigation in a diesel engine using carbon nanotubes blended water–diesel emulsion fuel. *Proceedings of the Institution of Mechanical Engineers Part A: Journal of Power and Energy* 2011;225:279-288.
- [23] Tewari P, Doijode E, Banapurmath NR, Yaliwal VS. Experimental investigations on a diesel engine fuelled with multiwalled carbon nanotubes blended biodiesel fuels. *Int J Emerg Technol Adv Eng* 2013;3:72-76.
- [24] Basha JS, Anand RB. Performance, emission and combustion characteristics of a diesel engine using Carbon Nanotubes blended Jatropha Methyl Ester Emulsions. *Alex Eng J* 2014;53:259-273.
- [25] Balaji G, Cheralathan M. Effect of CNT as additive with biodiesel on the performance and emission characteristics of a DI diesel engine. *Int J Chem Tech Res* 2015;7:1230-1236.
- [26] Singh N, Bharj RS. Effect of CNT-Emulsified Fuel on Performance Emission and Combustion Characteristics of Four Stroke Diesel Engine. *Int J Curr Eng Technol* 2015;5:477-485.
- [27] Ghafoori M, Ghobadian B, Najafi G, Layeghi M, Rashidi A, Mamat R. Effect of nanoparticles on the performance and emission of a diesel engine using biodiesel-diesel blend. *Int J Automot Mec Eng* 2015;12:3097-3108.
- [28] Maleney KH, Alisaraei AT, Ghobadian B, Mayvan AA. Analyzing and evaluation of carbon nanotubes additives to diesohol-B2 fuels on performance and emission of diesel engines. *Fuel* 2017;196:110-123.
- [29] Hosseini HS, Alisaraei AT, Ghobadian B, Mayvan AA. Performance and emission characteristics of a CI engine fuelled with carbon nanotubes and diesel-biodiesel blends. *Renew Energy* 2017;111:201-213.

- [30] Ghanbari M, Najafi G, Ghobadian B, Yusaf T, Carlucci AP, Kiani Deh Kiani M. Performance and emission characteristics of a CI engine using nano particles additives in biodiesel-diesel blends and modeling with GP approach. *Fuel* 2017;202:699-716.
- [31] Chen AF, Adzmi MA, Adam A, Fahmi M, Kamal M, Mrwan AG. Combustion characteristics, engine performances and emissions of a diesel engine using nano-particle-diesel fuel blends with aluminium oxide, carbon nanotubes and silicon oxide. *Energy Convers Manag* 2018;171:461-477.
- [32] Praveen A, Rao GLN, Balakrishna B. The combined effect of multiwalled carbon nanotubes and exhaust gas recirculation on the performance and emission characteristics of a diesel engine. *Int J Ambient Energy* 2017;40:791-799.
- [33] Basha JS. Impact of Carbon Nanotubes and Di-Ethyl Ether as additives with biodiesel emulsion fuels in a diesel engine e An experimental investigation. *J Energy Inst* 2018;91:289-303.
- [34] Hoseini SS, Najafi G, Ghobadian B, Mamat R, Ebadi M, Yusaf T. Novel environmentally friendly fuel: The effects of nanographene oxide additives on the performance and emission characteristics of diesel engines fuelled with *Ailanthus altissima* biodiesel. *Renew Energy* 2018;125:283-294.
- [35] Najafi G. Diesel engine combustion characteristics using nano-particles in biodiesel-diesel blends. *Fuel* 2018;212:668-678.

Appendix C1. The sample of GCMS results

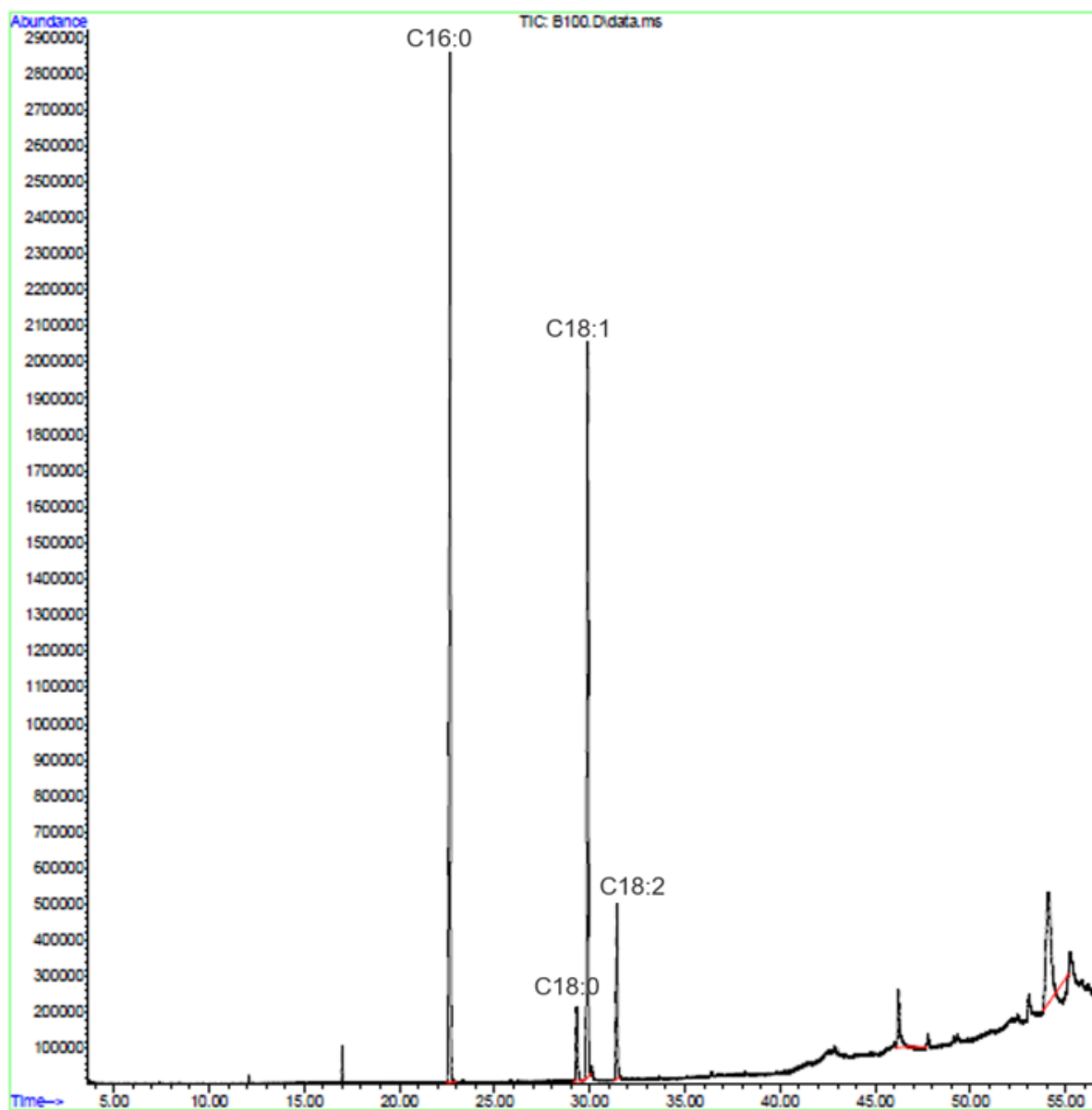



Figure 6-1: GCMS analysis of palm oil biodiesel sample

Appendix D1: Palm Methyl Ester specifications provided by the manufacturer


Mewah

BREMFIELD SDN. BHD. (735879-A)

SPECIFICATION SHEET **EN14214: 2012**

PALM METHYL ESTER **PME**

Test Parameter	Unit	Method	Specifications	
			min	max
Ester content	% (m/m)	EN 14103	96.5	
Density at 15°C	kg/m ³	EN ISO 12185	860	900
Kinematic viscosity at 40°C	mm ² /s	EN ISO 3104	3.5	5.0
Flash point	°C	EN ISO 2719	101	
Sulfur content	mg/kg	EN ISO 20846		10
Cetane Number	–	EN ISO 5165	51	
Sulfated ash content	% (m/m)	ISO 3987		0.02
Water content	mg/kg	EN ISO 12937		500
Total Contamination	mg/kg	EN 12662		24
Copper Strip Corrosion (3 hours at 50°C)	Rating	EN ISO 2160	Class 1	
Oxidation stability , 110°C (accelerated oxidation)	hours	EN 15751	8.0	
Acid value	mg KOH/g	EN 14104		0.5
Iodine value	g iodine/100g	EN 14111		120
Linolenic acid methyl ester	% (m/m)	EN 14103		12
Polyunsaturated (>= 4 Double bonds) methyl ester	% (m/m)	EN 15779		1
Methanol content	% (m/m)	EN 14110		0.2
Monoglyceride content	% (m/m)	EN 14105		0.7
Diglyceride content	% (m/m)	EN 14105		0.2
Triglyceride content	% (m/m)	EN 14105		0.2
Free glycerine	% (m/m)	EN 14105		0.02
Total glycerine	% (m/m)	EN 14105		0.25
Group I metals (Na + K)	mg/kg	EN 14108/9		5
Group II metals (Ca + Mg)	mg/kg	EN 14538		5
Phosphorus content	mg/kg	EN 14107		4
Cold Filter Plugging Point	°C	EN 116		15

Figure 6-2: The specification sheet of palm oil biodiesel provided by the manufacturer.

Appendix D2: Multiwalled Carbon Nanotubes specifications provided by the manufacturer

Table 6-3: Specifications of the MWCNTs (10-20 nm)

Name	US4306 Multi-Walled Carbon Nanotubes (MWNTs, MWCNTs)
Purity	> 95 wt% (carbon nanotubes) (from TGA & TEM) > 97 wt% (carbon content)
Outside diameter	10-20 nm (from HRTEM, Raman)
Inside diameter	5-10 nm
Length	10-30 μm (TEM)
SSA	200 m^2/g (BET)
Estimated number of walls	8-23
Color	Black
Ash	<1.5wt% (TGA)
Electrical conductivity	>100 s/cm
Tap density	0.22 g/cm^3
True density	~ 2.1 g/cm^3
Manufacturing method	CVD

Table 6-4: Table 6 3: Specifications of the MWCNTs (30-50 nm)

Name	US4312 Multi-Walled Carbon Nanotubes (MWNTs, MWCNTs)
Purity	> 95 wt% (carbon nanotubes) (from TGA & TEM) > 97 wt% (carbon content)
Outside diameter	30-50 nm (from HRTEM, Raman)
Inside diameter	5-12 nm
Length	10-20 μm (TEM)
SSA	60 m^2/g (BET)
Estimated number of walls	27-67
Color	Black
Ash	<1.5wt% (TGA)
Electrical conductivity	>120 s/cm
Tap density	0.22 g/cm^3
True density	~ 2.1 g/cm^3
Manufacturing method	CVD

Appendix E1: The schematic of the coflow bunsen burner used in the present study

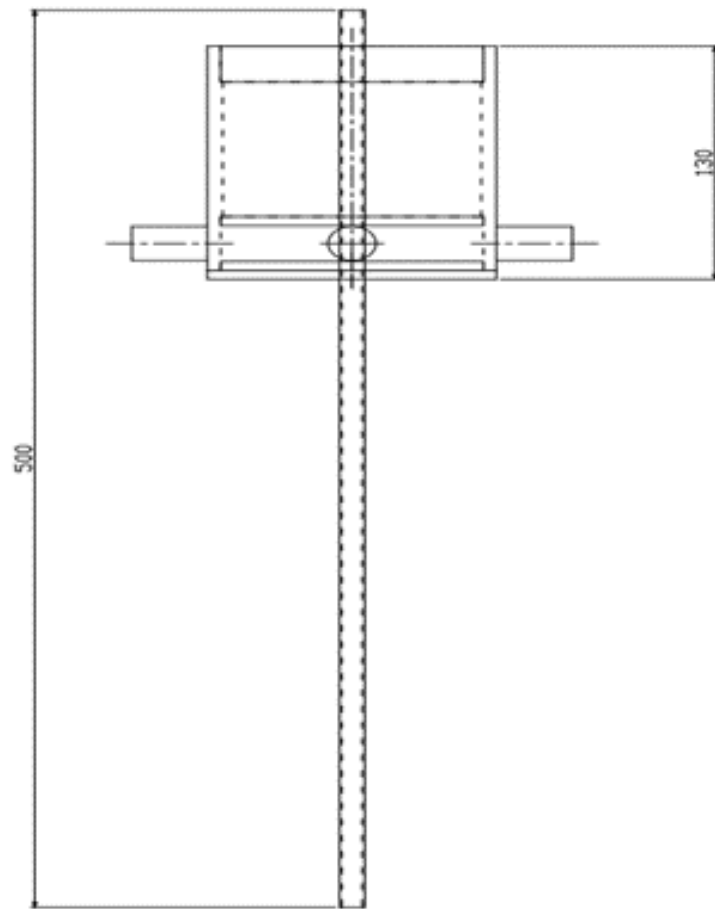











Figure 6-3: Schematic diagram of the coflow bunsen burner

Appendix E2. List of main equipment/items used in the present study

Table 6-5: The list of main components in the present experimental configuration.

No.	Name	Image	Description
1	Mass flow controller (MKS, 1179 A)		To control the flow of supplied gas
2	Readout controller (MKS, 247D 4 channel)		To control the flow of supplied gas
3	1/4" Stainless steel tube		To deliver the pre-vaporized mixture and pure gas to the nozzle.
4	Heating ropes (Omega, FGR-060)		To wrap the stainless steel to ensure the complete vaporization of liquid fuels.

5	Variable autotransformer variac		To control the voltage supply to the heating ropes, to control the applied temperature.
6	K-type thermocouples (Omega, SA3-K-72)		To measure the temperature of the heating ropes and pre-vaporized mixture.
7	Temperature readout (midi Logger GLB20)		To readout the measurement from the thermocouples.
8	Dry-test gas meter		To calibrate the MFCs per given gas.
9	Syringe pump (NE-300)		To supply the liquid fuels to the stainless steel line.

10	Glass syringe		To supply the liquid fuels to the stainless steel line.
11	Gas analyzer		To measure the produced emission at the nozzle exit.
12	Lens		Lens used in the schlieren setup.
13	Glass beads & Honeycomb		Glass beads and honeycomb are used to obtain the homogeneous flow of the coflow gas.

Enhancement of biogas/air combustion by hydrogen addition at elevated temperatures

Dastan Nurmukan¹ | Timothy Jie Ming Chen¹ | Yew Mun Hung¹ |
Mohd-Zulhilmi Ismadi¹ | Cheng Tung Chong² | Manh-Vu Tran¹ 

¹School of Engineering, Monash University Malaysia Selangor, Malaysia

²China-UK Low Carbon College Shanghai Jiao Tong University Shanghai, China

Correspondence

Manh-Vu Tran. School of Engineering, Monash University Malaysia Selangor, Malaysia.
Email: manhv.tran@monash.edu

Summary

In this study, combustion characteristics of various biogas/air mixtures with hydrogen addition at elevated temperatures were experimentally investigated using bunsen burner method. Methane, CH₄, was diluted with different concentrations of carbon dioxide, CO₂, 30 to 40% by volume, to prepare the biogas for testing. It is followed by the hydrogen, H₂, enrichment within the range of 0 to 40% by volume and the temperature elevation of unburned gas till 440 K. Blowoff velocities were measured by lowering the jet velocity until a premixed flame could be stabilized at the nozzle exit, while laminar burning velocities were calculated by analyzing the shape of the directly captured premixed bunsen flames. The results showed that hydrogen had a positive effect on the blowoff velocity for all three fuel samples. Nonlinear growth of the blowoff velocity with hydrogen addition was associated to the dominance of methane-inhibited hydrogen combustion process. It was also observed that the increase in the initial temperature of the unburned mixture led to a linear increase of the blowoff velocity. Moreover, specific changes in flame structure such as flame height, standoff distance, and the existence of tip opening were attributed to the change in the blowoff velocity. The effect of CO₂ content in the mixture was examined with regards to laminar burning velocity for all compositions. The outcome of the experiment showed that the biogas mixture with higher content of CO₂ possessed lower values of laminar burning velocity over the wide range of equivalence ratios. A reduced GRI-Mech 3.0 was used to simulate the combustion of biogas/air mixtures with different compositions using ANSYS Fluent. The numerically simulated stable conical flames were compared with the experimental flames, in terms of flame structure, showing that the reduced GRI-Mech 3.0 was suitable for modeling the combustion of biogas/air mixtures.

KEYWORDS

biogas, blowoff, burning velocity, hydrogen, numerical simulation

1 | INTRODUCTION

With the continuous decline of the environmental conditions as well as the increasing demand in energy supply, the interest in the development of renewable clean fuels has peaked over the last decade. Due to its strong accessibility, the abundance of its sources and environmentally friendly combustion, biogas has drawn lots of attention in the field of combustion research.¹ Although biogas brings these benefits, it has certain challenges restricting its use in the application of engine.² One of the significant problems of biogas is the high content of CO₂ in the mixture, which also varies in composition with the primary hydrocarbon, CH₄, based on the change of the temperature, pressure and the production method. This situation leads to the lower heating value, slower combustion speed, and the poor stability of a flame compared with the natural gas.³

To enhance the combustion characteristics of biogas, the addition of another fuel, having a high calorific value into the flowing stream of biogas, can be an effective solution. The past researches^{1,3-12} showed that hydrogen could be used as an additive to improve the combustion characteristics of fuels. Besides, from elevating the reactivity of the fuel blend, hydrogen is known as an environmentally friendly fuel as well, based on the production method. Mustafa et al⁴ showed that the increasing content of hydrogen results in a considerable decrease in the production of carbon monoxide, CO, emission. Results from this experimental study are in good agreement with the trends obtained via the numerical investigations, performed by Jeong et al⁵ and Esmail et al.⁶ While Hu and Zhang⁷ investigated the effect of hydrogen on the combustion characteristics of the low calorific value fuels using the constant volume combustion bomb, Yang and Wu¹¹ studied the influence of hydrogen on the properties of propane/air flames, using the burner with granular ceramic beds. They found that the addition of hydrogen in the fuel mixture led to a noticeable improvement in the flame propagation rate, regardless of the applied techniques and base fuel. Sun et al¹² used the constant-pressure spherical flame technique in order to calculate the laminar flame speeds of CO/H₂/air and CO/H₂/O₂/helium mixtures. The results showed that both mixtures experienced significant improvements in flame speed with the increase of H₂ content in the mixture. Hu and Zhang¹ discussed the effect of the CO₂/H₂ ratio on the development of the flame cells. It was shown that with the rising hydrogen ratio, the cellular instability of the flame increased resulting in the faster flame propagation. Wei et al³ investigated the effect of different compositions of CO₂ and H₂ on the heat transfer characteristics of biogas/hydrogen flames. It was shown that the increase in H₂ content resulted in the enhancement of total heat

transfer rate up to 50%, which varied depending on the CO₂ contents. Based on these studies, it is expected that the addition of the hydrogen into biogas leads to positive effects in terms of improved laminar burning velocity, heat transfer rate, and flame temperature. This statement is further supported by numerous researches, which can be referred for the detailed analyses^{2,8,10-14}. On the contrary, there is a research gap regarding the effect of the hydrogen addition on the blowoff velocity of premixed biogas/air mixtures. In the case of premixed laminar flame, the blowoff velocity is one of the main critical limits to ensure static stability. Furthermore, in some applications of low emission gas turbines, knowing blow-out velocities is crucial to prevent any severe problems in the case of the re-ignition system failure.¹⁵ As such, it can be understood that the study of the hydrogen effect on the blowoff velocity is required.

Most of the studies mentioned above for biogas have conducted their investigations at the room temperature condition. Effect of the initial temperature on the combustion of various fuels such as syngas and natural gas has been found in a few studies¹⁶⁻¹⁸. Natarajan et al¹⁶ conducted experiments in a bunsen burner and found that the laminar burning velocity of syngas was improved with the higher preheated temperature of the unburned gas. Robin et al¹⁷ and Ai et al¹⁸ employed the burner with the diverging channel and the spherical bomb configuration, respectively. All three reports showed that the temperature of the adiabatic flame was increased by heating the mixture of unburned gases, which consequently led to the improved laminar flame speed. Other research groups¹⁹⁻²¹ conducted experiments with different fuels, such as oxy-methane, methylcyclohexane, and methanol. They reported the same trends and supported the idea of increasing the temperature of the mixture enhanced combustion performance.

Besides the experimental studies mentioned earlier, there have been numerical studies determining the combustion characteristics of biogas fuels with various chemical mechanisms.^{19,20} Quintino et al²² and Xiang et al²³ assessed the effect of CO₂ on the combustion characteristics of CH₄/air flames using CANTERA with USC-Mech chemical-kinetic mechanism and PREMIX code with the GRI-Mech 3.0 chemical reaction mechanism, respectively. Furthermore, researchers²⁴⁻²⁶ performed numerical simulations of laminar premixed bunsen flames with different base fuels as well as the chemical mechanisms. While these studies have been performed in-depth, and, additionally, there is available literature on the usage of GRI-Mech 3.0 chemical mechanism in order to study the combustion characteristics of biogas/air flames,²⁷ the results were obtained based on the full mechanisms imposing a heavy computational burden. Thus, the applicability of the

reduced chemical mechanisms for modeling of the premixed bunsen flames becomes of importance.

Thus, the objective of this work is to experimentally investigate the enhancement of blowoff and laminar burning velocities with the addition of hydrogen at elevated initial temperatures of the unburned gases for different biogas compositions. Moreover, it is of interest to fill the knowledge gap on the application of the reduced GRI-Mech 3.0 chemical mechanism to simulate the biogas flames using ANSYS Fluent software. As such, the computational conical flames will be in direct comparison with the experimental bunsen flames to justify the use of the kinetic mechanism.

2 | EXPERIMENTAL APPARATUS AND SETUP

2.1 | Experimental setup

To perform the experimental investigation, the setup consisted of a coflow burner, multiple mass flow controllers, heating ropes, variable autotransformer variac, multiple thermocouples and a digital camera (Nikon D3000), as schematically shown in Figure 1. The central nozzle of the coflow burner was made of stainless steel with an inner diameter of 7.55 mm, the thickness of 1 mm and the length to be over 500 mm. This geometric profile was chosen to establish a fully developed parabolic profile of the velocity at the exit of the nozzle, regardless of the flow conditions.²⁸ The coflow burner was filled with glass beads and covered with a honeycomb in order to ensure a uniform coflow. Nitrogen (N_2) coflow was used to prevent the secondary diffusion flame while stabilizing premixed

bunsen flame. The nitrogen coflow was set at 5 cm/s and was used for all the conditions. Mass flow controllers (MKS, 1179 A) were used to control the flow rate of the gases via readout controller (MKS, 247D 4 channel). The calibration of these MFCs were done using a dry-test gas meter (Bios, Definer 220M). Methane (CH_4) and carbon dioxide (CO_2) were supplied to imitate the biogas fuel based on various compositions, referring to Table 1.

The biogas/air mixture was preheated by heating ropes (Omega) to investigate the effect of the temperature of the unburned mixture. The temperature of the heating ropes was controlled based on the supplied voltage from the autotransformer variac. The measurement of the temperature was done via a thermocouple (Omega, DP32PT) at the nozzle exit to ensure the temperature of the mixture was set at the desired condition. In order to confirm the uniformity of the heating, multiple thermocouples were attached throughout the supply line which was heated via the heating ropes. The temperature values were recorded by the temperature readout unit (midi LOGGER GLB20). Furthermore, the supplied mixture was ignited only when the temperature readout showed the desired value for the temperature, with an uncertainty of ± 1 K, of the unburned gas to ensure the accuracy of the experiment.

2.2 | Experimental methodology

2.2.1 | Blowoff velocity

The root of the premixed conical bunsen flame is the anchoring point which connects to the nozzle rim and leads to the stabilization of the flame as a result of the

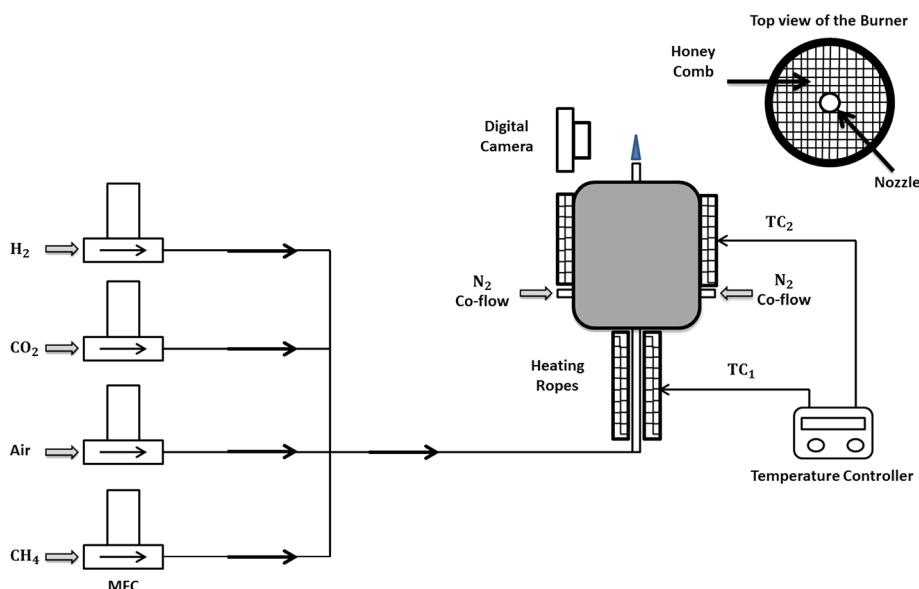


FIGURE 1 Schematic diagram of the experimental setup [Color figure can be viewed at wileyonlinelibrary.com]

TABLE 1 Biogas compositions used in this present work

Mixture Name	Biogas Composition, % by vol.	H ₂ Addition to Biogas, % by vol.	Gas Concentration in Fuel Mixture, % by vol.		
			CH ₄	CO ₂	H ₂
BG1	CH ₄ -CO ₂ 60-40%	0	60	40	0
BG1H10		10	54	36	10
BG1H20		20	48	32	20
BG1H30		30	42	28	30
BG1H40		40	36	24	40
BG2	CH ₄ -CO ₂ 65-35%	0	65	35	0
BG2H10		10	58.5	31.5	10
BG2H20		20	52	28	20
BG2H30		30	45.5	24.5	30
BG2H40		40	39	21	40
BG3	CH ₄ -CO ₂ 70-30%	0	70	30	0
BG3H10		10	63	27	10
BG2H20		20	56	24	20
BG3H30		30	49	21	30
BG4H40		40	42	18	40

heat transfer between these two mediums. Increasing the speed of the supplied mixture, relative to the velocity at which the flame is stable, pushes the flame further from the nozzle of a burner. As this distance increases, the heat transfer mechanism weakens resulting in instability of the flame, consequently leading to its blowoff at a specific flow velocity.²⁹ This critical nozzle exit velocity is known as the blowoff velocity of the flame. It is assumed that in order to experimentally determine this critical velocity, the premixed flame should firstly be established on the nozzle rim and followed by the continuous increase in the flow velocity until the flame blows off while maintaining the constant equivalence ratio of the mixture. Here equivalence ratio is defined as a measure of the fuel-air mixture relative to stoichiometric conditions. Among many factors that affect the blowoff phenomenon, laminar burning velocity plays an integral role in the behavior of the blowoff velocity. It showed that these two parameters, ie, blowoff and laminar burning velocities, had similar trends over the same range of equivalent ratio.³⁰ It is also known that the laminar burning velocity is dependent on the mixture's composition and temperature. Once the premixed flame is stabilized on the rim of the nozzle, there is a heat loss to the nozzle that causes a drop in the flame temperature. This occurrence negatively affects the laminar flame speed. On the other hand, the laminar burning velocity can get benefit from the heated nozzle as flame elevates the initial temperature of the mixture at the nozzle exit. Hence when

measuring the blowoff velocity, the time required to perform the measurements and change the velocity of the mixture would play a significant role in the outcome of the experiment. It was reported that using an increasing flow rate method could lead to inconsistent results.³⁰

Based on this observation, it was concluded that the decreasing flow rate method should be employed to determine the blowoff velocity of the premixed flame. In this study, the nozzle exit velocity was initially set at a high value where the flame was unable to be established. It is followed by the continuous decrease in the flow velocity when keeping the equivalence ratio constant until the flame was ignitable and stable at the nozzle rim. By following this approach, the heat loss from the flame to the nozzle was avoided, and the initial temperature of the unburned mixture was kept constant at the desirable conditions.

2.2.2 | Laminar burning velocity

Konnov et al³¹ reported a comprehensive review of measurements and data analysis of laminar burning velocities for various fuel/air mixtures in a wide range of various experimental configurations such as spherical bomb, counterflow, jet-wall stagnation, flat flame as well as the bunsen burner. It is worth noting that each of these experimental methods has its advantages and drawbacks. In the case of the bunsen burner method, there are two

well-known approaches in calculating the laminar burning velocity, namely the flame angle and the flame area methods.³¹ However, due to the non-uniform nature of the velocity distribution in the nozzle, the flame angle method cannot be used in this study. Hence, the bunsen burner with the flame area method was employed to obtain the values of the laminar flame speed.

Laminar burning velocity of a premixed bunsen flame is calculated as

$$S_u^0 = \frac{Q_u}{A_b} \quad (1)$$

The detailed explanation of the derivation was provided in multiple previous studies, which can be found in Konnov et al.³¹

While the volumetric flow rate of the unburned gas is defined by the experimental conditions, the area of the flame surface is found based on the image processing method of the given flame. The most challenging part of this segment is to identify the location of the flame front. Theoretically, the most accurate edge of the flame front is the location where the deviation of the temperature of the fresh gas starts to occur.²⁹ The most known methods of imaging process are schlieren, shadow graphing and the direct photographs of the flame; each of the mentioned methods produces different flame boundaries.²⁹ It was reported in Konnov et al.³¹ that the boundary with the highest brightness in a flame can be used as the flame front for calculation purposes. It is worth noting in Lewis and Von Elbe²⁹ that the inner boundary of the visible flame was shown to be coinciding or slightly overlapping with the outer edge of the shadow boundary. In order to validate this statement, the shadowed image of a premixed bunsen flame was obtained as shown in Figure 2A, whereas Figure 2B illustrates the greyscaled version of the flame, captured by direct imaging. The inner boundary of the visible flame was highlighted by identifying the highest rate of

change in pixel brightness in each column of the direct flame image, as displayed by the red dots in Figure 2B. As such, by identifying the pixel location and overlaying them on the shadowgraph image of the respective flame, Figure 2A, it was shown that both direct imaging and shadow graphing methods produce almost identical outcomes of flame surface area, which is used in calculation of the laminar burning velocity. For comparison purposes, the laminar burning velocity of CH₄/air mixture at $\phi = 1$ was calculated to be 34.78 cm/s by shadow graphing and 34.57 cm/s by direct imaging. However, employing the shadow graphing method brings additional difficulties as the thickness of the flame varies based on the distance between the flame and the camera.²⁹ This phenomenon is clearly shown in Figures 2C and 2D. Hence, it was decided to use the inner boundary of a visible flame from the direct photographs to define the area of the flame surface in this study. The image post-processing analysis was done using the MATLAB program.

2.3 | Measurement uncertainties

In this experimental study, there are two main sources of uncertainties; one is associated with the flow metering system which corresponds to the determination of the blowoff velocity while the other comes from the calculation of a flame area to obtain the laminar burning velocity of the flame.³¹ As mentioned earlier, the gases were supplied via mass flow controllers calibrated using the dry-test gas meter, which resulted in $\pm 2\%$ accuracy per gas. Hence, based on the root sum of squares method, the combined uncertainty for the total mixture (four gases) is calculated to be around $\pm 4\%$. In the case of the flame area calculation, five images were captured for each flame, and due to the axisymmetric nature of the bunsen flame, the calculation was done using the half image at a time. The final conical flame surface area was the average value of the five flames.

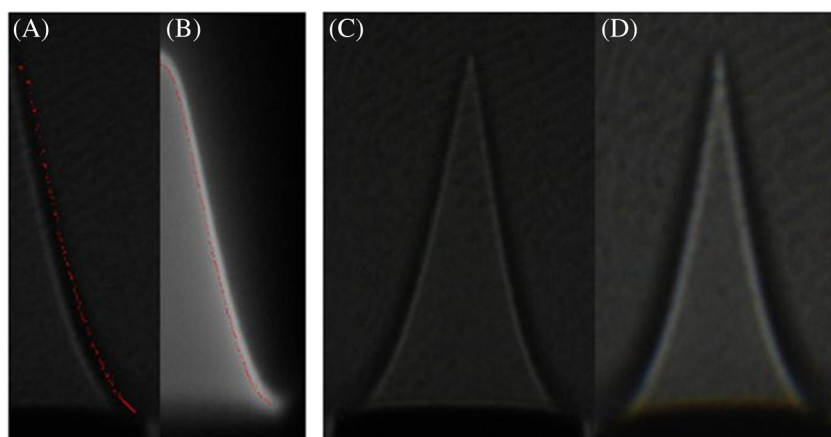


FIGURE 2 Flame image captured by shadowgraph technique; B, greyscaled direct photograph. Shadow boundary thickness changes with the distance between the camera and the flame, (C) 0.4856 mm and (D) 0.6143 mm [Color figure can be viewed at wileyonlinelibrary.com]

The maximum deviation, in the area of the flame front between a single image and the averaged value based on all the images, is roughly $\pm 3\%$. This produces the accuracy of $\pm 1\%$ for the mean flame area used in the calculation of the laminar burning velocity. Thus, the maximum uncertainty in the measurement of blowoff velocity is calculated to be $\pm 4\%$ while for the laminar flame speed is $\pm 5\%$.

3 | NUMERICAL SIMULATION

A steady-state simulation was modeled with non-swirling 2D axis-symmetric geometry using ANSYS Fluent 17.2. The reactive fluid flow was solved with three fundamental conservation equations in steady-state forms^{32,33}:

1. Continuity equation,

$$\nabla \cdot (\rho \vec{U}) = 0. \quad (2)$$

2. Navier-Stoke equation,

$$\nabla \cdot (\rho \vec{U} \vec{U}) = -\nabla p + \nabla \cdot \vec{\tau} + \rho \vec{g}. \quad (3)$$

3. Energy equation,

$$\begin{aligned} & \nabla \cdot \left[\vec{U} \left(\rho \left(h - \frac{p}{\rho} + \frac{U^2}{2} \right) + p \right) \right] \\ &= \nabla \cdot \left[k \nabla T - \sum_i h_i \vec{J}_i + \left(\vec{\tau} \cdot \vec{U} \right) \right] - \sum_i \frac{h_i^0}{M_i} \mathfrak{R}_i. \end{aligned} \quad (4)$$

where

$$\nabla \cdot \vec{U} = \frac{\partial U_x}{\partial x} + \frac{\partial U_y}{\partial y} + \frac{U_z}{y}, \quad (5)$$

and,

$$\vec{\tau} = \nabla \cdot \mu \left[\left(\nabla \vec{U} + \nabla \vec{U}^T \right) - \frac{2}{3} \nabla \cdot \vec{U} \vec{\delta} \right]. \quad (6)$$

Pressure-based solver was chosen with laminar as viscous model. Species transport species model was chosen for ideal gas with volumetric reaction activated and wall reaction deactivated. GRI-Mech 3.0 chemical mechanism³⁴ containing 325 reactions and 53 species was chosen. However, for the purpose of the present study, the dimension reduction was carried out to yield 13 species (H_2 , H , O , O_2 , OH , H_2O , HO_2 , CH_3 , CH_4 , CO , CO_2 , CH_2O , and N_2) as recommended and proved by the

number of research groups³⁵⁻³⁷ to account for methane and biogas only. This reduced mechanism was used to lessen the computational burden, while producing the same level of results, by employing the most relevant reactions and species on the combustion in the given chemical mechanism. Stiff chemistry solver, which uses ISAT table to increase solving speed,³² was configured with ISAT error tolerance of 5×10^{-5} . Coupled solver scheme with second-order upwind spatial discretization was selected for higher accuracy.

Figure 3 shows the geometry and the computational grid of the coflow burner for simulation. It is worth mentioning the importance of the inlet location for fuel/air mixture in the geometry of the model. Based on the main findings from the studies related to the combustion of the bunsen flames^{38,39}, the present study adopted the idea of setting the fuel/air inlet at 70 mm upstream from the nozzle exit. This is done in order to promote a more realistic velocity profile at the nozzle exit, as applying the fuel inlet boundary conditions at the nozzle exit tends to produce overestimation of the results. Mesh convergence test was performed by comparing the temperature profile along the central axial direction. Based on the mesh convergence results, the geometry with the total mesh elements of 44,104 quadrilateral cells with radial edge element sizing of 0.2 mm, 2/3 mm, 1 mm for fuel-air inlet, nozzle wall, coflow inlet and axial edge sizing of 0.2 mm was selected for the simulation study. Nozzle dimensions followed those of the experiment. Coflow velocity was radially uniform at 5 cm/s while fuel/air mixture velocity followed a parabolic function with maximum velocity $U_{\max} = 2U_0$. Nonslip wall condition and inlet temperature of 298 K were applied. Volume was initialized at 298 K and 1 atm.

For the first 200 iterations, reaction was deactivated to ensure steady flow. Then the activation of reaction to solve for the following 2500 iterations was selected to achieve steady bunsen flame. Temperature contour was plotted to define flame geometry.

4 | RESULTS AND DISCUSSION

The main objective of this work is to investigate the blowoff velocity of various biogas/air mixtures; specifically, to understand the behavioral change in blowoff velocity due to the addition of hydrogen and the elevated temperatures of the unburned mixture. Moreover, in order to fill the knowledge gap in this field of research, the numerical investigation of the biogas/air flame, using the reduced GRI-Mech 3.0 chemical mechanism, was conducted. In this section, experimental and numerical

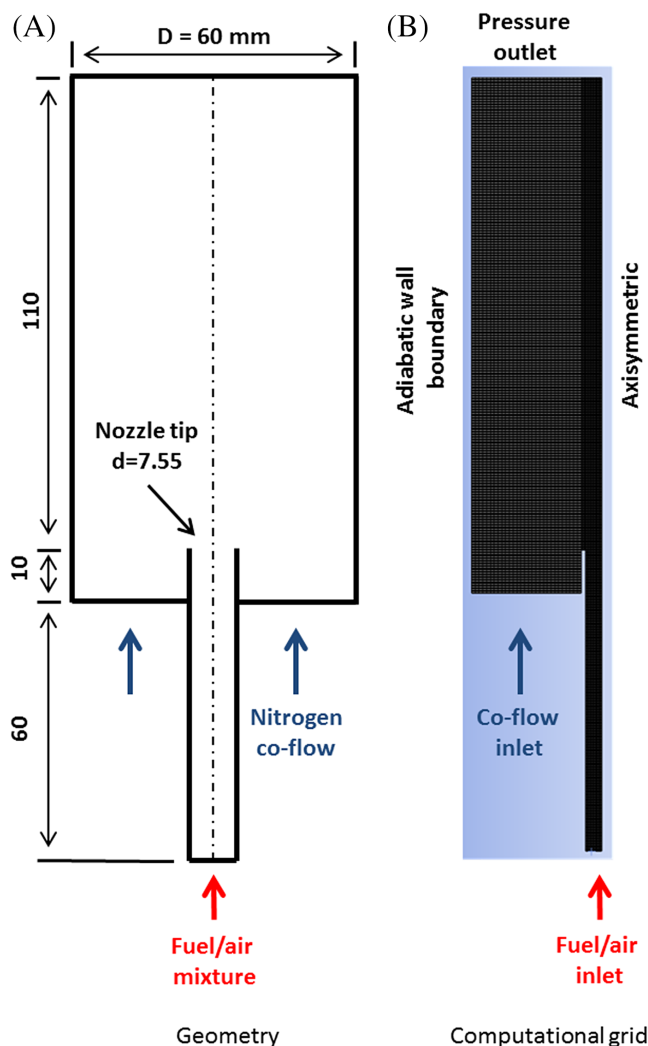


FIGURE 3 (A) Geometry and (B) computational grid of the coflow burner with its boundary conditions [Color figure can be viewed at wileyonlinelibrary.com]

results for CH_4/air flame are compared with literature data to validate our experimental setup and numerical model. Then the effects of hydrogen addition, elevated initial temperature, and CO_2 composition in the biogas/air mixtures are discussed next.

4.1 | Experimental validation

In order to validate the above-mentioned methodologies, combustion characteristics such as blowoff and laminar burning velocities were experimentally determined at room temperature and atmospheric pressure conditions for methane/air flames and illustrated in Figures 4A and 4B, respectively. As shown in Figure 4, both values, from the present study, are in good agreement with the literature data^{30,40-43}. Although there are some minor discrepancies between this study and the literature, the similarity in the trends is obvious. Moreover, these

differences can be caused by the variation in the experimental setup as well as in the methods of determining these parameters.³¹ However, the discrepancies are within the calculated uncertainties range represented by the error bars. Thus, the proposed methodologies, as well as the reduced GRI-Mech 3.0 chemical mechanism were validated and could be used for the determination of the laminar flame speed of the biogas/air mixture.

4.2 | Effect of elevated initial temperatures

The unburned gas temperature of the biogas/air mixture was heated within the range of 298 to 440 K, with the incremental steps of 20 K. Figure 5 illustrates the effect of initial temperature variation on the blowoff velocity of various stoichiometric biogas/air mixtures, with different CH_4 and CO_2 compositions. It is clearly seen that blowoff

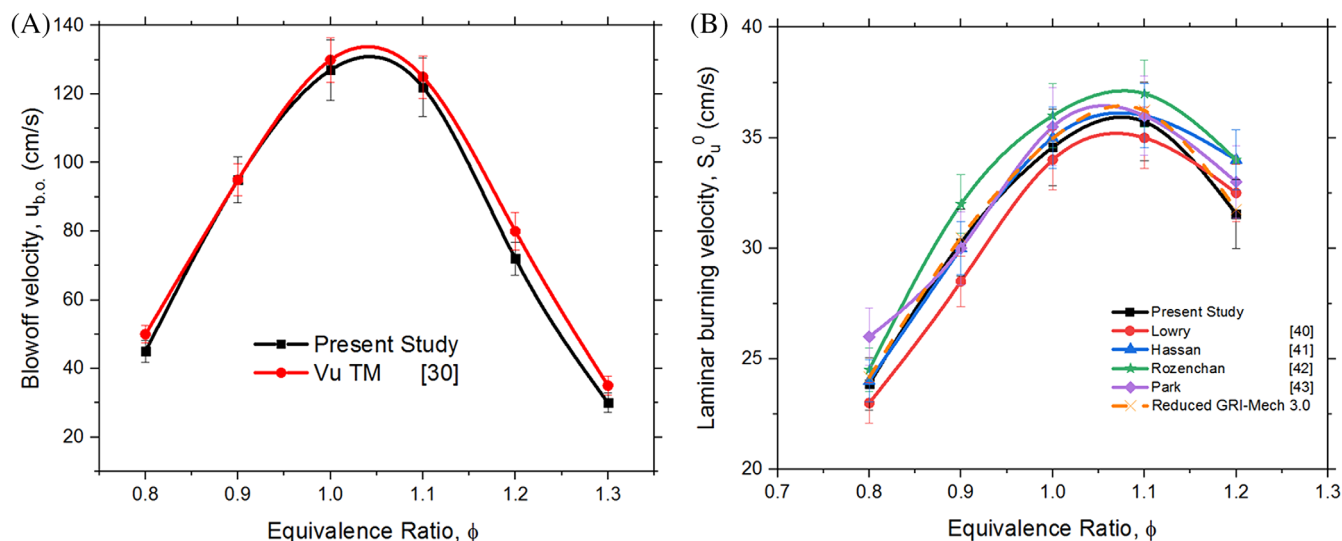


FIGURE 4 Comparison of the experimental and numerical data for CH₄/air mixture; A, blowoff velocity; B, laminar flame speed [Color figure can be viewed at [wileyonlinelibrary.com](#)]

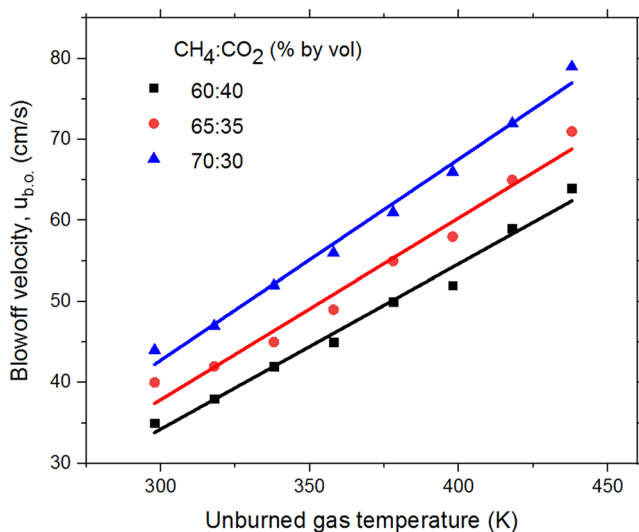


FIGURE 5 Effect of elevated unburned gas temperature on the blowoff velocity of stoichiometric biogas/air mixtures at atmospheric pressure condition [Color figure can be viewed at [wileyonlinelibrary.com](#)]

velocities are linearly increasing with the initial temperature of the mixture, regardless of CO₂ content. This behavior occurs as the result of a higher content of enthalpy present in the heated biogas mixture. To observe the impact of elevated initial temperatures of the unburned gas, flame photographs at three different initial temperatures of the unburned gas, ie, 298, 373, and 440 K, were taken at the same inlet velocity of 35 cm/s for the fuel sample BG1, as shown in Figure 6A. Moreover, the settings in the digital camera were kept constant (1/60 s and $f = 1.2$) for the purpose of the direct comparison between the flame observations. From Figure 6A, it

was found that the height of the flame had decreased with an increase in the initial temperature of the mixture. As an example, for the fuel sample BG1 at $\phi = 1.0$, the flame height was reduced from 2.281 mm to 2.016 mm at the initial temperatures of 298 K and 440 K respectively. As the local flow velocity was kept constant for the comparison purposes, it was observed that the reduction in flame height resulted in an increase of the cone angle. It is also known that the calculation of the laminar burning velocity is closely associated with the cone angle and the local flow velocity. Therefore, the change in flame height can be considered as the indicator of change in both laminar burning velocity as well as the blowoff velocity.

The standoff distance, which is the distance between the flame base and the nozzle rim, plays an essential role in the flame stabilization as the heat transfer takes place between these two mediums^{30,44}. Although the anchoring mechanism of the flame based on the nozzle rim is complicated and consists of various combustion properties, the standoff distance of the flame can be another indicator to predict the behavior of the blowoff velocity. This situation is in good agreement with the observation of flame images from Figure 6A. It can be seen that the standoff distance of the flame was decreased with the elevated temperature of the biogas/air mixture, which results in a stronger stabilization mechanism indicating the increase in blowoff velocity. Figure 6B illustrates the enhancement in the blowoff velocity of the BG1 flames with regards to their respective elevated initial temperatures. The blowoff velocities were found to be 35, 50 and 64 cm/s for initial temperatures of 298, 373, and 440 K respectively. Although the increase in flame height can be attributed to the increased flow rate of the unburned mixture, the decrease in standoff distance can be

observed, which indicates the stronger anchoring mechanism at the nozzle rim.

4.3 | Effect of hydrogen addition

All three compositions of biogas were enriched with the hydrogen in the range of 10 to 40%, as shown in Table 1. The effect of this additive on the blowoff velocity was experimentally investigated at atmospheric pressure and 298 ± 1 K, over the wide range of equivalence ratios, ie, 0.8 to 1.3.

Figure 7 shows the enhancement of blowoff velocities of biogas/air mixtures with the addition of hydrogen at the stoichiometric condition. Unlike the linear increase of the blowoff velocity due to the elevated temperature of the unburned gas, the blowoff velocity increased nonlinearly with the increasing content of hydrogen in the mixture, for all three biogas compositions, BG1, BG2, and

BG3. It is obvious to note that the fuel sample with the lower content of CO_2 underwent a more significant rise in blowoff velocity with the hydrogen enrichment. This behavior is more apparent with the increasing content of the hydrogen in the mixture. For example, with 20% of hydrogen content in the mixture, BG1, BG2, and BG3 achieved the improvements of 100, 140, and 170% in the blowoff velocities, respectively. It can be explained based on the fact that the temperature of the combustion and the active radicals are increased with the higher content of H_2 as well as the lower concentration of CO_2 added into the biogas mixtures. This behavior is similar to the case of the laminar burning velocity of hydrogen-enriched fuels, which was shown in literature^{2,3,10}.

Figures 8A and 8B depict the effect of hydrogen addition on the blowoff as well as the laminar burning velocities of the BG1 mixture over the wide range of equivalence ratios. As a result of the addition of hydrogen into the mixture, more active radicals are produced, and

FIGURE 6 Direct photographs of stoichiometric premixed bunsen flame (BG1) with elevated temperatures; A, all three flames are at the same inlet velocity of 35 cm/s; B, flames are at their critical velocity just prior to blowoff [Color figure can be viewed at wileyonlinelibrary.com]

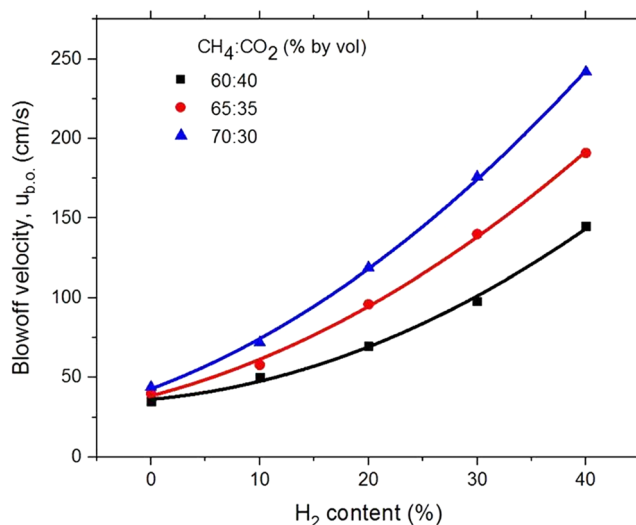
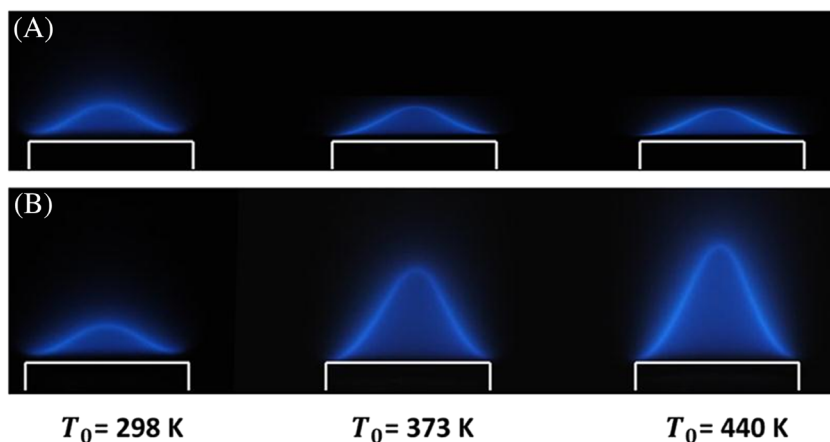


FIGURE 7 Effect of hydrogen addition on the blowoff velocities of stoichiometric biogas/air mixtures [Color figure can be viewed at wileyonlinelibrary.com]

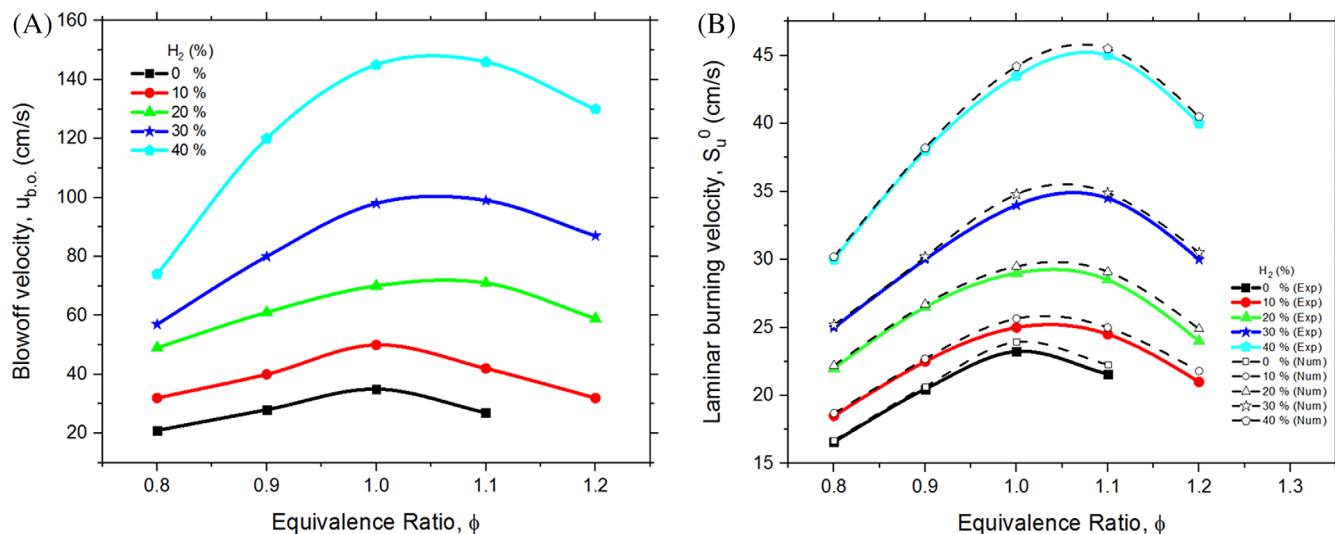


FIGURE 8 Effect of the hydrogen addition on: (A) blowoff velocity and (B) laminar burning velocity of BG1 mixture over the wide range of equivalence ratios [Color figure can be viewed at wileyonlinelibrary.com]

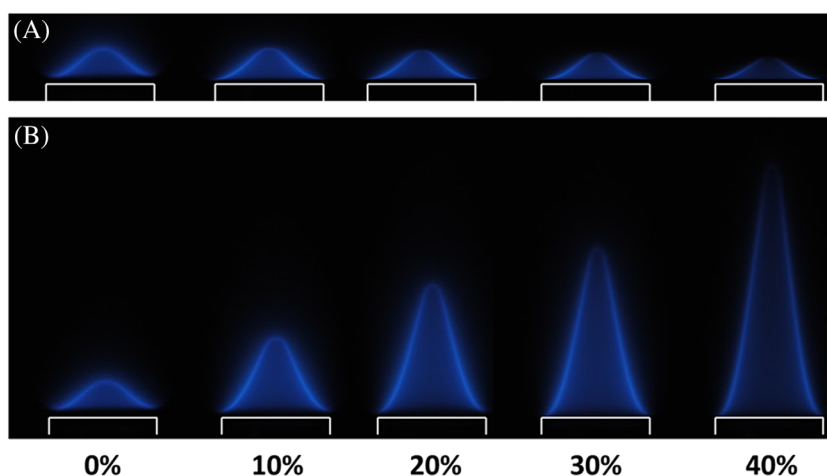
the temperature of the unburned mixture is increased. These changes lead to the enhancement of the thermal diffusivity. This phenomenon was discussed by Wei et al.,³ who also predicted that the thermal diffusivity was higher in the rich hydrogen-enriched-biogas mixtures compared with the lean mixtures. This prediction is in good agreement with the experimental results of the present study, shown in Figure 8A, as the improvements in stoichiometric and rich mixtures were more apparent compared with lean mixtures. Moreover, it is worth noting that the significant growth in the burning velocity can be attributed to the higher contribution of hydrogen towards the combustion process of the fuel blends. Erjiang et al.⁴⁵ performed a numerical investigation on the combustion of methane/hydrogen/air mixture and showed that there were three regimes of the combustion. One of them is the transition regime where the combustion was governed by both hydrogen and methane fuels. As a result of their combined physiochemical properties, the growth in flame burning velocity was non-linear compared with the linear increase for purely methane or hydrogen dominated combustion regimes. Jun et al.⁴⁶ reported a similar observation while studying the combustion characteristics of hydrogen/ammonia/air mixture. The results showed that the changes in the burning velocity are non-linear with the hydrogen content of 30 to 50% in the mixture. The effect of this non-linear growth can be seen in Figure 8, where the improvements in blowoff and laminar burning velocities change dramatically with the hydrogen fraction of 30% and above.

Blowoff velocity of a flame can generally be predicted by the trend of the laminar burning velocity for a given

flame. This is because the laminar burning velocity is associated with the temperature of the flame, which plays a major role in the heat transfer mechanism between the root of the premixed bunsen flame and the nozzle. This is in good agreement with the present results, illustrated in Figures 8A and 8B. However, it must be noted that the relationship between these two characteristics is far more complex due to the possible occurrence of the stretch of the flame surface, heat losses, quenching effects as well as the dilution with the ambient gas.

To perform the flame observation, the direct photographs of stoichiometric premixed bunsen flames of BG2 mixture with different concentrations of hydrogen, 0 to 40%, are shown in Figure 9A. For the purpose of the comparison, the flame photographs were taken at the same inlet velocity of 40 cm/s. In Figure 9B, the flames were taken at their respective blowoff velocities, which were found to be 40, 58, 96, 140, and 191 cm/s for 0 to 40% of hydrogen addition respectively. As the hydrogen content increases in the mixture, the diffusion rate drops in the reaction zone and enhances in the preheat zone. This leads to the following changes: more active radicals, elevated temperature of the unburned gas, rise in the rates of reactions as well as the improved blowoff and laminar flame speed. On the contrary, the upstream side of the flame experiences early low-temperature reactions which lead to a steeper temperature gradient of the flame. Hence, the reaction zone thickness is decreased, as seen in Figure 9A. This observation is in good agreement with the mathematical relation discussed by Kanury.⁴⁷ It showed that the ratio of the temperature difference between burned and unburned gases to the maximum temperature

FIGURE 9 Direct photographs of stoichiometric premixed bunsen flames (BG2) with H₂ additions; A, all five flames are at the same inlet velocity of 40 cm/s; B, flames are at their critical velocity just prior to blowoff [Color figure can be viewed at wileyonlinelibrary.com]



gradient of the flame could be used to represent the flame thickness.⁴⁷

Another observation from the flame images, shown in Figure 9A, is the existence of the flame tip opening at 40% H₂ addition in the fuel blends. The two main factors associated with the tip opening of premixed bunsen flames are stretch rate, which is characterized by the curvature of the flame tip, and the preferential diffusion, which is associated with the disproportion of molecular diffusion of the components within the mixture.⁴⁸ As illustrated in Figure 9A, fuel enrichment with hydrogen resulted in the reduction in the flame height at the given unburned gas velocity. The reduction in flame height increases the curvature at the flame tip, which dominates the stretch effect and weakens the negative stretch. Moreover, flow strain exists due to the high mass diffusivity of hydrogen causing the positive stretch effect. Yasuhiro et al²⁶ conducted a numerical study to understand the tip opening mechanism of bunsen flames. The results of the simulation showed that the fuel concentration is not homogeneous throughout the flame structure. It decreases along the direction of the flow, ie, in the axial direction, due to the outward radial diffusion, while the oxidant concentration is constant. As such, there was a reduction in the fuel consumption rate in the downstream of the flame, due to the leaner nature of the mixture, which led to the lower local combustion intensity at the flame tip. Hence, there is a competitive relationship between the impact of the flame curvature and the fuel consumption rate at the tip of the flame. With the higher fraction of H₂ in the mixture, the flame height reduces while increasing the curvature of the flame tip at the given unburned gas velocity. On the other hand, the intensity of the combustion at the flame tip enhances due to the increased hydrogen ratio. Thus, the tip opening depends on whichever of the two mentioned effects are more dominant at the given hydrogen concentration. This behavior is more apparent with the higher

concentration of hydrogen which is consistent with the present experimental results. In this work, the tip opening of the flame occurred at 40% addition of H₂, where the flame curvature weakened the negative flame stretch, and its influence was more dominant compared with the local combustion intensity at the tip of the flame. Additionally, Vu et al⁴⁹ showed that the existence of tip opening was independent of the unburned gas velocity at the given equivalence ratio, which is supported with the present study findings shown in Figure 9. The flame images were taken at the same gas velocity of 40 cm/s as shown in Figure 9A whereas in Figure 9B, the flame images were taken at their respective blowoff velocities. In both scenarios, the tip opening of the flame was present at the hydrogen concentration of 40%, irrespective of the jet velocity.

4.4 | Effect of CO₂ composition in biogas mixture

Figures 10A and 10B illustrate the variation of the laminar flame speed of biogas/air mixtures over the wide range of equivalence ratios, for all three mixture compositions with and without H₂ addition respectively. It can be observed that the increase in CO₂ content in the mixture causes a consistent reduction in the laminar burning velocity of the biogas/air mixtures. In addition, the reduction of laminar burning velocity due to the dilution with CO₂ is noticeably higher for richer biogas mixtures compared with lean and stoichiometric conditions. Figure 10A shows that the peak of laminar burning velocity of biogas with H₂ addition shifts from the richer towards stoichiometric mixture conditions with the increase of CO₂ content in biogas fuel, while the peak of laminar burning velocity is at stoichiometric for the biogas without H₂ enrichment as can be seen from Figure 10B. These behaviors can be explained by the

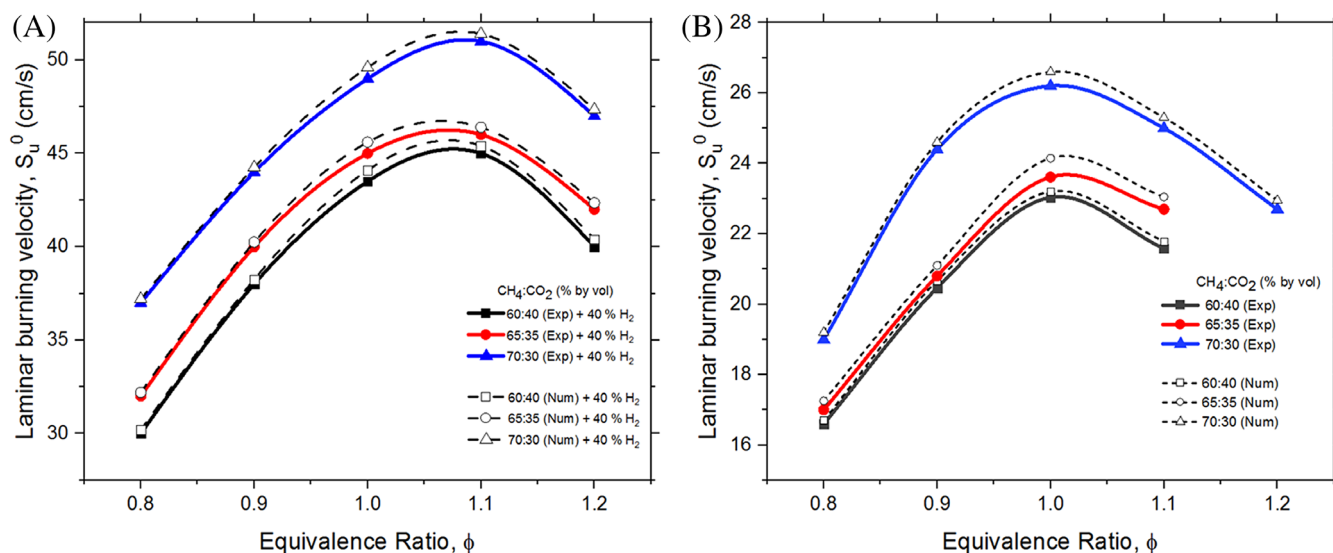
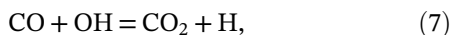


FIGURE 10 Laminar burning velocity of biogas/air mixtures (A) with 40% of H₂ addition and (B) pure biogas/air mixtures, at room temperature and atmospheric pressure [Color figure can be viewed at wileyonlinelibrary.com]

combination of dilution, thermal, chemical and radiation effects of CO₂ in the mixture^{22,50}. As mentioned above, CO₂ is a chemically passive agent and its addition to the mixture results in the reduction of the fuel content due to the dilution effect. Thermal effect is characterized by the reduction in adiabatic flame temperature, due to the non-reactive nature of CO₂, which plays the role of the heat sink in the mixture.⁵⁰ Hence, the laminar flame speed decreased with the higher dilution ratio of CO₂, as shown in Figure 10B, due to its dependency on the temperature of the flame. The result is in good agreement with our numerical adiabatic flame temperatures, which were recorded to be 2110, 2130 and 2158 K for BG1, BG2, and BG3 respectively.

Besides, CO₂ is one of the major products of combustion. It has been reported the chemical kinetics of fuel/air mixture modifications, invoked by the addition of 1CO₂, can be associated with the following major reactions^{22,23,27,50}:



The presence of CO₂ in the mixture results in the reduction of H radicals through the reverse reaction of $\text{CO} + \text{OH} = \text{CO}_2 + \text{H}$. Whereas, $\text{H} + \text{O}_2 = \text{O} + \text{OH}$ reaction is the most influential on the combustion, based on the sensitivity analysis. Therefore, the lack of H radicals resulted by Equation 7 influences Equation 8, thereby decreasing the reaction rate of the overall combustion for the given mixture. However, it is important to note that the chemical effect of CO₂ is more pronounced near

stoichiometric conditions. The content of the fuel increases with the equivalence ratio, allowing more H radicals in the mixture to be available in Equation 8, thereby strengthening the effect of chemical kinetics for the rich fuel mixtures. This can explain the shift in the peak of laminar burning velocity from the rich side of biogas with H₂ addition, Figure 10A, to the stoichiometric side of biogas without H₂ addition, Figure 10B.

Figure 10B shows that the richer biogas mixtures experience a more notable reduction in laminar burning velocities with CO₂ dilution rate. This is attributed to the radiation effect of CO₂ in the mixture. Carlos et al⁵¹ reported the existence of the linear relation between the temperature loss through radiation and CO₂ dilution rate. In addition, with both experiment and numerical simulation, Lee et al⁵² reported that CO₂ can be considered as a radiating medium, and thereby resulting in the radiation heat loss as well as the total heat loss.

Another observation from Figures 10A and 10B is the drastic change in laminar burning velocity of the biogas mixtures between BG2 and BG3. This behavior can be explained by the findings from Lee et al,⁵² where the steeper temperature drops were observed through the radiation loss, between 30% and 40% of CO₂ dilution in the mixture. This difference has also exerted its influence on the physical appearance of the bunsen flames. To further support the above-mentioned statement, the flame observations for all three compositions were conducted, as shown in Figure 11. The results, indeed, showed that BG3 depicted the brightest flame indicating the highest flame temperature as well as the highest presence of active radicals among the three tested biogas mixtures, which directly affects the rates of reactions in the combustion process.

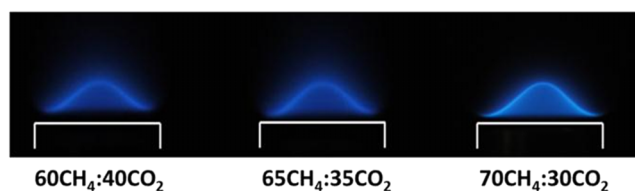


FIGURE 11 Comparison of stoichiometric biogas/air with three different compositions at room temperature and atmospheric pressure and unburned gas velocity of 35 cm/s [Color figure can be viewed at wileyonlinelibrary.com]

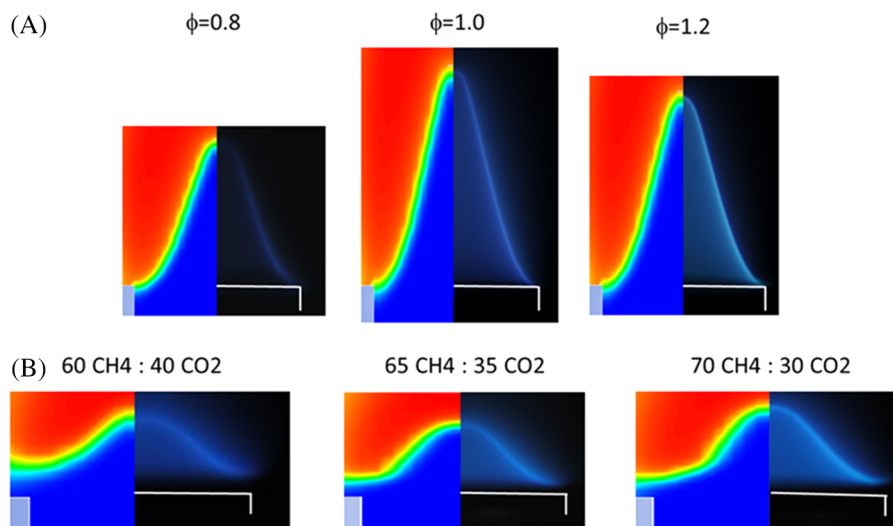


FIGURE 12 Comparison between numerical and experimental results; A, CH_4/air mixtures at $\phi = 0.8, 1.0$, and 1.2 (from left to right); B biogas/air mixtures at the stoichiometric condition ($\phi = 1.0$) [Color figure can be viewed at wileyonlinelibrary.com]

4.5 | Comparison between numerical and experimental flames

While there are a number of studies on combustion characteristics of biogas/air flames using the GRI-Mech 3.0 chemical mechanism, the information on the application of reduced GRI-Mech 3.0 chemical mechanism is scarce. Thus, the applicability of the reduced chemical mechanisms for modeling of the premixed biogas/air flames becomes of importance.

In this study, the reduced GRI-Mech 3.0 mechanism is applied to study the combustion of CH_4/air flames in order to ensure the accuracy of the model. This is done as CH_4 is one of the major components in the biogas fuel, which is the main interest of this study. The numerically obtained data of laminar burning velocity, then, was compared with the experimental results, as shown in Figure 4B. It can be seen that the results are in good agreement and well within the literature scatter.

Upon the completion of the numerical study on CH_4/air flames, the same reduced mechanism was applied to investigate the effect of CO_2 and H_2 content on the combustion characteristics of the biogas/air flames. As expected, the laminar burning velocity decreased with a higher concentration of CO_2 in the mixture and increased

with the addition of H_2 . These behaviors are in good agreement with the experimental results. Figure 10 shows the laminar burning velocity of biogas/air mixtures with different concentrations of CO_2 and their enrichment with H_2 addition. As can be seen, numerical and experimental results are in good agreement with each other. While Figure 10A shows only 40% of H_2 addition to the three different biogas compositions, Figure 8B can be referred to view the change in laminar burning velocity of BG1 fuel sample with the various H_2 concentrations.

Figures 12A and 12B illustrate the direct comparison of the flame structures between the numerically and experimentally obtained premixed bunsen flames, for both CH_4/air and biogas/air flames. In ensuring the validity of the results, CH_4/air flames were compared at three equivalence ratio conditions such as fuel-lean ($\phi = 0.8$, $U_0 = 50$ cm/s), stoichiometric ($\phi = 1.0$, $U_0 = 125$ cm/s) and fuel-rich ($\phi = 1.2$, $U_0 = 80$ cm/s) as shown in Figure 12A. Whereas in Figure 12B, the flame of biogas/air mixtures were captured at the stoichiometric condition with their respective gas flow velocities of 35 cm/s (for $60\text{CH}_4:40\text{CO}_2$), 40 cm/s (for $65\text{CH}_4:35\text{CO}_2$) and 44 cm/s (for $70\text{CH}_4:30\text{CO}_2$). From the observation, it is clear to note that both flame heights and standoff

distances of the experimental flames are in good agreement with the computational results. It must be highlighted that the location of the fuel/air inlet boundary condition is essential as it highly affects the velocity profile at the nozzle exit. It was found that applying the fuel/air inlet boundary condition at the nozzle exit area leads to an overestimation in flame height and standoff distance.

5 | CONCLUDING REMARKS

In the present study, the biogas mixtures with the CO₂ concentration of 30 to 40% were enriched by H₂ within the range of 0 to 40% by volume and preheated in the range of 298 to 440 K. Combustion characteristics, such as blowoff and laminar burning velocities, of these biogas/air flames were experimentally examined using the bunsen burner method. The computational results were obtained using the ANSYS Fluent with reduced GRI-Mech 3.0 chemical mechanism and compared with the experimental results of the premixed bunsen flames. The major conclusions of the study are as follows:

1. Blowoff velocity increases linearly with the increasing of the unburned gas temperature. The improvements in blowoff velocity are indicated by the reduction in flame height as well as the shortening of standoff distance.
2. Blowoff and laminar burning velocities of biogas/air flames increase with the H₂ enrichment of the mixture. The relationship of blowoff velocity and H₂ addition is non-linear and attributed to the dominance of methane-inhibited hydrogen combustion process. The improvements in burning velocities are more apparent in the stoichiometric and rich fuels compared with lean mixtures. Additionally, the tip opening of the flame was observed with the H₂ concentration of 40% in the mixture irrespective of the jet velocity.
3. Laminar burning velocity decreases with the addition of CO₂ into the biogas/air mixture. The flame structure changes in terms of the brightness of the flame as well as the reduction in flame temperature. Furthermore, the fuel samples with 30% of CO₂ (BG3) show a big difference in laminar burning velocity compared with BG1 (40%) and BG2 (35%).
4. The reduced GRI-Mech 3.0 chemical mechanism is suitable to simulate the premixed bunsen flames of biogas/air mixtures. The flame height and standoff distance and the laminar burning velocity are in good agreement between the computational and experimental results. It is highlighted that setting the fuel/air inlet boundary condition at 70 mm upstream is

required as applying the inlet boundary conditions at the nozzle exit leads to overestimation of the results.

NOMENCLATURE

A_b	flame surface area, m ²
g	gravitational acceleration, m·s ⁻²
h	sensible enthalpy, m ² ·s ⁻²
J	diffusive flux, kg·m ⁻² ·s ⁻¹
k	thermal conductivity, W·m ⁻¹ ·K ⁻¹
M	molecular weight, kg·kgmol ⁻¹
P	pressure, kg·m ⁻¹ ·s ⁻²
Q_u	total unburned gas volumetric flow rate, m ³ ·s ⁻¹
R_i	volumetric rate of creation of species, mol·m ⁻³ ·s ⁻¹
S_u^0	laminar burning velocity, m·s ⁻¹
T	temperature, K
TC	thermocouple
U	velocity, m·s ⁻¹
U_{\max}	maximum velocity of parabolic profile, m·s ⁻¹
U_0	average speed of the profile, m·s ⁻¹
$u_{b,o}$	blowoff velocity, m·s ⁻¹
x	axial coordinate
y	radial coordinate
ϕ	equivalence ratio
ρ	density, kg·m ⁻³
μ	dynamic viscosity, kg·m ⁻¹ ·s ⁻¹
$\bar{\tau}$	stress tensor, kg·m ⁻¹ ·s ⁻²
$\bar{\delta}$	isotropic tensor, kg·m ⁻¹ ·s ⁻²

ORCID

Manh-Vu Tran  <https://orcid.org/0000-0002-6713-4201>

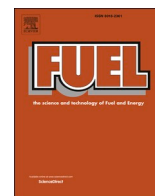
REFERENCES

1. Hu Z, Zhang X. Experimental study on flame stability of biogas/hydrogen combustion. *Int J Hydrogen Energy*. 2019;44:5607-5614.
2. Liu J, Zhang X, Wang T, Hou X, Zhang J, Zheng S. Numerical study of the chemical, thermal and diffusion effects of H₂ and CO addition on the laminar flame speeds of methane-air mixture. *Int J Hydrogen Energy*. 2015;40:8475-8483.
3. Wei ZL, Leung CW, Cheung CS, Huang ZH. Effects of H₂ and CO₂ addition on the heat transfer characteristics of laminar premixed biogas-hydrogen Bunsen flame. *Int J Heat Mass Transf*. 2016;98:359-366.
4. Mustafa İ, İlker Y. Experimental analysis of the effects of hydrogen addition on methane combustion. *Int J Energy Res*. 2012;36:643-647.
5. Jeong P, Dong JH, June SP, et al. Hydrogen utilization as a fuel: hydrogen-blending effects inflame structure and NO emission behavior of CH₄-Air flame. *Int J Energy Res*. 2007;31:472-485.
6. Esmail MAM, Yinka SS, Mohamed AH. Numerical study of hydrogen-enriched methane-air combustion under ultra-lean conditions. *Int J Energy Res*. 2016;40:743-762.

7. Hu Z, Zhang X. Study on laminar combustion characteristic of low calorific value gas blended with hydrogen in a constant volume combustion bomb. *Int J Hydrogen Energy*. 2019;44:487-493.
8. Zhen HS, Leung CW, Cheung CS. Effects of hydrogen addition on the characteristics of a biogas diffusion flame. *Int J Hydrogen Energy*. 2013;38:6874-6881.
9. Leung T, Wierzbka I. The effect of hydrogen addition on biogas non-premixed jet flame stability in a co-flowing air stream. *Int J Hydrogen Energy*. 2008;33:3856-3862.
10. Li Z, Cheng X, Wei W, Qiu L, Wu H. Effects of hydrogen addition on laminar flame speeds of methane, ethane and propane: Experimental and numerical analysis. *Int J Hydrogen Energy*. 2017;42:24055-24066.
11. Yang SI, Wu MS. Properties of premixed hydrogen/propane/air flame in ceramic granular beds. *Int J Hydrogen Energy*. 2014;39:17347-17357.
12. Sun HY, Yang SI, Jomaas G, Law CK. High-pressure laminar flame speeds and kinetic modeling of carbon monoxide/hydrogen combustion. *Proc Combust Inst*. 2007;31:439-446.
13. Ma F, Wang Y, Liu H, Li Y, Wang J, Ding S. Effects of hydrogen addition on cycle-by-cycle variations in a lean burn natural gas spark-ignition engine. *Int J Hydrogen Energy*. 2008;33:823-831.
14. Porpatham E, Ramesh A, Nagalingam B. Effect of hydrogen addition on the performance of a biogas fuelled spark ignition engine. *Int J Hydrogen Energy*. 2007;32:2057-2065.
15. Schefer RW. Hydrogen enrichment for improved lean flame stability. *Int J Hydrogen Energy*. 2003;28:1131-1141.
16. Natarajan J, Kochar Y, Lieuwen T, Seitzman J. Pressure and preheat dependence of laminar flame speeds of $H_2/CO/CO_2/O_2/He$ mixtures. *Proc Combust Inst*. 2009;32:1261-1268.
17. Robin JV, Harshal K, Vishnu H, Sudarshan K. Effect of CO content on laminar burning velocities of syngas-air premixed flames at elevated temperatures. *Fuel*. 2018;214:144-153.
18. Ai Y, Zhou Z, Chen Z, Kong W. Laminar flame speed and Markstein length of syngas at normal and elevated pressures and temperatures. *Fuel*. 2014;137:339-345.
19. Hu X, Yu Q. Effect of the elevated initial temperature on the laminar flame speeds of oxy-methane mixtures. *Energy*. 2018;147:876-883.
20. Vladimir AA, Sergey SM, Ivan VC, Sergey GM. Laminar burning velocities of methylcyclohexane + air flames at room and elevated temperatures: A comparative study. *Combust Flame*. 2018;196:99-107.
21. Amit K, Asad M, Minaev S, Sudarshan K. Measurement of laminar burning velocities of methanol-air mixtures at elevated temperatures. *Fuel*. 2016;182:57-63.
22. Quintino FM, Fernandes EC. Analytical correlation to model diluent concentration repercussions on the burning velocity of biogas lean flames: Effect of CO_2 and N_2 . *Biomass Bioenergy*. 2018;119:354-363.
23. Xiang L, Chu H, Ren F, Gu M. Numerical analysis of the effect of CO_2 on combustion characteristics of laminar premixed methane/air flames. *J Energy Inst*. 2018;92(5):1487-1501.
24. Wang J, Zhilong W, Senbin Y, et al. Effects of stretch and preferential diffusion on tip opening of laminar premixed Bunsen flames of syngas/air mixtures. *Fuel*. 2016;148:1-8.
25. Zerrin T-R, Rajnish NS, Robert RR. Two-dimensional simulation of premixed laminar flame at microscale. *Chem Eng Sci*. 2015;138:414-431.
26. Yasuhiro M, Taisuke N, Tadao T. Numerical study of tip opening of hydrogen/air Bunsen flame. *Proc Combust Inst*. 2019;37:1775-1781.
27. Nonaka HOB, Pereira FM. Experimental and numerical study of CO_2 content effects on the laminar burning velocity of biogas. *Fuel*. 2016;182:382-390.
28. White FM. *Fluid Mechanics*. 4th ed. New York: McGraw-Hill, p. 331, 1998.
29. Bernard L, Guenther VE. *Combustion, Flames and Explosions of Gases*. 2nd ed. Pittsburgh, Pennsylvania: Academic Press, INC; 1961.
30. Vu TM, Won SH, Ombrello T, Cha MS. Stability enhancement of ozone-assisted laminar premixed Bunsen flames in nitrogen co-flow. *Combust Flame*. 2014;161:917-926.
31. Alexander AK, Akram M, Velamati RK, Nam K, Chockalingam P, Sudarshan K. A comprehensive review of measurements and data analysis of laminar burning velocities for various fuel + air mixtures. *Prog Energy Combust Sci*. 2018;68:197-267.
32. ANSYS, ANSYS Fluent 15.0 Theory Guide, Canonsburg, PA, 2013, pp. 2-4, pp. 133-5, pp. 187-8, pp. 289-90.
33. Batchelor GK. *An introduction to fluid dynamics*. Cambridge: Cambridge Uni. Press; 2000.
34. Smith GP, Golden DM, Frenklach M, et al. GRI-MECH 3.0. Available at. http://www.me.berkeley.edu/gri_mech/
35. Ren Z, Goldin GM, Hiremath V, Pope BS. Simulations of a turbulent non-premixed flame using combined dimension reduction and tabulation for combustion chemistry. *Fuel*. 2013;105:636-644.
36. Belcadi A, Assou M, Affad E, Chatri E. Construction of a reduced mechanism for modeling premixed combustion of methane-air. *Combust Theory Model*. 2007;11:603-613.
37. Kuo KK. *Principles of Combustion*. 2nd ed. John Wiley & Sons, Inc., p. 732.
38. Cha MS, Son JW, Yoon SH, Luong HT, Deanna AL, Sohn CH. Vortex formation mechanism within fuel streams in laminar nonpremixed jet flames. *Combust Flame*. 2019;199:46-53.
39. Nasreldin MM, Fuwu Y, Yu W. Effects of fuel inlet boundary condition on aromatic species formation in coflow diffusion flames. *J Energy Inst*. 2018;92:288-297.
40. Lowry W, de Vries J, Krejci M, et al. Laminar flame speed measurements and modeling of pure alkanes and alkane blends at elevated pressures. *J Eng Gas Turbines Power*. 2011;133(9):091501-091509.
41. Hassan MI, Aung KT, Kwon OC, Faeth GM. Properties of laminar premixed hydrocarbon/Air flames at various pressures. *J Propuls Power*. 1998;14:479-488.
42. Rozenchan G, Zhu D, Law C, Tse S. Outward propagation, burning velocities, and chemical effects of methane flames up to 60atm. *Proc Combust Inst*. 2002;29:1461-1470.
43. Park O, Veloo PS, Liu N, Egolfopoulos FN. Combustion characteristics of alternative gaseous fuels. *Proc Combust Inst*. 2011;33:887-894.
44. Hu X, Yu Q, Liu J, Sun N. Investigation of laminar flame speeds of $CH_4/O_2/CO_2$ mixtures at ordinary pressure and kinetic simulation. *Energy*. 2014;70:626-634.

45. Erjiang H, Zuohua H, Jiajia H, Chun J, Jianjun Z. Experimental and numerical study on laminar burning characteristics of premixed methane–hydrogen–air flames. *Int J Hydrogen Energy*. 2009;34:4876–4888.
46. Jun L, Hongyu H, Noriyuki K, Zhaohong H, Yoshihiro N. Study on using hydrogen and ammonia as fuels: Combustion characteristics and NO_x formation. *Int J Energy Res*. 2014;38:1214–1223.
47. Kanury AM. *Introduction to Combustion Phenomena*. New York: Breach Science Publishers; 1975.
48. Jinhua W, Zhilong W, Senbin Y, et al. Effects of stretch and preferential diffusion on tip opening of laminar premixed Bunsen flames of syngas/air mixtures. *Fuel*. 2015;148:1–8.
49. Vu TM, Cha MS, Lee BJ, Chung SH. Tip opening of premixed bunsen flames: extinction with negative stretch and local Karlovitz number. *Combust Flame*. 2015;162:1614–1621.
50. Chen Z, Tang C, Fu J, et al. Experimental and numerical investigation on diluted DME flames: thermal and chemical kinetic effects on laminar flame speeds. *Fuel*. 2012;102:567–573.
51. Carlos DG, Arrieta AA, Suárez JL. Comparison of combustion properties of simulated biogas and methane. *C.T.F Cienc. Tecnol. Futuro*. 2009;3:225–236.
52. Lee K, Kim H, Park P, Yang S, Ko Y. CO₂ radiation heat loss effects on NO_x emissions and combustion instabilities in lean premixed flames. *Fuel*. 2013;106:682–689.

How to cite this article: Nurmukan D, Chen TJM, Hung YM, Ismadi M-Z, Chong CT, Tran M-V. Enhancement of biogas/air combustion by hydrogen addition at elevated temperatures. *Int J Energy Res*. 2020;44:1519–1534. <https://doi.org/10.1002/er.4912>



Full Length Article

Experimental study on laminar lifted flames of pre-vaporized palm oil biodiesel

Dastan Nurmukan^a, Manh-Vu Tran^{a,*}, Ji Jinn Foo^a, Gianfranco Scribano^b, Cheng Tung Chong^c, Thanh Cong Huynh^d

^a School of Engineering, Monash University Malaysia, Jalan Lagoon Selatan, 47500 Bandar Sunway, Selangor, Malaysia

^b Department of Mechanical, Materials and Manufacturing Engineering, The University of Nottingham Malaysia Campus, Jalan Broga, 43500 Semenyih, Selangor, Malaysia

^c China-UK Low Carbon College, Shanghai Jiao Tong University, Lingang, Shanghai 201306, China

^d Department of Science & Technology, Vietnam National University, Ho Chi Minh City, Viet Nam

ARTICLE INFO

Keywords:

Biodiesel
Buoyancy
Lift-off
Lifted flame
Tribrachial flame

ABSTRACT

Characteristics of laminar lifted flame of pre-vaporized palm oil biodiesel have been experimentally investigated by varying fuel mole fraction at elevated unburnt gas temperatures. The biodiesel fuel was pre-vaporized and mixed with pre-heated nitrogen at a range of fuel mole fractions of 0.01 – 0.02. The unburnt gas temperature was varied from 500 K to 650 K. The results showed that the increase in jet flow velocity influenced the lift-off of the laminar non-premixed flame. Furthermore, the higher fuel mole fractions and the elevated unburnt gas temperatures led to a reduction in the lift-off height of the flame. Hence, a limited range of conditions, where the lifted flame occurred was determined for a given unburnt gas temperature and fuel mole fraction. At some of the experimental conditions such as 500 K and 550 K, the flames still experienced lift-off even at smaller jet velocities compared to stoichiometric laminar burning velocity of the same mixture. This behavior was believed to associate with the buoyant force produced at the nozzle of the rim, causing secondary entrainment of the mixture flow at relatively low jet flow velocities. The results suggested a correlation between the lift-off height and jet flow velocity, with the inclusion of the stoichiometric laminar burning velocity, regardless of the unburnt gas temperature and fuel mole fraction in the mixture. The adaptation of the buoyancy-induced velocity to the lift-off velocity correlated well with the stoichiometric laminar burning velocity, showing the significance of the buoyant force near the nozzle exit.

1. Introduction

Economic development due to the spikes in oil prices, ongoing debates on the possible shortage of the fossil fuels in the future, and the currently increasing awareness on the effect of greenhouse gasses on global warming and climate change have led to an increased interest in the development of the renewable clean fuels [1–5]. Among many available options, biodiesel fuel has drawn the attention of the scientific community due to its availability and variety of its feedstock sources, and its cleaner combustion nature compared to the traditional fossil fuels, all the while requiring minimal to no modification of the existing engines [6].

As one of its advantages, biodiesel can be produced from a wide range of feedstocks, both from edible [7] and non-edible sources [8],

which result in a variety of chemical and physical properties of the fuel. A number of research groups have studied combustion characteristics of different biodiesels such as soybean, coconut, rapeseed, sunflower, palm oil, and others [7–10]. Upon their observations, the results showed that palm oil biodiesel has a slight advantage over the other fuels extracted from sunflower, rapeseed and soybean, because it has a higher cetane number and heating value as well as higher oil content resulting in advantageous economic factor. Furthermore, palm oil biodiesel achieves more complete combustion due to the presence of oxygen in the fuel, leading to a lower soot production compared to traditional fossil fuels. It is also important to note that most studies in literature have been conducted in engines [11,12], there have been very few works studying the fundamental combustion characteristics of different types of biodiesel.

Despite all the positive findings of palm oil biodiesel, it has some

* Corresponding author.

E-mail address: manhvu.tran@monash.edu (M.-V. Tran).

<https://doi.org/10.1016/j.fuel.2020.119697>

Received 5 July 2020; Received in revised form 4 September 2020; Accepted 5 November 2020

Available online 16 November 2020

0016-2361/© 2020 Elsevier Ltd. All rights reserved.

significant drawbacks such as low heating value as well as high freezing point. Thus, biodiesel is mainly blended with the standard fossil fuel in order to obtain the optimal fuel characteristics in terms of cleanliness and combustion efficiency [11,12]. Since palm oil biodiesel is generally blended with traditional diesel fuels, it is of utmost importance to identify the limitation of the flame stability for biofuels to avoid the degradation of the fuel blend.

There are three main parameters that can characterize the stabilization mechanism of laminar non-premixed flames in practical combustors, known as liftoff velocity (U_{LO}), liftoff height (H_L), and blowoff velocity (U_{BO}). Understanding of the behavior of the lifted flames is also critical in the development of industrial burners [13]. There is a wide range of applications where the lifted flames occur, such as gas turbines, power systems as well as the traditional diesel engines [14]. As such, the stabilization of the lifted flames has been extensively studied both numerically and experimentally at various conditions such as fuel types, dilution effect, the inclusion of partial premixing as well as different coflow velocities [14–22].

Choi and Chung [16] conducted an experimental study to investigate the lifted flames of pre-vaporized *n*-heptane at both non-autoignited and autoignited temperatures. The results showed that, for non-autoignited lifted flames, there was an existence of tribrachial flame structure at the edge of the stationary lifted flames, which was similar to the flame structure of the gaseous fuels. The tribrachial flame edge was described by its triple-layer, where the rich and lean premixed wings were both connected to the trailing diffusion flame [18]. On the contrary, within the autoignited regime, lifted flames experienced mild combustion, which resulted in a different flame structure compared to the gaseous fuels [20]. Choi and Chung [16] also showed the correlation between the stoichiometric laminar burning velocity and liftoff velocity with the inclusion of the buoyancy effect created near the nozzle rim. A similar study was conducted by Al-Noman et al. [17] to investigate the behavior of *iso*-octane flames. The results showed that in the autoignited regime, the flames experienced higher liftoff heights for *iso*-octane compared to *n*-heptane, which was associated with the prolonged ignition delay.

While the previous studies produced significant data in understanding the stabilization of the lifted flames, it is important to note that they have focused on pure fuels. However, in practical cases, traditional fuels consist of various compounds, having different combustion characteristics and transport properties. Quattrocchi et al. [14] conducted a numerical investigation on the effect of syngas compositions on the flame stability parameters such as liftoff and blowout velocities. To further enrich the knowledge on the stabilization mechanism of lifted flames, Choi and Chung [20] and Van et al. [21] conducted experimental and numerical studies, respectively, to investigate the stability of the flames with Schmid numbers less than unity. While Van et al. [21] focused on the behavior of the diluted methane jet flames, Choi and Chung [20] emphasized the effect of the coflow temperature on the stability of the lifted flames. The results concluded that the laminar non-premixed lifted flames could be obtained even at the condition of Schmid numbers being less than unity. Despite the fact of having all the findings from the research groups mentioned above, it is essential to highlight that the studies focused mainly on the primary reference fuels as well as natural gasses.

Due to the increasing interest in the study of alternative cleaner fuels as well as the lack of studies on the stabilization of the non-premixed heavy biofuels, palm oil biodiesel was selected for investigation in the study. Thus, the main objective of the present study is to experimentally investigate the characteristics of laminar lifted flame of the palm oil biodiesel by varying fuel mole fraction at elevated unburnt gas temperatures. This study provides reasonable correlations between the liftoff height and jet flow velocity, as well as the buoyancy effect and liftoff velocity. Furthermore, blends of palm oil biodiesel and standard diesel at different biodiesel/diesel ratios were prepared to study the liftoff characteristic of the blends.

2. Experiment

2.1. Experimental setup

The experimental setup, schematically shown in Fig. 1, consisted of a coflow burner, fuel supply line, mass flow controllers (MKS, 1179 A), syringe pump (NE-300), heating ropes (Omega), thermocouples (Omega, SA3-K-72), variable autotransformer variac, the temperature readout unit (midi LOGGER GLB20) and a digital camera (Fujifilm X-T20). A stainless-steel tube with an inner diameter of 4.35 mm and a thickness of 1 mm was employed as the central nozzle of the burner. In the case of the central nozzle, in order to achieve a fully parabolic velocity profile at the outlet of the nozzle, the length of the tube was chosen to be over 500 mm [23]. The biodiesel fuel was delivered to the central nozzle via a syringe pump, where the fuel was pre-vaporized and diluted by the pre-heated carrier gas of N_2 . The autotransformer variac controlled the output of the supplied voltage to the heating ropes to achieve the desired temperature. Multiple thermocouples (TC₁₋₃) were attached throughout the system to confirm the uniformity of heating temperature, and the ceramic wool insulators were installed to mitigate the heat loss to the environment. One of the thermocouples (TC₃) was placed at the nozzle exit to ensure the temperature of the mixture was set at the desired conditions. Air was used as the coflow gas to stabilize the lifted flames above the burner. The uniformity of the air coflow was achieved by filling the burner with glass beads and utilizing a honeycomb as a pathway. The air coflow velocity was set at 10 cm/s and was kept constant for all the experimental cases. The flow rates of both air coflow and N_2 carrier gas were controlled by mass flow controllers and readout controller (MKS, 247D 4 channel). To minimize the potential errors, the mass flow controllers were calibrated using a dry-test gas meter (Bios, Definer 220 M) for each specific gas accordingly. The pre-heated temperature of N_2 carrier gas was kept constant at 483 K, which is its boiling temperature, to avoid the condensation of vaporized fuel during the mixing process. In this experimental study, the fuel mixtures were heated at the temperature range of 500 K – 650 K, and the fuel mole fraction was varied from 0.01 to 0.02. For biodiesel/diesel cases, the blends were prepared based on the volumetric fractions and the homogeneity of the blends was assured by using an ultrasonicator with 55% amplitude for 10 min at 10/5 pulse. The lifted flames were visualized via direct photography employing the digital camera, and liftoff heights, which is the distance between the nozzle rim and the base of the lifted flame, were measured in post-analysis via image processing using MATLAB.

Palm oil biodiesel, which is known as palm methyl esters (PME), was supplied by Mewah Oils Sdn. Bhd., Malaysia while diesel with ultra-low sulphur concentration was purchased from a commercial petrol station, Shell. The quality of the PME and diesel is within the European Union's EN14214 standards. The properties of the fuels and the composition of PME are shown in Tables 1 and 2 respectively. The compositions of PME were obtained via GC–MS analysis using Agilent 7890A (GC) & 5975C (MS) [24,25].

3. Results and discussion

The objective of this work was to experimentally study the behavior of the lifted flames of PME for different fuel mole fractions in the mixture at elevated unburnt gas temperatures. The lifted flames were achieved by varying the jet flow velocity at a specified temperature per given fuel mole fraction in the mixture. To describe the behavior of the lifted flames, the correlations between the liftoff height and jet flow velocity, as well as the buoyancy effect and liftoff velocity, were obtained.

3.1. Experimental validation

Since palm oil biodiesel is a liquid fuel, *n*-heptane [16] and *iso*-octane [17] were chosen as the reference fuels in order to validate the accuracy

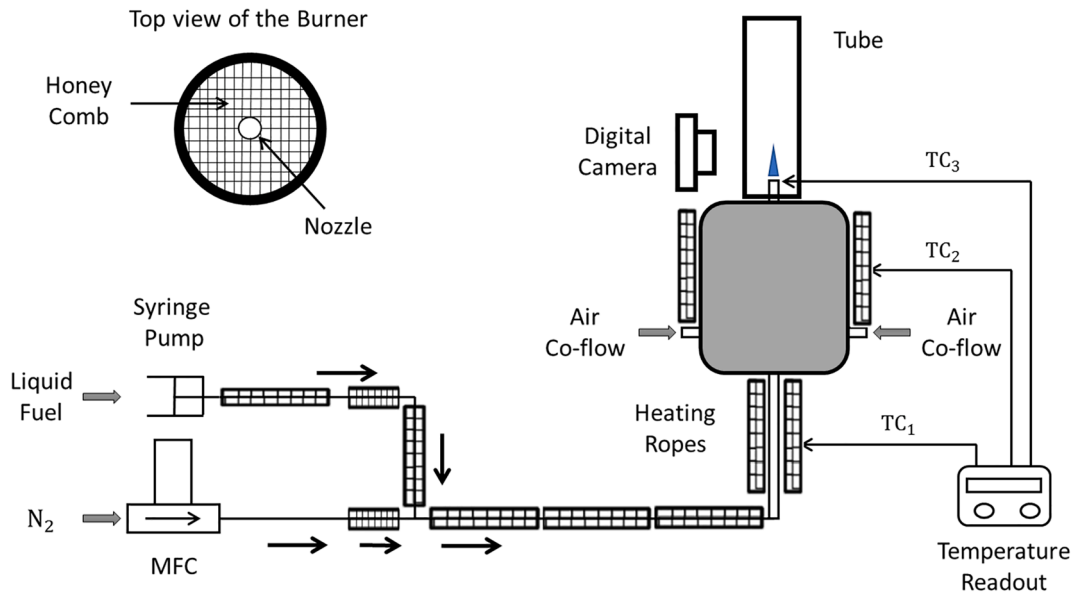


Fig. 1. Schematic diagram of the experimental setup.

Table 1

Diesel and Palm methyl esters (PME) properties.

	Diesel	PME
Density at 25 °C [kg/m ³]	820	872
Kinematic viscosity at 40 °C [mm ² /s]	3.05	4.1
Flash point [°C]	79	101
Boiling point [°C]	> 180	> 210
Cetane number [-]	49	51
Molecular weight [g/mol]	190	281
High heating value [MJ/kg]	46.2	39.9

Table 2

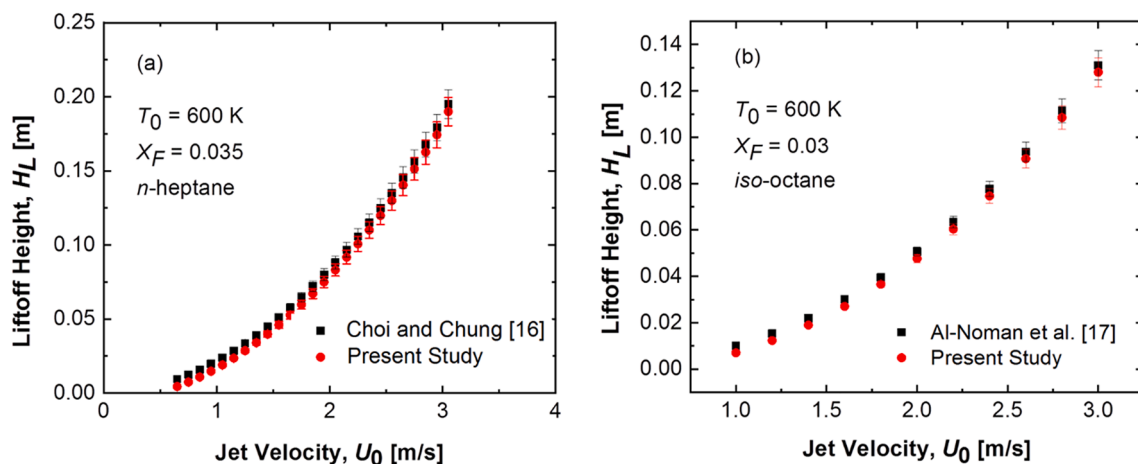
Compositions of fatty acids in palm methyl esters (PME).

Fatty acid	No. of carbon: double bond	Composition (% wt)
Palmitic	(C16:0)	47.50
Oleic	(C18:1)	39.55
Linoleic	(C18:2)	8.42
Stearic	(C18:0)	4.53

of the present experimental setup. The same conditions were applied, such as the non-autoignited regime and the molar fraction of the fuel, which was kept in the range of 0.02–0.04. Fig. 2(a) and (b) show the direct comparison between the results from this study and the literature. It can be seen that the results are in good agreement both value-wise as well as trend-wise. Thus, it can be concluded that the current experimental setup is acceptable to produce adequate results.

3.2. Stabilization of non-premixed laminar lifted flames

The characteristics of laminar lifted flame are influenced by multiple parameters such as the unburnt gas temperature, T_0 , fuel mole fraction in the mixture, X_F , as well as the jet flow velocity, U_0 [22]. Fig. 3 displays direct photographs of the typical laminar diffusion lifted flames of biodiesel. Fig. 3(a) shows the effect of increasing U_0 on the liftoff height of the flames and Fig. 3(b) illustrates the behavior of the lifted flames for $U_0 = 0.7$ m/s and $X_F = 0.02$ at different unburnt gas temperatures. As can be observed from the direct images, the liftoff height increased with the increasing jet flow velocity (Fig. 3(a)). On the contrary, elevation in the unburnt gas temperature led to a reduced liftoff height per given fuel mole fraction (Fig. 3(b)). While the edges of the lifted flames were not shown in detail to represent the tribrachial structure, Al-Noman et al.

Fig. 2. Comparison of the liftoff heights with literature values for (a) *n*-heptane, (b) *iso*-octane.

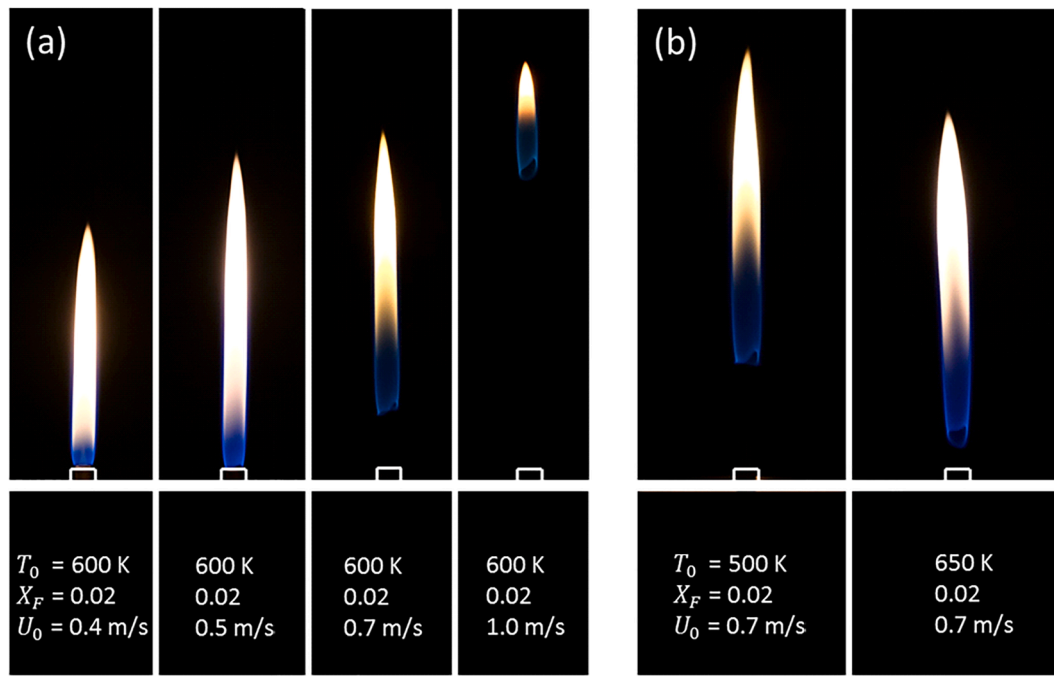


Fig. 3. Visible images of the laminar diffusion flames of biodiesel.

[19] showed that the tribrachial edge was associated with lifted flame even when it was not clearly visible from the direct photography. Furthermore, the existence of the tribrachial structure at the edges of lifted flames was shown for both gaseous fuels [20] and liquid fuels [16,17]. This means that the lifted flames have the triple structure where the point of lean and rich premixed flame wings is connected and trailed by a diffusion flame [18]. It should be noted that the edges of the flames remained to have a tribrachial structure regardless of changes in T_0 , X_F , and U_0 .

To further study the behavior of the lifted flames, lifted height as a function of jet fuel velocity at $T_0 = 500$ K and $X_F = 0.02$ are plotted in Fig. 4(a). It can be observed that the flame was initially established and attached to the nozzle rim at relatively low jet flow velocity ($U_0 \leq 0.35$ m/s). As the jet flow velocity increased, the laminar non-premixed flames lifted off from the nozzle rim and stabilized at a specific height. It was followed by a non-linear increment in the liftoff height of the flame until it reached a critical jet flow velocity where the blowout took place. The non-linear progression, shown in Fig. 4(a), can be expressed in terms of a power law with the correlation coefficient of 0.98:

$$H_L = 0.1495 \times U_0^{2.842} \quad (1)$$

As the unburnt gas temperature increases, the heat transfer between the nozzle rim and the lifted flame enhances [23,26]. This led to a reduced liftoff height of the flames due to the elevated unburnt gas temperatures, which can be seen in Fig. 4(b). At the given fuel mole fraction of $X_F = 0.02$ and jet flow velocity of $U_0 = 0.6$ m/s, the flame experienced the liftoff height of 0.036 m at $T_0 = 500$ K and blowout at a slightly lower temperature. In contrast, the flame at the same fuel mole fraction and jet flow velocity is fully attached to the nozzle at the temperature of 650 K.

Based on the obtained results, it was expected that the lifted flames could be achieved in a limited domain in terms of the fuel mole fraction and the unburnt gas temperature, as shown in Fig. 5. The blue lines represent the lower limit of the domain. When the fuel mole fraction in the mixture was below the blue lines at a given temperature, the flame could not be stabilized due to the high dilution ratio of the inert gas (N_2). On the contrary, the red lines represent the upper limit of the domain. When the fuel mole fraction in the mixture was above the red lines at

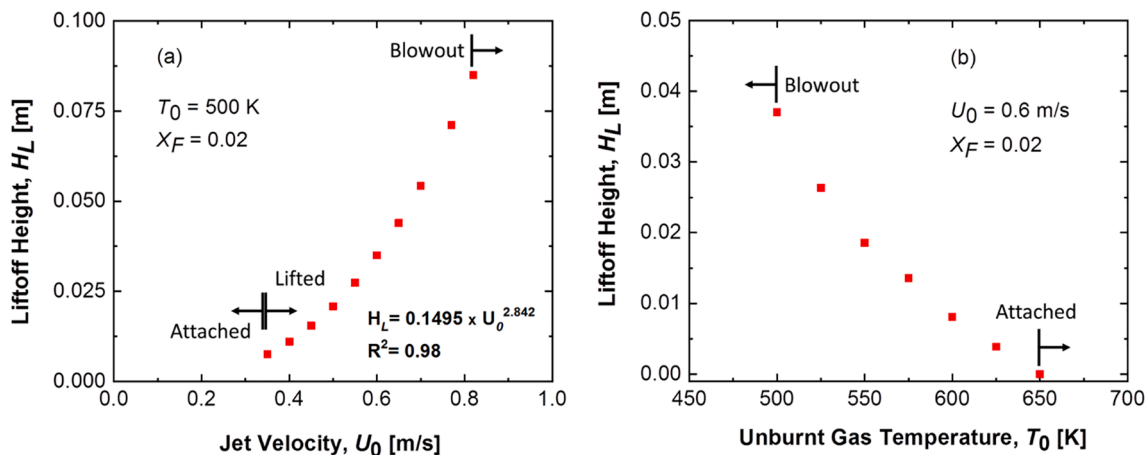


Fig. 4. Liftoff heights for various (a) jet flow velocities at $T_0 = 500$ K and $X_F = 0.02$, (b) unburnt gas temperatures at $U_0 = 0.6$ m/s and $X_F = 0.02$.

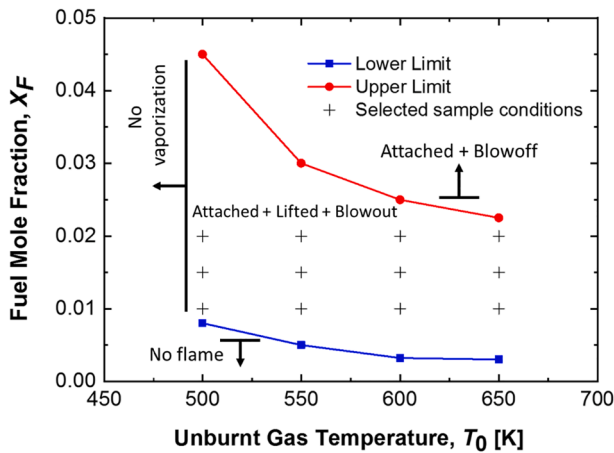


Fig. 5. The domain of existence of the lifted flames.

given temperature, the stable flame could be established on the nozzle rim at low jet flow velocities. However, as the jet flow velocity increased and reached a critical value, the flame blew off without having a liftoff effect. In this study, experiments were conducted at the unburnt gas conditions represented with “+” sign, as shown in Fig. 5. The results showed that the flames, with the conditions within the domain, experienced all three stages of the flame development. The laminar non-premixed flames were established on the nozzle rim at the sufficiently low jet flow velocity, followed by the liftoff due to the increasing jet flow velocity and experienced the blowout once the velocity reached a critical value. It was noted that 483 K is the lowest set temperature at the nozzle exit to achieve the complete vaporization. Below this temperature, the experiments could not be conducted as the fuel could not be vaporized completely.

3.3. Effect of elevated unburnt gas temperatures

As mentioned earlier, the liftoff height of the flames can be influenced by multiple parameters such as the unburnt gas temperature, the fuel mole fraction in the mixture as well as the jet flow velocity. Fig. 6 shows the liftoff height as a function of jet flow velocity for varying fuel mole fraction as well as unburnt gas temperature. In order to highlight the fairly linear correlation between the liftoff heights and the jet flow velocities, at different temperatures and fuel mole fractions, a log–log scale was used. However, it was observed that the linear relation between the liftoff heights and the jet flow velocities weakened with an increase in unburnt gas temperature. On the other hand, higher unburnt

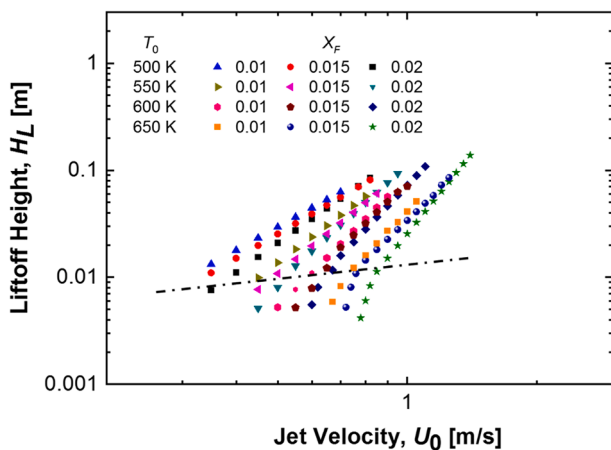


Fig. 6. Liftoff height as a function of jet flow velocity for various unburnt gas temperatures and fuel mole fractions.

gas temperatures resulted in a steeper slope of the data, regardless of the fuel mole fraction in the mixture. Furthermore, the linear trend seems to deteriorate only at relatively low liftoff height, which are illustrated by the points below the dashed-dotted line in Fig. 6. This behavior can be explained based on the observation made by Won et al. [27]. They have found that the lifted flames could be stabilized in either developing or developed regions of the jet, which were corresponding to the areas near the nozzle and further away from the nozzle rim, respectively. Won et al. [27] suggested that the length of the developing region is approximated by cold jet theory, where centerline velocity U_{CL} must be smaller than U_{max} , with U_{max} the maximum jet flow velocity ($U_{max} = 2U_0$).

$$U_{CL} = \frac{U_0^2 d^2}{8\nu x} \quad (2)$$

where d is the inner diameter of the nozzle, ν is the kinematic viscosity of the unburnt gas, and x is the axial distance. Since the fuel mole fraction was notably smaller than the mole fraction of the carrier gas, the kinematic viscosity of N_2 was adopted to calculate the centerline velocity. Furthermore, the temperature influences the kinematic viscosity of the gas, hence, the length of the developing region is appreciably influenced by temperature. The changes in slope and non-linearity within the developing region were demonstrated by the dashed-dotted line, which was the locus of cross-points of the experimental results. This behavior is in good agreement with the findings related to the lifted flames of the pre-vaporized *n*-heptane [16] and *iso*-octane [17] but disagrees with the pure gaseous fuels [20,22]. One of the most significant differences between these studies is that pre-vaporized liquid fuels were prepared with a much higher dilution ratio of N_2 as they required a carrier gas, unlike pure gaseous fuels. Thus, to explain the significance of the dilution ratio in gaseous fuels, Van et al. [21] experimentally studied the laminar lifted nitrogen-diluted methane jet flames. Their results showed that, within the developing region of the jet, the highly diluted gaseous flames experienced the non-linear behavior between H_L and U_0 , which agreed with the behavior observed in the present study.

The stabilized lifted flame, having a tribrachial structure, is associated with the balance mechanism between the local flow velocity along the contour of stoichiometry and the burning velocity of the tribrachial flame. The existence of the tribrachial structure in lifted flames implies that there is a relation between the tribrachial edge propagation speed and its associated stoichiometric laminar burning velocity of the given mixture [18]. As such, it can be assumed that the liftoff velocity and, subsequently, liftoff height can be related and dependent on the stoichiometric laminar burning velocity. Hence, all the obtained data were replotted in Fig. 7 to further emphasize the role of the stoichiometric laminar burning velocity, S_{st}^0 . The results showed that the liftoff height is

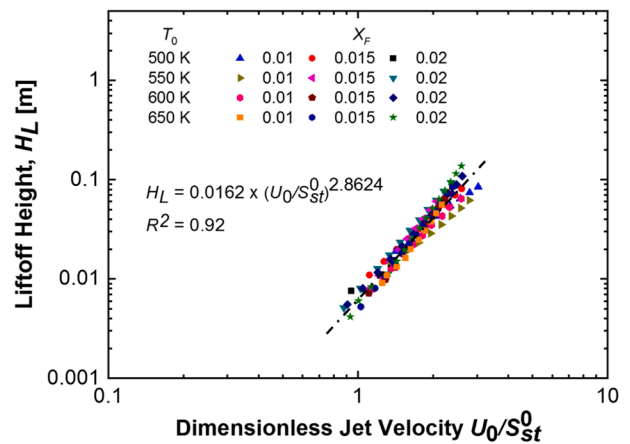


Fig. 7. Liftoff height as a function of jet flow velocity scaled by the stoichiometric laminar burning velocity for various unburnt gas temperatures and fuel mole fractions.

significantly influenced by the stoichiometric laminar burning velocity, regardless of the fuel mole fraction and the unburnt gas temperature. It is noted that the stoichiometric laminar burning velocity of the flame, per given mixture, was obtained via the PREMIX code in Chemkin using the kinetic mechanism developed by Kuti et al. [28]. The compositions of the palm oil biodiesel were used in accordance with the values in Table 2. The overall correlation between the liftoff height and dimensionless jet flow velocity, U_0/S_{st}^0 , was successfully established with the correlation coefficient of 0.92. Hence, the changes in the slopes of H_L versus U_0 between developing or developed regions in Fig. 6 were attributed to the varying of the unburnt gas temperature as well as the fuel mole fraction in the mixture. This is due to the differential diffusion between the fuel and carrier gas, which directly affects the fuel mole fraction in the stoichiometric region of the flame [22]. As a result, the stoichiometric laminar burning velocity is changed, thereby influencing the burning velocity of the tribrachial flame.

3.4. Jet flow velocity of the lifted flames

From Fig. 4(a), it can be seen that the flame initially attached to the nozzle rim at relatively low jet flow velocity. Once it reached a certain velocity, the flame abruptly experienced liftoff. This velocity is known to be the liftoff velocity, U_{LO} . In Fig. 8, liftoff velocities of biodiesel flame were plotted as a function of stoichiometric laminar burning velocity, together with the liftoff condition shown as the dashed line. Ko and Chung [29] and Lee et al. [30] explained that, for the liftoff to take place, the jet flow velocity must be higher than the stoichiometric laminar burning velocity of the mixture. Hence, the flames that experience $U_{LO} < S_{st}^0$, theoretically, could not be lifted. However, as can be seen from Fig. 8, there are some discrepancies for the previously mentioned statement. This contradiction can be associated with the buoyancy effect [31].

Based on the general structure of the non-premixed laminar lifted flames, it can be understood that there are temperature and density differences between the unburnt and burnt gases. As a result, the flame can experience a driving force of buoyancy, known as a buoyant force. This force has the highest impact near the nozzle rim, where it leads to an increase in flow velocity as it causes the entrainment of the flow of the mixture, thereby leading to the buoyancy-induced velocity of the flame, U_B . Therefore, considering the presence of buoyancy, the overall local flow velocity becomes higher, resulting in $U_{LO}^* = U_{LO} + U_B$. Thus, the condition for the existence of lifted flames ($U_{LO}^* > S_{st}^0$), can be fully satisfied.

Bédard and Cheng [31] showed the effect of the buoyancy on the premixed flame stabilization. Based on their work, the impact of

buoyancy on the flow rate of the mixture was approximated using the following expression:

$$U_B = \sqrt{(\Delta\rho/\rho_u)gd} \quad (3)$$

with the density difference between the unburnt and burnt gases $\Delta\rho = \rho_u - \rho_b$, densities of the unburnt gas ρ_u and burnt gas ρ_b , gravitational acceleration, and the inner diameter of the nozzle d . Hence, Fig. 9 was plotted by including the effect of buoyancy-induced velocity to the liftoff velocity, $(U_{LO}U_B)^{1/2}$. This graph shows that the scaled expression of $(U_{LO}U_B)^{1/2}$ is a good indicator in demonstrating the significance of the buoyancy effect on the lifted flames, with the correlation coefficient of 0.97. This implies, together with the observations from Fig. 8, that the buoyancy effect reduced the liftoff velocity of the flame. Lastly, it is essential to note that the expression used for the approximation of the buoyancy, $\sqrt{(\Delta\rho/\rho_u)gd}$, is sensitive to the change in unburnt gas temperature. Hence, with the increasing unburnt gas temperature, the flow entrainment at the nozzle rim caused by the buoyancy is mitigated, as shown in Fig. 8.

3.5. Biodiesel/diesel blends

Fig. 10 displays direct photographs of laminar diffusion lifted flames of pure biodiesel (B100), pure diesel (D100) and their blends at the same unburnt gas temperature of 550 K, fuel mole fraction of 0.02 and jet flow velocity of 0.9 m/s. It can be seen that the liftoff height decreased with the increasing concentration of diesel in the fuel blend. Hence, the pure diesel flame stabilized at lower liftoff height as compared to pure biodiesel flame at the same conditions. This phenomenon is attributed to the difference in the laminar burning velocity that plays an essential role in flame stabilization. It is noted that the stoichiometric laminar burning velocities of biodiesel and diesel at atmospheric pressure and unburnt gas temperature of 550 K were measured to be 103 cm/s and 112 cm/s respectively.

Fig. 11 illustrates the liftoff height as a function of jet flow velocity at $T_0 = 550$ K and $X_F = 0.02$ for diffusion flames of B100, D100 and their blends. It can be seen that the liftoff heights of the D100 and biodiesel/diesel diffusion flames increased nonlinearly with jet flow velocity which are similar to the trend of B100 lifted flame. Also, it can be observed that D100 flame was able to stabilize at much higher jet flow velocity compared to B100 flame, indicating a stronger stabilization mechanism of diesel fuel. Since we focused on the characteristics of biodiesel lifted flame in the present study, a detailed explanation of the stabilization mechanism of diesel lifted flame should be addressed in a future study, where in-depth experimental and numerical investigations

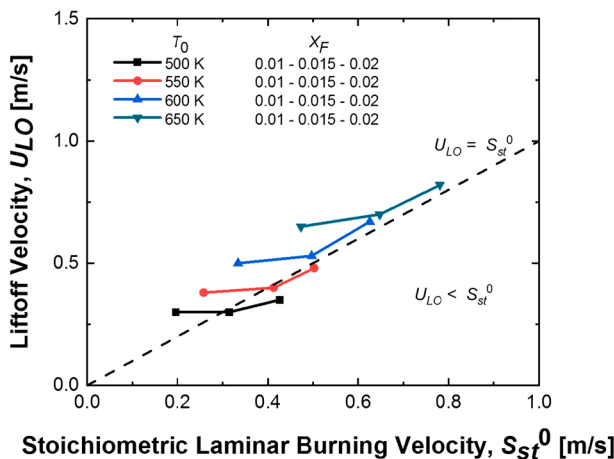


Fig. 8. Liftoff velocity as a function of the stoichiometric laminar burning velocity for various unburnt gas temperatures and fuel mole fractions.

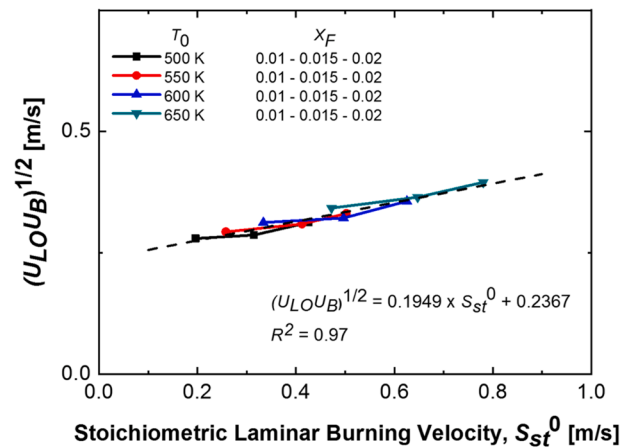


Fig. 9. Effect of the buoyancy-induced velocity on the liftoff with respect to stoichiometric laminar burning velocity for various unburnt gas temperatures and fuel mole fractions.

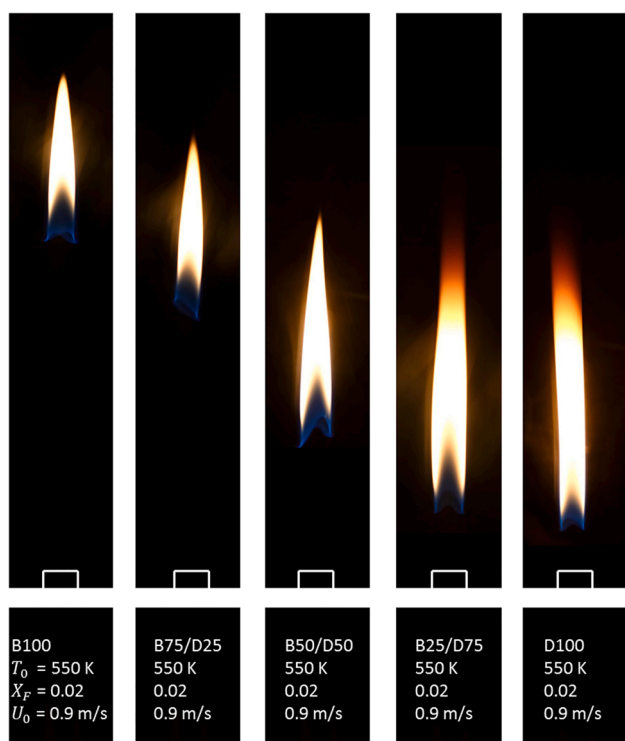


Fig. 10. Visible images of the laminar diffusion flames of various biodiesel/diesel blends. B100 represents pure biodiesel, D100 represents pure diesel, B50/D50 represents 50% biodiesel/50% diesel blend.

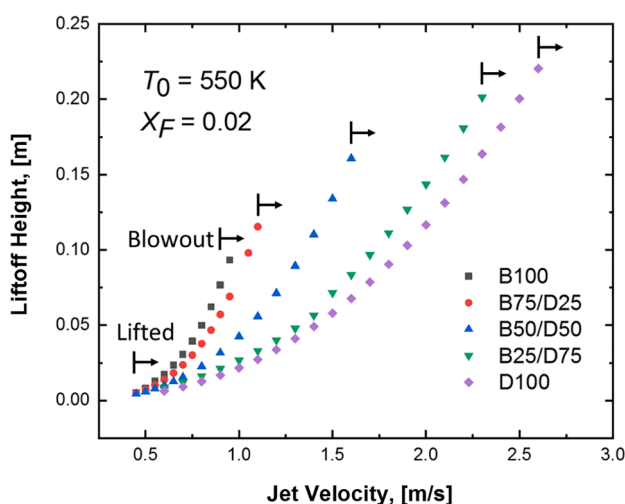


Fig. 11. Lift-off height as a function of jet flow velocity for various biodiesel/diesel blends at $T_0 = 550$ K and $X_F = 0.02$.

are required.

4. Concluding remarks

In the present study, the lift-off characteristics of palm oil biodiesel were studied by varying the jet flow velocity per given fuel mole fraction and unburnt gas temperature. The fuel mole fraction and unburnt gas temperature ranges were 0.01 – 0.02 and 500 K – 650 K, respectively. The fuel was pre-vaporized and mixed with pre-heated nitrogen which was used as the carrier gas. The major conclusions of the study are as follows:

1. The lift-off height increased with the higher jet flow velocity. The unburnt gas temperature and the fuel mole fraction had a similar effect on the lifted flames, because the increase in either of those parameters enhanced the heat transfer mechanism between the flame base and the nozzle rim, which resulted in lower lift-off heights. Based on these observations, the limited range of the conditions where the lifted flames occurred had been obtained per given unburnt gas temperature and fuel mole fraction.
2. The existence of the tribrachial structure implies the balance between the stoichiometric laminar burning velocity and local jet flow velocity. Thus, the dimensionless jet flow velocity, U_0/S_{st}^0 , was calculated to illustrate its correlation with the lift-off height of the flames. Furthermore, the changes in the slope and non-linear relationship between the lift-off height and the jet flow velocity were attributed to the nature of the developing region of the jet.
3. For the lift-off to take place, the jet flow velocity must be higher than the stoichiometric laminar burning velocity of the given mixture. It was noted that there were few cases where this criterion was not fulfilled, and this behavior was associated with the buoyancy effect on the flames. Hence, buoyancy-induced velocity was calculated and its correlation with the stoichiometric laminar burning velocity was obtained.
4. The lift-off height decreased with the increasing concentration of diesel in the fuel blend. Hence, B100 flame stabilized at higher lift-off height as compared to D100 flame due to the lower laminar burning velocity of biodiesel flame. Similar to the B100 lifted flame, the lift-off heights of the D100 and biodiesel/diesel diffusion flames increased nonlinearly with jet flow velocity.

CRediT authorship contribution statement

Dastan Nurmukan: Investigation, Writing - original draft. **Manh-Vu Tran:** Supervision, Conceptualization, Writing - review & editing. **Ji Jinn Foo:** Conceptualization, Writing - review & editing. **Gianfranco Scribano:** Conceptualization, Writing - review & editing. **Cheng Tung Chong:** Conceptualization, Writing - review & editing. **Thanh Cong Huynh:** Conceptualization, Writing - review & editing.

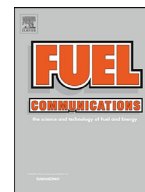
Declaration of Competing Interest

The authors declare that they have no known competing financial interests or personal relationships that could have appeared to influence the work reported in this paper.

References

- [1] Mohd Noor CW, Noor MM, Mamat R. Biodiesel as alternative fuel for marine diesel engine applications: A review. *Renew Sustain Energy Rev* 2018;94:127–42. <https://doi.org/10.1016/j.rser.2018.05.031>.
- [2] Unglert M, Bockey D, Bofinger C, Buchholz B, Fisch G, Luther R, Müller M, Schaper K, Schmitt J, Schröder O, Schumann U, Tschöke H, Remmele E, Wicht R, Winkler M, Krahel J. Action areas and the need for research in biofuels. *Fuel* 2020; 268:117227. <https://doi.org/10.1016/j.fuel.2020.117227>.
- [3] Adeniyi OM, Azimov U, Burluka A. Algae biofuel: Current status and future applications. *Renew Sustain Energy Rev* 2018;90:316–35. <https://doi.org/10.1016/j.rser.2018.03.067>.
- [4] Najafi G. Diesel engine combustion characteristics using nano-particles in biodiesel-diesel blends. *Fuel* 2018;212:668–78. <https://doi.org/10.1016/j.fuel.2017.10.001>.
- [5] Elkelay M, Alm-Eldin Bastawissi H, Esmaili KK, Radwan AM, Panchal H, Sadasivuni KK, Ponnammam D, Walvekar R. Experimental studies on the biodiesel production parameters optimization of sunflower and soybean oil mixture and DI engine combustion, performance, and emission analysis fueled with diesel/biodiesel blends. *Fuel* 2019;255:115791. <https://doi.org/10.1016/j.fuel.2019.115791>.
- [6] Singh D, Sharma D, Soni SL, Sharma S, Kumari D. Chemical compositions, properties, and standards for different generation biodiesels: A review. *Fuel* 2019; 253:60–71. <https://doi.org/10.1016/j.fuel.2019.04.174>.
- [7] Raman LA, Deepanraj B, Rajakumar S, Sivasubramanian V. Experimental investigation on performance, combustion and emission analysis of a direct injection diesel engine fuelled with rapeseed oil biodiesel. *Fuel* 2019;246:69–74. <https://doi.org/10.1016/j.fuel.2019.02.106>.

- [8] Wang R, Zhou W-W, Hanna MA, Zhang Y-P, Bhadury PS, Wang Y, Song B-A, Yang S. Biodiesel preparation, optimization, and fuel properties from non-edible feedstock, *Datura stramonium* L. Fuel 2012;91(1):182–6. <https://doi.org/10.1016/j.fuel.2011.07.001>.
- [9] Chong CT, Chiong M-C, Teyo ZY, Ng J-H, Chong WWF, Tran M-V, Lam SS, Valera-Medina A. Pool Fire Burning Characteristics of Biodiesel. Fire Technol 2020;56(4):1703–24. <https://doi.org/10.1007/s10694-020-00949-3>.
- [10] Moser BR. Influence of Blending Canola, Palm, Soybean, and Sunflower Oil Methyl Esters on Fuel Properties of Biodiesel †. Energy Fuels 2008;22(6):4301–6. <https://doi.org/10.1021/ef800588x>.
- [11] Temizer İ, Cihan Ö, Eskici B. Numerical and experimental investigation of the effect of biodiesel/diesel fuel on combustion characteristics in CI engine. Fuel 2020;270:117523. <https://doi.org/10.1016/j.fuel.2020.117523>.
- [12] Ge JC, Kim HY, Yoon SK, Choi NJ. Optimization of palm oil biodiesel blends and engine operating parameters to improve performance and PM morphology in a common rail direct injection diesel engine. Fuel 2020;260:116326. <https://doi.org/10.1016/j.fuel.2019.116326>.
- [13] Wu Y. Handbook of Combustion. Weinheim: Wiley-VCH Verlag GmbH & Co. KGaA, cop. 2010. pp. 121–139.
- [14] Quattrocchi S, Aggarwal SK, Katta VR. Liftoff and blowout characteristics of laminar syngas nonpremixed flames. Int J Hydrogen Energy 2018;43(12):6421–33. <https://doi.org/10.1016/j.ijhydene.2018.01.194>.
- [15] Chan SMS, Torii S, Yano T. Enhancement of turbulent jet diffusion flame blowout limits by annular counterflow. Int. J. Energy Res. 2001;25(12):1091–105. <https://doi.org/10.1002/er.742>.
- [16] Choi SK, Chung SH. Autoignited and non-autoignited lifted flames of pre-vaporized n-heptane in coflow jets at elevated temperatures. Combust Flame 2013;160(9):1717–24. <https://doi.org/10.1016/j.combustflame.2013.03.028>.
- [17] Al-Noman SM, Choi SK, Chung SH. Autoignition characteristics of laminar lifted jet flames of pre-vaporized iso -octane in heated coflow air. Fuel 2015;162:171–8. <https://doi.org/10.1016/j.fuel.2015.09.006>.
- [18] Chung SH. Stabilization, propagation and instability of tribrachial triple flames. Proc Combust Inst 2007;31(1):877–92. <https://doi.org/10.1016/j.proci.2006.08.117>.
- [19] Al-Noman SM, Choi BC, Chung SH. Autoignited lifted flames of dimethyl ether in heated coflow air. Combust Flame 2018;195:75–83. <https://doi.org/10.1016/j.combustflame.2018.04.020>.
- [20] Choi BC, Chung SH. Autoignited laminar lifted flames of methane, ethylene, ethane, and n-butane jets in coflow air with elevated temperature. Combust Flame 2010;157(12):2348–56. <https://doi.org/10.1016/j.combustflame.2010.06.011>.
- [21] Van K, Jung KS, Yoo CS, Oh S, Lee BJ, Cha MS, Park J, Chung SH. Decreasing liftoff height behavior in diluted laminar lifted methane jet flames. Proc Combust Inst 2019;37(2):2005–12. <https://doi.org/10.1016/j.proci.2018.05.031>.
- [22] Kim KN, Won SH, Chung SH. Characteristics of laminar lifted flames in coflow jets with initial temperature variation. Proc Combust Inst 2007;31(1):947–54. <https://doi.org/10.1016/j.proci.2006.08.012>.
- [23] Nurmukan D, Chen TJM, Hung YM, Ismadi M-Z, Chong CT, Tran M-V. Enhancement of biogas/air combustion by hydrogen addition at elevated temperatures. Int J Energy Res 2020;44(3):1519–34. <https://doi.org/10.1002/er.4912>.
- [24] Maulidiyah, Nurdin M, Fatma F, Natsir M, Wibowo D. Characterization of methyl ester compound of biodiesel from industrial liquid waste of crude palm oil processing. Anal Chem Res 2017;12:1–9. <https://doi.org/10.1016/j.ancr.2017.01.002>.
- [25] El-Araby R, Amin A, El Morsi AK, El-Ibiari NN, El-Diwani GI. Study on the characteristics of palm oil–biodiesel–diesel fuel blend. Egypt J Pet 2018;27(2):187–94. <https://doi.org/10.1016/j.ejpe.2017.03.002>.
- [26] Alekseev VA, Matveev SS, Chechet IV, Matveev SG, Konnov AA. Laminar burning velocities of methylcyclohexane + air flames at room and elevated temperatures: A comparative study. Combust Flame 2018;196:99–107.
- [27] Won SH, Chung SH, Cha MS, Lee BJ. Lifted flame stabilization in developing and developed regions of coflow jets for highly diluted propane. Proc Combust Inst 2000;28(2):2093–9. [https://doi.org/10.1016/S0082-0784\(00\)80618-9](https://doi.org/10.1016/S0082-0784(00)80618-9).
- [28] Kuti O, Sarathy M, Nishida K, Roberts W. Numerical studies of spray combustion processes of palm oil biodiesel and diesel fuels using reduced chemical kinetic mechanisms. SAE Technical Paper 2014-01-1143.
- [29] Ko YS, Chung SH. Propagation of unsteady tribrachial flames in laminar non-premixed jets. Combust Flame 1999;118(1-2):151–63. [https://doi.org/10.1016/S0010-2180\(98\)00154-0](https://doi.org/10.1016/S0010-2180(98)00154-0).
- [30] Lee J, Won SH, Jin SH, Chung SH, Fujita O, Ito K. Propagation speed of tribrachial (triple) flame of propane in laminar jets under normal and micro gravity conditions. Combust Flame 2003;134(4):411–20. [https://doi.org/10.1016/S0010-2180\(03\)00115-9](https://doi.org/10.1016/S0010-2180(03)00115-9).
- [31] Bédard B, Cheng RK. Effects of buoyancy on premixed flame stabilization. Combust Flame 1996;107:13–26.



Effect of multi-walled carbon nanotubes on pre-vaporized palm oil biodiesel/air premixed flames

Dastan Nurmukan^a, Manh-Vu Tran^{a,*}, Yew Mun Hung^a, Gianfranco Scribano^b,
Cheng Tung Chong^c

^a School of Engineering, Monash University Malaysia, Jalan Lagoon Selatan, 47500 Bandar Sunway, Selangor, Malaysia

^b Department of Mechanical, Materials and Manufacturing Engineering, The University of Nottingham Malaysia Campus, Jalan Broga, 43500, Semenyih, Selangor, Malaysia

^c China-UK Low Carbon College, Shanghai Jiao Tong University, Lingang, Shanghai 201306, China

ARTICLE INFO

Article history:

Received 22 November 2020

Revised 10 April 2021

Accepted 16 April 2021

Keywords:

Biodiesel

Blowoff

Multi-walled carbon nanotubes

Laminar burning velocity

Nitrogen oxides (NO_x) and carbon monoxide (CO)

ABSTRACT

In regard to the current state of global energy, the high demand for traditional fossil fuels and their negative environmental impact have led to an increase of interest in the development of renewable clean fuels. Recently, nano-additives such as carbon nanotubes (CNTs) have been considered as a potential additive to increase fuel combustion performance. Thus, we experimentally studied the combustion characteristics of multi-walled carbon nanotubes (MWCNTs) blended palm-oil biodiesel/air mixtures at a wide range of equivalence ratios, 0.7–1.6. Experiments were conducted at atmospheric pressure and a temperature of 550 K to ensure full vaporization of the liquid biodiesel fuel. Concentrations of the MWCNTs in the mixture were varied from 25 to 200 ppm for two different groups of nanotubes having outer diameter ranges of 10–20 nm and 30–50 nm. The results showed that both laminar burning velocity and blowoff velocity were increased with the additions of MWCNTs. Besides, the flammability limits of MWCNTs blended biodiesel/air premixed flames were also extended at both fuel-lean and fuel-rich conditions. It was also observed that the MWCNTs of 10–20 nm experienced more noticeable improvements in the combustion characteristics compared to the MWCNTs of 30–50 nm. After reaching the highest enhancement, a further increase in the concentration of MWCNTs generally caused less improvement in the laminar burning velocities of the premixed flames. Besides, the addition of MWCNTs increased nitrogen oxides and decreased carbon monoxide concentrations in the combustion products.

© 2021 The Authors. Published by Elsevier Ltd.

This is an open access article under the CC BY-NC-ND license (<http://creativecommons.org/licenses/by-nc-nd/4.0/>)

1. Introduction

The primary use of traditional fossil fuels in agriculture, manufacturing as well as transportation applications has led to the apparent concerns of fuel supply capacity. Furthermore, the combustion of fossil fuels produces a large amount of greenhouse, which, in turn, directly influences the rate of climate change [1]. Thus, there is a demand for developing alternative fuels that can replace or supplement the existing hydrocarbon-based fuels. One of the ways to reduce emission production is to employ cleaner combustion. In this regard, the studies [2,3] showed that biodiesel fuels can be considered as one of the most promising renewable and sustainable solutions. Biodiesel fuels can be obtained from a vari-

ety of feedstock sources such as vegetable oils (palm, soybean, and canola) and animal fats via the transesterification process [4].

Fuel enrichment is one of the most widely accepted methods of altering the fuel combustion properties in order to improve the performance characteristics of engines without modification in design. Over the past decade, there has been an increasing interest in the application of various nano-particles as an additive to biodiesel fuels [5–14]. These studies showed that nano-additives could, in fact, enhance combustion parameters, reduce fuel consumption, and lower the production of harmful exhaust emissions. It is essential to note that there are different classes of nano-additives such as metal-based, metal oxide-based, magnetic nano-fluids, nano-organic additives, carbon-based, as well as mixed nano-particles [6,8]. Sivakumar et al. [5] and Venu and Madhavan [9] showed a reduction in the break specific fuel consumption (BSFC), improvement in the brake thermal efficiency, and reduced concentrations

* Corresponding author.

E-mail address: manhvu.tran@monash.edu (M.-V. Tran).

of oxides of nitrogen (NO_x), unburnt hydrocarbon (UHC), and carbon monoxide (CO) productions with the addition of aluminum oxide (Al_2O_3) to the fuel. It was also reported that similar behavior was observed by Sajith et al. [10] and Vairamuthu et al. [11] when cerium oxide (CeO_2) nano-particles were used as a fuel additive. Manigandan et al. [7] and Chen et al. [12] conducted comparative studies between various nano-additives and, in contrast, showed that carbon nanotubes (CNTs) could provide a different effect as compared to other nano-particles due to their properties such as free metal compound nature, higher energy density, and higher thermal conductivity. By experiments with diesel fuel, Chen et al. [12] revealed that the addition of CNTs led to a reduction of NO_x concentration and an increase in UHC, CO, and CO_2 emissions at 0, 50%, and 75% engine loads. However, it was observed that the presence of CNTs resulted in insignificant differences in NO_x production at the engine load of 25%. Furthermore, at 100% engine load, the increase in CNTs resulted in the opposite effect, where the production of CO emissions was reduced. In addition, Ghanbari et al. [13] experimentally showed that the engine's brake power and torque were increased while decreasing the BSFC at any load, with the addition of CNTs to the fuel. Najafi [14] conducted an experiment to analyze the changes in the combustion behavior of CNTs blended diesel and biodiesel mixtures. The results revealed that CNTs blended fuels experienced a shorter ignition delay, lower pressure in the cylinder, and faster heat release rate. These findings were attributed to the catalytic nature of CNTs, which acted as an agent accelerating fuel combustion reaction. While the studies mentioned above claim the benefits of nano-additives on the combustion of fuels, it is apparent to conclude that all the experiments were conducted to merely assess the performance of engines rather than the fundamental combustion characteristics of CNTs added fuels, creating the knowledge gap in this research area.

Laminar burning velocity and blowoff velocity are amongst the main fundamental combustion characteristics of fuels. These parameters are essential in understanding the fuel behavior in various practical applications and as data in the development of kinetic mechanisms. As such, many studies have been conducted to measure the laminar burning velocity of gaseous fuels over a wide range of equivalence ratios, ϕ , at different pressures [15] and temperatures [16], using various methodologies [17]. However, regarding liquid fuels, the vast majority of the existing literature is focused on single component hydrocarbon fuels [18–24]. Even though the existing literature has shown an increasing interest in biodiesel fuels, there are limited data, both experimental and numerical, on the fundamental combustion characteristics such as laminar burning velocity. The lack of such data can be attributed to the complexity of the fuel structure and variability of the composition, depending on the feedstock sources. In the case of laminar premixed flame, blowoff velocity is another important parameter from which the critical burning limits of a given fuel can be analyzed. Furthermore, knowing the limits of flame stability is crucial in preventing potential system failures due to re-ignition behavior in applications such as low emission gas turbines.

Although the potential benefits of carbon-based nano-additives have drawn a lot of attention, it can be noticed that the current knowledge is mainly limited to compression ignition engine applications. In addition to that, data on the fundamental combustion characteristics of palm oil biodiesel flames, such as laminar burning velocity and blowoff velocity, are still scarce. In this regard, the present study focused on investigating the fundamental combustion characteristics of pre-vaporized palm oil biodiesel premixed flames with and without the addition of multi-walled carbon nanotubes, MWCNTs. The present study results could provide an adequate set of data on MWCNTs blended palm oil biodiesel and pure palm oil biodiesel, which can be

Table 1

Palm methyl esters (PME) properties.

Properties	Value
Density at 25 °C [kg/m^3]	872
Kinematic viscosity at 40 °C [mm^2/s]	4.1
Flash point [°C]	101
Boiling point [°C]	> 210
Cetane number [-]	51
Molecular weight [g/mol]	281
High heating value [MJ/kg]	39.9

Table 2

Compositions of fatty acids in palm methyl esters (PME).

Fatty acid	No. of carbon: double bond	Composition (% wt.)
Palmitic	(C16:0)	47.50
Oleic	(C18:1)	39.55
Linoleic	(C18:2)	8.42
Stearic	(C18:0)	4.53

useful for practical applications and the development of kinetic mechanisms.

2. Experiment

2.1. Experimental setup

A detailed schematic of the present setup is illustrated in Fig. 1. The overall system consisted of a coflow burner, a syringe pump (NE-300) that delivered the liquid fuel to a stainless steel supply line wrapped with heating ropes (Omega, FGR-060). The temperature of the heating ropes was controlled by a variable autotransformer variac and measured via thermocouples, TC_{1-3} (Omega, SA3-K-72), at multiple locations to ensure the desired temperature. The temperatures measured by TC_{1-3} were displayed by a temperature readout unit (midi Logger GLB20). The setup also included two mass flow controllers (MKS, 1179 A) and a readout controller (MKS, 247D 4 channel) to deliver the air and nitrogen, N_2 coflow to the system. The mass flow controllers were calibrated using a dry-test gas meter (Bios, Definer 220 M) to improve the accuracy of the experiment. The central nozzle of the coflow burner was made of a stainless steel tube with an inner diameter of 7.55 mm and a thickness of 1 mm. The length of this tube was set to be over 500 mm in order to achieve a fully parabolic velocity profile at the nozzle rim [16]. Since the boiling temperature of the palm oil biodiesel is 483 K, the liquid fuel was preheated and mixed with air at a constant temperature of 550 K in the system to ensure complete vaporization. The stainless steel supply line and burner were insulated by ceramic wool to minimize the heat loss to the environment and avoid any potential condensation of vaporized fuel. To stabilize a premixed flame while preventing secondary diffusion flame development, N_2 coflow at 10 cm/s was employed for all the experimental conditions. It should be noted that the N_2 coflow was supplied to the burner independently from the mainstream of the fuel/air premixed mixture. As such, it is possible to maintain the same flow rate of the N_2 coflow for all the velocity conditions of the fuel/air mixture in the experiment. Based on [16,17], the impact of the coflow velocity was negligible on the measurement of laminar burning velocity.

In the present study, the palm oil biodiesel, also known as palm methyl esters (PME), was supplied by Mewah Oils Sdn. Bhd., Malaysia. Furthermore, GC–MS analysis, using Agilent 7890 A (GC) & 5975C (MS), was performed to obtain the composition of PME used in the experiment [25]. Table 1 shows the fuel properties, which are well within the European Union's EN14214 standards, while Table 2 illustrates the composition of PME. Multi-walled car-

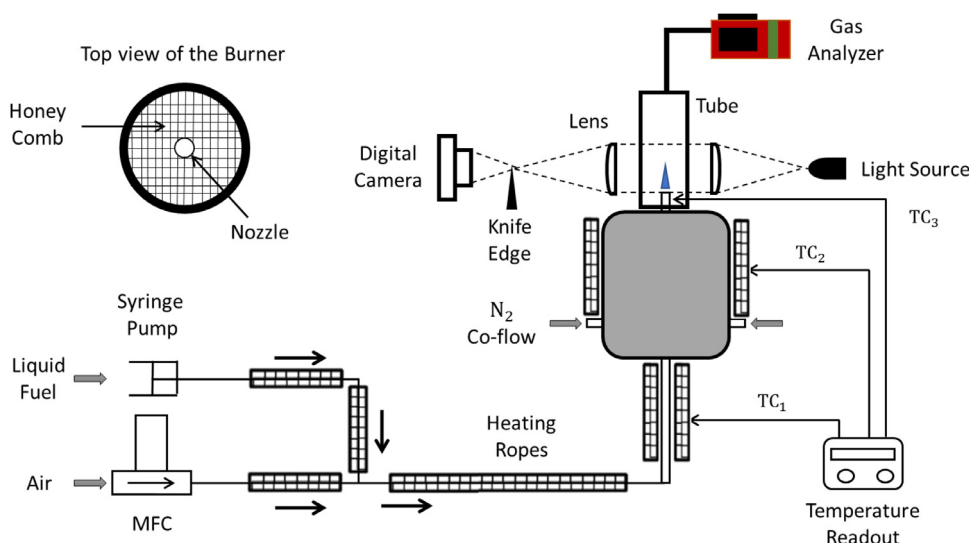


Fig. 1. Schematic diagram of the experimental setup.

Table 3
Properties of the MWCNTs.

Property	10–20 nm	30–50 nm
Purity (carbon content, wt.%)	97	97
Inner diameter (nm)	5–10	5–12
Length (μm)	10–30	10–20
Specific surface area (m ² /g)	> 200	> 60
True density (g/cm ³)	2.1	2.1
Estimated number of walls (-)	8–23	27–67

bon nanotubes having outer diameter ranges of 10–20 and 30–50 nm were supplied by BT Science Sdn. Bhd., Malaysia, and their properties are illustrated in Table 3. The concentration of nano-additives in the mixture was varied from 25 to 200 ppm. It is worth mentioning that MWCNTs with the outer diameter of 10–20 nm were used as the main additive to study the effect of the nanotubes on the combustion characteristics of the fuel, while the nanotubes with an outer diameter of 30–50 nm were employed to analyze the significance of nanotubes geometry. MWCNTs blended fuel samples were prepared using an ultrasonicator (Cole Parmer) at the amplitude of 55% and the pulse of 10/5 for 45 min. The images of premixed flames were captured via direct photography using a digital camera (Sony, A6000). In the case of the emission measurement, the concentrations of NO_x and CO in the exhaust gasses were obtained via an exhaust gas analyzer (Kane, 905), which was placed at the end of the quartz tube aligned with the central nozzle.

2.2. Experimental methodology

2.2.1. Blowoff velocity

The stabilization of the premixed bunsen flame at the nozzle rim is associated with the heat transfer mechanism between the nozzle rim and the root of the premixed flame. The distance between the nozzle rim and the flame root is known as a standoff distance, and it increases with the higher jet velocity, U_{jet} [26]. The premixed flame can experience a blowoff effect at a critical jet velocity due to the weaker heat transfer mechanism as a result of a high standoff distance. This is known as the blowoff velocity of the premixed flame [27].

In the case of experimental measurement of the blowoff velocity, the findings from the literature showed that the increasing flow rate method could result in inconsistent data [26]. It was assumed

that the blowoff velocity can be measured by establishing a stable flame at the nozzle rim and gradually increasing the jet velocity until the flame experiences the blowoff effect. However, the time taken to change the jet velocity of the mixture is significant enough such that the heat loss from the flame to the nozzle rim can increase the temperature of the unburnt mixture. As a result of this observation, Vu et al. [26] concluded that the blowoff velocity should be determined using the decreasing flow rate method. In the present study, the jet velocity was firstly set at a high value at which the flame was unable to ignite. It was followed by the gradual decrease in jet velocity, in the step of 1 cm/s, until the flame was successfully established at the nozzle rim, while the equivalence ratio of the mixture remained constant. Hence, this method allowed keeping the unburnt mixture and the nozzle temperatures unchanged by preventing the heat loss from the flame to the nozzle rim.

2.2.2. Laminar burning velocity

The laminar burning velocity is a fundamental combustion characteristic that describes the propagation of a premixed fuel-air flame at a given temperature and pressure for a specific equivalence ratio. Based on the literature [17], laminar burning velocity was extensively studied for gaseous fuels using various experimental configurations such as constant volume combustion chamber, flat flame burner, counterflow burner, and coflow burner.

In the present study, the coflow burner was employed to obtain the conical premixed flames. The calculation of laminar burning velocity was performed based on the weighted average of the area over the entire flame surface method [28]

$$S_u^0 = Q_u / A_b \quad (1)$$

where S_u^0 is the laminar burning velocity, Q_u is the total volumetric flow rate of the unburnt mixture, and A_b is the flame surface area. While the value of Q_u was varied based on the experimental conditions, the flame surface areas were calculated from the flame images. There are three widely known flame imaging methods: schlieren, shadowgraphing, and direct photography [27]. Although all three methods can produce adequate laminar burning velocity results, it is also known that the schlieren method is the most accurate among them [17]. Hence, the flame surface area in the present study was defined based on the visible flame boundary from the schlieren images, as shown in Fig. 2. The flame boundary was identified using the image processing tools from MATLAB, which was used to calculate the surface area of the revolution.

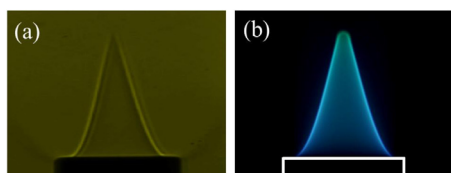


Fig. 2. (a) Schlieren image, (b) direct photograph of PME/air flame at $\phi = 1.1$ and $U_{jet} = 100$ cm/s.

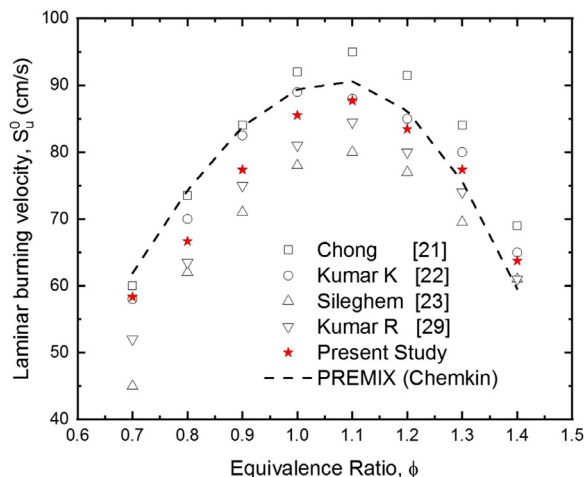


Fig. 3. Laminar burning velocities of *n*-heptane/air flame at atmospheric pressure and the unburnt gas temperature of 470 K obtained from the present study and literature.

3. Results and discussion

In the present study, the effect of MWCNTs addition on fundamental combustion characteristics of the PME/air premixed flames was experimentally investigated. Laminar burning velocities were obtained over the wide range of equivalence ratios, $\phi = 0.7$ – 1.3 , and at the unburnt gas temperature of 550 K and atmospheric pressure. The blowoff effect was achieved at all the equivalence ratios, and the changes in flammability limits were identified at both fuel-lean and fuel-rich regions. Lastly, the exhaust gas analyzer was used to measure NO_x and CO concentrations as the result of the combustion of MWCNTs blended PME fuel.

3.1. Experimental validation

Based on the literature findings, there are some studies done on laminar burning velocity and blowoff velocity of liquid fuels such as *n*-heptane [21–23,29], while data for PME/air premixed flame are still limited. Hence, the laminar burning velocity of *n*-heptane flame was measured using the present setup in order to validate the accuracy of the current experiment. To perform a direct comparison, experiments were conducted at the same conditions as the literature conditions at the atmospheric pressure with the unburnt gas temperature of 470 K and the equivalence ratio varying from 0.7 to 1.4. Furthermore, the experimental results were also compared with the numerically obtained results using PREMIX code of Chemkin, with CRECK mechanism [30]. As illustrated in Fig. 3, it can be seen that the results from the present study are well within the range of the literature findings [21–23,29] and in good agreement with the numerical results. The discrepancies between the literature results can be attributed to the differences in the experimental setups and the use of different burner configurations.

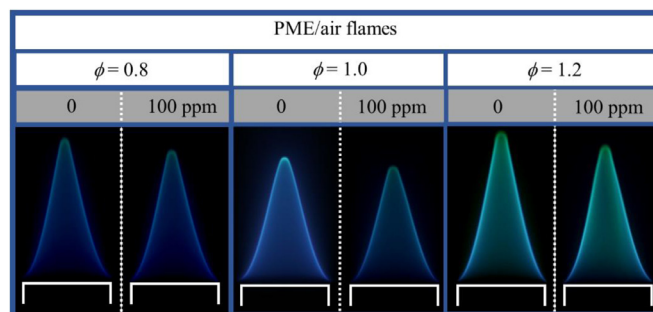


Fig. 4. Direct photographs of PME/air premixed flames without and with MWCNTs (10–20 nm) of 100 ppm addition at lean, rich, and stoichiometric conditions at $U_{jet} = 120$ cm/s.

3.2. Blowoff velocity

PME/air premixed mixtures were enriched with MWCNTs of 10–20 nm at the concentration of 100 ppm to study the effect of nano-additives on the behavior of the premixed flames. Fig. 4 illustrates the laminar premixed flames stabilized at the nozzle rim, for all three, lean ($\phi = 0.8$), rich ($\phi = 1.2$) and stoichiometric ($\phi = 1.0$) conditions at the jet velocity of 120 cm/s. All direct images were captured at the same camera settings (ISO, shutter speed, and white balance) in order to perform the direct comparison in the structure of premixed flames with and without the addition of MWCNTs.

As can be seen from Fig. 4, the flame height was shorter when MWCNTs were added to the mixture regardless of the equivalence ratio. As an example, for the PME/air flame at the rich condition, the height was decreased from 12.6 mm to 11.9 mm with MWCNTs of 100 ppm addition to the mixture. This behavior can be attributed to the improved fuel-air mixing with the presence of nanotubes in the mixture due to the occurrence of micro explosions during the vaporization and combustion process. In other words, MWCNTs helped the fuel react with more oxygen in the mixture. This is in alignment with the observations made by Hua et al. [31] and Mazas et al. [32], where they showed that the height of the reaction zone in flames decreased with the higher content of oxygen in the fuel/air mixtures. In regard to the structure of a premixed bunsen flame, the balance between the laminar burning velocity and the local flow velocity determines the flame tip angle. Hence, it is understood that any changes in the two parameters can lead to a change in the conical premixed flame angle, resulting in a flame height modification. In fact, when the jet velocity is kept constant for the mixture with and without MWCNTs addition, a decrease in the flame height of the premixed flame is a good indicator of the improvement in laminar burning velocity and blowoff velocity.

In premixed flame, standoff distance, which is defined as the height of the flame base from the nozzle rim, determines the heat transfer mechanism between the flame and the nozzle rim. Blowoff occurs when the standoff distance reaches its critical value at a certain jet velocity [27]. Hence, it can be understood that the standoff distance is another parameter in predicting the behavior of the blowoff velocity of a premixed bunsen flame. The effect of MWCNTs on the PME/air premixed flames was further investigated at the fuel-rich conditions of the mixture by increasing the equivalence ratio towards the rich limit. It can be observed from Fig. 5 that there is a decrease in the standoff distance of the flame with the addition of MWCNTs. Furthermore, the typical conical shape of the premixed bunsen flames was distorted, and the rotating flames were observed at $\phi \geq 1.35$. By gradually increasing the equivalence ratio of the PME/air mixture, the extinction limit of the flame with-

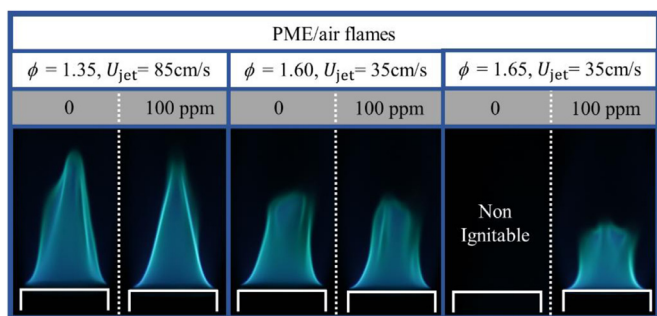


Fig. 5. Direct photographs of very rich PME/air premixed flames without and with MWCNTs (10–20 nm) of 100 ppm addition.

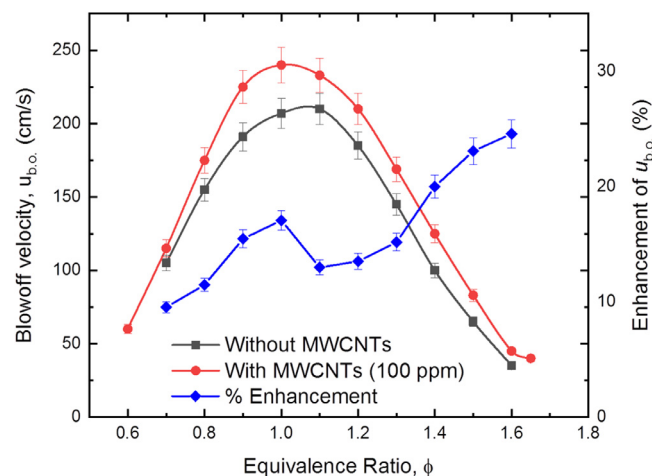


Fig. 6. Comparison of blowoff velocities of PME/air premixed flames without and with MWCNTs (10–20 nm) of 100 ppm addition.

out the addition of MWCNTs was found to be at $\phi = 1.6$. However, it was found that the flammability was further extended to $\phi = 1.65$ with the MWCNTs of 100 ppm addition to the mixture. While it is an adequate conclusion to state that the nano-additives could improve the stability of the premixed flames, it should be highlighted that a more detailed study of the chemical kinetics involving the MWCNTs blended PME/air premixed flames is required.

Fig. 6 depicts the effect of MWCNTs on the blowoff velocity of PME/air flames over the wide range of equivalence ratios. The results showed that there was an improvement in blowoff velocities regardless of the equivalence ratio. From the absolute values of blowoff velocities, it can be observed that the flames around the stoichiometric condition experienced the most significant improvement. However, it is worth noting that, based on the enhancement percentage, the flames at very rich conditions ($\phi \geq 1.4$) experienced a more improvement compared to the flames at $\phi < 1.4$. Furthermore, the flammability limits at both lean and rich regions were improved with the addition of 100 ppm of MWCNTs to PME/air premixed flames. The improvements of blowoff velocities were associated with the enhancement of the heat transfer to the nozzle rim due to the decrease of standoff distance, as can be seen in Fig. 5. In their studies, Hosseini et al. [33] and El-Seesy et al. [34] showed two favoring properties of carbon-based nanotubes, such as high thermal conductivity and high surface to volume ratio, made them a promising fuel-borne catalyst. Hence, it can be understood that the high surface to volume ratio of MWCNTs enabled an improved thermal exchange between nano-additives and fuel-air droplets, leading to the occurrence of micro explosions during the vaporization and combustion processes. This resulted in improving combustion performance due to the enhancement of

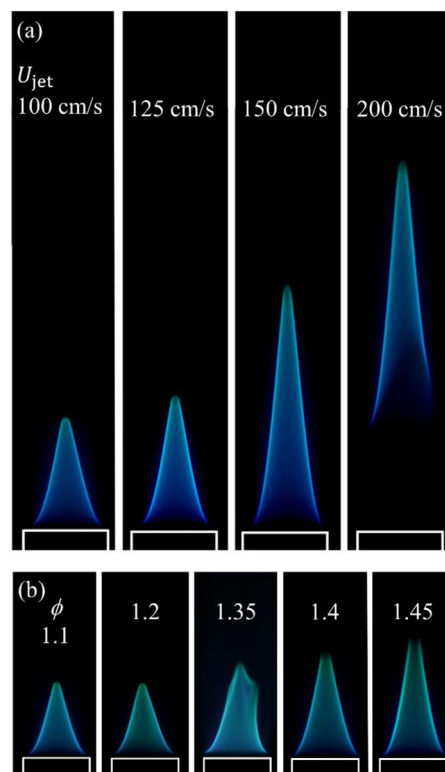


Fig. 7. Direct photographs of PME/air premixed flames, (a) increasing the jet velocity until blowoff at $\phi = 1.0$, (b) presence of tip opening with the increasing of equivalence ratio at $U_{jet} = 90$ cm/s.

fuel-air mixing, which, in turn, improved the oxidation of the mixture.

Another observation made during the present study regarding the flame structure was the presence of tip opening in the premixed bunsen flame. Fig. 7(a) illustrates the typical behavior of the premixed flame with the increasing jet velocity, $U_{jet} = 100, 125, 150$, and 200 cm/s, at the stoichiometric condition of the mixture. As can be seen in Fig. 7(a), the flame tip did not open even though the flame experienced the blowoff effect. This indicates the independence of the tip opening with regard to the jet velocity of the flame. Fig. 7(b) shows the premixed flames with the increasing equivalence ratio, $\phi = 1.1, 1.2, 1.35, 1.4$, and 1.45 , at the jet velocity of 90 cm/s. It can be observed that the flame did not experience any tip opening at the equivalence ratios of 1.1 and 1.2 . However, it started experiencing the flame structure breakouts at $\phi = 1.35$ and followed by the clear tip opening at $\phi = 1.4$, which grew wider when the mixture became richer, at $\phi = 1.45$. It was observed that the presence of tip opening led to the stabilization of the flame front, and the breakouts of the flame structure disappeared. In general, the occurrence of flame tip opening is associated with the negative stretch rate of the curvature at the flame tip and the preferential diffusion, represented by the Lewis number, from the imbalance of thermal and mass diffusions in the flame [35,36]. Regarding the premixed bunsen flames, Mizobuchi et al. [37] showed that the fuel concentration was not homogeneous throughout the flame structure as it decreased along the axial direction. Furthermore, the findings from [35,36] showed a gradual decrease in the maximum concentration of OH radicals downstream along the flame front with the increasing equivalence ratio of the rich mixtures. In addition to that, the localized concentration of OH radicals was weakened at the tip for the flames that experienced the tip opening phenomenon [35]. Hence, the preferential diffusion between the fuel and oxidant molecules led to a weaker

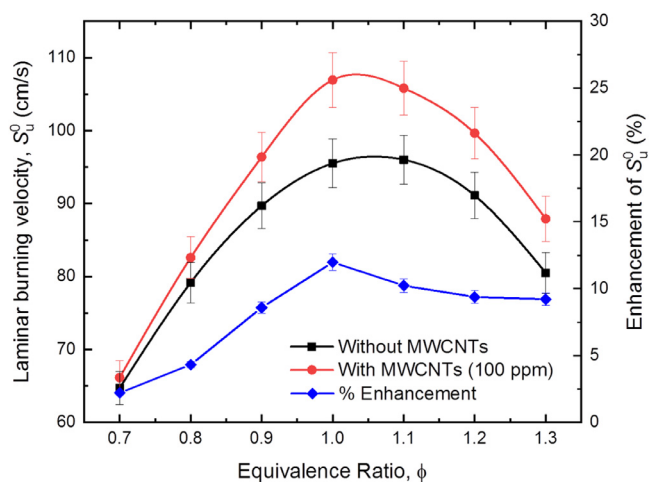


Fig. 8. Comparison of laminar burning velocities of PME/air premixed flames with and without MWCNTs (10–20 nm) of 100 ppm addition.

local combustion intensity at the flame tip. Additionally, it can be seen from Fig. 7(b) that the flame height was increased with the increasing equivalence ratio of the premixed flame, which, in turn, caused a stronger flame stretch rate at the tip. As such, the flame tip opening can be addressed with the weaker combustion intensity and the stronger flame stretch rate at the tip of the flame with the increasing equivalence ratio of the mixture.

3.3. Laminar burning velocity

Fig. 8 shows the laminar burning velocities of PME/air premixed flames with and without MWCNTs addition over the wide range of equivalence ratios, $\phi = 0.7$ – 1.3 , at atmospheric pressure and the preheat temperature of 550 K. While the richer mixtures, $\phi = 1.35$ – 1.6 , were ignitable, it is important to highlight that the measurement of laminar burning velocity was limited to $\phi = 1.3$. Regarding the premixed bunsen flame, laminar burning velocity can be obtained either via angle or flame surface area method. It is worth noting that both mentioned methods require the assumption of a flame being in a conical shape with symmetry about its axial direction. Hence, as shown in Fig. 5, the flames with $\phi > 1.3$ can be considered irregular and asymmetrical. Furthermore, the existence of tip opening at the fuel-rich conditions can result in greater uncertainties in calculating the surface area method, which in return leads to errors in the calculation of laminar burning velocity. As illustrated in Fig. 8, the results showed that the laminar burning velocities of PME/air premixed flames were noticeably improved with the addition of MWCNTs for all the experimental cases. Alenezi et al. [38] explained that the presence of MWCNTs in the fuel blends led to an accelerated fuel reaction in the combustion process due to the catalytic nature of carbon-based nanotubes. It was further explained that the thermos-physical properties, such as thermal conductivity and mass diffusivity, of the fuel were enhanced with the addition of nano-additives, resulting in improving combustion performance [39]. In addition to the overall improvement of laminar burning velocity, the results from the present study showed that the effect of nano-additives was more impactful at the fuel-rich and stoichiometric conditions as compared to the fuel-lean conditions of PME/air mixtures, as represented by the enhancement percentage curve in Fig. 8. This behavior is quite similar in trend to the enhancement percentage for the blowoff velocity at the specific range of equivalence ratios, $\phi = 0.7$ – 1.3 , as shown in Fig. 6. Furthermore, the laminar burning velocity against the equivalence ratio trend is similar to the trend of blowoff velocity for PME/air premixed flames, as compared between Figs. 6 and

8. As such, it can be stated that the behavior of the laminar burning velocity can be used as a preliminary parameter to predict the behavior of the blowoff velocity per given mixture. Although these two parameters have a codependency with each other, it is essential to highlight that the relationship is far more complex due to the potential coupling effect of the flame stretch, heat losses as well as quenching.

To further understand how the carbon-based nanotubes affect the combustion of PME/air premixed flames, the concentration of MWCNTs in the mixture was varied between 25 and 200 ppm. Furthermore, to assess the significance of nanotubes' diameter on the laminar burning velocity of the premixed flame, the mixture was blended with two different groups of nano-additives, 10–20 nm, and 30–50 nm diameter ranges. As can be seen from Fig. 9(a), the maximum improvement of 13.6% in laminar burning velocity was achieved at the stoichiometric condition with 125 ppm of MWCNTs (10–20 nm) addition. It was followed by the flames at fuel-rich conditions, which experienced the most improvement in laminar burning velocity at 150 ppm of MWCNTs. On the other hand, the flames at lean conditions experienced the least improvement in the laminar burning velocity, which peaked at about 125 ppm of MWCNTs in the mixture to reach about 4% improvement. From these observations, it can be concluded that for the smaller MWCNTs (10–20 nm), the MWCNTs of 125–150 ppm range can be considered as the optimal concentration across the equivalence ratios. On the other hand, PME/air mixtures with the addition of larger MWCNTs (30–50 nm) experienced a much lower improvement in laminar burning velocity, as shown in Fig. 9(b). The highest increase in laminar burning velocity with larger MWCNTs (30–50 nm) is about 6% compared to 13.6% improvement with smaller MWCNTs (10–20 nm). This behavior can be explained based on the difference in surface to volume ratio, which can be quantified from the specific surface area of the MWCNTs. As can be seen from Table 3, the specific surface area of the smaller nanotubes is much higher than that of the larger nanotubes, indicating the higher thermal conductivity of the smaller nanotubes. This is in good agreement with the findings of Fujii et al. [40], where it was reported that the thermal conductivity of MWCNTs increased as their outer diameter decreased. This phenomenon is associated with the number of walls per nanotube as nanotubes with larger outer diameter contain a higher number of walls than smaller nanotubes. Furthermore, the present results revealed that the biodiesel flames with larger MWCNTs addition showed an unpredictable behavior in enhancing the laminar burning velocity. As can be seen from Fig. 9(b), the fuel-rich and stoichiometric mixtures experienced the most enhancement in the laminar burning velocity of PME/air with MWCNTs (30–50 nm) of 100–125 ppm addition. In contrast, the fuel-lean mixture experienced less impact, in which the most enhancement in laminar burning velocity occurred at 75 ppm. While it was expected that the laminar burning velocity would gradually increase with the concentration of MWCNTs in the mixture, it was observed that the mixtures experienced lesser improvements in laminar burning velocity when the MWCNTs concentration reached a critical value in the mixture, regardless of the size of the nanotubes and equivalence ratio. For both groups of nanotubes (10–20 nm and 30–50 nm), the decline in the laminar burning velocity was associated with the excessive concentration of nano-additives in the mixture. While MWCNTs possess beneficial thermos-physical properties that can enhance the combustion of the given fuel, exceeding a specific concentration of nano-additives could dilute the overall mixture. The dilution effect was confirmed when some blends could not even get ignited with concentrations of MWCNTs above 150 ppm, as shown in Fig. 9(b). Furthermore, it can be explained that the heat absorption of the MWCNTs in the mixture becomes more significant with the increasing of concentration, resulting in a reduction in the unburnt

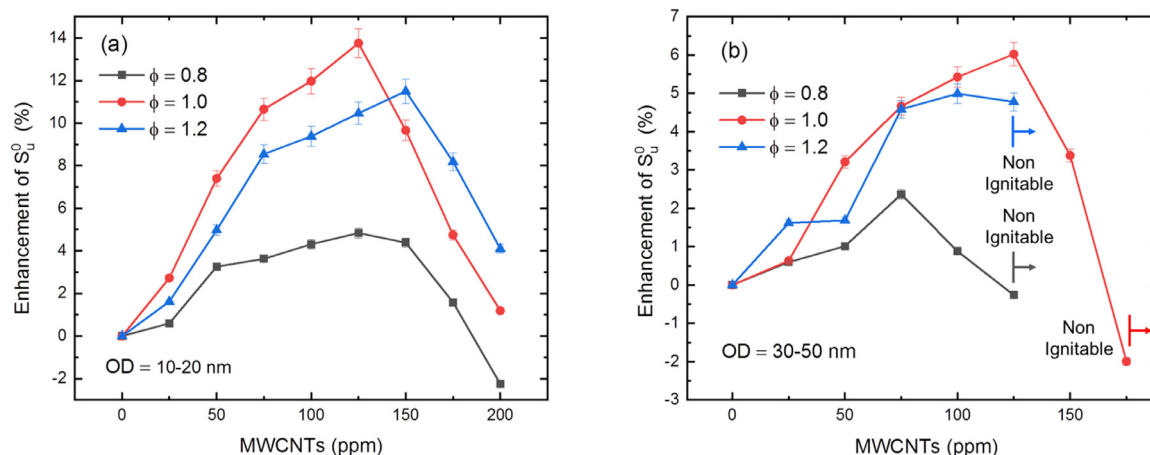


Fig. 9. Enhancement of laminar burning velocities of PME/air premixed flames with MWCNTs addition with the outer diameters of (a) 10–20 nm, (b) 30–50 nm.

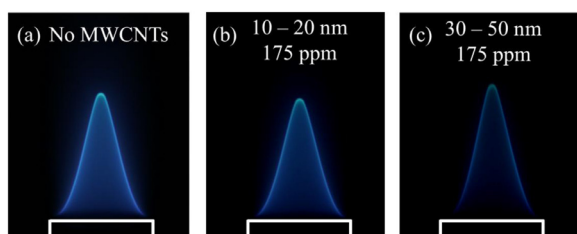


Fig. 10. Direct photographs of PME/air premixed flames (a) without MWCNTs and with MWCNTs addition of 175 ppm with the outer diameter of (b) 10–20 nm, (c) 30–50 nm, at $\phi = 1.0$ and $U_{jet} = 120$ cm/s.

mixture temperature. This observation was in agreement with the findings of Hariram et al. [41], where the effect of CNTs on the compression ignition engine performance running with oxygenated jojoba biodiesel-diesel blends was investigated. The results suggested that the fuel sample with 100 ppm of MWCNTs had the optimal engine performance compared to the fuel samples with 50 and 150 ppm of MWCNTs.

The flame structure changes, such as flame height and standoff distance, with the presence of MWCNTs with two different outer diameters, were visualized in Fig. 10. While Fig. 10(a) shows the premixed flame with no nanotubes in the mixture, Figs. 10(b and c) show the flames of the same mixture with the addition of MWCNTs of 175 ppm with 10–20 and 30–50 nm outer diameters, respectively. The jet velocity was kept constant at 120 cm/s to perform the direct comparison between the flames. As can be observed from Fig. 10, the height of the flame with MWCNTs (10–20 nm) addition was decreased by 7.4%, whereas the flame with MWCNTs (30–50 nm) addition was increased by 3.9% as compared to the flame without MWCNTs. Furthermore, the standoff distance became shorter for the flame with MWCNTs (10–20 nm) addition, whereas the flame with MWCNTs (30–50 nm) addition was pushed further away from the nozzle rim. These changes in the flame structure can be attributed to the changes in the laminar burning velocity of premixed flames with the presence of MWCNTs. From Fig. 9(a), it can be viewed that the laminar burning velocity of the stoichiometric mixture was enhanced by about 4% by adding MWCNTs (10–20 nm) of 175 ppm. Hence, this improvement in laminar burning velocity resulted in shorter flame height and standoff distance. On the contrary, Fig. 9(b) shows that the laminar burning velocity of the stoichiometric mixture was reduced by about 2% with MWCNTs (30–50 nm) of 175 ppm addition. Besides, it can also be observed that the intensity of flame luminosity decreased with the addition of carbon-based nanotubes.

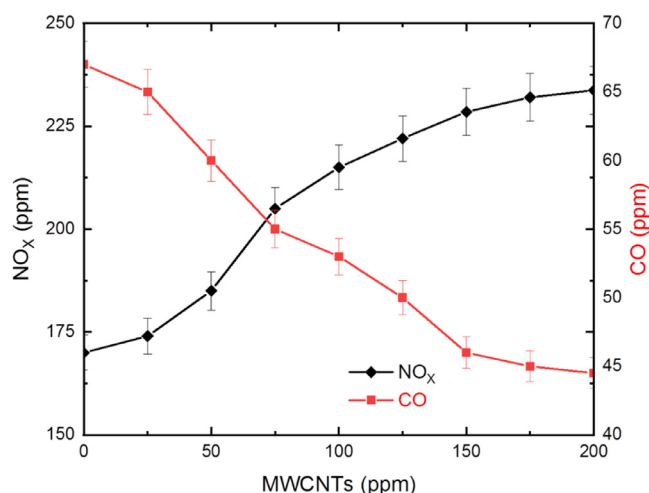


Fig. 11. NO_x and CO emissions from PME/air premixed flames at the stoichiometric condition with MWCNTs (10–20 nm) addition.

3.4. NO_x and CO emissions

It is known that transportation is one of the most significant sectors in terms of fossil-based fuel consumption. As such, they are recognized as one of the main contributors towards the production of pollutant emissions. Based on the literature, the usage of biodiesel in diesel engines allows reducing the concentration of UHC, CO₂, CO, and solid particles in the exhaust gasses. However, this also leads to a higher content of NO_x emissions [13]. In regard to this behavior, Fig. 11 illustrates the effect of MWCNTs in the mixture on the NO_x and CO emissions. The results showed that NO_x was continuously increasing while CO gradually decreased with the increasing content of MWCNTs in the mixture. It can also be observed that with the content of MWCNTs of 150 ppm and higher, the changes in the concentration of pollutants were relatively small, which were less than 2% for both NO_x and CO productions.

The reduction in CO was mainly attributed to the enhancement of combustion performance with the presence of MWCNTs. Furthermore, MWCNTs in the fuel-air mixture could improve the chemical reactivity of the overall blend [34,38]. It could be attributed to the properties of the carbon-based nanotubes, such as a high area to volume ratio and high thermal conductivity, which resulted in the accelerated combustion of the mixture, thereby lead-

ing to a higher heat release rate. This resulted in mitigating the chemical energy loss in the process leading to the reduction in CO formation. Furthermore, the process of CO oxidization in the preheated zone could be improved due to the increased temperature of the premixed flame with MWCNTs addition.

In engine application, the formation of NO_x emission is predominantly dependent on the parameters such as injection timing, combustion timing, heat release rate, and temperature of the fuels. In the present laboratory scaled experiment, the injection and combustion timing were not considered to be the relevant parameters. There are three opportunities for NO_x formation including thermal NO_x, fuel NO_x, and prompt NO_x in which thermal NO_x is the main mechanism of NO_x formation [42]. In the present study, the addition of MWCNTs to PME/air mixture could raise the flame temperature as a result of the enhancement of combustion performance due to the presence of MWCNTs in the mixture. Hence, the increase in NO_x formation can be attributed to the thermal NO_x mechanism. This is also in good agreement with the improvements found in laminar burning velocity, as it has been reported that the higher flame temperature leads to a higher laminar burning velocity. Furthermore, the improved chemical reactivity of the blend could result in a higher heat release rate. As such, these changes in the combustion behavior, due to the presence of MWCNTs in the mixture, resulted in a higher content of NO_x formation.

4. Concluding remarks

In the present study, the fundamental combustion characteristics of PME/air premixed mixtures with the addition of MWCNTs were investigated using the coflow burner configuration. The parameters such as laminar burning velocity, blowoff velocity, and NO_x and CO concentrations were experimentally measured over the wide range of equivalence ratios at atmospheric pressure and the preheated temperature of 550 K. The main findings are as follows:

- 1 Blowoff velocity increased with MWCNTs addition to the mixture regardless of the equivalence ratio. The impact of nano-additives was more significant in fuel-rich conditions, whereas the fuel-lean mixtures experienced less improvement in blowoff velocity. Furthermore, the flammability limits were extended at both lean and rich conditions.
- 2 Laminar burning velocity increased with MWCNTs addition to the mixture, with the highest enhancement observed around the stoichiometric condition. However, further increase the concentration of nano-additives in the mixture beyond the critical concentrations (125–150 ppm and 75–125 ppm for MWCNTs of 10–20 nm and 30–50 nm, respectively) generally caused less improvement in the laminar burning velocities of the premixed flames. It was observed that the nanotubes with the larger outer diameter were less effective than the smaller nanotubes.
- 3 The improvements in blowoff velocity and laminar burning velocity were indicated by the reduction in standoff distance and shortening of flame height with the addition of MWCNTs. Furthermore, PME/air premixed flames experienced tip opening at very fuel-rich conditions ($\phi \geq 1.4$). It was shown that the tip opening occurred irrespective of the jet velocity and was primarily affected by the fuel concentration in the mixture.
- 4 NO_x was continuously increasing, while CO gradually decreased with the increasing content of MWCNTs in the mixture. These emissions production behaviors were mainly attributed to the accelerated and enhanced combustion performance due to the presence of MWCNTs in the mixture.

Declaration of Competing Interests

The authors declare that they have no known competing financial interests or personal relationships that could have appeared to influence the work reported in this paper.

References

- [1] Martin U, Dieter B, Christine B, Bert B, Georg F, Rolf L, Martin M, Kevin S, Jennifer S, Olaf S, Ulrike S, Helmut T, Edgar R, Richard W, Markus W, Jürgen K. Action areas and the need for research in biofuels. *Fuel* 2020;268:117227.
- [2] Digambar S, Dilip S, Shyam LS, Sumit S, Deepika K. Chemical compositions, properties, and standards for different generation biodiesels: a review. *Fuel* 2019;253:60–71.
- [3] Anantha RL, Deepanraj B, Rajakumar S, Sivasubramanian V. Experimental investigation on performance, combustion and emission analysis of a direct injection diesel engine fuelled with rapeseed oil biodiesel. *Fuel* 2019;246:69–74.
- [4] Medhat E, Hagar AEB, Khaled KE, Ahmed MR, Hitesh P, Kishor KS, Deepalekshmi P, Rashmi W. Experimental studies on the biodiesel production parameters optimization of sunflower and soybean oil mixture and DI engine combustion, performance, and emission analysis fueled with diesel/biodiesel blends. *Fuel* 2019;255:115791.
- [5] Sivakumar M, Sundaram NS, Kumar RR, Thasthagir MHS. Effect of aluminum oxide nano-particles blended pongamia methyl ester on performance, combustion and emission characteristics of diesel engine. *Renew Energy* 2018;116:518–26.
- [6] Lee CC, Tran M-V, Tan BT, Scribano G, Chong CT. A comprehensive review on the effects of additives on fundamental combustion characteristics and pollutant formation of biodiesel and ethanol. *Fuel* 2021;288:119749.
- [7] Manigandan S, Sarweswaran R, Devi PB, Sohret Y, Kondratiev A, Venkatesh S, Vimal MR, Joshua JJ. Comparative study of nanoadditives TiO₂, CNT, Al₂O₃, CuO and CeO₂ on reduction of diesel engine emission operating on hydrogen fuel blends. *Fuel* 2020;262:116336.
- [8] Shaafi T, Sairam K, Gopinath A, Kumaresan G, Velraj R. Effect of dispersion of various nanoadditives on the performance and emission characteristics of a CI engine fuelled with diesel, biodiesel and blends—A review. *Renew Sust Energy Rev* 2015;49:563–73.
- [9] Venu H, Madhavan V. Effect of Al₂O₃ nano-particles in biodiesel-diesel-ethanol blends at various injection strategies: performance, combustion and emission characteristics. *Fuel* 2016;186:176–89.
- [10] Sajith V, Sobhan CB, Peterson GP. Experimental Investigations on the Effects of Cerium Oxide Nanoparticle Fuel Additives on Biodiesel. *Adv Mech Eng* 2015;2:1–6.
- [11] Vairamuthu G, Sundarapandian S, Kailasanathan C, Thangagiri B. Experimental investigation on the effects of cerium oxide nano-particle on Calophyllum inophyllum (Punnai) biodiesel blended with diesel fuel in DI diesel engine modified by nozzle geometry. *J Energy Inst* 2016;89:668–82.
- [12] Chen AF, Adzmi MA, Adam A, Fahmi M, Kamal M, Mrwan AG. Combustion characteristics, engine performances and emissions of a diesel engine using nano-particle- diesel fuel blends with aluminium oxide, carbon nanotubes and silicon oxide. *Energy Convers Manag* 2018;171:461–77.
- [13] Ghanbari M, Najafi G, Ghobadian B, Yusaf T, Carlucci AP, Kiani Deh Kiani M. Performance and emission characteristics of a CI engine using nano particles additives in biodiesel-diesel blends and modeling with GP approach. *Fuel* 2017;202:699–716.
- [14] Najafi G. Diesel engine combustion characteristics using nano-particles in biodiesel-diesel blends. *Fuel* 2018;212:668–78.
- [15] Yi W, Bjorn R, Vincent M, Xilong Y, Linlin W, Frédéric G. Laminar flame speed of lignocellulosic biomass-derived oxygenates and blends of gasoline/oxygenates. *Fuel* 2017;202:572–82.
- [16] Nurmukan D, Chen TJM, Hung YM, Ismadi M-Z, Chong CT, Tran M-V. Enhancement of biogas/air combustion by hydrogen addition at elevated temperatures. *Int J Energy Res* 2020;44:1519–34.
- [17] Alexander AK, Akram M, Velamati RK, Nam K, Chockalingam P, Sudarshan K. A comprehensive review of measurements and data analysis of laminar burning velocities for various fuel + air mixtures. *Prog Energy Combust Sci* 2018;68:197–267.
- [18] Wei L, Yong J, Yi J, Xianli Z. Investigation of the influence of DMMP on the laminar burning velocity of methane/air premixed flames. *Fuel* 2019;235:1294–300.
- [19] Sileghem L, Alekseev VA, Vancoillie J, Van Geem KM, Nilsson EJK, Verhelst S, Konnov AA. Laminar burning velocity of gasoline and the gasoline surrogate components iso-octane, n-heptane and toluene. *Fuel* 2013;112:355–65.
- [20] Rau F, Hartl S, Voss S, Still M, Hasse C, Trimis D. Laminar burning velocity measurements using the Heat Flux method and numerical predictions of iso-octane/ethanol blends for different preheat temperatures. *Fuel* 2015;140:10–16.
- [21] Chong CT, Hochgreb S. Measurements of laminar flame speeds of liquid fuels: jet-A1, diesel, palm methyl esters and blends using particle imaging velocimetry (PIV). *Proc Comb Inst* 2011;33:979–86.
- [22] Kumar K, Freeh JE, Sung CJ, Huang Y. Laminar Flame Speeds of Preheated Iso-Octane/O₂/N₂ and n-Heptane/O₂/N₂Mixtures. *J Propul Power* 2007;23:428–36.

- [23] Sileghem L, Alekseev VA, Vancoillie J, Van Geem KM, Nilsson EJK, Verhelst S, Konnov AA. Laminar Burning Velocity of Gasoline and the Gasoline Surrogate Components Iso-Octane, nHeptane and Toluene. *Fuel* 2013;112:355–65.
- [24] Meng Z, Liang K, Fang J. Laminar burning velocities of iso-octane, toluene, 1-hexene, ethanol and their quaternary blends at elevated temperatures and pressures. *Fuel* 2019;237:630–6.
- [25] Nurmukan D, Tran M-V, Foo JJ, Scribano G, Chong CT, Huynh TC. Experimental study on laminar lifted flames of pre-vaporized palm oil biodiesel. *Fuel* 2021;288:119697.
- [26] Vu TM, Won SH, Ombrello T, Cha MS. Stability enhancement of ozone-assisted laminar premixed Bunsen flames in nitrogen co-flow. *Combust Flame* 2014;161:917–26.
- [27] Bernard L, Guenther VE. Combustion, flames and explosions of gases, INC. 2nd ed. Pittsburgh, Pennsylvania: Academic Press; 1961.
- [28] Munajat NF, Erlich C, Fakhrai R, Fransson TH. Influence of water vapour and tar compound on laminar flame speed of gasified biomass gas. *Appl Energy* 2012;98:114–21.
- [29] Kumar R, Singhal A, Katoch A, Kumar S. Experimental Investigations on laminar burning velocities of n-heptane + air mixtures at higher mixture temperatures using externally heated diverging channel method. *Energy Fuels* 2020;34:2405–16.
- [30] Ranzi E, Frassoldati A, Stagni A, Pelucchi M, Cuoci A, Faravelli T. Reduced kinetic schemes of complex reaction systems: fossil and biomass-derived transportation fuels. *Int J Chem Kinetics* 2014;46:512–42.
- [31] Hua Y, Qiu L, Liu F, Qian Y, Meng S. Numerical investigation into the effects of oxygen concentration on flame characteristics and soot formation in diffusion and partially premixed flames. *Fuel* 2020;268:117398.
- [32] Mazas AN, Fiorina B, Lacoste DA, Schuller T. Effects of water vapor addition on the laminar burning velocity of oxygen-enriched methane flames. *Combust Flame* 2011;158:2428–40.
- [33] Hosseini SH, Alisarai AT, Ghobadian B, Mayvan AA. Performance and emission characteristics of a CI engine fuelled with carbon nanotubes and diesel-biodiesel blends. *Renew Energy* 2017;111:201–13.
- [34] El-Seesy AI, Abdel-Rahman AK, Bady M, Ookawara S. Performance, combustion, and emission characteristics of a diesel engine fueled by biodiesel-diesel mixtures with multi-walled carbon nanotubes additives. *Energy Convers Manag* 2017;135:373–93.
- [35] Vu TM, Cha MS, Lee BJ, Chung SH. Tip opening of premixed bunsen flames: extinction with negative stretch and local Karlovitz number. *Combust Flame* 2015;162:1614–21.
- [36] Wang J, Nie Y, Cai X, Guo S, Zhang W, Xie Y, Huang Z. Investigation on the highly negative curved syngas Bunsen flame and the critical local Karlovitz number when tip opening. *Fuel* 2018;215:429–37.
- [37] Mizobuchi Y, Nambu T, Takeno T. Numerical study of tip opening of hydrogen/air Bunsen flame. *Proc Comb Inst* 2019;37:1775–81.
- [38] Alenezi RA, Norkhizan AM, Mamat R, Erdiawansyah Najafi G, Mazlan M. Investigating the contribution of carbon nanotubes and diesel-biodiesel blends to emission and combustion characteristics of diesel engine. *Fuel* 2021;285:119046.
- [39] Ficarella A, Carlucci AP, Chehroudi B, Laforgia D, Strafella L. Multi-Walled Carbon Nanotubes (MWCNTs) bonded with Ferrocene particles as ignition agents for air-fuel mixtures. *Fuel* 2017;208:734–45.
- [40] Fujii M, Zhang X, Xie H, Ago H, Takahashi K, Ikuta T, Abe H, Shimizu T. Measuring the thermal conductivity of a single carbon nanotube. *Phys Rev Lett* 2005;95:065502.
- [41] Hariram V, Udhayakumar V, Karthick P, Abraham Eben Andrews A, Arunraja A, Seralathan S, Micha Premkumar T. Effect of carbon nanotubes on oxygenated jojoba biodiesel-diesel blends in direct injection ci engines. *Int J Veh Struct Syst* 2018;10:423–32.
- [42] Miller JA, Bowman CT. Mechanism and modeling of nitrogen chemistry in combustion. *Prog Energy Comb Sci* 1989;15:287–338.